



## 1 Global Carbon Budget 2024

2 Pierre Friedlingstein [1,2], Michael O'Sullivan [1], Matthew W. Jones [3], Robbie M. Andrew [4], Judith Hauck  
3 [5,6], Peter Landschützer [7], Corinne Le Quéré [3], Hongmei Li [8,9], Ingrid T. Lujckx [10], Are Olsen [11,12],  
4 Glen P. Peters [4], Wouter Peters [10,13], Julia Pongratz [14,9], Clemens Schwingshackl [14], Stephen Sitch  
5 [1], Josep G. Canadell [15], Philippe Ciais [16], Robert B. Jackson [17], Simone R. Alin [18], Almut Arneth  
6 [19], Vivek Arora [20], Nicholas R. Bates [21], Meike Becker [11,12], Nicolas Bellouin [22], Carla F. Berghoff  
7 [23], Henry C. Bittig [24], Laurent Bopp [2], Patricia Cadule [2], Katie Campbell [25], Matthew A.  
8 Chamberlain [26], Naveen Chandra [27], Frédéric Chevallier [16], Louise P. Chini [28], Thomas Colligan [29],  
9 Jeanne Decayeux [30], Laique M. Djeutchouang [31,32], Xinyu Dou [33], Carolina Duran Rojas [1], Kazutaka  
10 Enyo [34], Wiley Evans [25], Amanda R. Fay [35], Richard A. Feely [18], Daniel. J. Ford [1], Adrianna Foster  
11 [36], Thomas Gasser [37], Marion Gehlen [16], Thanos Gkritzalis [7], Giacomo Grassi [38], Luke Gregor [39],  
12 Nicolas Gruber [39], Özgür Gürses [5], Ian Harris [40], Matthew Hefner [41,42], Jens Heinke [43], George C.  
13 Hurtt [28], Yosuke Iida [34], Tatiana Ilyina [44,8,9], Andrew R. Jacobson [45], Atul K. Jain [46], Tereza  
14 Jarníková [47], Annika Jersild [29], Fei Jiang [48], Zhe Jin [49,50], Etsushi Kato [51], Ralph F. Keeling [52],  
15 Kees Klein Goldewijk [53], Jürgen Knauer [54,15], Jan Ivar Korsbakken [4], Siv K. Lauvset [55,12], Nathalie  
16 Lefèvre [56], Zhu Liu [33], Junjie Liu [57,58], Lei Ma [28], Shamil Maksyutov [59], Gregg Marland [41,42],  
17 Nicolas Mayot [60], Patrick C. McGuire [61], Nicolas Metzl [56], Natalie M. Monacci [62], Eric J. Morgan  
18 [52], Shin-Ichiro Nakaoka [59], Craig Neill [26], Yosuke Niwa [59], Tobias Nützel [14], Lea Olivier [5],  
19 Tsuneo Ono [63], Paul I. Palmer [64,65], Denis Pierrot [66], Zhangcai Qin [67], Laure Resplandy [68], Alizée  
20 Roobaert [7], Thais M. Rosan [1], Christian Rödenbeck [69], Jörg Schwinger [55,12], T. Luke Smallman  
21 [64,65], Stephen M. Smith [70], Reinel Sospedra-Alfonso [71], Tobias Steinhoff [72,55], Qing Sun [73],  
22 Adrienne J. Sutton [18], Roland Séférian [30], Shintaro Takao [59], Hiroaki Tatebe [74,75], Hanqin Tian [76],  
23 Bronte Tilbrook [26,77], Olivier Torres [2], Etienne Tourigny [78], Hiroyuki Tsujino [79], Francesco Tubiello  
24 [80], Guido van der Werf [10], Rik Wanninkhof [66], Xuhui Wang [50], Dongxu Yang [81], Xiaojuan Yang  
25 [82], Zhen Yu [83], Wenping Yuan [84], Xu Yue [85], Sönke Zachle [69], Ning Zeng [86, 29], Jiye Zeng [59].  
26

- 27 1. Faculty of Environment, Science and Economy, University of Exeter, Exeter EX4 4QF, UK  
28 2. Laboratoire de Météorologie Dynamique, Institut Pierre-Simon Laplace, CNRS, Ecole Normale Supérieure,  
29 Université PSL, Sorbonne Université, Ecole Polytechnique, Paris, France  
30 3. Tyndall Centre for Climate Change Research, School of Environmental Sciences, University of East Anglia,  
31 Norwich Research Park, Norwich NR4 7TJ, UK  
32 4. CICERO Center for International Climate Research, Oslo 0349, Norway  
33 5. Alfred-Wegener-Institut, Helmholtz-Zentrum für Polar- und Meeresforschung, Am Handelshafen 12, 27570  
34 Bremerhaven, Germany  
35 6. Universität Bremen, Bremen, Germany  
36 7. Flanders Marine Institute (VLIZ), Jacobsenstraat 1, 8400, Ostend, Belgium  
37 8. Helmholtz-Zentrum Hereon, Max-Planck-Straße 1, 21502 Geesthacht, Germany



- 38 9. Max Planck Institute for Meteorology, Bundesstraße 53, 20146 Hamburg, Germany
- 39 10. Wageningen University, Environmental Sciences Group, P.O. Box 47, 6700AA, Wageningen, The
- 40 Netherlands
- 41 11. Geophysical Institute, University of Bergen, Allégaten 70, 5007 Bergen, Norway
- 42 12. Bjerknes Centre for Climate Research, Bergen, Norway
- 43 13. University of Groningen, Centre for Isotope Research, Groningen, The Netherlands
- 44 14. Ludwig-Maximilians-Universität München, Luisenstr. 37, 80333 München, Germany
- 45 15. CSIRO Environment, Canberra, ACT 2101, Australia
- 46 16. Laboratoire des Sciences du Climat et de l'Environnement, LSCE/IPSL, CEA-CNRS-UVSQ, Université
- 47 Paris-Saclay, F-91198 Gif-sur-Yvette, France
- 48 17. Department of Earth System Science, Woods Institute for the Environment, and Precourt Institute for
- 49 Energy, Stanford University, Stanford, CA 94305–2210, United States of America
- 50 18. National Oceanic and Atmospheric Administration, Pacific Marine Environmental Laboratory
- 51 (NOAA/PMEL), 7600 Sand Point Way NE, Seattle, WA 98115, USA
- 52 19. Karlsruhe Institute of Technology, Institute of Meteorology and Climate Research/Atmospheric
- 53 Environmental Research, 82467 Garmisch-Partenkirchen, Germany
- 54 20. Canadian Centre for Climate Modelling and Analysis, Environment and Climate Change Canada, Victoria,
- 55 BC, Canada
- 56 21. ASU-BIOS, Bermuda Institute of Ocean Sciences, 31 Biological Lane, Ferry Reach, St. Georges,, GE01,
- 57 Bermuda
- 58 22. Department of Meteorology, University of Reading, Reading, RG6 6BB, UK
- 59 23. Instituto Nacional de Investigación y Desarrollo Pesquero, Paseo Victoria Ocampo N°1, Escollera Norte,
- 60 B7602HSA, Mar del Plata, Argentina
- 61 24. Leibniz Institute for Baltic Sea Research Warnemuende (IOW), Seestrasse 15, 18119 Rostock, Germany
- 62 25. Hakai Institute, British Columbia, V0P 1H0, Canada
- 63 26. CSIRO Environment, Castray Esplanade, Hobart, Tasmania 7004, Australia
- 64 27. Research Institute for Global Change, JAMSTEC, 3173-25 Showa-machi, Kanazawa, Yokohama, 236-0001,
- 65 Japan
- 66 28. Department of Geographical Sciences, University of Maryland, College Park, Maryland 20742, USA
- 67 29. Earth System Science Interdisciplinary Center, University of Maryland, College Park, MD 20740, USA
- 68 30. Centre National de Recherches Météorologiques, Université de Toulouse, Météo-France, CNRS UMR 3589,
- 69 Toulouse, France
- 70 31. School for Climate Studies, Stellenbosch University, Private Bag X1, Matieland, Stellenbosch, 7602, South
- 71 Africa
- 72 32. Southern Ocean Carbon – Climate Observatory, CSIR, Rosebank, Cape Town, 7700, South Africa
- 73 33. Department of Earth System Science, Tsinghua University, Beijing, China
- 74 34. Japan Meteorological Agency, 3-6-9 Toranomon, Minato City, Tokyo 105-8431, Japan
- 75 35. Columbia University and Lamont-Doherty Earth Observatory, New York, NY, USA



- 76 36. Climate and Global Dynamics Laboratory, National Center for Atmospheric Research, Boulder, CO 80305,  
77 USA
- 78 37. International Institute for Applied Systems Analysis (IIASA), Schlossplatz 1, A-2361 Laxenburg, Austria
- 79 38. European Commission, Joint Research Centre, 21027 Ispra (VA), Italy
- 80 39. Environmental Physics Group, ETH Zürich, Institute of Biogeochemistry and Pollutant Dynamics and  
81 Center for Climate Systems Modeling (C2SM), Zürich, Switzerland
- 82 40. NCAS-Climate, Climatic Research Unit, School of Environmental Sciences, University of East Anglia,  
83 Norwich Research Park, Norwich, NR4 7TJ, UK
- 84 41. Research Institute for Environment, Energy, and Economics, Appalachian State University, Boone, North  
85 Carolina, USA
- 86 42. Department of Geological and Environmental Sciences, Appalachian State University, Boone, North  
87 Carolina, USA
- 88 43. Potsdam Institute for Climate Impact Research (PIK), member of the Leibniz Association, P.O. Box 60 12  
89 03, 14412 Potsdam, Germany
- 90 44. Universität Hamburg, Bundesstraße 55, 20146 Hamburg, Germany
- 91 45. Cooperative Institute for Research in Environmental Sciences, CU Boulder and NOAA Global Monitoring  
92 Laboratory, Boulder, USA
- 93 46. Department of Climate, Meteorology and Atmospheric Sciences, University of Illinois, Urbana, IL 61821,  
94 USA
- 95 47. University of East Anglia, Norwich, UK
- 96 48. Jiangsu Provincial Key Laboratory of Geographic Information Science and Technology, International  
97 Institute for Earth System Science, Nanjing University, Nanjing, 210023, China
- 98 49. State Key Laboratory of Tibetan Plateau Earth System and Resource Environment, Institute of Tibetan  
99 Plateau Research, Chinese Academy of Sciences, Beijing 100101, China
- 100 50. Institute of Carbon Neutrality, Sino-French Institute for Earth System Science, College of Urban and  
101 Environmental Sciences, Peking University, Beijing 100871, China
- 102 51. Institute of Applied Energy (IAE), Minato-ku, Tokyo 105-0003, Japan
- 103 52. University of California, San Diego, Scripps Institution of Oceanography, La Jolla, CA 92093-0244, USA
- 104 53. Utrecht University, Faculty of Geosciences, Department IMEW, Copernicus Institute of Sustainable  
105 Development, Heidelberglaan 2, P.O. Box 80115, 3508 TC, Utrecht, the Netherlands
- 106 54. Hawkesbury Institute for the Environment, Western Sydney University, Penrith, New South Wales,  
107 Australia
- 108 55. NORCE Norwegian Research Centre, Jahnebakken 5, 5007 Bergen, Norway
- 109 56. LOCEAN/IPSL laboratory, Sorbonne Université, CNRS/IRD/MNHN, Paris, 75252, France
- 110 57. Jet Propulsion Laboratory, California Institute of Technology, Pasadena, CA, USA
- 111 58. California Institute of Technology, Pasadena, CA, USA
- 112 59. Earth System Division, National Institute for Environmental Studies, 16-2 Onogawa, Tsukuba, Ibaraki, 305-  
113 8506 Japan
- 114 60. Sorbonne Université, Laboratoire d'Océanographie de Villefranche, Villefranche-sur-Mer, France



- 115 61. Department of Meteorology & National Centre for Atmospheric Science (NCAS), University of Reading,  
116 Reading, UK
- 117 62. University of Alaska Fairbanks, College of Fisheries and Ocean Sciences, Fairbanks, AK, 99709, USA
- 118 63. Fisheries Research and Education Agency, 2-12-4 Fukuura, Kanazawa-Ku, Yokohama 236-8648, Japan
- 119 64. National Centre for Earth Observation, University of Edinburgh, EH9 3FF, UK
- 120 65. School of GeoSciences, University of Edinburgh, EH9 3FF, UK
- 121 66. NOAA Atlantic Oceanographic and Meteorological Laboratory (NOAA/AOML), 4301 Rickenbacker  
122 Causeway, Miami, Florida 33149, USA
- 123 67. School of Atmospheric Sciences, Sun Yat-sen University, Zhuhai 519000, China
- 124 68. Princeton University, Department of Geosciences and Princeton Environmental Institute, Princeton, NJ,  
125 USA
- 126 69. Max Planck Institute for Biogeochemistry, P.O. Box 600164, Hans-Knöll-Str. 10, 07745 Jena, Germany
- 127 70. Smith School of Enterprise and the Environment, University of Oxford, Oxford, UK
- 128 71. Canadian Centre for Climate Modelling and Analysis, Environment and Climate Change Canada, Victoria,  
129 British Columbia, Canada
- 130 72. GEOMAR Helmholtz Centre for Ocean Research Kiel, Wischhofstr. 1-3, 24148 Kiel, Germany
- 131 73. Institute for Climate and Environmental Physics, Bern, Switzerland
- 132 74. Research Center for Environmental Modeling and Application, Japan Agency for Marine-Earth Science and  
133 Technology, Yokohama, Japan
- 134 75. Advanced Institute for Marine Ecosystem Change, Japan Agency for Marine-Earth Science and Technology,  
135 Yokohama, Japan
- 136 76. Schiller Institute of Integrated Science and Society, Department of Earth and Environmental Sciences,  
137 Boston College, Chestnut Hill, MA 02467, USA
- 138 77. Australian Antarctic Partnership Program, University of Tasmania, Hobart, Australia
- 139 78. Barcelona Supercomputing Center, Barcelona, Spain
- 140 79. JMA Meteorological Research Institute, Tsukuba, Ibaraki, Japan
- 141 80. Statistics Division, Food and Agriculture Organization of the United Nations, Via Terme di Caracalla, Rome  
142 00153, Italy
- 143 81. Institute of Atmospheric Physics, Chinese Academy of Sciences, Beijing, China
- 144 82. Climate Change Science Institute and Environmental Sciences Division, Oak Ridge National Lab, Oak  
145 Ridge, TN 37831, USA.
- 146 83. School of Ecology and Applied Meteorology, Nanjing University of Information Science and Technology,  
147 Nanjing 210044, PR. China
- 148 84. Institute of Carbon Neutrality, College of Urban and Environmental Sciences, Peking University, Beijing  
149 100091, China
- 150 85. School of Environmental Science and Engineering, Nanjing University of Information Science and  
151 Technology (NUIST), Nanjing, 210044, China
- 152 86. Department of Atmospheric and Oceanic Science, University of Maryland, Maryland, USA
- 153



154

155

156 *Correspondence to:* Pierre Friedlingstein (p.friedlingstein@exeter.ac.uk)

157 **1. Abstract**

158 Accurate assessment of anthropogenic carbon dioxide (CO<sub>2</sub>) emissions and their redistribution among the  
159 atmosphere, ocean, and terrestrial biosphere in a changing climate is critical to better understand the global  
160 carbon cycle, support the development of climate policies, and project future climate change. Here we describe  
161 and synthesise datasets and methodologies to quantify the five major components of the global carbon budget  
162 and their uncertainties. Fossil CO<sub>2</sub> emissions (E<sub>FOS</sub>) are based on energy statistics and cement production data,  
163 while emissions from land-use change (E<sub>LUC</sub>) are based on land-use and land-use change data and bookkeeping  
164 models. Atmospheric CO<sub>2</sub> concentration is measured directly, and its growth rate (G<sub>ATM</sub>) is computed from the  
165 annual changes in concentration. The ocean CO<sub>2</sub> sink (S<sub>OCEAN</sub>) is estimated with global ocean biogeochemistry  
166 models and observation-based  $f$ CO<sub>2</sub>-products. The terrestrial CO<sub>2</sub> sink (S<sub>LAND</sub>) is estimated with dynamic  
167 global vegetation models. Additional lines of evidence on land and ocean sinks are provided by atmospheric  
168 inversions, atmospheric oxygen measurements and Earth System Models. The sum of all sources and sinks  
169 results in the carbon budget imbalance (B<sub>IM</sub>), a measure of imperfect data and incomplete understanding of the  
170 contemporary carbon cycle. All uncertainties are reported as  $\pm 1\sigma$ .

171 For the year 2023, E<sub>FOS</sub> increased by 1.3% relative to 2022, with fossil emissions at  $10.1 \pm 0.5$  GtC yr<sup>-1</sup> ( $10.3 \pm$   
172  $0.5$  GtC yr<sup>-1</sup> when the cement carbonation sink is not included), E<sub>LUC</sub> was  $1.0 \pm 0.7$  GtC yr<sup>-1</sup>, for a total  
173 anthropogenic CO<sub>2</sub> emission (including the cement carbonation sink) of  $11.1 \pm 0.9$  GtC yr<sup>-1</sup> ( $40.6 \pm 3.2$  GtCO<sub>2</sub>  
174 yr<sup>-1</sup>). Also, for 2023, G<sub>ATM</sub> was  $5.9 \pm 0.2$  GtC yr<sup>-1</sup> ( $2.79 \pm 0.1$  ppm yr<sup>-1</sup>), S<sub>OCEAN</sub> was  $2.9 \pm 0.4$  GtC yr<sup>-1</sup> and  
175 S<sub>LAND</sub> was  $2.3 \pm 1.0$  GtC yr<sup>-1</sup>, with a near zero B<sub>IM</sub> ( $-0.02$  GtC yr<sup>-1</sup>). The global atmospheric CO<sub>2</sub> concentration  
176 averaged over 2023 reached  $419.3 \pm 0.1$  ppm. Preliminary data for 2024, suggest an increase in E<sub>FOS</sub> relative to  
177 2023 of +0.8% (-0.3% to 1.9%) globally, and atmospheric CO<sub>2</sub> concentration increased by 2.8 ppm reaching  
178 422.5 ppm, 52% above pre-industrial level (around 278 ppm in 1750). Overall, the mean and trend in the  
179 components of the global carbon budget are consistently estimated over the period 1959-2023, with a near-zero  
180 overall budget imbalance, although discrepancies of up to around 1 GtC yr<sup>-1</sup> persist for the representation of  
181 annual to semi-decadal variability in CO<sub>2</sub> fluxes. Comparison of estimates from multiple approaches and  
182 observations shows: (1) a persistent large uncertainty in the estimate of land-use changes emissions, (2) a low  
183 agreement between the different methods on the magnitude of the land CO<sub>2</sub> flux in the northern extra-tropics,  
184 and (3) a discrepancy between the different methods on the mean ocean sink.

185 This living data update documents changes in methods and datasets applied to this most-recent global carbon  
186 budget as well as evolving community understanding of the global carbon cycle. The data presented in this  
187 work are available at <https://doi.org/10.18160/GCP-2024> (Friedlingstein et al., 2024).



188 **2. Executive Summary**

189 **Global fossil CO<sub>2</sub> emissions (including cement carbonation) are expected to further increase in 2024 by**  
190 **0.8%.** The 2023 emission increase was 0.14 GtC yr<sup>-1</sup> (0.5 GtCO<sub>2</sub> yr<sup>-1</sup>) relative to 2022, bringing 2023 fossil CO<sub>2</sub>  
191 emissions to 10.1 ± 0.5 GtC yr<sup>-1</sup> (36.8 ± 1.8 GtCO<sub>2</sub> yr<sup>-1</sup>). Preliminary estimates based on data available suggest  
192 fossil CO<sub>2</sub> emissions to increase further in 2024, by 0.8% relative to 2023 (-0.3% to 1.9%), bringing emissions  
193 to 10.2 GtC yr<sup>-1</sup> (37.4 GtCO<sub>2</sub> yr<sup>-1</sup>).<sup>1</sup>

194 Emissions from coal, oil and gas in 2024 are expected to be slightly above their 2023 levels (by 0.2%, 0.9% and  
195 2.4% respectively). Regionally, fossil emissions in 2024 are expected to decrease by 3.8% in the European  
196 Union reaching 0.7 GtC (2.4 GtCO<sub>2</sub>), and by 0.6% in the United States (1.3 GtC, 4.9 GtCO<sub>2</sub>). Emissions in  
197 China are expected to increase in 2024 by 0.2%, reaching 3.3 GtC, (12.0 GtCO<sub>2</sub>). Fossil emissions are also  
198 expected to increase by 4.6% in India (0.9 GtC, 3.2 GtCO<sub>2</sub>) and by 1.1% for the rest of the world (4.0 GtC, 14.5  
199 GtCO<sub>2</sub>) in 2024. Emissions from international aviation and shipping (IAS) are also expected to increase by 7.8%  
200 (0.3 GtC, 1.2 GtCO<sub>2</sub>) in 2024.

201 **Fossil CO<sub>2</sub> emissions decreased significantly in 22 countries with significantly growing economies during**  
202 **the decade 2014-2023.** Altogether, these 22 countries contribute about 2.2 GtC yr<sup>-1</sup> (8.1 GtCO<sub>2</sub>) fossil fuel CO<sub>2</sub>  
203 emissions over the last decade, representing about 23% of world CO<sub>2</sub> fossil emissions.

204 **Global CO<sub>2</sub> emissions from land-use, land-use change, and forestry (LULUCF) averaged 1.1 ± 0.7 GtC yr<sup>-1</sup>**  
205 **(4.1 ± 2.6 GtCO<sub>2</sub> yr<sup>-1</sup>) for the 2014-2023 period with a similar preliminary projection for 2024 of 1.1 ±**  
206 **0.7 GtC yr<sup>-1</sup> (4.2 ± 2.6 GtCO<sub>2</sub> yr<sup>-1</sup>).** Since the late-1990s, emissions from LULUCF show a statistically  
207 **significant decrease at a rate of around 0.2 GtC per decade.** Emissions from deforestation, the main driver of  
208 global gross sources, remain high at around 1.7 GtC yr<sup>-1</sup> over the 2014-2023 period, highlighting the strong  
209 potential of halting deforestation for emissions reductions. Sequestration of 1.2 GtC yr<sup>-1</sup> through re-  
210 /afforestation and forestry offsets two third of the deforestation emissions. Further, smaller emissions are due to  
211 other land-use transitions and peat drainage and peat fire. The highest emitters during 2014-2023 in descending  
212 order were Brazil, Indonesia, and the Democratic Republic of the Congo, with these 3 countries contributing  
213 more than half of global land-use CO<sub>2</sub> emissions.

214 **Total anthropogenic emissions (fossil and LULUCF, including the carbonation sink) were 11.1 GtC yr<sup>-1</sup>**  
215 **(40.6 GtCO<sub>2</sub> yr<sup>-1</sup>) in 2023, with a marginally higher preliminary estimate of 11.3 GtC yr<sup>-1</sup> (41.6 GtCO<sub>2</sub> yr<sup>-1</sup>)**  
216 **for 2024. Total anthropogenic emissions have been stable over the last decade (zero growth rate over**  
217 **the 2014-2023 period), much slower than over the previous decade (2004-2013) with an average growth**  
218 **rate of 2.0% yr<sup>-1</sup>.**

219 **The remaining carbon budget for a 50% likelihood to limit global warming to 1.5°C, 1.7°C and 2°C above**  
220 **the 1850-1900 level has respectively been reduced to 65 GtC (235 GtCO<sub>2</sub>), 160 GtC (585 GtCO<sub>2</sub>) and 305**

---

<sup>1</sup> All 2024 growth rates use a leap year adjustment that corrects for the extra day in 2024.



221 **GtC (1110 GtCO<sub>2</sub>) from the beginning of 2025, equivalent to around 6, 14 and 27 years, assuming 2024**  
222 **emissions levels.**

223 **The concentration of CO<sub>2</sub> in the atmosphere is set to reach 422.5 ppm in 2024, 52% above pre-industrial**  
224 **levels.** The atmospheric CO<sub>2</sub> growth was  $5.2 \pm 0.02$  GtC yr<sup>-1</sup> (2.5 ppm) during the decade 2014-2023 (48% of  
225 total CO<sub>2</sub> emissions) with a preliminary 2024 growth rate estimate of around 5.9 GtC (2.8 ppm).

226 **The ocean CO<sub>2</sub> sink has been stagnant since 2016 after rapid growth during 2002-2016, largely in**  
227 **response to large inter-annual climate variability.** The ocean CO<sub>2</sub> sink was  $2.9 \pm 0.4$  GtC yr<sup>-1</sup> during the  
228 decade 2014-2023 (26% of total CO<sub>2</sub> emissions). A slightly higher value of 3.0 GtC yr<sup>-1</sup> is preliminarily  
229 estimated for 2024, which marks an increase in the sink since 2023 due to the prevailing El Niño and neutral  
230 conditions in 2024.

231 **The land CO<sub>2</sub> sink continued to increase during the 2014-2023 period primarily in response to increased**  
232 **atmospheric CO<sub>2</sub>, albeit with large interannual variability.** The land CO<sub>2</sub> sink was  $3.2 \pm 0.9$  GtC yr<sup>-1</sup> during  
233 the 2014-2023 decade (30% of total CO<sub>2</sub> emissions). The land sink in 2023 was  $2.3 \pm 1$  GtC yr<sup>-1</sup>, 1.6 GtC lower  
234 than in 2022, and the lowest estimate since 2015. This reduced sink is primarily driven by a response of tropical  
235 land ecosystems to the onset of the 2023-2024 El Niño event, combined with large wildfires in Canada in 2023.  
236 The preliminary 2024 estimate is around 3.2 GtC yr<sup>-1</sup>, similar to the decadal average, consistent with a land sink  
237 emerging from the El Niño state.

238 **So far in 2024, global fire CO<sub>2</sub> emissions have been 11-32% higher than the 2014-2023 average due to**  
239 **high fire activity in both North and South America, reaching 1.6-2.2 GtC during January-September.** In  
240 Canada, emissions through September were 0.2-0.3 GtC yr<sup>-1</sup>, down from 0.5-0.8 GtC yr<sup>-1</sup> in 2023 but still more  
241 than twice the 2014-2023 average. In Brazil, fires through September emitted 0.2-0.3 GtC yr<sup>-1</sup>, 91-118% above  
242 the 2014-2023 average due to intense drought. These fire emissions estimates should not be directly compared  
243 with the land use emissions or the land sink, because they represent a gross carbon flux to the atmosphere and  
244 do not account for post-fire recovery or distinguish between natural, climate-driven, and land-use-related fires.

245



246

## 247 **1 Introduction**

248 The concentration of carbon dioxide (CO<sub>2</sub>) in the atmosphere has increased from approximately 278 parts per  
249 million (ppm) in 1750 (Gulev et al., 2021), the beginning of the Industrial Era, to  $419.3 \pm 0.1$  ppm in 2023 (Lan  
250 et al., 2024; Figure 1). The atmospheric CO<sub>2</sub> increase above pre-industrial levels was, initially, primarily caused  
251 by the release of carbon to the atmosphere from deforestation and other land-use change activities (Canadell et  
252 al., 2021). While emissions from fossil fuels started before the Industrial Era, they became the dominant source  
253 of anthropogenic emissions to the atmosphere from around 1950 and their relative share has continued to  
254 increase until present. Anthropogenic emissions occur on top of an active natural carbon cycle that circulates  
255 carbon between the reservoirs of the atmosphere, ocean, and terrestrial biosphere on time scales from sub-daily  
256 to millennial, while exchanges with geologic reservoirs occur on longer timescales (Archer et al., 2009).

257 The global carbon budget (GCB) presented here refers to the mean, variations, and trends in the perturbation of  
258 CO<sub>2</sub> in the environment, referenced to the beginning of the Industrial Era (defined here as 1750). This paper  
259 describes the components of the global carbon cycle over the historical period with a stronger focus on the  
260 recent period (since 1958, onset of robust atmospheric CO<sub>2</sub> measurements), the last decade (2014-2023), the last  
261 year (2023) and the current year (2024). Finally, it provides cumulative emissions from fossil fuels and land-use  
262 change since the year 1750, and since the year 1850 (the reference year for historical simulations in IPCC AR6)  
263 (Eyring et al., 2016).

264 We quantify the input of CO<sub>2</sub> to the atmosphere by emissions from human activities, the growth rate of  
265 atmospheric CO<sub>2</sub> concentration, and the resulting changes in the storage of carbon in the land and ocean  
266 reservoirs in response to increasing atmospheric CO<sub>2</sub> levels, climate change and variability, and other  
267 anthropogenic and natural changes (Figure 2). An understanding of this perturbation budget over time and the  
268 underlying variability and trends of the natural carbon cycle is necessary to understand the response of natural  
269 sinks to changes in climate, CO<sub>2</sub> and land-use change drivers, and to quantify emissions compatible with a given  
270 climate stabilisation target.

271 The components of the CO<sub>2</sub> budget that are reported annually in this paper include separate and independent  
272 estimates for the CO<sub>2</sub> emissions from (1) fossil fuel combustion and oxidation from all energy and industrial  
273 processes; also including cement production and carbonation ( $E_{FOS}$ ; GtC yr<sup>-1</sup>) and (2) the emissions resulting  
274 from deliberate human activities on land, including those leading to land-use change ( $E_{LUC}$ ; GtC yr<sup>-1</sup>); and their  
275 partitioning among (3) the growth rate of atmospheric CO<sub>2</sub> concentration ( $G_{ATM}$ ; GtC yr<sup>-1</sup>), and the uptake of  
276 CO<sub>2</sub> (the ‘CO<sub>2</sub> sinks’) in (4) the ocean ( $S_{OCEAN}$ ; GtC yr<sup>-1</sup>) and (5) on land ( $S_{LAND}$ ; GtC yr<sup>-1</sup>). The CO<sub>2</sub> sinks as  
277 defined here conceptually include the response of the land (including inland waters and estuaries) and ocean  
278 (including coastal and marginal seas) to elevated CO<sub>2</sub> and changes in climate and other environmental  
279 conditions, although in practice not all processes are fully accounted for (see Section 2.10). Global emissions  
280 and their partitioning among the atmosphere, ocean and land are in balance in the real world. Due to the  
281 combination of imperfect spatial and/or temporal data coverage, errors in each estimate, and smaller terms not





282 included in our budget estimate (discussed in Section 2.10), the independent estimates (1) to (5) above do not  
283 necessarily add up to zero. We hence estimate a budget imbalance ( $B_{IM}$ ), which is a measure of the mismatch  
284 between the estimated emissions and the estimated changes in the atmosphere, land and ocean, as follows:

$$285 \quad B_{IM} = E_{FOS} + E_{LUC} - (G_{ATM} + S_{OCEAN} + S_{LAND}) \quad (1)$$

286  $G_{ATM}$  is usually reported in  $\text{ppm yr}^{-1}$ , which we convert to units of carbon mass per year,  $\text{GtC yr}^{-1}$ , using  $1 \text{ ppm}$   
287  $= 2.124 \text{ GtC}$  (Ballantyne et al., 2012; Table 1). Units of gigatonnes of  $\text{CO}_2$  (or billion tonnes of  $\text{CO}_2$ ) used in  
288 policy are equal to 3.664 multiplied by the value in units of  $\text{GtC}$ .

289 We also assess a set of additional lines of evidence derived from global atmospheric inversion system results  
290 (Section 2.7), observed changes in oxygen concentration (Section 2.8) and Earth System Models (ESMs)  
291 simulations (Section 2.9), all of these methods closing the global carbon balance (zero  $B_{IM}$ ).

292 We further quantify  $E_{FOS}$  and  $E_{LUC}$  by country, including both territorial and consumption-based accounting for  
293  $E_{FOS}$  (see Section 2), and discuss missing terms from sources other than the combustion of fossil fuels (see  
294 Section 2.10, Supplement S1 and S2). We also assess carbon dioxide removal (CDR) (see Sect. 2.2 and 2.3).  
295 Land-based CDR is significant, but already accounted for in  $E_{LUC}$  in equation (1) (Sect 3.2.2). Other CDR  
296 methods, not based on vegetation, are currently several orders of magnitude smaller than the other components  
297 of the budget (Sect. 3.3), hence these are not included in equation (1), or in the global carbon budget tables or  
298 figures (with the exception of Figure 2 where CDR is shown primarily for illustrative purpose).

299 The global  $\text{CO}_2$  budget has been assessed by the Intergovernmental Panel on Climate Change (IPCC) in all  
300 assessment reports (Prentice et al., 2001; Schimel et al., 1995; Watson et al., 1990; Denman et al., 2007; Ciais et  
301 al., 2013; Canadell et al., 2021), and by others (e.g. Ballantyne et al., 2012). The Global Carbon Project (GCP,  
302 www.globalcarbonproject.org, last access: 28 October 2024) has coordinated this cooperative community effort  
303 for the annual publication of global carbon budgets for the year 2005 (Raupach et al., 2007; including fossil  
304 emissions only), year 2006 (Canadell et al., 2007), year 2007 (GCP, 2008), year 2008 (Le Quéré et al., 2009),  
305 year 2009 (Friedlingstein et al., 2010), year 2010 (Peters et al., 2012a), year 2012 (Le Quéré et al., 2013; Peters  
306 et al., 2013), year 2013 (Le Quéré et al., 2014), year 2014 (Le Quéré et al., 2015a; Friedlingstein et al., 2014),  
307 year 2015 (Jackson et al., 2016; Le Quéré et al., 2015b), year 2016 (Le Quéré et al., 2016), year 2017 (Le Quéré  
308 et al., 2018a; Peters et al., 2017a), year 2018 (Le Quéré et al., 2018b; Jackson et al., 2018), year 2019  
309 (Friedlingstein et al., 2019; Jackson et al., 2019; Peters et al., 2020), year 2020 (Friedlingstein et al., 2020; Le  
310 Quéré et al., 2021), year 2021 (Friedlingstein et al., 2022a; Jackson et al., 2022), year 2022 (Friedlingstein et al.,  
311 2022b), and most recently the year 2023 (Friedlingstein et al., 2023). Each of these papers updated previous  
312 estimates with the latest available information for the entire time series.

313 We adopt a range of  $\pm 1$  standard deviation ( $\sigma$ ) to report the uncertainties in our global estimates, representing a  
314 likelihood of 68% that the true value will be within the provided range if the errors have a gaussian distribution,  
315 and no bias is assumed. This choice reflects the difficulty of characterising the uncertainty in the  $\text{CO}_2$  fluxes  
316 between the atmosphere and the ocean and land reservoirs individually, particularly on an annual basis, as well



317 as the difficulty of updating the CO<sub>2</sub> emissions from land-use change. A likelihood of 68% provides an  
318 indication of our current capability to quantify each term and its uncertainty given the available information.  
319 The uncertainties reported here combine statistical analysis of the underlying data, assessments of uncertainties  
320 in the generation of the datasets, and expert judgement of the likelihood of results lying outside this range. The  
321 limitations of current information are discussed in the paper and have been examined in detail elsewhere  
322 (Ballantyne et al., 2015; Zscheischler et al., 2017). We also use a qualitative assessment of confidence level to  
323 characterise the annual estimates from each term based on the type, amount, quality, and consistency of the  
324 different lines of evidence as defined by the IPCC (Stocker et al., 2013).

325 This paper provides a detailed description of the datasets and methodology used to compute the global carbon  
326 budget estimates for the industrial period, from 1750 to 2024, and in more detail for the period since 1959. This  
327 paper is updated every year using the format of ‘living data’ to keep a record of budget versions and the changes  
328 in new data, revision of data, and changes in methodology that lead to changes in estimates of the carbon  
329 budget. Additional materials associated with the release of each new version will be posted at the Global Carbon  
330 Project (GCP) website (<http://www.globalcarbonproject.org/carbonbudget>, last access: 28 October 2024), with  
331 fossil fuel emissions also available through the Global Carbon Atlas (<http://www.globalcarbonatlas.org>, last  
332 access: 28 October 2024). All underlying data used to produce the budget can also be found at  
333 <https://globalcarbonbudget.org/> (last access: 28 October 2024). With this approach, we aim to provide the  
334 highest transparency and traceability in the reporting of CO<sub>2</sub>, the key driver of climate change.

## 335 **2 Methods**

336 Multiple organisations and research groups around the world generated the original measurements and data used  
337 to complete the global carbon budget. The effort presented here is thus mainly one of synthesis, where results  
338 from individual groups are collated, analysed, and evaluated for consistency. We facilitate access to original  
339 data with the understanding that primary datasets will be referenced in future work (see Table 2 for how to cite  
340 the datasets, and Section on data availability). Descriptions of the measurements, models, and methodologies  
341 follow below, with more detailed descriptions of each component provided as Supplementary Information (S1 to  
342 S5).

343 This is the 19<sup>th</sup> version of the global carbon budget and the 13<sup>th</sup> revised version in the format of a living data  
344 update in Earth System Science Data. It builds on the latest published global carbon budget of Friedlingstein et  
345 al. (2023). The main changes this year are: the inclusion of (1) data to year 2023 and a projection for the global  
346 carbon budget for year 2024; and (2) an estimate of the 2024 projection of fossil emissions from Carbon  
347 Monitor. Other methodological differences between recent annual carbon budgets (2020 to 2024) are  
348 summarised in Table 3 and previous changes since 2006 are provided in Table S9.



349 **2.1 Fossil CO<sub>2</sub> emissions (E<sub>FOS</sub>)**

350 **2.1.1 Historical period 1850-2023**

351 The estimates of global and national fossil CO<sub>2</sub> emissions (E<sub>FOS</sub>) include the oxidation of fossil fuels through  
352 both combustion (e.g., transport, heating) and chemical oxidation (e.g. carbon anode decomposition in  
353 aluminium refining) activities, and the decomposition of carbonates in industrial processes (e.g. the production  
354 of cement). We also include CO<sub>2</sub> uptake from the cement carbonation process. Several emissions sources are not  
355 estimated or not fully covered: coverage of emissions from lime production are not global, and decomposition of  
356 carbonates in glass and ceramic production are included only for the “Annex 1” countries of the United Nations  
357 Framework Convention on Climate Change (UNFCCC) for lack of activity data. These omissions are  
358 considered to be minor. Short-cycle carbon emissions - for example from combustion of biomass - are not  
359 included here but are accounted for in the CO<sub>2</sub> emissions from land use (see Section 2.2).

360 Our estimates of fossil CO<sub>2</sub> emissions rely on data collection by many other parties. Our goal is to produce the  
361 best estimate of this flux, and we therefore use a prioritisation framework to combine data from different  
362 sources that have used different methods, while being careful to avoid double counting and undercounting of  
363 emissions sources. The CDIAC-FF emissions dataset, derived largely from UN energy data, forms the  
364 foundation, and we extend emissions to 2023 using energy growth rates reported by the Energy Institute (a  
365 dataset formerly produced by BP). We then proceed to replace estimates using data from what we consider to be  
366 superior sources, for example Annex 1 countries’ official submissions to the UNFCCC. All data points are  
367 potentially subject to revision, not just the latest year. For full details see Andrew and Peters (2024).

368 Other estimates of global fossil CO<sub>2</sub> emissions exist, and these are compared by Andrew (2020a). The most  
369 common reason for differences in estimates of global fossil CO<sub>2</sub> emissions is a difference in which emissions  
370 sources are included in the datasets. Datasets such as those published by the Energy Institute, the US Energy  
371 Information Administration, and the International Energy Agency’s ‘CO<sub>2</sub> emissions from fuel combustion’ are  
372 all generally limited to emissions from combustion of fossil fuels. In contrast, datasets such as PRIMAP-hist,  
373 CEDS, EDGAR, and GCP’s dataset aim to include all sources of fossil CO<sub>2</sub> emissions. See Andrew (2020a) for  
374 detailed comparisons and discussion.

375 Cement absorbs CO<sub>2</sub> from the atmosphere over its lifetime, a process known as ‘cement carbonation’. We  
376 estimate this CO<sub>2</sub> sink, from 1931 onwards, as the average of two studies in the literature (Cao et al., 2020; Guo  
377 et al., 2021). Both studies use the same model, developed by Xi et al. (2016), with different parameterisations  
378 and input data, with the estimate of Guo and colleagues being a revision of Xi et al. (2016). The trends of the  
379 two studies are very similar. Since carbonation is a function of both current and previous cement production, we  
380 extend these estimates to 2023 by using the growth rate derived from the smoothed cement emissions (10-year  
381 smoothing) fitted to the carbonation data. In the present budget, we always include the cement carbonation  
382 carbon sink in the fossil CO<sub>2</sub> emission component (E<sub>FOS</sub>).



383 We use the Kaya Identity for a simple decomposition of CO<sub>2</sub> emissions into the key drivers (Raupach et al.,  
384 2007). While there are variations (Peters et al., 2017a), we focus here on a decomposition of CO<sub>2</sub> emissions into  
385 population, GDP per person, energy use per GDP, and CO<sub>2</sub> emissions per energy. Multiplying these individual  
386 components together returns the CO<sub>2</sub> emissions. Using the decomposition, it is possible to attribute the change  
387 in CO<sub>2</sub> emissions to the change in each of the drivers. This method gives a first-order understanding of what  
388 causes CO<sub>2</sub> emissions to change each year.

### 389 **2.1.2 2024 projection**

390 We provide a projection of global fossil CO<sub>2</sub> emissions in 2024 by combining separate projections for China,  
391 USA, EU, India, and for all other countries combined. The methods are different for each of these. For China we  
392 combine monthly fossil fuel production data from the National Bureau of Statistics and trade data from the  
393 Customs Administration, giving us partial data for the growth rates to date of natural gas, petroleum, and  
394 cement, and of the apparent consumption itself for raw coal. We then use a regression model to project full-year  
395 emissions based on historical observations. For the USA our projection is taken directly from the Energy  
396 Information Administration's (EIA) Short-Term Energy Outlook (EIA, 2024), combined with the year-to-date  
397 growth rate of cement clinker production. For the EU we use monthly energy data from Eurostat to derive  
398 estimates of monthly CO<sub>2</sub> emissions through July, with coal emissions extended through September using a  
399 statistical relationship with reported electricity generation from coal and other factors. For natural gas we use  
400 Holt-Winters to project the last four months of the year. EU emissions from oil are derived using the EIA's  
401 projection of oil consumption for Europe. EU cement emissions are based on available year-to-date data from  
402 three of the largest producers, Germany, Poland, and Spain. India's projected emissions are derived from  
403 estimates through August (July for coal) using the methods of Andrew (2020b) and extrapolated assuming  
404 seasonal patterns from before 2019. Emissions from international transportation (bunkers) are estimated  
405 separately for aviation and shipping. Changes in aviation emissions are derived primarily from OECD monthly  
406 estimates, extrapolated using the growth rates of global flight miles from Airportia, and then the final months  
407 are projected assuming normal patterns from previous years. Changes in shipping emissions are derived from  
408 OECD monthly estimates for global shipping. Emissions for the rest of the world are derived for coal and  
409 cement using projected growth in economic production from the IMF (2023) combined with extrapolated  
410 changes in emissions intensity of economic production; for oil using a global constraint from EIA; and for  
411 natural gas using a global constraint from IEA. More details on the E<sub>FOS</sub> methodology and its 2024 projection  
412 can be found in Supplement S.1.

413 For the first time this year, we cross check our 2024 projection with a 2024 projection from Carbon Monitor.  
414 Carbon Monitor is an open access dataset (<https://carbonmonitor.org/>) of daily emissions constructed using  
415 hourly to daily proxy data (e.g., electricity consumption, travel patterns, etc) instead of energy use data.  
416 Available Carbon Monitor estimated emissions from January to August are combined to a new projection for  
417 September to December to give a full year 2024 estimate. The September to December projections are estimated  
418 by leveraging seasonal patterns from 2019-2023 daily CO<sub>2</sub> emission data from Carbon Monitor. A regression  
419 model is applied separately for individual countries to obtain their respective 4-month forecast. First, the



420 seasonality component for each month is assessed based on daily average emissions from 2019 to 2023,  
421 excluding 2020 due to the COVID-19 pandemic. Then, a linear regression model is constructed using the  
422 calculated seasonal components and the daily average emissions for the months from January to August 2024.  
423 The resulting model is used to project carbon emissions for the remaining months of 2024. The uncertainty  
424 range is calculated by using historical monthly variance of seasonal components.

## 425 **2.2 CO<sub>2</sub> emissions from land-use, land-use change and forestry (E<sub>LUC</sub>)**

### 426 **2.2.1 Historical period 1850-2023**

427 The net CO<sub>2</sub> flux from land-use, land-use change and forestry (E<sub>LUC</sub>, called land-use change emissions in the  
428 rest of the text) includes CO<sub>2</sub> fluxes from deforestation, afforestation, logging and forest degradation (including  
429 harvest activity), shifting cultivation (cycle of cutting forest for agriculture, then abandoning), regrowth of  
430 forests (following wood harvest or agriculture abandonment), peat burning, and peat drainage.

431 Four bookkeeping approaches (updated estimates each of BLUE (Hansis et al., 2015), OSCAR (Gasser et al.,  
432 2020), and H&C2023 (Houghton and Castanho, 2023), and new estimates of LUCE (Qin et al. 2024) were used  
433 to quantify gross emissions and gross removals and the resulting net E<sub>LUC</sub>. Emissions from peat burning and peat  
434 drainage are added from external datasets, peat drainage being averaged from three spatially explicit  
435 independent datasets (see Supplement S.2.1). Uncertainty estimates were derived from the Dynamic Global  
436 Vegetation Models (DGVMs) ensemble for the time period prior to 1960, and using for the recent decades an  
437 uncertainty range of  $\pm 0.7$  GtC yr<sup>-1</sup>, which is a semi-quantitative measure for annual and decadal emissions and  
438 reflects our best value judgement that there is at least 68% chance ( $\pm 1\sigma$ ) that the true land-use change emission  
439 lies within the given range, for the range of processes considered here.

440 The GCB E<sub>LUC</sub> estimates follow the CO<sub>2</sub> flux definition of global carbon cycle models and differ from IPCC  
441 definitions adopted in National GHG Inventories (NGHGI) for reporting under the UNFCCC. The latter  
442 typically include terrestrial fluxes occurring on all land that countries define as managed, following the IPCC  
443 managed land proxy approach (Grassi et al., 2018). This partly includes fluxes due to environmental change  
444 (e.g. atmospheric CO<sub>2</sub> increase), which are part of S<sub>LAND</sub> in our definition. As a result, global emission estimates  
445 are smaller for NGHGI than for the global carbon budget definition (Grassi et al., 2023). The same is the case  
446 for the Food Agriculture Organization (FAO) estimates of carbon fluxes on forest land, which include both  
447 anthropogenic and natural fluxes on managed land (Tubiello et al., 2021). We translate the GCB and NGHGI  
448 definitions to each other, to provide a comparison of the anthropogenic carbon budget as reported in GCB to the  
449 official country reporting to the UNFCCC convention. We further compare these estimates with the net  
450 atmosphere-to-land flux from atmospheric inversion systems (see Section 2.7), averaged over managed land  
451 only.

452 E<sub>LUC</sub> contains a range of fluxes that are related to Carbon Dioxide Removal (CDR). CDR is defined as the set of  
453 anthropogenic activities that remove CO<sub>2</sub> from the atmosphere, additional to the Earth's natural processes, and  
454 store it in durable form, such as in forest biomass and soils, long-lived products, or in geological or ocean



455 reservoirs. Here, we quantify vegetation-based CDR that is implicitly or explicitly captured by land-use fluxes  
456 (CDR not based on vegetation is discussed in Section 2.3; IPCC, 2023). We quantify re/afforestation from the  
457 four bookkeeping estimates by separating forest regrowth in shifting cultivation cycles from permanent  
458 increases in forest cover (see Supplement S.2.1). The latter count as CDR, but it should be noted that the  
459 permanence of the storage under climate risks such as fire is increasingly questioned. Other CDR activities  
460 contained in  $E_{LUC}$  include the transfer of carbon to harvested wood products (HWP), bioenergy with carbon  
461 capture and storage (BECCS); and biochar production. Note that the different bookkeeping models represent  
462 HWP with varying details concerning product usage and their lifetimes. Bookkeeping and TRENDY models  
463 currently only represent BECCS and biochar with regard to the  $CO_2$  removal through photosynthesis, but do not  
464 account for the durable storage. HWP, BECCS, and biochar are typically counted as CDR when the transfer to  
465 the durable storage site occurs and not when the  $CO_2$  is removed from the atmosphere, which complicates a  
466 direct comparison to the GCB approach to quantify annual fluxes to and from the atmosphere. Estimates for  
467 CDR through HWP, BECCS, and biochar are thus not indicated in this budget, but can be found elsewhere (see  
468 Section 3.2.2).

#### 469 **2.2.2 2024 Projection**

470 We project the 2024 land-use emissions for BLUE, H&C2023, OSCAR, and LUCE based on their  $E_{LUC}$   
471 estimates for 2023 and adding the change in carbon emissions from peat fires and tropical deforestation and  
472 degradation fires (2024 emissions relative to 2023 emissions) estimated using active fire data (MCD14ML;  
473 Giglio et al., 2016). Peat drainage is assumed to be unaltered as it has low interannual variability. More details  
474 on the  $E_{LUC}$  methodology can be found in Supplement S.2.

#### 475 **2.3 Carbon Dioxide Removal (CDR) not based on vegetation**

476 While some CDR involves  $CO_2$  fluxes via land-use and is included in  $E_{LUC}$ , (such as afforestation, biochar,  
477 HWP, and BECCS) other CDR occurs through fluxes of  $CO_2$  directly from the air to the geosphere. The  
478 majority of this derives from enhanced weathering through the application of crushed rock to soils, with a  
479 smaller contribution from Direct Air Carbon Capture and Storage (DACCS). We use data from the State of  
480 CDR Report (Smith et al., 2024), which compiles and harmonises reported removal rates from a combination of  
481 existing databases, surveys and novel research. Currently there are no internationally agreed methods for  
482 reporting these types of CDR, meaning estimates are based on self-disclosure by projects following their own  
483 protocols. As such, the fractional uncertainty on these numbers should be viewed as substantial, and they are  
484 liable to change in future years as protocols are harmonised and improved.

#### 485 **2.4 Growth rate in atmospheric $CO_2$ concentration ( $G_{ATM}$ )**

##### 486 **2.4.1 Historical period 1850-2023**

487 The rate of growth of the atmospheric  $CO_2$  concentration is provided for years 1959-2023 by the US National  
488 Oceanic and Atmospheric Administration Global Monitoring Laboratory (NOAA/GML; Lan et al., 2024),



489 which includes recent revisions to the calibration scale of atmospheric CO<sub>2</sub> measurements (WMO-CO<sub>2</sub>-X2019;  
490 Hall et al., 2021). For the 1959-1979 period, the global growth rate is based on measurements of atmospheric  
491 CO<sub>2</sub> concentration averaged from the Mauna Loa and South Pole stations, as observed by the CO<sub>2</sub> Program at  
492 Scripps Institution of Oceanography (Keeling et al., 1976). For the 1980-2021 time period, the global growth  
493 rate is based on the average of multiple stations selected from the marine boundary layer sites with well-mixed  
494 background air (Ballantyne et al., 2012), after fitting a smooth curve through the data for each station as a  
495 function of time, and averaging by latitude band (Masarie and Tans, 1995). The annual growth rate is estimated  
496 by Lan et al. (2024) from atmospheric CO<sub>2</sub> concentration by taking the average of the most recent December-  
497 January months corrected for the average seasonal cycle and subtracting this same average one year earlier. The  
498 growth rate in units of ppm yr<sup>-1</sup> is converted to units of GtC yr<sup>-1</sup> by multiplying by a factor of 2.124 GtC per  
499 ppm, assuming instantaneous mixing of CO<sub>2</sub> throughout the atmosphere (Ballantyne et al., 2012; Table 1).

500 The uncertainty around the atmospheric growth rate is due to four main factors. First, the long-term  
501 reproducibility of reference gas standards (around 0.03 ppm for 1σ from the 1980s; Lan et al., 2024). Second,  
502 small unexplained systematic analytical errors that may have a duration of several months to two years come  
503 and go. They have been simulated by randomising both the duration and the magnitude (determined from the  
504 existing evidence) in a Monte Carlo procedure. Third, the network composition of the marine boundary layer  
505 with some sites coming or going, gaps in the time series at each site, etc (Lan et al., 2024). The latter uncertainty  
506 was estimated by NOAA/GML with a Monte Carlo method by constructing 100 "alternative" networks (Masarie  
507 and Tans, 1995; NOAA/GML, 2019). The second and third uncertainties, summed in quadrature, add up to  
508 0.085 ppm on average (Lan et al., 2024). Fourth, the uncertainty associated with using the average CO<sub>2</sub>  
509 concentration from a surface network to approximate the true atmospheric average CO<sub>2</sub> concentration (mass-  
510 weighted, in 3 dimensions) as needed to assess the total atmospheric CO<sub>2</sub> burden. In reality, CO<sub>2</sub> variations  
511 measured at the stations will not exactly track changes in total atmospheric burden, with offsets in magnitude  
512 and phasing due to vertical and horizontal mixing. This effect must be very small on decadal and longer time  
513 scales, when the atmosphere can be considered well mixed. The CO<sub>2</sub> increase in the stratosphere lags the  
514 increase (meaning lower concentrations) that we observe in the marine boundary layer, while the continental  
515 boundary layer (where most of the emissions take place) leads the marine boundary layer with higher  
516 concentrations. These effects nearly cancel each other. In addition, the growth rate is nearly the same  
517 everywhere (Ballantyne et al., 2012). We therefore maintain an uncertainty around the annual growth rate based  
518 on the multiple stations dataset ranges between 0.11 and 0.72 GtC yr<sup>-1</sup>, with a mean of 0.61 GtC yr<sup>-1</sup> for 1959-  
519 1979 and 0.17 GtC yr<sup>-1</sup> for 1980-2023, when a larger set of stations were available as provided by Lan et al.  
520 (2024). We estimate the uncertainty of the decadal averaged growth rate after 1980 at 0.02 GtC yr<sup>-1</sup> based on the  
521 calibration and the annual growth rate uncertainty but stretched over a 10-year interval. For years prior to 1980,  
522 we estimate the decadal averaged uncertainty to be 0.07 GtC yr<sup>-1</sup> based on a factor proportional to the annual  
523 uncertainty prior and after 1980 (0.02 \* [0.61/0.17] GtC yr<sup>-1</sup>).

524 We assign a high confidence to the annual estimates of G<sub>ATM</sub> because they are based on direct measurements  
525 from multiple and consistent instruments and stations distributed around the world (Ballantyne et al., 2012; Hall  
526 et al., 2021).



527 To estimate the total carbon accumulated in the atmosphere since 1750 or 1850, we use an atmospheric CO<sub>2</sub>  
528 concentration of  $278.3 \pm 3$  ppm or  $285.1 \pm 3$  ppm, respectively (Gulev et al., 2021). For the construction of the  
529 cumulative budget shown in Figure 3, we use the fitted estimates of CO<sub>2</sub> concentration from Joos and Spahni  
530 (2008) to estimate the annual atmospheric growth rate using the conversion factors shown in Table 1. The  
531 uncertainty of  $\pm 3$  ppm (converted to  $\pm 1\sigma$ ) is taken directly from the IPCC's AR5 assessment (Ciais et al., 2013).  
532 Typical uncertainties in the growth rate in atmospheric CO<sub>2</sub> concentration from ice core data are equivalent to  
533  $\pm 0.1$ - $0.15$  GtC yr<sup>-1</sup> as evaluated from the Law Dome data (Etheridge et al., 1996) for individual 20-year intervals  
534 over the period from 1850 to 1960 (Bruno and Joos, 1997).

#### 535 **2.4.2 2024 projection**

536 We provide an assessment of  $G_{\text{ATM}}$  for 2024 as the average of two methods. The GCB regression method  
537 models monthly global-average atmospheric CO<sub>2</sub> concentrations and derives the increment and annual average  
538 from these. The model uses lagged observations of concentration (Lan et al., 2024): both a 12-month lag, and  
539 the lowest lag that will allow model prediction to produce an estimate for the following January, recalling that  
540 the  $G_{\text{ATM}}$  increment is derived from December/January pairs. The largest driver of interannual changes is the  
541 ENSO signal (Betts et al., 2016), so the monthly ENSO 3.4 index (Huang et al., 2023) is included in the model.  
542 Given the natural lag between sea-surface temperatures and effects on the biosphere, and in turn effects on  
543 globally mixed atmospheric CO<sub>2</sub> concentration, a lagged ENSO index is used, and we use both a 5-month and a  
544 6-month lag. The combination of the two lagged ENSO values helps reduce possible effects of noise in a single  
545 month. To help characterise the seasonal variation, we add month as a categorical variable. Finally, we flag the  
546 period affected by the Pinatubo eruption (August 1991 - November 1993) as a categorical variable. Note that  
547 while emissions of CO<sub>2</sub> are the largest driver of the trend in atmospheric CO<sub>2</sub> concentration, our goal here is to  
548 predict divergence from that trend. Because changes in emissions from year to year are relatively minor in  
549 comparison to total emissions, this has little effect on the variation of concentration from the trend line. Even the  
550 relatively large drop in emissions in 2020 due to the COVID-19 pandemic does not cause any problems for the  
551 model.

552 We also use the multi-model mean and uncertainty of the 2024  $G_{\text{ATM}}$  estimated by the ESMs prediction system  
553 (see Section 2.9). We then take the average of the GCB regression and ESMs  $G_{\text{ATM}}$  estimates, with their  
554 respective uncertainty combined quadratically.

555 Similarly, the projection of the 2024 global average CO<sub>2</sub> concentration (in ppm), is calculated as the average of  
556 the estimates from the two methods. For the GCB regression method, it is the annual average of global  
557 concentration over the 12 months of 2024; for the ESMs, it is the observed global average CO<sub>2</sub> concentration for  
558 2023 plus the annual increase in 2024 of the global average CO<sub>2</sub> concentration predicted by the ESMs multi-  
559 model mean.





## 560 2.5 Ocean CO<sub>2</sub> sink

### 561 2.5.1 Historical period 1850-2023

562 The reported estimate of the global ocean anthropogenic CO<sub>2</sub> sink  $S_{\text{OCEAN}}$  is derived as the average of two  
563 estimates. The first estimate is derived as the mean over an ensemble of ten global ocean biogeochemistry  
564 models (GOBMs, Table 4 and Table S2). The second estimate is obtained as the mean over an ensemble of eight  
565 surface ocean  $f\text{CO}_2$ -observation-based data-products (Table 4 and Table S3). A ninth  $f\text{CO}_2$ -product (UEXP-FFN-  
566 U) is shown but is not included in the ensemble average as it differs from the other products by adjusting the  
567 flux to a cool, salty ocean surface skin. In previous editions of the GCB, this product was following the Watson  
568 et al. (2020) method but has been updated following the method of Dong et al. (2022, see Supplement S.3.1 for  
569 a discussion). The GOBMs simulate both the natural and anthropogenic CO<sub>2</sub> cycles in the ocean. They constrain  
570 the anthropogenic air-sea CO<sub>2</sub> flux (the dominant component of  $S_{\text{OCEAN}}$ ) by the transport of carbon into the  
571 ocean interior, which is also the controlling factor of present-day ocean carbon uptake in the real world. They  
572 cover the full globe and all seasons and were evaluated against surface ocean carbon observations, suggesting  
573 they are suitable to estimate the annual ocean carbon sink (Hauck et al., 2020). The  $f\text{CO}_2$ -products are tightly  
574 linked to observations of  $f\text{CO}_2$  (fugacity of CO<sub>2</sub>, which equals  $p\text{CO}_2$  corrected for the non-ideal behaviour of the  
575 gas; Pfeil et al., 2013), which carry imprints of temporal and spatial variability, but are also sensitive to  
576 uncertainties in gas-exchange parameterizations and data-sparsity (Fay et al., 2021, Gloege et al., 2021, Hauck  
577 et al., 2023a). Their asset is the assessment of the mean spatial pattern of variability and its seasonality (Hauck  
578 et al., 2020, Gloege et al. 2021, Hauck et al., 2023a). To benchmark trends derived from the  $f\text{CO}_2$ -products, we  
579 additionally performed a model subsampling exercise following Hauck et al. (2023a, see section S3). In  
580 addition, two diagnostic ocean models are used to estimate  $S_{\text{OCEAN}}$  over the industrial era (1781-1958).

581 The global  $f\text{CO}_2$ -based flux estimates were adjusted to remove the pre-industrial ocean source of CO<sub>2</sub> to the  
582 atmosphere of  $0.65 \pm 0.3 \text{ GtC yr}^{-1}$  from river input to the ocean (Regnier et al., 2022), to satisfy our definition of  
583  $S_{\text{OCEAN}}$  (Hauck et al., 2020). The river flux adjustment was distributed over the latitudinal bands using the  
584 regional distribution of Lacroix et al. (2020; North:  $0.14 \text{ GtC yr}^{-1}$ , Tropics:  $0.42 \text{ GtC yr}^{-1}$ , South:  $0.09 \text{ GtC yr}^{-1}$ ).  
585 Acknowledging that this distribution is based on only one model, the advantage is that a gridded field is  
586 available, and the river flux adjustment can be calculated for the three latitudinal bands and the RECCAP  
587 regions (REgional Carbon Cycle Assessment and Processes (RECCAP2; Ciais et al., 2020, Poulter et al., 2022,  
588 DeVries et al., 2023). This dataset suggests that more of the riverine outgassing is located in the tropics than in  
589 the Southern Ocean and is thus opposed to the previously used dataset of Aumont et al. (2001). Accordingly, the  
590 regional distribution is associated with a major uncertainty in addition to the large uncertainty around the global  
591 estimate (Crisp et al., 2022; Gruber et al., 2023). Anthropogenic perturbations of river carbon and nutrient  
592 transport to the ocean are not considered (see Section 2.10 and Supplement S.6.3).

593 We derive  $S_{\text{OCEAN}}$  from GOBMs by using a simulation (sim A) with historical forcing of climate and  
594 atmospheric CO<sub>2</sub> from GCB (Section 2.4), accounting for model biases and drift from a control simulation (sim  
595 B) with constant atmospheric CO<sub>2</sub> and normal year climate forcing. A third simulation (sim C) with historical



596 atmospheric CO<sub>2</sub> increase and normal year climate forcing is used to attribute the ocean sink to CO<sub>2</sub> (sim C  
597 minus sim B) and climate (sim A minus sim C) effects. A fourth simulation (sim D; historical climate forcing  
598 and constant atmospheric CO<sub>2</sub>) is used to compare the change in anthropogenic carbon inventory in the interior  
599 ocean (sim A minus sim D) to the observational estimate of Gruber et al. (2019) with the same flux components  
600 (steady state and non-steady state anthropogenic carbon flux). The *f*CO<sub>2</sub>-products are adjusted with respect to  
601 their original publications to represent the full ice-free ocean area, including coastal zones and marginal seas,  
602 when the area coverage is below 99%. This is done by either area filling following Fay et al. (2021) or a simple  
603 scaling approach. GOBMs and *f*CO<sub>2</sub>-products fall within the observational constraints over the 1990s ( $2.2 \pm 0.7$   
604 GtC yr<sup>-1</sup>, Ciais et al., 2013) before and after applying adjustments.

605 *S*<sub>OCEAN</sub> is calculated as the average of the GOBM ensemble mean and the *f*CO<sub>2</sub>-product ensemble mean from  
606 1990 onwards. Prior to 1990, it is calculated as the GOBM ensemble mean plus half of the offset between  
607 GOBMs and *f*CO<sub>2</sub>-products ensemble means over 1990-2001.

608 We assign an uncertainty of  $\pm 0.4$  GtC yr<sup>-1</sup> to the ocean sink based on a combination of random (ensemble  
609 standard deviation) and systematic uncertainties (GOBMs bias in anthropogenic carbon accumulation,  
610 previously reported uncertainties in *f*CO<sub>2</sub>-products; see Supplement S.3.4). While this approach is consistent  
611 within the GCB, an independent uncertainty assessment of the *f*CO<sub>2</sub>-products alone suggests a somewhat larger  
612 uncertainty of up to 0.7 GtC yr<sup>-1</sup> (Ford et al. 2024, accepted). We assess a medium confidence level to the  
613 annual ocean CO<sub>2</sub> sink and its uncertainty because it is based on multiple lines of evidence, it is consistent with  
614 ocean interior carbon estimates (Gruber et al., 2019, see Section 3.6.5) and the interannual variability in the  
615 GOBMs and data-based estimates is largely consistent and can be explained by climate variability. We refrain  
616 from assigning a high confidence because of the deviation between the GOBM and *f*CO<sub>2</sub>-product trends  
617 between around 2002 and 2020. More details on the *S*<sub>OCEAN</sub> methodology can be found in Supplement S.3.

## 618 **2.5.2 2024 Projection**

619 The ocean CO<sub>2</sub> sink forecast for the year 2024 is based on the annual historical time-series and our estimated  
620 2024 atmospheric CO<sub>2</sub> concentration (Lan et al 2024), the historical and our estimated 2024 annual global fossil  
621 fuel emissions from this year's carbon budget, and the spring (March, April, May) Oceanic Niño Index (ONI)  
622 (NCEP, 2024). Using a non-linear regression approach, i.e., a feed-forward neural network, atmospheric CO<sub>2</sub>,  
623 ONI, and the fossil fuel emissions are used as training data to best match the annual ocean CO<sub>2</sub> sink (i.e.  
624 combined *S*<sub>OCEAN</sub> estimate from GOBMs and data products) from 1959 through 2023 from this year's carbon  
625 budget. Using this relationship, the 2024 *S*<sub>OCEAN</sub> can then be estimated from the projected 2024 input data using  
626 the non-linear relationship established during the network training. To avoid overfitting, the neural network was  
627 trained with a variable number of hidden neurons (varying between 2-5) and 20% of the randomly selected  
628 training data were withheld for independent internal testing. Based on the best output performance (tested using  
629 the 20% withheld input data), the best performing number of neurons was selected. In a second step, we trained  
630 the network 10 times using the best number of neurons identified in step 1 and different sets of randomly  
631 selected training data. The mean of the 10 trainings is considered our best forecast, whereas the standard



632 deviation of the 10 ensembles provides a first order estimate of the forecast uncertainty. This uncertainty is then  
633 combined with the  $S_{OCEAN}$  uncertainty ( $0.4 \text{ GtC yr}^{-1}$ ) to estimate the overall uncertainty of the 2024 projection.  
634 As an additional line of evidence, we also assess the 2024 atmosphere-ocean carbon flux from the ESM  
635 prediction system (see Section 2.9).

## 636 **2.6 Land CO<sub>2</sub> sink**

### 637 **2.6.1 Historical Period 1850-2023**

638 The terrestrial land sink ( $S_{LAND}$ ) is thought to be due to the combined effects of rising atmospheric CO<sub>2</sub>,  
639 increasing N inputs, and climate change, on plant growth and terrestrial carbon storage.  $S_{LAND}$  does not include  
640 land sinks directly resulting from land-use and land-use change (e.g., regrowth of vegetation) as these are part of  
641 the land-use flux ( $E_{LUC}$ ), although system boundaries make it difficult to attribute exactly CO<sub>2</sub> fluxes on land  
642 between  $S_{LAND}$  and  $E_{LUC}$  (Erb et al., 2013).

643  $S_{LAND}$  is estimated from the multi-model mean of 20 DGVMs (Table 4 and Table S1). DGVMs simulations  
644 include all climate variability and CO<sub>2</sub> effects over land. In addition to the carbon cycle represented in all  
645 DGVMs, 14 models also account for the nitrogen cycle and hence can include the effect of N inputs on  $S_{LAND}$ .  
646 The DGVMs estimate of  $S_{LAND}$  does not include the export of carbon to aquatic systems or its historical  
647 perturbation, which is discussed in Supplement S.6.3. DGVMs need to meet several criteria to be included in  
648 this assessment. In addition, we use the International Land Model Benchmarking system (ILAMB; Collier et al.,  
649 2018) for the DGVMs evaluation (see Supplement S.4.2), with an additional comparison of DGVMs with a  
650 data-informed, Bayesian model-data fusion framework (CARDAMOM) (Bloom and Williams, 2015; Bloom et  
651 al., 2016). The uncertainty on  $S_{LAND}$  is taken from the DGVMs standard deviation. More details on the  $S_{LAND}$   
652 methodology can be found in Supplement S.4.

### 653 **2.6.2 2024 Projection**

654 Like for the ocean forecast, the land CO<sub>2</sub> sink ( $S_{LAND}$ ) forecast for the year 2024 is based on the annual  
655 historical (Lan et al., 2024) and our estimated 2024 atmospheric CO<sub>2</sub> concentration, historical and our estimated  
656 2024 annual global fossil fuel emissions from this year's carbon budget, and the summer (June, July, August)  
657 ONI (NCEP, 2024). All training data are again used to best match  $S_{LAND}$  from 1959 through 2023 from this  
658 year's carbon budget using a feed-forward neural network. To avoid overfitting, the neural network was trained  
659 with a variable number of hidden neurons (varying between 2-15), larger than for  $S_{OCEAN}$  prediction due to the  
660 stronger land carbon interannual variability. As done for  $S_{OCEAN}$ , a pre-training selects the optimal number of  
661 hidden neurons based on 20% withheld input data, and in a second step, an ensemble of 10 forecasts is produced  
662 to provide the mean forecast plus uncertainty. This uncertainty is then combined with the  $S_{LAND}$  uncertainty for  
663 2023 ( $1.0 \text{ GtC yr}^{-1}$ ) to estimate the overall uncertainty of the 2024 projection.



## 664 2.7 Atmospheric inversion estimate

665 The world-wide network of in-situ atmospheric measurements and satellite derived atmospheric CO<sub>2</sub> column  
666 (xCO<sub>2</sub>) observations put a strong constraint on changes in the atmospheric abundance of CO<sub>2</sub>. This is true  
667 globally (hence our large confidence in G<sub>ATM</sub>), but also in regions with sufficient observational density found  
668 mostly in the extra-tropics. This allows atmospheric inversion methods to constrain the magnitude and location  
669 of the combined total surface CO<sub>2</sub> fluxes from all sources, including fossil and land-use change emissions and  
670 land and ocean CO<sub>2</sub> fluxes. The inversions assume E<sub>FOS</sub> to be well known, and they solve for the spatial and  
671 temporal distribution of land and ocean fluxes from the residual gradients of CO<sub>2</sub> between stations that are not  
672 explained by fossil fuel emissions. By design, such systems thus close the carbon balance (B<sub>IM</sub> = 0) and thus  
673 provide an additional perspective on the independent estimates of the ocean and land fluxes.

674 This year's release includes fourteen inversion systems that are described in Table S4. Each system is rooted in  
675 Bayesian inversion principles but uses different methodologies. These differences concern the selection of  
676 atmospheric CO<sub>2</sub> data or xCO<sub>2</sub>, and the choice of a-priori fluxes to refine. They also differ in spatial and  
677 temporal resolution, assumed correlation structures, and mathematical approach of the models (see references in  
678 Table S4 for details). Importantly, the systems use a variety of transport models, which was demonstrated to be  
679 a driving factor behind differences in atmospheric inversion-based flux estimates, and specifically their  
680 distribution across latitudinal bands (Gaubert et al., 2019; Schuh et al., 2019). Eight inversion systems used  
681 surface observations from the global measurement network (Schuldt et al., 2023, 2024). Six inversion systems  
682 (CAM5-FT24r1, CMS-flux, GONGGA, COLA, GCASv2, NTFVAR) used satellite xCO<sub>2</sub> retrievals from  
683 GOSAT and/or OCO-2, scaled to the WMO 2019 calibration scale, of which three inversions this year (CMS-  
684 Flux, COLA, NTFVAR) used these xCO<sub>2</sub> datasets in addition to the in-situ observational CO<sub>2</sub> mole fraction  
685 records.

686 The original products delivered by the inverse modellers were modified to facilitate the comparison to the other  
687 elements of the budget, specifically on two accounts: (1) global total fossil fuel emissions including cement  
688 carbonation CO<sub>2</sub> uptake, and (2) riverine CO<sub>2</sub> transport. We note that with these adjustments the inverse results  
689 no longer represent the net atmosphere-surface exchange over land/ocean areas as sensed by atmospheric  
690 observations. Instead, for land, they become the net uptake of CO<sub>2</sub> by vegetation and soils that is not exported  
691 by fluvial systems, similar to the DGVMs estimates. For oceans, they become the net uptake of anthropogenic  
692 CO<sub>2</sub>, similar to the GOBMs estimates.

693 The inversion systems prescribe global fossil fuel emissions based on e.g. the GCP's Gridded Fossil Emissions  
694 Dataset versions 2024.0 (GCP-GridFED; Jones et al., 2024a), which are updates to GCP-GridFEDv2021  
695 presented by Jones et al. (2021b). GCP-GridFEDv2024.0 scales gridded estimates of CO<sub>2</sub> emissions from  
696 EDGARv4.3.2 (Janssens-Maenhout et al., 2019) within national territories to match national emissions  
697 estimates provided by the GCB for the years 1959-2023, which were compiled following the methodology  
698 described in Section 2.1. Small differences between the systems due to for instance regridding to the transport  
699 model resolution, or use of different fossil fuel emissions than GCP-GridFEDv2024.0, are adjusted in the



700 latitudinal partitioning we present, to ensure agreement with the estimate of  $E_{\text{FOS}}$  in this budget. We also note  
701 that the ocean fluxes used as prior by 8 out of 14 inversions are part of the suite of the ocean process model or  
702  $f\text{CO}_2$ -products listed in Section 2.5. Although these fluxes are further adjusted by the atmospheric inversions  
703 (except for Jena CarboScope), it makes the inversion estimates of the ocean fluxes not completely independent  
704 of  $\text{SOCEAN}$  assessed here.

705 To facilitate comparisons to the independent  $\text{SOCEAN}$  and  $\text{SLAND}$ , we used the same adjustments for transport and  
706 outgassing of carbon transported from land to ocean, as done for the observation-based estimates of  $\text{SOCEAN}$  (see  
707 Supplement S.3).

708 The atmospheric inversions are evaluated using vertical profiles of atmospheric  $\text{CO}_2$  concentrations (Figure S5).  
709 More than 30 aircraft programs over the globe, either regular programs or repeated surveys over at least 9  
710 months (except for SH programs), have been used to assess system performance (with space-time observational  
711 coverage sparse in the SH and tropics, and denser in NH mid-latitudes; Table S8). The fourteen systems are  
712 compared to the independent aircraft  $\text{CO}_2$  measurements between 2 and 7 km above sea level between 2001 and  
713 2023. Results are shown in Figure S5 and discussed in Supplement S.5.2.

714 With a relatively small ensemble of systems that cover at least one full decade ( $N=10$ ), and which moreover  
715 share some a-priori fluxes used with one another, or with the process-based models, it is difficult to justify using  
716 their mean and standard deviation as a metric for uncertainty across the ensemble. We therefore report their full  
717 range (min-max) without their mean. More details on the atmospheric inversion methodology can be found in  
718 Supplement S.5.

## 719 **2.8 Atmospheric oxygen based estimate**

720 Long-term atmospheric  $\text{O}_2$  and  $\text{CO}_2$  observations allow estimation of the global ocean and land carbon sinks,  
721 due to the coupling of  $\text{O}_2$  and  $\text{CO}_2$  with distinct exchange ratios for fossil fuel emissions and land uptake, and  
722 uncoupled  $\text{O}_2$  and  $\text{CO}_2$  ocean exchange (Keeling and Manning, 2014). The global ocean and net land carbon  
723 sinks were calculated following methods and constants used in Keeling and Manning (2014) but modified to  
724 also include the effective  $\text{O}_2$  source from metal refining (Battle et al., 2023). For the exchange ratio of the net  
725 land sink at value of 1.05 is used, following Resplandy et al. (2019). For fossil fuels, the following values are  
726 used: gas: 1.95 (+/-) 0.04, liquid: 1.44 (+/-) 0.03, solid: 1.17 (+/-) 0.03, cement: 0 (+/-) 0, gas flaring: 1.98 (+/-)  
727 0.07 (Keeling, 1988). Atmospheric  $\text{O}_2$  is observed as  $\delta(\text{O}_2/\text{N}_2)$  and combined with  $\text{CO}_2$  mole fraction  
728 observations into Atmospheric Potential Oxygen (APO, Stephens et al., 1998). The APO observations from  
729 1990 to 2024 were taken from a weighted average of flask records from three stations in the Scripps  $\text{O}_2$  program  
730 network (Alert, Canada (ALT), La Jolla, California (LJO), and Cape Grim, Australia (CGO), weighted per  
731 Keeling and Manning (2014). Observed  $\text{CO}_2$  was taken from the globally averaged marine surface annual mean  
732 growth rate from the NOAA/GML Global Greenhouse Gas Reference Network (Lan et al., 2024). The  $\text{O}_2$  source  
733 from ocean warming is based on ocean heat content from updated data from NOAA/NCEI (Levitus et al., 2012).  
734 The effective  $\text{O}_2$  source from metal refining is based on production data from Bray (2020), Flanagan (2021), and  
735 Tuck (2022). Uncertainty was determined through a Monte Carlo approach with 20,000 iterations, using



736 uncertainties prescribed in Keeling and Manning (2014), including observational uncertainties from Keeling et  
737 al. (2007) and autoregressive errors in fossil fuel emissions (Ballantyne et al., 2015). The reported uncertainty is  
738 1 standard deviation of the ensemble. The difference between the atmospheric O<sub>2</sub> estimate for GCB2023 is due  
739 to a revision to the Scripps O<sub>2</sub> program CO<sub>2</sub> data. As for the atmospheric inversions, the O<sub>2</sub> based estimates also  
740 closes the carbon balance ( $B_{IM} = 0$ ) by design and provides another independent estimate of the ocean and land  
741 fluxes. Note that the O<sub>2</sub> method requires a correction for global air-sea O<sub>2</sub> flux, which has the largest uncertainty  
742 at annual time scales, but which is still non negligible for decadal estimates (Nevison et al., 2008).

## 743 **2.9 Earth System Models estimate**

744 Reconstructions and predictions from decadal prediction systems based on Earth system models (ESMs) provide  
745 a novel line of evidence in assessing the atmosphere-land and atmosphere-ocean carbon fluxes in the past  
746 decades and predicting their changes for the current year. The decadal prediction systems based on ESMs used  
747 here consist of three sets of simulations: (i) uninitialized freely evolving historical simulations (1850-2014); (ii)  
748 assimilation reconstruction incorporating observational data into the model (1960-2023); (iii) initialised  
749 prediction simulations for the 1981-2024 period, starting every year from initial states obtained from the above  
750 assimilation simulations. The assimilations are designed to reconstruct the actual evolution of the Earth system  
751 by assimilating essential fields from data products. The assimilations' states, which are expected to be close to  
752 observations, are used to start the initialised prediction simulations used for the current year (2024) global  
753 carbon budget. Similar initialised prediction simulations starting every year (Nov. 1st or Jan. 1st) over the 1981-  
754 2023 period (i.e., hindcasts) are also performed for predictive skill quantification and for bias correction. More  
755 details on the illustration of a decadal prediction system based on an ESM can refer to Figure 1 of Li et al.  
756 (2023).

757 By assimilating physical atmospheric and oceanic data products into the ESMs, the models are able to reproduce  
758 the historical variations of the atmosphere-sea CO<sub>2</sub> fluxes, atmosphere-land CO<sub>2</sub> fluxes, and atmospheric CO<sub>2</sub>  
759 growth rate (Li et al., 2016, 2019; Lovenduski et al., 2019a,b; Ilyina et al., 2021; Li et al., 2023). Furthermore,  
760 the ESM-based predictions have proven their skill in predicting the air-sea CO<sub>2</sub> fluxes for up to 6 years, the air-  
761 land CO<sub>2</sub> fluxes and atmospheric CO<sub>2</sub> growth for 2 years (Lovenduski et al., 2019a,b; Ilyina et al., 2021; Li et  
762 al., 2023). The reconstructions from the fully coupled model simulations ensure a closed budget within the Earth  
763 system, i.e., no budget imbalance term.

764 Five ESMs, i.e., CanESM5 (Swart et al., 2019; Sospedra-Alfonso et al., 2021), EC-Earth3-CC (Döscher et al.  
765 2021; Bilbao et al., 2021; Bernardello et al., 2024), IPSL-CM6A-CO2-LR (Boucher et al., 2020), MIROC-ES2L  
766 (Watanabe et al., 2020), and MPI-ESM1-2-LR (Mauritsen et al., 2019; Li et al., 2023), have performed the set of  
767 prediction simulations. Each ESM uses a different assimilation method and combination of data products  
768 incorporated in the system, more details on the models configuration can be found in Table 4 and Supplementary  
769 Table S5. The ESMs use external forcings from the Coupled Model Intercomparison Project Phase 6 (CMIP6)  
770 historical (1960-2014) plus SSP2-4.5 baseline and CovidMIP two-year blip scenario (2015-2024) (Eyring et al.,  
771 2016; Lamboll et al., 2021). The CO<sub>2</sub> emissions forcing from 2015-2024 are substituted by GCB-GridFED



772 (v2024.0, Jones et al., 2024a) to provide a consistent CO<sub>2</sub> forcing. Reconstructions of atmosphere-ocean CO<sub>2</sub>  
773 fluxes (S<sub>OCEAN</sub>) and atmosphere-land CO<sub>2</sub> fluxes (S<sub>LAND-ELUC</sub>) for the time period from 1960-2023 are assessed  
774 here. Predictions of the atmosphere-ocean CO<sub>2</sub> flux, atmosphere-land CO<sub>2</sub> flux, and atmospheric CO<sub>2</sub> growth for  
775 2024 are calculated based on the predictions at a lead time of 1 year. The predictions are bias corrected using the  
776 1985-2014 climatology mean of GCB2022 (Friedlingstein et al., 2022), more details on methods can be found in  
777 Boer et al. (2016) and Li et al. (2023). The ensemble size of initialized prediction simulations is 10, and the  
778 ensemble mean for each individual model is used here. The ESMs are used here to support the assessment of  
779 S<sub>OCEAN</sub> and net atmosphere-land CO<sub>2</sub> flux (S<sub>LAND</sub> - E<sub>ELUC</sub>) over the 1960-2023 period, and to provide an estimate  
780 of the 2024 projection of G<sub>ATM</sub>.

## 781 2.10 Processes not included in the global carbon budget

782 The contribution of anthropogenic CO and CH<sub>4</sub> to the global carbon budget is not fully accounted for in Eq. (1)  
783 and is described in Supplement S.6.1. The contributions to CO<sub>2</sub> emissions of decomposition of carbonates not  
784 accounted for is described in Supplement S.6.2. The contribution of anthropogenic changes in river fluxes is  
785 conceptually included in Eq. (1) in S<sub>OCEAN</sub> and in S<sub>LAND</sub>, but it is not represented in the process models used to  
786 quantify these fluxes. This effect is discussed in Supplement S.6.3. Similarly, the loss of additional sink capacity  
787 from reduced forest cover is missing in the combination of approaches used here to estimate both land fluxes  
788 (E<sub>ELUC</sub> and S<sub>LAND</sub>) and its potential effect is discussed and quantified in Supplement S.6.4.

## 789 3 Results

790 For each component of the global carbon budget, we present results for three different time periods: the full  
791 historical period, from 1850 to 2023, the decades in which we have atmospheric concentration records from  
792 Mauna Loa (1960-2023), a specific focus on last year (2023), and the projection for the current year (2024).  
793 Subsequently, we assess the estimates of the budget components of the last decades against the top-down  
794 constraints from inverse modelling of atmospheric observations, the land/ocean partitioning derived from the  
795 atmospheric O<sub>2</sub> measurements, and the budget components estimates from the ESMs assimilation simulations.  
796 Atmospheric inversions further allow for an assessment of the budget components with a regional breakdown of  
797 land and ocean sinks.

### 798 3.1 Fossil CO<sub>2</sub> Emissions

#### 799 3.1.1 Historical period 1850-2023

800 Cumulative fossil CO<sub>2</sub> emissions for 1850-2023 were 490 ± 25 GtC, including the cement carbonation sink  
801 (Figure 3, Table 8, with all cumulative numbers rounded to the nearest 5GtC). In this period, 46% of global  
802 fossil CO<sub>2</sub> emissions came from coal, 35% from oil, 15% from natural gas, 3% from decomposition of  
803 carbonates, and 1% from flaring. In 1850, the UK stood for 62% of global fossil CO<sub>2</sub> emissions. In 1893 the  
804 combined cumulative emissions of the current members of the European Union reached and subsequently  
805 surpassed the level of the UK. Since 1917 US cumulative emissions have been the largest. Over the entire



806 period 1850-2023, US cumulative emissions amounted to 120GtC (24% of world total), the EU's to 80 GtC  
807 (16%), China's to 75 GtC (15%), and India's to 15 GtC (3%).

808 In addition to the estimates of fossil CO<sub>2</sub> emissions that we provide here (see Section 2.1), there are three global  
809 datasets with long time series that include all sources of fossil CO<sub>2</sub> emissions: CDIAC-FF (Hefner and Marland,  
810 2024), CEDS version 2024\_07\_08 (Hoesly et al., 2024) and PRIMAP-hist version 2.6 (Gütschow et al., 2016;  
811 Gütschow et al., 2024), although these datasets are not entirely independent from each other (Andrew, 2020a).  
812 CEDS has cumulative emissions over 1750-2022 at 480 GtC, CDIAC-FF has 481 GtC, GCP 484 GtC,  
813 PRIMAP-hist CR 490 GtC, and PRIMAP-hist TR 492 GtC. CDIAC-FF excludes emissions from lime  
814 production. CEDS estimates higher emissions from international shipping in recent years, while PRIMAP-hist  
815 has higher fugitive emissions than the other datasets. However, in general these four datasets are in relative  
816 agreement as to total historical global emissions of fossil CO<sub>2</sub>.

### 817 **3.1.2 Recent period 1960-2023**

818 Global fossil CO<sub>2</sub> emissions, E<sub>FOS</sub> (including the cement carbonation sink), have increased every decade from an  
819 average of  $3.0 \pm 0.2$  GtC yr<sup>-1</sup> for the decade of the 1960s to an average of  $9.7 \pm 0.5$  GtC yr<sup>-1</sup> during 2014-2023  
820 (Table 7, Figure 2 and Figure 5). The growth rate in these emissions decreased between the 1960s and the  
821 1990s, from 4.3% yr<sup>-1</sup> in the 1960s (1960-1969), 3.2% yr<sup>-1</sup> in the 1970s (1970-1979), 1.6% yr<sup>-1</sup> in the 1980s  
822 (1980-1989), to 1.0% yr<sup>-1</sup> in the 1990s (1990-1999). After this period, the growth rate began increasing again in  
823 the 2000s at an average growth rate of 2.8% yr<sup>-1</sup>, decreasing to 0.6% yr<sup>-1</sup> for the last decade (2014-2023).  
824 China's emissions increased by +1.9% yr<sup>-1</sup> on average over the last 10 years dominating the global trend, and  
825 India's emissions increased by +3.6% yr<sup>-1</sup>, while emissions decreased in EU27 by 2.1% yr<sup>-1</sup>, and in the USA by  
826 1.2% yr<sup>-1</sup>. Figure 6 illustrates the spatial distribution of fossil fuel emissions for the 2014-2023 period.

827 E<sub>FOS</sub> reported here includes the uptake of CO<sub>2</sub> by cement via carbonation which has increased with increasing  
828 stocks of cement products, from an average of 20 MtC yr<sup>-1</sup> (0.02 GtC yr<sup>-1</sup>) in the 1960s to an average of 200MtC  
829 yr<sup>-1</sup> (0.2 GtC yr<sup>-1</sup>) during 2014-2023 (Figure 5).

### 830 **3.1.3 Final year 2023**

831 Global fossil CO<sub>2</sub> emissions were slightly higher, 1.4%, in 2023 than in 2022, with an increase of 0.14 GtC to  
832 reach  $10.1 \pm 0.5$  GtC (including the 0.21 GtC cement carbonation sink) in 2023 (Figure 5), distributed among  
833 coal (41%), oil (32%), natural gas (21%), cement (4%), flaring (<1%), and others (<1%). Compared to 2022, the  
834 2023 emissions from coal, oil, and gas increased by 1.4%, 2.5%, and 0.1% respectively, while emissions from  
835 cement decreased by 2%. All annual growth rates presented are adjusted for the leap year, unless stated  
836 otherwise.

837 In 2023, the largest absolute contributions to global fossil CO<sub>2</sub> emissions were from China (31%), the USA  
838 (13%), India (8%), and the EU27 (7%). These four regions account for 59% of global fossil CO<sub>2</sub> emissions,  
839 while the rest of the world contributed 41%, including international aviation and marine bunker fuels (3% of the





840 total). Growth rates for these countries from 2022 to 2023 were 4.9% (China), -3.3% (USA), -8.4% (EU27), and  
841 8.2% (India), with +0.7% for the rest of the world, including international aviation and marine bunker fuels  
842 (+9.5%). The per-capita fossil CO<sub>2</sub> emissions in 2023 were 1.3 tC person<sup>-1</sup> yr<sup>-1</sup> for the globe, and were 3.9  
843 (USA), 2.3 (China), 1.5 (EU27) and 0.6 (India) tC person<sup>-1</sup> yr<sup>-1</sup> for the four highest emitters (Figure 5).

### 844 **3.1.4 Year 2024 Projection**

845 Globally, we estimate that global fossil CO<sub>2</sub> emissions (including cement carbonation, -0.21 GtC) will grow by  
846 0.8% in 2024 (-0.3% to +1.9%) to 10.2 GtC (37.4 GtCO<sub>2</sub>), an historical record high<sup>2</sup>. Carbon Monitor projects a  
847 similar 2024 increase of 0.6% (-0.7% to 1.9%). GCB estimates of changes in 2024 emissions per fuel types,  
848 relative to 2023, are projected to be 0.2% (range -1.0% to 1.4%) for coal, +0.9% (range 0.0% to 1.8%) for oil,  
849 +2.4% (range 1.1% to 3.8%) for natural gas, and -2.8% (range -4.7% to -0.9%) for cement.

850 For China, projected fossil emissions in 2024 are expected to increase slightly by 0.2% (range -1.6% to 2.0%)  
851 compared with 2023 emissions, bringing 2023 emissions for China around 3.3 GtC yr<sup>-1</sup> (12.0 GtCO<sub>2</sub> yr<sup>-1</sup>). In  
852 comparison, the Carbon Monitor estimate projects a 2024 decrease of 0.8% (range -3.8% to 1.9%). Our  
853 projected changes by fuel for China are +0.3% for coal, -0.8% for oil, +8%.0 natural gas, and -8.1% for cement.

854 For the USA, using the Energy Information Administration (EIA) emissions projection for 2024 combined with  
855 cement clinker data from USGS, we project a decrease of 0.6% (range -2.9% to 1.7%) compared to 2023,  
856 bringing USA 2023 emissions to around 1.3 GtC yr<sup>-1</sup> (4.9 GtCO<sub>2</sub> yr<sup>-1</sup>). Carbon Monitor projects a 2024 increase  
857 in USA emissions of 1.2% (-1.0% to 3.5%). Our projected changes by fuel are -3.5% for coal, -0.7% for oil,  
858 +1.0% for natural gas, and -5.8% for cement.

859 For the European Union, our projection for 2024 is for a decrease of 3.8% (range -6.2% to -1.4%) relative to  
860 2023, with 2024 emissions around 0.7 GtC yr<sup>-1</sup> (2.4 GtCO<sub>2</sub> yr<sup>-1</sup>). The Carbon Monitor projection for the EU27 is  
861 slightly lower than GCB with a decrease of 5.5% (-9.2% to -1.9%). Our projected changes by fuel are -15.8%  
862 for coal, +0.2% for oil, -1.3% for natural gas, and -3.5% for cement.

863 For India, our projection for 2024 is an increase of 4.6% (range of 3.0% to 6.1%) over 2023, with 2024  
864 emissions around 0.9 GtC yr<sup>-1</sup> (3.2 GtCO<sub>2</sub> yr<sup>-1</sup>). The Carbon Monitor projection for India is an increase of 5.5%  
865 (1.9% to 9.1%). Our projected changes by fuel are +4.5% for coal, +3.6% for oil, +11.8% for natural gas, and  
866 +4.0% for cement.

867 International aviation and shipping are projected to increase by 7.8% in 2024, with international aviation  
868 projected to be up 14% over 2023, continuing to recover from pandemic lows, and international shipping  
869 projected to rise by 3%. The Carbon Monitor projects international aviation and shipping to increase by 3.3% in  
870 2024.

---

<sup>2</sup> Growth rates in this section use a leap year adjustment that corrects for the extra day in 2024.



871 For the rest of the world, the expected change for 2024 is an increase of 1.1% (range -1.0% to 3.3%) with 2024  
872 emissions around 4.0 GtC yr<sup>-1</sup> (14.5 GtCO<sub>2</sub> yr<sup>-1</sup>), similar to the Carbon Monitor projection of 1.1% (range -0.1%  
873 to 2.3%). The fuel-specific projected 2024 growth rates for the rest of the world are: +0.5% for coal, +0.5% for  
874 oil, +2.2% for natural gas, +2.0% for cement.

875 For traceability, Table S6 provides a comparison of annual projections from GCB since 2015 with the actual  
876 emissions assessed in the subsequent GCB annual report.

### 877 **3.2 Emissions from Land Use Change**

#### 878 **3.2.1 Historical period 1850-2023**

879 Cumulative CO<sub>2</sub> emissions from land-use change (ELUC) for 1850-2023 were 225 ± 65 GtC (Table 8; Figure 3;  
880 Figure 16). The cumulative emissions from ELUC show a large spread among individual estimates of 150 GtC  
881 (H&C2023), 205 GtC (OSCAR), 250 GtC (LUCE) and 285 GtC (BLUE) for the four bookkeeping models and a  
882 similar wide estimate of 250 ± 85 GtC for the DGVMs (all cumulative numbers are rounded to the nearest 5  
883 GtC). Vegetation biomass observations provide independent constraints on the ELUC estimates (Li et al., 2017).  
884 Over the 1901-2012 period, the GCB bookkeeping models cumulative ELUC amounts to 165 GtC [105 to 210  
885 GtC], similar to the observation-based estimate of 155 ± 50 GtC (Li et al., 2017).

#### 886 **3.2.2 Recent period 1960-2023**

887 In contrast to growing fossil emissions, CO<sub>2</sub> emissions from land-use, land-use change, and forestry remained  
888 relatively constant (around 1.5 GtC yr<sup>-1</sup>) over the 1960-1999 period. Since then, they have shown a statistically  
889 significant decrease of about 0.2 GtC per decade, reaching 1.1 ± 0.7 GtC yr<sup>-1</sup> for the 2014-2023 period (Table  
890 7), but with significant spread, from 0.8 to 1.3 GtC yr<sup>-1</sup> across the four bookkeeping models (Table 5, Figure 7).  
891 Different from the bookkeeping average, the DGVMs average grows slightly larger over the 1980-2010 period  
892 and shows no sign of decreasing emissions in the recent decades, apart from in the most recent decade (Table 5,  
893 Figure 7). This is, however, expected as DGVM-based estimates include the loss of additional sink capacity,  
894 which grows with time, while the bookkeeping estimates do not (Supplement S.6.4).

895 We separate net ELUC into five component fluxes to gain further insight into the drivers of net emissions:  
896 deforestation, forest (re-)growth, wood harvest and other forest management, peat drainage and peat fires, and  
897 all other transitions (Figure 7c; supplemental Sec. S.2.1). We further decompose the deforestation and the forest  
898 (re-)growth term into contributions from shifting cultivation vs permanent forest cover changes (Figure 7d).  
899 Averaged over the 2014-2023 period and over the four bookkeeping estimates, fluxes from deforestation amount  
900 to 1.7 [1.4 to 2.3] GtC yr<sup>-1</sup> (Table 5), of which 1.0 [0.8, 1.1] GtC yr<sup>-1</sup> are from permanent deforestation. Fluxes  
901 from forest (re-)growth amount to -1.2 [-1.5, -0.9] GtC yr<sup>-1</sup> (Table 5), of which -0.5 [-0.7, -0.3] GtC yr<sup>-1</sup> are from  
902 re/afforestation and the remainder from forest regrowth in shifting cultivation cycles. Emissions from wood  
903 harvest and other forest management (0.3 [0.0, 0.6] GtC yr<sup>-1</sup>), peat drainage and peat fires (0.2 [0.2, 0.3] GtC yr<sup>-1</sup>)  
904 and the net flux from other transitions (0.1 [0.0, 0.1] GtC yr<sup>-1</sup>) are substantially less important globally (Table



905 5). However, the small net flux from wood harvest and other forest management contains substantial gross  
906 fluxes that largely compensate each other (see Figure S8):  $1.4 [0.9, 2.0]$   $\text{GtC yr}^{-1}$  emissions result from the  
907 decomposition of slash and the decay of wood products and  $-1.1 [-1.4, -0.8]$   $\text{GtC yr}^{-1}$  removals result from  
908 regrowth after wood harvesting.

909 The split into component fluxes clarifies the potentials for emission reduction and carbon dioxide removal: the  
910 emissions from permanent deforestation - the largest of our component fluxes - could be halted (largely) without  
911 compromising carbon uptake by forests, contributing substantially to emissions reduction. By contrast, reducing  
912 wood harvesting would have limited potential to reduce emissions as it would be associated with less forest  
913 regrowth; removals and emissions cannot be decoupled here on long timescales. A similar conclusion applies to  
914 removals and emissions from shifting cultivation, which we have therefore separated out. Carbon Dioxide  
915 Removal (CDR) in forests could instead be increased by permanently increasing the forest cover through  
916 re/afforestation. Our estimate of about  $-0.5 \text{ GtC yr}^{-1}$  removed on average each year during 2014-2023 by  
917 re/afforestation is similar to independent estimates that were derived from NGHGs for CDR in managed forests  
918 (through re/afforestation plus forest management) for 2013-2022 ( $-0.5 \text{ GtC yr}^{-1}$ , Pongratz et al., 2024).  
919 Re/afforestation constitutes the vast majority of all current CDR (Pongratz et al., 2024). Though they cannot be  
920 compared directly to annual fluxes from the atmosphere, CDR through transfers between non-atmospheric  
921 reservoirs such as in durable HWPs, biochar, or BECCS comprise much smaller amounts of carbon.  $218 \text{ MtC}$   
922  $\text{yr}^{-1}$  have been estimated to be transferred to HWPs, averaged over 2013-2022. The net flux of HWPs,  
923 considering the re-release of  $\text{CO}_2$  through their decay, amounts to  $91 \text{ MtC yr}^{-1}$  over that period (Pongratz et al.,  
924 2024). Note that some double-counting between the CDR through HWPs and the CDR through re/afforestation  
925 exists if the HWPs are derived from newly forested areas. BECCS projects have been estimated to store  $0.1 \text{ MtC}$   
926  $\text{yr}^{-1}$  in geological projects worldwide in 2023, biochar projects  $0.2 \text{ MtC yr}^{-1}$  (Pongratz et al., 2024). “Blue  
927 carbon”, i.e. coastal wetland management such as restoration of mangrove forests, saltmarshes and seagrass  
928 meadows, though at the interface of land and ocean carbon fluxes, are counted towards the land-use sector as  
929 well. Currently, bookkeeping models do not include blue carbon; however, current CDR deployment in coastal  
930 wetlands is small globally, less than  $0.003 \text{ MtC yr}^{-1}$  (Powis et al., 2023).

931 The statistically significant decrease in  $E_{\text{LUC}}$  since the late-1990s, including the larger drop within the most  
932 recent decade, is due to the combination of decreasing emissions from deforestation (in particular permanent  
933 deforestation) and increasing removals from forest regrowth (with those from re/afforestation stagnating  
934 globally in the last decade). Emissions in 2014-2023 are 28% lower than in the late-1990s (1995-2004) and 20%  
935 lower than in 2004-2013. The steep drop in  $E_{\text{LUC}}$  after 2015 is due to the combined effect from a peak in peat  
936 fire emissions in 2015 and a long-term decline in deforestation emissions in many countries over the 2010-2020  
937 period with largest declines in the Democratic Republic of the Congo, Brazil, China, and Indonesia. Since the  
938 processes behind gross removals, foremost forest regrowth and soil recovery, are all slow, while gross emissions  
939 include a large instantaneous component, short-term changes in land-use dynamics, such as a temporary  
940 decrease in deforestation, influences gross emissions dynamics more than gross removals dynamics, which  
941 rather are a response to longer-term dynamics. Component fluxes often differ more across the four bookkeeping  
942 estimates than the net flux, which is expected due to different process representation; in particular, the treatment



943 of shifting cultivation, which increases both gross emissions and removals, differs across models, but also net  
944 and gross wood harvest fluxes show high uncertainty. By contrast, models agree relatively well for emissions  
945 from permanent deforestation.

946 Overall, highest land-use emissions occur in the tropical regions of all three continents. The top three emitters  
947 (both cumulatively 1959-2023 and on average over 2014-2023) are Brazil (in particular the Amazon Arc of  
948 Deforestation), Indonesia and the Democratic Republic of the Congo, with these 3 countries contributing 0.7  
949 GtC yr<sup>-1</sup> or 60% of the global net land-use emissions (average over 2014-2023) (Figure 6b, Figure 7b). This is  
950 related to massive expansion of cropland, particularly in the last few decades in Latin America, Southeast Asia,  
951 and sub-Saharan Africa (Hong et al., 2021), to a substantial part for export of agricultural products (Pendrell et  
952 al., 2019). Emission intensity is high in many tropical countries, particularly of Southeast Asia, due to high rates  
953 of land conversion in regions of carbon-dense and often still pristine, undegraded natural forests (Hong et al.,  
954 2021). Emissions are further increased by peat fires in equatorial Asia (GFED4s, van der Werf et al., 2017). Our  
955 estimates of high ELUC in China has been revised down since the 1980s as compared to GCB2023 related to  
956 the update of the land-use forcing, which is now based on the cropland dataset by Yu et al. (2022) (see  
957 Supplement S.2.2), which suggests lower cropland expansion and thus less deforestation than the previous  
958 datasets assumed. Uptake due to land-use change occurs in several regions of the world (Figure 6b) particularly  
959 because of re/afforestation. Highest CDR in the last decade is seen in China, where our estimates show an even  
960 larger uptake since 2010 compared to GCB2023 related to the updated land-use forcing, in the EU27, partly  
961 related to expanding forest area as a consequence of the forest transition in the 19<sup>th</sup> and 20<sup>th</sup> century and  
962 subsequent regrowth of forest (Mather 2001; McGrath et al., 2015), and in the U.S. Substantial uptake through  
963 re/afforestation also exists in other regions such as Brazil, Myanmar or Russia, where, however, emissions from  
964 deforestation and other land-use changes dominate the net flux.

965 While the mentioned patterns are robust and supported by independent literature, we acknowledge that model  
966 spread is substantially larger on regional than global levels, as has been shown for bookkeeping models (Bastos  
967 et al., 2021) as well as DGVMs (Obermeier et al., 2021). Assessments for individual regions are being  
968 performed as part of REgional Carbon Cycle Assessment and Processes (RECCAP2; Ciais et al., 2020, Poulter  
969 et al., 2022) or already exist for selected regions (e.g., for Europe by Petrescu et al., 2020, for Brazil by Rosan et  
970 al., 2021, for 8 selected countries/regions in comparison to inventory data by Schwingshackl et al., 2022). The  
971 revisions since GCB2023 reflect such uncertainties: The integration of a fourth bookkeeping model alters our  
972 estimates, though only to a limited extent given that the new model LUCE lies in between the other three  
973 models for the global ELUC estimates. Larger changes are obvious at regional level due to the revisions of the  
974 land-use forcing with a general update to more recent FAO input for agricultural areas and wood harvest, new  
975 MapBiomass input for Brazil and Indonesia and the updated cropland dataset in China.

976 The NGHGI data under the LULUCF sector and the LULUCF estimates from FAOSTAT differ from the global  
977 models' definition of ELUC (see Section 2.2.1). In the NGHGI reporting, the natural fluxes ( $S_{LAND}$ ) are counted  
978 towards ELUC when they occur on managed land (Grassi et al., 2018). To compare our results to the NGHGI  
979 approach, we perform a translation of our ELUC estimates by adding  $S_{LAND}$  in managed forest from the DGVMs



980 simulations (following the methodology described in Grassi et al., 2023) to the bookkeeping  $E_{LUC}$  estimate (see  
981 Supplement S.2.3). For the 2014-2023 period, we estimate that 1.8 GtC yr<sup>-1</sup> of  $S_{LAND}$  occurred in managed  
982 forests. Adding this sink to  $E_{LUC}$  changes  $E_{LUC}$  from being a source of 1.1 GtC yr<sup>-1</sup> to a sink of 0.7 GtC yr<sup>-1</sup>, very  
983 similar to the NGHGI estimate that yields a sink of 0.8 GtC yr<sup>-1</sup> (Figure 8, Table S10). We further apply a mask  
984 of managed land to the net atmosphere-to-land flux estimate from atmospheric inversions to obtain inverse  
985 estimates that are comparable to the NGHGI estimates and to the translated  $E_{LUC}$  estimates from bookkeeping  
986 models (see Supplement S.2.3). The inversion-based net flux in managed land indicates a sink of 0.7 GtC yr<sup>-1</sup>  
987 for 2014-2023, which agrees very well with the NGHGI and the translated  $E_{LUC}$  estimates (Figure 8, Table S10).  
988 Additionally, the interannual variability of the inversion estimates and the translated  $E_{LUC}$  estimates show a  
989 remarkable agreement (Pearson correlation of 0.81 in 2000-2023), which supports the suggested translation  
990 approach.

991 The translation approach has been shown to be generally applicable also at the country-level (Grassi et al., 2023;  
992 Schwingshackl et al., 2022). Country-level analysis suggests, e.g., that the bookkeeping method estimates higher  
993 deforestation emissions than the national report in Indonesia, but less CO<sub>2</sub> removal by afforestation than the  
994 national report in China. The fraction of the natural CO<sub>2</sub> sinks that the NGHGI estimates include differs  
995 substantially across countries, related to varying proportions of managed vs total forest areas (Schwingshackl et  
996 al., 2022). By comparing  $E_{LUC}$  and NGHGI on the basis of the component fluxes used above, we find that our  
997 estimates reproduce very closely the NGHGI estimates for emissions from permanent deforestation, peat  
998 emissions, and other transitions (Figure 8), although a difference in sign for the latter (small source in  
999 bookkeeping estimates, small sink in NGHGI) creates a notable difference between NGHGI and bookkeeping  
1000 estimates. Fluxes due to forest (re-)growth & other forest management, that is, (re-)growth from re/afforestation  
1001 plus the net flux from wood harvesting and other forest management and emissions and removals in shifting  
1002 cultivation cycles, constitute a large sink in the NGHGI (-1.9 GtC yr<sup>-1</sup> averaged over 2014-2023), since they  
1003 also include  $S_{LAND}$  in managed forests. Summing up the bookkeeping estimates of (re-)growth from  
1004 re/afforestation, the net flux from wood harvesting and other forest management, and the emissions and  
1005 removals in shifting cultivation cycles, and adding  $S_{LAND}$  in managed forests yields a flux of -2.0 GtC yr<sup>-1</sup>  
1006 (averaged over 2014-2023), which compares well with the NGHGI estimate. Though estimates between  
1007 NGHGI, FAOSTAT and the translated budget estimates still differ in value and need further analysis, the  
1008 approach suggested by Grassi et al. (2023), which we adopt here, provides a feasible way to relate the global  
1009 models' and NGHGI approach to each other and thus link the anthropogenic carbon budget estimates of land  
1010 CO<sub>2</sub> fluxes directly to the Global Stocktake, as part of the UNFCCC Paris Agreement.

### 1011 3.2.3 Final year 2023

1012 The global CO<sub>2</sub> emissions from land-use change are estimated as  $1.0 \pm 0.7$  GtC in 2023, similar to the 2022  
1013 estimate. However, confidence in the annual change remains low. Despite El Niño conditions, which in general  
1014 lead to more fires in deforestation areas, peat fire emissions in Indonesia remained below average (GFED4.1s;  
1015 updated from van der Werf et al., 2017). In South America, emissions from tropical deforestation and



1016 degradation fires have been about average, as effects of the El Niño in the Amazon, such as droughts, are not  
1017 expected before 2024.

### 1018 **3.2.4 Year 2024 Projection**

1019 In Southeast Asia, peat fire emissions have further dropped (from 27 Tg C in 2023 to 1 Tg C in 2024 through  
1020 October 17 2024; GFED4.1s, van der Werf et al., 2017), as have tropical deforestation and degradation fires  
1021 (from 33 Tg C to 6 Tg C) as the El Niño conditions ceased. By contrast, emissions from tropical deforestation  
1022 and degradation fires in South America have risen from 121 Tg C in 2023 to 324 Tg C in 2024 up until October  
1023 17, as the impacts of the El Niño unfold, in particular drought conditions since 2023. The 2024 South American  
1024 fire emissions are among the highest values in the record, which started in 1997. Part of the increase is due to  
1025 elevated fire activity in the wetlands of the Pantanal. Disentangling the degree to which interannual variability in  
1026 rainfall patterns and stronger environmental protection measures in both Indonesia after their 2015 high fire  
1027 season and in Brazil after the change in government play a role in fire trends is an important research topic.  
1028 Cumulative 2024 fire emission estimates through October 17 2024 are 422 Tg C for global deforestation and  
1029 degradation fires and 1 Tg C for peatland fires in Southeast Asia.

1030 Based on these estimates, we expect  $E_{LUC}$  emissions of around 1.1 GtC (4.2 GtCO<sub>2</sub>) in 2024, slightly above the  
1031 2023 level. Note that although our extrapolation includes tropical deforestation and degradation fires, the  
1032 degradation attributable to selective logging, edge-effects or fragmentation is not captured. Further,  
1033 deforestation and fires in deforestation zones may become more disconnected, partly due to changes in  
1034 legislation in some regions. For example, Van Wees et al. (2021) found that the contribution from fires to forest  
1035 loss decreased in the Amazon and in Indonesia over the period of 2003-2018.

### 1036 **3.3 CDR not based on vegetation**

1037 Besides the CDR through land use (Sec. 3.2), the atmosphere to geosphere flux of carbon resulting from carbon  
1038 dioxide removal (CDR) activity in 2023 is estimated at 0.011 MtC/yr. This results primarily from 0.009 MtC/yr  
1039 of enhanced weathering projects and 0.001 MtC/yr of DACCS. While it represents a growth of 200% in the  
1040 anthropogenic sink, from the 0.0036 MtC/yr estimate in 2022, it remains about a million times smaller than  
1041 current fossil CO<sub>2</sub> emissions.

### 1042 **3.4 Total anthropogenic emissions**

1043 Cumulative anthropogenic CO<sub>2</sub> emissions (fossil and land use) for 1850-2023 totalled  $710 \pm 70$  GtC ( $2605 \pm$   
1044  $260$  GtCO<sub>2</sub>), of which 70% (500 GtC) occurred since 1960 and 34% (240 GtC) since 2000 (Table 7 and 8).  
1045 Total anthropogenic emissions more than doubled over the last 60 years, from  $4.6 \pm 0.7$  GtC yr<sup>-1</sup> for the decade  
1046 of the 1960s to an average of  $10.8 \pm 0.9$  GtC yr<sup>-1</sup> during 2014-2023, and reaching  $11.1 \pm 0.9$  GtC ( $40.6 \pm 3.2$   
1047 GtCO<sub>2</sub>) in 2023. However, total anthropogenic CO<sub>2</sub> emissions have been stable over the last decade (zero  
1048 growth rate over the 2014-2023 period), much slower than the 2.0% growth rate over the previous decade  
1049 (2004-2013).



1050 During the historical period 1850-2023, 31% of historical emissions were from land use change and 69% from  
1051 fossil emissions. However, fossil emissions have grown significantly since 1960 while land use changes have  
1052 not, and consequently the contributions of land use change to total anthropogenic emissions were smaller during  
1053 recent periods, 18% during the period 1960-2023 and down to 10% over the last decade (2014-2023).

1054 For 2024, we project global total anthropogenic CO<sub>2</sub> emissions from fossil and land use changes to be around  
1055 11.3 GtC (41.6 GtCO<sub>2</sub>), 2% above the 2023 level. All values here include the cement carbonation sink (currently  
1056 about 0.2 GtC yr<sup>-1</sup>).

1057

### 1058 **3.5 Atmospheric CO<sub>2</sub>**

#### 1059 **3.5.1 Historical period 1850-2023**

1060 Atmospheric CO<sub>2</sub> concentration was approximately 278 parts per million (ppm) in 1750, reaching 300 ppm in  
1061 the late 1900s, 350 ppm in the late 1980s, and reaching 419.31 ± 0.1 ppm in 2023 (Lan et al., 2024; Figure 1).  
1062 The mass of carbon in the atmosphere increased by 51% from 590 GtC in 1750 to 890 GtC in 2023. Current  
1063 CO<sub>2</sub> concentrations in the atmosphere are unprecedented in the last 2 million years and the current rate of  
1064 atmospheric CO<sub>2</sub> increase is at least 10 times faster than at any other time during the last 800,000 years  
1065 (Canadell et al., 2021).

#### 1066 **3.5.2 Recent period 1960-2023**

1067 The growth rate in atmospheric CO<sub>2</sub> level increased from 1.7 ± 0.07 GtC yr<sup>-1</sup> in the 1960s to 5.2 ± 0.02 GtC yr<sup>-1</sup>  
1068 during 2014-2023 with important decadal variations (Table 7, Figure 3 and Figure 4). During the last decade  
1069 (2014-2023), the growth rate in atmospheric CO<sub>2</sub> concentration continued to increase, albeit with large  
1070 interannual variability (Figure 4).

1071 The airborne fraction (AF) is defined as the ratio of atmospheric CO<sub>2</sub> growth rate to total anthropogenic  
1072 emissions:

$$1073 \quad AF = G_{ATM} / (E_{FOS} + E_{LUC}) \quad (2)$$

1074 It provides a diagnostic of the relative strength of the land and ocean carbon sinks in removing part of the  
1075 anthropogenic CO<sub>2</sub> perturbation. The evolution of AF over the last 60 years shows no significant trend,  
1076 remaining at around 44%, albeit showing a large interannual and decadal variability driven by the year-to-year  
1077 variability in G<sub>ATM</sub> (Figure 10). The observed stability of the airborne fraction over the 1960-2023 period  
1078 indicates that the ocean and land CO<sub>2</sub> sinks have been increasing in pace with the total anthropogenic emissions  
1079 over that period, removing on average about 56% of the emissions (see Sections 3.6.2 and 3.7.2).



1080 **3.5.3 Final year 2023**

1081 The growth rate in atmospheric CO<sub>2</sub> concentration was  $5.9 \pm 0.2$  GtC ( $2.79 \pm 0.08$  ppm) in 2023 (Figure 4; Lan  
1082 et al., 2024), well above the 2022 growth rate ( $4.6 \pm 0.2$  GtC) or the 2014-2023 average ( $5.2 \pm 0.02$  GtC), as to  
1083 be expected during an El Niño year. The 2023 atmospheric CO<sub>2</sub> growth rate was the 4th largest over the 1959-  
1084 2023 atmospheric observational record, closely following 2015, 2016 and 1998, all strong El Niño years.

1085 **3.5.4 Year 2024 Projection**

1086 The 2024 growth in atmospheric CO<sub>2</sub> concentration ( $G_{ATM}$ ) is projected to be about 5.9 GtC (2.76 ppm), still  
1087 high, which is common for the year after a strong El Niño year. This is the average of the GCB regression  
1088 method (5.6 GtC, 2.64 ppm) and ESMs the multi-model mean (6.1 GtC, 2.88 ppm). The 2024 atmospheric CO<sub>2</sub>  
1089 concentration, averaged over the year, is expected to reach the level of 422.5 ppm, 52% over the pre-industrial  
1090 level.

1091 **3.6 Ocean Sink**

1092 **3.6.1 Historical period 1850-2023**

1093 Cumulated since 1850, the ocean sink adds up to  $185 \pm 35$  GtC, with more than two thirds of this amount ( $130 \pm$   
1094  $25$  GtC) being taken up by the global ocean since 1960. Over the historical period, the ocean sink increased in  
1095 pace with the anthropogenic emissions exponential increase (Figure 3). Since 1850, the ocean has removed 26%  
1096 of total anthropogenic emissions.

1097 **3.6.2 Recent period 1960-2023**

1098 The ocean CO<sub>2</sub> sink increased from  $1.2 \pm 0.4$  GtC yr<sup>-1</sup> in the 1960s to  $2.9 \pm 0.4$  GtC yr<sup>-1</sup> during 2014-2023  
1099 (Table 7), with interannual variations of the order of a few tenths of GtC yr<sup>-1</sup> (Figure 4, Figure 11). The ocean-  
1100 borne fraction ( $S_{OCEAN}/(E_{FOS}+E_{LUC})$ ) has been remarkably constant around 25% on average (Figure 10c), with  
1101 variations around this mean illustrating the decadal variability of the ocean carbon sink. So far, there is no  
1102 indication of a decrease in the ocean-borne fraction from 1960 to 2022. The increase of the ocean sink is  
1103 primarily driven by the increased atmospheric CO<sub>2</sub> concentration, with the strongest CO<sub>2</sub> induced signal in the  
1104 North Atlantic and the Southern Ocean (Figure 12a). The effect of climate change is much weaker, reducing the  
1105 ocean sink globally by  $0.17 \pm 0.05$  GtC yr<sup>-1</sup> (-5.9% of  $S_{OCEAN}$ ) during 2014-2023 (all models simulate a  
1106 weakening of the ocean sink by climate change, range -3.4 to -10.7%), and does not show clear spatial patterns  
1107 across the GOBMs ensemble (Figure 12b). This is the combined effect of change and variability in all  
1108 atmospheric forcing fields, previously attributed to wind and temperature changes (LeQuéré et al., 2010, Bunsen  
1109 et al., 2024). The effect of warming is smaller than expected from offline calculation due to a stabilising  
1110 feedback from limited exchange between surface and deep waters (Bunsen et al., 2024).

1111 The global net air-sea CO<sub>2</sub> flux is a residual of large natural and anthropogenic CO<sub>2</sub> fluxes into and out of the  
1112 ocean with distinct regional and seasonal variations (Figure 6 and S1). Natural fluxes dominate on regional





1113 scales, but largely cancel out when integrated globally (Gruber et al., 2009). Mid-latitudes in all basins and the  
1114 high-latitude North Atlantic dominate the ocean CO<sub>2</sub> uptake where low temperatures and high wind speeds  
1115 facilitate CO<sub>2</sub> uptake at the surface (Takahashi et al., 2009). In these regions, formation of mode, intermediate  
1116 and deep-water masses transport anthropogenic carbon into the ocean interior, thus allowing for continued CO<sub>2</sub>  
1117 uptake at the surface. Outgassing of natural CO<sub>2</sub> occurs mostly in the tropics, especially in the equatorial  
1118 upwelling region, and to a lesser extent in the North Pacific and polar Southern Ocean, mirroring a well-  
1119 established understanding of regional patterns of air-sea CO<sub>2</sub> exchange (e.g., Takahashi et al., 2009, Gruber et  
1120 al., 2009). These patterns are also noticeable in the Surface Ocean CO<sub>2</sub> Atlas (SOCAT) dataset, where an ocean  
1121  $f$ CO<sub>2</sub> value above the atmospheric level indicates outgassing (Figure S1). This map further illustrates the data-  
1122 sparsity in the Indian Ocean and the southern hemisphere in general.

1123 The largest variability in the ocean sink occurs on decadal time-scales (Figure 11). The ensemble means of  
1124 GOBMs and  $f$ CO<sub>2</sub>-products show the same patterns of decadal variability, although with a larger amplitude of  
1125 variability in the  $f$ CO<sub>2</sub>-products than in the GOBMs. The ocean sink stagnated in the 1990s and strengthened  
1126 between the early 2000s and the mid-2010s (Figure 11; Le Quéré et al., 2007; Landschützer et al., 2015, 2016;  
1127 DeVries et al., 2017; Hauck et al., 2020; McKinley et al., 2020, Gruber et al., 2023). More recently, the sink  
1128 seems to have entered a phase of stagnation since 2016, largely in response to large inter-annual climate  
1129 variability. Different explanations have been proposed for the decadal variability in the 1990s and 2000s,  
1130 ranging from the ocean's response to changes in atmospheric wind systems (e.g., Le Quéré et al., 2007, Keppler  
1131 and Landschützer, 2019), including variations in upper ocean overturning circulation (DeVries et al., 2017) to  
1132 the eruption of Mount Pinatubo in the 1990s (McKinley et al., 2020). The main origin of the decadal variability  
1133 is a matter of debate with a number of studies initially pointing to the Southern Ocean (see review in Canadell et  
1134 al., 2021), but also contributions from the North Atlantic and North Pacific (Landschützer et al., 2016, DeVries  
1135 et al., 2019), or a global signal (McKinley et al., 2020) were proposed.

1136 On top of the decadal variability, interannual variability of the ocean carbon sink is driven by climate variability  
1137 with a first-order effect from a stronger ocean sink during large El Niño events (e.g., 1997-1998) (Figure 11;  
1138 Rödenbeck et al., 2014, Hauck et al., 2020; McKinley et al. 2017) leading to a reduction in CO<sub>2</sub> outgassing from  
1139 the Tropical Pacific. During 2010-2016, the ocean CO<sub>2</sub> sink appears to have intensified in line with the expected  
1140 increase from atmospheric CO<sub>2</sub> (McKinley et al., 2020). This effect is similar in the  $f$ CO<sub>2</sub>-products (Figure 11,  
1141 ocean sink 2016 minus 2010, GOBMs:  $+0.42 \pm 0.11$  GtC yr<sup>-1</sup>,  $f$ CO<sub>2</sub>-products:  $+0.44$  GtC yr<sup>-1</sup>, range 0.18 to 0.72  
1142 GtC yr<sup>-1</sup>). The reduction of  $-0.18$  GtC yr<sup>-1</sup> (range:  $-0.41$  to  $-0.03$  GtC yr<sup>-1</sup>) in the ocean CO<sub>2</sub> sink in 2017 is  
1143 consistent with the return to normal conditions after the El Niño in 2015/16, which caused an enhanced sink in  
1144 previous years. After an increasing  $S_{\text{OCEAN}}$  in 2018 and 2019, the GOBM and  $f$ CO<sub>2</sub>-product ensemble means  
1145 suggest a decrease of  $S_{\text{OCEAN}}$ , related to the triple La Niña event 2020-2022, followed by a rebound in 2023  
1146 linked to the onset of an El Niño event.

1147 Although all individual GOBMs and  $f$ CO<sub>2</sub>-products fall within the observational constraint, the ensemble means  
1148 of GOBMs, and  $f$ CO<sub>2</sub>-products (adjusted for the riverine flux) show a mean offset increasing from 0.31 GtC yr<sup>-1</sup>  
1149 in the 1990s to 0.49 GtC yr<sup>-1</sup> in the decade 2014-2023 and a slightly lower offset of 0.3 GtC yr<sup>-1</sup> in 2023. In this



1150 version of the GCB, the  $S_{OCEAN}$  positive trend diverges over time by a factor of 1.4 since 2002 (GOBMs:  $0.25 \pm$   
1151  $0.04 \text{ GtC yr}^{-1}$  per decade,  $fCO_2$ -products:  $0.35 \text{ GtC yr}^{-1}$  per decade [ $0.17$  to  $0.79 \text{ GtC yr}^{-1}$  per decade],  $S_{OCEAN}$ :  
1152  $0.30 \text{ GtC yr}^{-1}$  per decade), but the uncertainty ranges overlap. This divergence is smaller than reported in  
1153 previous GCB versions, because of the updated lower sink estimates by the  $fCO_2$ -products for recent years. This  
1154 also leads to agreement on the trend since 2010 (GOBMs:  $0.18 \pm 0.06 \text{ GtC yr}^{-1}$  per decade,  $fCO_2$ -products:  $0.18$   
1155  $\text{GtC yr}^{-1}$  per decade [ $-0.36$  to  $0.73 \text{ GtC yr}^{-1}$  per decade]  $S_{OCEAN}$ :  $0.18 \text{ GtC yr}^{-1}$  per decade). A hybrid approach  
1156 recently constrained the trend 2000-2022 to  $0.42 \pm 0.06 \text{ GtC yr}^{-1} \text{ decade}^{-1}$  (Mayot et al., 2024), which aligns  
1157 with the updated trends of  $S_{OCEAN}$  ( $0.39 \text{ GtCyr}^{-1} \text{ decade}^{-1}$ ) and of the  $fCO_2$ -products ( $0.45 [0.28, 0.84] \text{ GtCyr}^{-1}$   
1158  $\text{decade}^{-1}$ ), while the GOBMs result in a lower trend ( $0.32 \pm 0.04 \text{ GtC yr}^{-1}$  per decade) over the same period.

1159 In the current dataset, the discrepancy between the two types of estimates stems from a persistently larger  
1160  $S_{OCEAN}$  in the  $fCO_2$ -products in the northern extra-tropics since around 2002 and an intermittently larger  $S_{OCEAN}$   
1161 in the southern extra-tropics in the period 2008-2020 (Figure 14). Note that the discrepancy in the mean flux,  
1162 which was located in the Southern Ocean in GCB 2022 and earlier, was reduced due to the choice of the  
1163 regional river flux adjustment (Lacroix et al., 2020 instead of Aumont et al., 2001). This comes at the expense of  
1164 a discrepancy in the mean  $S_{OCEAN}$  of about  $0.2 \text{ GtC yr}^{-1}$  in the tropics. Likely explanations for the discrepancy in  
1165 the trends and decadal variability in the high-latitudes are data sparsity and uneven data distribution (Bushinsky  
1166 et al., 2019, Gloege et al., 2021, Hauck et al., 2023a, Mayot et al., 2024). In particular, two  $fCO_2$ -products were  
1167 shown to overestimate the Southern Ocean  $CO_2$  flux trend by 50 and 130% based on current sampling in a  
1168 model subsampling experiment (Hauck et al., 2023a) and the largest trends in the  $fCO_2$ -products occurred in a  
1169 data void region in the North Pacific (Mayot et al., 2024). In this respect it is highly worrisome that the coverage  
1170 of  $fCO_2$  observations continues to decline (Dong et al 2024), and is now down to that of the early 2000s (Fig.  
1171 11). Another likely contributor to the discrepancy between GOBMs and  $fCO_2$ -products are model biases (as  
1172 indicated by the comparison with Mayot et al., 2024, by the large model spread in the South, Figure 14, and the  
1173 larger model-data  $fCO_2$  mismatch, Figure S2).

1174 The reported  $S_{OCEAN}$  estimate from GOBMs and  $fCO_2$ -products is  $2.2 \pm 0.4 \text{ GtC yr}^{-1}$  over the period 1994 to  
1175 2007, which is in agreement with the ocean interior estimate of  $2.2 \pm 0.4 \text{ GtC yr}^{-1}$ , which accounts for the  
1176 climate effect on the natural  $CO_2$  flux of  $-0.4 \pm 0.24 \text{ GtC yr}^{-1}$  (Gruber et al., 2019) to match the  
1177 definition of  $S_{OCEAN}$  used here (Hauck et al., 2020). This comparison depends critically on the estimate of the  
1178 climate effect on the natural  $CO_2$  flux, which is smaller from the GOBMs ( $-0.1 \text{ GtC yr}^{-1}$ ) than in Gruber et al.  
1179 (2019). Uncertainties of these two estimates would also overlap when using the GOBM estimate of the climate  
1180 effect on the natural  $CO_2$  flux. Similarly, the  $S_{OCEAN}$  estimates integrated over the decades 1994-2004 ( $21.5 \text{ GtC}$   
1181  $\text{yr}^{-1}$ ) and 2004-2014 ( $25.6 \text{ GtC yr}^{-1}$ ) agree with the interior ocean-based estimates of Müller et al. (2023;  $21.4 \pm$   
1182  $2.8$  and  $26.5 \pm 1.3 \text{ GtC yr}^{-1}$ ), but depend critically on assumptions of the climate effect on natural carbon, which  
1183 in turn, are based on the  $fCO_2$ -products in Müller et al. (2023).



1184 **3.6.3 Final year 2023**

1185 The estimated ocean CO<sub>2</sub> sink is  $2.9 \pm 0.4$  GtC for 2023. This is a small increase of 0.16 GtC compared to 2022,  
1186 in line with the expected sink strengthening from the 2023 El Niño conditions. GOBM and *f*CO<sub>2</sub>-product  
1187 ensemble mean estimates consistently result in an S<sub>OCEAN</sub> increase in 2023 (GOBMs:  $0.17 \pm 0.15$  GtC, *f*CO<sub>2</sub>-  
1188 products: 0.14 [-0.04,0.30] GtC). Eight GOBMs and six *f*CO<sub>2</sub>-products show an increase in S<sub>OCEAN</sub>, while only  
1189 two GOBMs and two *f*CO<sub>2</sub>-products show a minor decrease in S<sub>OCEAN</sub> of less than 0.05 GtC (Figure 11). The  
1190 *f*CO<sub>2</sub>-products have a larger uncertainty at the end of the reconstructed time series, potentially linked to  
1191 uncertainties related to fewer available observations in the final year and the shift from La Niña to El Niño (see  
1192 e.g. Watson et al 2020, Pérez et al 2024). Specifically, the *f*CO<sub>2</sub>-products' estimate of the last year is regularly  
1193 adjusted in the following release owing to the tail effect and an incrementally increasing data availability. While  
1194 the monthly grid cells covered may have a lag of only about a year (Figure 11 inset), the values within grid cells  
1195 may change with 1-5 years lag (see absolute number of observations plotted in previous GCB releases),  
1196 potentially resulting in annual changes in the flux magnitude from *f*CO<sub>2</sub>-products.

1197 **3.6.4 Year 2024 Projection**

1198 Using a feed-forward neural network method (see Section 2.5.2) we project an ocean sink of 3.0 GtC for 2024,  
1199 only 0.1 GtC higher than for the year 2023, consistent with El Niño to neutral conditions in 2024. The set of  
1200 ESMs predictions support this estimate with a 2024 ocean sink of around 3.0 [2.9, 3.1] GtC.

1201 **3.6.5 Evaluation of Ocean Models and *f*CO<sub>2</sub>-products**

1202 The process-based model evaluation draws a generally positive picture with GOBMs scattered around the  
1203 observational values for Southern Ocean sea-surface salinity, Southern Ocean stratification index and surface  
1204 ocean Revelle factor (Section S3.3 and Table S11). However, the Atlantic Meridional Overturning Circulation at  
1205 26°N is underestimated by 8 out of 10 GOBMs and overestimated by one GOBM. It is planned to derive skill  
1206 scores for the GOBMs in future releases based on these metrics.

1207 The model simulations allow to separate the anthropogenic carbon component (steady state and non-steady  
1208 state, sim D - sim A) and to compare the model flux and DIC inventory change directly to the interior ocean  
1209 estimate of Gruber et al. (2019) without further assumptions (Table S11). The GOBMs ensemble average of  
1210 anthropogenic carbon inventory changes 1994-2007 amounts to 2.4 GtC yr<sup>-1</sup> and is thus lower than the  $2.6 \pm 0.3$   
1211 GtC yr<sup>-1</sup> estimated by Gruber et al. (2019) although within the uncertainty. Only three models fall within the  
1212 range reported by Gruber et al. (2019). This suggests that the majority of the GOBMs underestimate  
1213 anthropogenic carbon uptake by 10-20% and some models even more. Comparison to the decadal estimates of  
1214 anthropogenic carbon accumulation (Müller et al., 2023) are close to the interior ocean data based estimate for  
1215 the decade 2004-2014 (GOBMs sim D minus sim A,  $24.7 \pm 3.6$  GtC yr<sup>-1</sup>, Müller et al.  $27.3 \pm 2.5$  GtC yr<sup>-1</sup>), but  
1216 do not reproduce the supposedly higher anthropogenic carbon accumulation in the earlier period 1994-2004  
1217 (GOBMs sim D minus sim A,  $21.1 \pm 3.0$  GtC yr<sup>-1</sup>, Müller et al.  $29.3 \pm 2.5$  GtC yr<sup>-1</sup>). Analysis of Earth System  
1218 Models indicate that an underestimation by about 10% may be due to biases in ocean carbon transport and



1219 mixing from the surface mixed layer to the ocean interior (Goris et al., 2018, Terhaar et al., 2021, Bourgeois et  
1220 al., 2022, Terhaar et al., 2022), biases in the chemical buffer capacity (Revelle factor) of the ocean (Vaittinada  
1221 Ayar et al., 2022; Terhaar et al., 2022) and partly due to a late starting date of the simulations (mirrored in  
1222 atmospheric CO<sub>2</sub> chosen for the preindustrial control simulation, Table S2, Bronselaer et al., 2017, Terhaar et  
1223 al., 2022; 2024). Interestingly, and in contrast to the uncertainties in the surface CO<sub>2</sub> flux, we find the largest  
1224 mismatch in interior ocean carbon accumulation in the tropics, with smaller contributions from the north and the  
1225 south. The large discrepancy in accumulation in the tropics highlights the role of interior ocean carbon  
1226 redistribution for those inventories (Khatiwala et al., 2009, DeVries et al., 2023).

1227 The evaluation of the ocean estimates with the *f*CO<sub>2</sub> observations from the SOCAT v2024 dataset for the period  
1228 1990-2023 shows an RMSE from annually detrended data of 0.2 to 2.4 μatm for the eight *f*CO<sub>2</sub>-products over  
1229 the globe (Figure S2). The GOBMs RMSEs are larger and range from 2.7 to 4.9 μatm. The RMSEs are  
1230 generally larger at high latitudes compared to the tropics, for both the *f*CO<sub>2</sub>-products and the GOBMs. The  
1231 *f*CO<sub>2</sub>-products have RMSEs of 0.3 to 2.9 μatm in the Tropics, 0.6 to 2.4 μatm in the North, and 0.8 to 2.4 μatm  
1232 in the South. Note that the *f*CO<sub>2</sub>-products are based on the SOCAT v2024 database, hence SOCAT is not an  
1233 independent dataset for the evaluation of the *f*CO<sub>2</sub>-products. The GOBMs RMSEs are more spread across  
1234 regions, ranging from 2.4 to 3.9 μatm in the tropics, 2.8 to 5.9 μatm in the North, and 2.7 to 6.0 μatm in the  
1235 South. The higher RMSEs occur in regions with stronger climate variability, such as the northern and southern  
1236 high latitudes (poleward of the subtropical gyres). Additionally, this year we evaluate the trends derived from a  
1237 subset of *f*CO<sub>2</sub>-products by subsampling four GOBMs used in Friedlingstein et al. (2023; covering the period up  
1238 to the year 2022) following the approach of Hauck et al. (2023a) and evaluating the air-sea CO<sub>2</sub> flux trend for  
1239 the 2001-2021 period, i.e. the period of strong divergence in the air-sea CO<sub>2</sub> exchange excluding the final year  
1240 to remove the tail effect, against trend biases identified by the GOBM reconstruction. The results indicate a  
1241 relationship between reconstruction bias and strength of the decadal trends (see Figure S3), indicating a  
1242 tendency of the *f*CO<sub>2</sub>-products ensemble to overestimate the air-sea CO<sub>2</sub> flux trends in agreement with a recent  
1243 study by Mayot et al. (2024).

## 1244 **3.7 Land Sink**

### 1245 **3.7.1 Historical period 1850-2023**

1246 Cumulated since 1850, the terrestrial CO<sub>2</sub> sink amounts to 220 ± 60 GtC, 31% of total anthropogenic emissions.  
1247 As for the ocean, more than two thirds of this amount (150 ± 40 GtC) have been taken up by terrestrial  
1248 ecosystems since 1960. Over the historical period, the sink increased in pace with the anthropogenic emissions  
1249 increase (Figure 3).

### 1250 **3.7.2 Recent period 1960-2023**

1251 The terrestrial CO<sub>2</sub> sink *S*<sub>LAND</sub> increased from 1.2 ± 0.5 GtC yr<sup>-1</sup> in the 1960s to 3.2 ± 0.9 GtC yr<sup>-1</sup> during 2014-  
1252 2023, with important interannual variations of up to 2 GtC yr<sup>-1</sup> generally showing a decreased land sink during  
1253 El Niño events (Figure 9), responsible for the corresponding enhanced growth rate in atmospheric CO<sub>2</sub>



1254 concentration. The larger land CO<sub>2</sub> sink during 2014-2023 compared to the 1960s is reproduced by all the  
1255 DGVMs in response to the increase in both atmospheric CO<sub>2</sub>, nitrogen deposition, and the changes in climate,  
1256 and is consistent with the residual estimated from the other budget terms ( $E_{\text{FOS}}+E_{\text{LUC}}-G_{\text{ATM}}-S_{\text{OCEAN}}$ , Table 5).

1257 Over the period 1960 to present the increase in the global terrestrial CO<sub>2</sub> sink is largely attributed to the CO<sub>2</sub>  
1258 fertilisation effect (Prentice et al., 2001, Piao et al., 2009, Schimel et al., 2015) and increased nitrogen  
1259 deposition (Huntzinger et al., 2017, O’Sullivan et al., 2019), directly stimulating plant photosynthesis and  
1260 increased plant water use in water limited systems, with a small negative contribution of climate change (Figure  
1261 12). There is a range of evidence to support a positive terrestrial carbon sink in response to increasing  
1262 atmospheric CO<sub>2</sub>, albeit with uncertain magnitude (Walker et al., 2021). As expected from theory, the greatest  
1263 CO<sub>2</sub> effect is simulated in the tropical forest regions, associated with warm temperatures and long growing  
1264 seasons (Hickler et al., 2008) (Figure 12a). However, evidence from tropical intact forest plots indicate an  
1265 overall decline in the land sink across Amazonia (1985-2011), attributed to enhanced mortality offsetting  
1266 productivity gains (Brienen et al., 2015, Hubau et al., 2020). During 2014-2023 the land sink is positive in all  
1267 regions (Figure 6) with the exception of eastern Brazil, Bolivia, northern Venezuela, Southwest USA, central  
1268 Europe and Central Asia, North and South Africa, and eastern Australia, where the negative effects of climate  
1269 variability and change (i.e. reduced rainfall and/or increased temperature) counterbalance CO<sub>2</sub> effects. This is  
1270 clearly visible on Figure 12 where the effects of CO<sub>2</sub> (Figure 12a) and climate (Figure 12b) as simulated by the  
1271 DGVMs are isolated. The negative effect of climate can be seen across the globe, and is particularly strong in  
1272 most of South America, Central America, Southwest US, Central Europe, western Sahel, southern Africa,  
1273 Southeast Asia and southern China, and eastern Australia (Figure 12b). Globally, over the 2014-2023 period,  
1274 climate change reduces the land sink by  $0.87 \pm 0.56 \text{ GtC yr}^{-1}$  (27% of  $S_{\text{LAND}}$ ).

1275 Most DGVMs have similar  $S_{\text{LAND}}$  averaged over 2014-2023, and 14/20 models fall within the  $1\sigma$  range of the  
1276 residual land sink [ $1.8\text{-}3.7 \text{ GtC yr}^{-1}$ ] (see Table 5), and all models but one are within the  $2\sigma$  range [ $0.8\text{-}4.6 \text{ GtC}$   
1277  $\text{yr}^{-1}$ ]. The ED model is an outlier, with a land sink estimate of  $5.1 \text{ GtC yr}^{-1}$  for the 2014-2023 period, driven by a  
1278 strong CO<sub>2</sub> fertilisation effect ( $6.3 \text{ GtC yr}^{-1}$  in the CO<sub>2</sub> only (S1) simulation). There are no direct global  
1279 observations of the land sink ( $S_{\text{LAND}}$ ), or the CO<sub>2</sub> fertilisation effect, and so we are not yet in a position to rule  
1280 out models based on component fluxes if their net land sink ( $S_{\text{LAND}}-E_{\text{LUC}}$ ) is within the observational uncertainty  
1281 provided by atmospheric inversions or O<sub>2</sub> measurements (Table 5). Furthermore, DGVMs were compared  
1282 against a model-data fusion based analysis of the land carbon cycle (CARDAMOM) (Bloom and Williams,  
1283 2015; Bloom et al., 2016). Results suggest good correspondence between approaches at the interannual  
1284 timescales, but divergence in the recent trend in  $S_{\text{LAND}}$  with CARDAMOM simulating a stronger trend than the  
1285 DGVM multi-model mean (Figure 9).

1286 Since 2020 the globe has experienced La Niña conditions which would be expected to lead to an increased land  
1287 carbon sink. This 3-year long period of La Niña conditions came to an end by the second half of 2023 and  
1288 transitioned to an El Niño which lasted until mid-2024. A clear transition from maximum to a minimum in the  
1289 global land sink is evident in  $S_{\text{LAND}}$ , from 2022 to 2023 and we find that a El Niño- driven decrease in tropical  
1290 land sink is offset by a smaller increase in the high latitude land sink. In the past years several regions



1291 experienced record-setting fire events (see also section 3.8.3). While global burned area has declined over the  
1292 past decades mostly due to declining fire activity in savannas (Andela et al., 2017), forest fire emissions are  
1293 rising and have the potential to counter the negative fire trend in savannas (Zheng et al., 2021). Noteworthy  
1294 extreme fire events include the 2019-2020 Black Summer event in Australia (emissions of roughly 0.2 GtC; van  
1295 der Velde et al., 2021), Siberia in 2021, where emissions approached 0.4 GtC or three times the 1997-2020  
1296 average according to GFED4s, and Canada in 2023 (Byrne et al., 2024). While other regions, including Western  
1297 US and Mediterranean Europe, also experienced intense fire seasons in 2021 their emissions are substantially  
1298 lower.

1299 Despite these regional negative effects of climate change on  $S_{\text{LAND}}$ , the efficiency of land to remove  
1300 anthropogenic  $\text{CO}_2$  emissions has remained broadly constant over the last six decades, with a land-borne  
1301 fraction ( $S_{\text{LAND}}/(E_{\text{FOS}}+E_{\text{LUC}})$ ) of around 30% (Figure 10b).

### 1302 **3.7.3 Final year 2023**

1303 The terrestrial  $\text{CO}_2$  sink from the DGVMs ensemble  $S_{\text{LAND}}$  was  $2.3 \pm 1.0$  GtC in 2023, 41% below the 2022 La  
1304 Niña induced strong sink of  $3.9 \pm 1.0$  GtC, and also below the 2014-2023 average of  $3.2 \pm 0.9$  GtC yr<sup>-1</sup> (Figure  
1305 4, Table 7). We estimate that the 2023 land sink was the lowest since 2015. The severe reduction in the land  
1306 sink in 2023 is likely driven by the El Niño conditions, leading to a 58% reduction in  $S_{\text{LAND}}$  in the tropics (30N-  
1307 30S) from 2.8 GtC in 2022 to 1.2 GtC in 2023. This is combined with intense wildfires in Canada that led to a  
1308 significant  $\text{CO}_2$  source (see also Section 3.8.3). We note that the  $S_{\text{LAND}}$  DGVMs estimate for 2023 of  $2.3 \pm 1.0$   
1309 GtC is very similar to the  $2.2 \pm 1.0$  GtC yr<sup>-1</sup> estimate from the residual sink from the global budget ( $E_{\text{FOS}}+E_{\text{LUC}}-  
1310 G_{\text{ATM-SOCEAN}}$ , Table 5).

### 1311 **3.7.4 Year 2024 Projection**

1312 Using a feed-forward neural network method we project a land sink of 3.2 GtC for 2024, 0.9 GtC larger than the  
1313 2023 estimate. As for the ocean sink, we attribute this to the transition from the El Niño conditions in 2023 to a  
1314 neutral state. The ESMs do not provide an additional estimate of  $S_{\text{LAND}}$  as they only simulate the net  
1315 atmosphere-land carbon flux ( $S_{\text{LAND}}-E_{\text{LUC}}$ ).

### 1316 **3.7.5 Land Models Evaluation**

1317 The evaluation of the DGVMs shows generally higher agreement across models for runoff, and to a lesser extent  
1318 for GPP, and ecosystem respiration. These conclusions are supported by a more comprehensive analysis of  
1319 DGVM performance in comparison with benchmark data (Sitch et al., 2024). A relative comparison of DGVM  
1320 performance (Figure S4) suggests several DGVMs (CABLE-POP, CLASSIC, OCN, ORCHIDEE) may  
1321 outperform others at multiple carbon and water cycle benchmarks. However, results from Seiler et al., 2022,  
1322 also show how DGVM differences are often of similar magnitude compared with the range across observational  
1323 datasets. All models score high enough over the metrics tests to support their use here. There are a few



1324 anomalously low scores for individual metrics from a single model, and these can direct the effort to improve  
1325 models for use in future budgets.

### 1326 **3.8 Partitioning the carbon sinks**

#### 1327 **3.8.1 Global sinks and spread of estimates**

1328 In the period 2014-2023, the bottom-up view of global net ocean and land carbon sinks provided by the GCB,  
1329  $S_{\text{OCEAN}}$  for the ocean and  $S_{\text{LAND}} - E_{\text{LUC}}$  for the land, agrees closely with the top-down global carbon sinks  
1330 delivered by the atmospheric inversions. This is shown in Figure 13, which visualises the individual decadal  
1331 mean atmosphere-land and atmosphere-ocean fluxes from each, along with the constraints on their sum offered  
1332 by the global fossil  $\text{CO}_2$  emissions flux minus the atmospheric growth rate ( $E_{\text{FOS}} - G_{\text{ATM}}$ ,  $4.4 \pm 0.5 \text{ Gt C yr}^{-1}$ ,  
1333 Table 7, shown as diagonal line on Figure 13). The GCB estimate for net atmosphere-to-surface flux ( $S_{\text{OCEAN}} +$   
1334  $S_{\text{LAND}} - E_{\text{LUC}}$ ) during 2014-2023 is  $4.9 \pm 1.2 \text{ Gt C yr}^{-1}$  (Table 7), with the difference to the diagonal representing  
1335 the budget imbalance ( $B_{\text{IM}}$ ) of  $0.4 \text{ Gt C yr}^{-1}$  discussed in Section 3.9. By virtue of the inversion methodology, the  
1336 atmospheric inversions estimate of the net atmosphere-to-surface flux during 2014-2023 is  $4.5 \text{ Gt C yr}^{-1}$ , with a  
1337  $< 0.1 \text{ Gt C yr}^{-1}$  imbalance, and thus scatter across the diagonal, with inverse models trading land for ocean fluxes  
1338 in their solution. The independent constraint on the net atmosphere-to-surface flux based on atmospheric  $\text{O}_2$  by  
1339 design also closes the balance and is  $4.5 \pm 0.9 \text{ Gt C yr}^{-1}$  over the 2014-2023 period (orange symbol on Figure  
1340 13), while the ESMs estimate for the net atmosphere-to-surface flux over that period average to  $4.7 [3.0, 5.8]$   
1341  $\text{Gt C yr}^{-1}$  (Tables 5 and 6).

1342 The distributions based on the individual models and  $f\text{CO}_2$ -products reveal substantial spread but converge near  
1343 the decadal means quoted in Tables 5 to 7. Sink estimates for  $S_{\text{OCEAN}}$  and from inverse systems are mostly non-  
1344 Gaussian, while the ensemble of DGVMs appears more normally distributed justifying the use of a multi-model  
1345 mean and standard deviation for their errors in the budget. Noteworthy is that the tails of the distributions  
1346 provided by the land and ocean bottom-up estimates would not agree with the global constraint provided by the  
1347 fossil fuel emissions and the observed atmospheric  $\text{CO}_2$  growth rate. This illustrates the power of the  
1348 atmospheric joint constraint from  $G_{\text{ATM}}$  and the global  $\text{CO}_2$  observation network it derives from.

##### 1349 **3.8.1.1 Net atmosphere-to-land flux**

1350 The GCB estimate of the net atmosphere-to-land flux ( $S_{\text{LAND}} - E_{\text{LUC}}$ ), calculated as the difference between  
1351  $S_{\text{LAND}}$  from the DGVMs and  $E_{\text{LUC}}$  from the bookkeeping models, amounts to a  $2.1 \pm 1.1 \text{ Gt C yr}^{-1}$  sink during  
1352 2014-2023 (Table 5). Estimates of net atmosphere-to-land flux ( $S_{\text{LAND}} - E_{\text{LUC}}$ ) from the DGVMs alone ( $1.7 \pm$   
1353  $0.6 \text{ Gt C yr}^{-1}$ , Table 5, green symbol on Figure 13) are slightly lower, although within the uncertainty of the GCB  
1354 estimate and also within uncertainty of the global carbon budget constraint ( $E_{\text{FOS}} - G_{\text{ATM}} - S_{\text{OCEAN}}$ ,  $1.6 \pm 0.6 \text{ Gt C}$   
1355  $\text{yr}^{-1}$ ; Table 7). Also, for 2014-2023, the inversions estimate the net atmosphere-to-land flux is a  $1.4 [0.3, 2.2]$   
1356  $\text{Gt C yr}^{-1}$  sink, slightly lower than the mean of the DGVMs estimates (purple versus grey symbols on Figure 13).  
1357 The independent constraint based on atmospheric  $\text{O}_2$  is even lower,  $1.0 \pm 0.8 \text{ Gt C yr}^{-1}$  (orange symbol in Figure  
1358 13), although its large uncertainty overlaps with the uncertainty range from other approaches. Last, the ESMs



1359 estimate for the net atmosphere-to-land flux during 2014-2023 is a 2.2 [0.3, 3.6] GtC yr<sup>-1</sup> sink, more consistent  
1360 with the GCB estimates of  $S_{\text{LAND}} - \bar{E}_{\text{LUC}}$  (Figure 14 top row).

1361 As discussed in Section 3.5.3, the atmospheric growth rate of CO<sub>2</sub> was very high in 2023, 5.9 GtC (2.79 ppm)  
1362 the 4<sup>th</sup> largest on record. Both DGVMs and inversions assign this large CO<sub>2</sub> growth rate to a severe decrease of  
1363 the net atmosphere to land flux, and in particular in the tropics (Figure 14). DGVMs simulate a 2023 global the  
1364 net atmosphere-to-land flux of 1.1 GtC yr<sup>-1</sup>, a 55% decline relative to the 2.4 GtC yr<sup>-1</sup> sink in 2022, primarily  
1365 driven by the severe reduction in  $S_{\text{LAND}}$  (-41%, see Section 3.7.3). The tropics (30N-30S) are recording a  
1366 dramatic decrease in the net atmosphere-to-land flux from 1.5 GtC yr<sup>-1</sup> in 2022 to 0.1 GtC yr<sup>-1</sup> in 2023. The  
1367 atmospheric inversion shows a similar story with the global net atmosphere-to-land flux declining from 2.6 GtC  
1368 yr<sup>-1</sup> in 2022 to 0.9 GtC yr<sup>-1</sup> in 2023 (-64%), with the tropics turning from a 1.0 GtC yr<sup>-1</sup> sink in 2022 to a 0.4  
1369 GtC yr<sup>-1</sup> source in 2023. Our results are broadly consistent with the Ke et al. (2024) study which reported a  
1370 global atmosphere-to-land flux of  $0.4 \pm 0.2$  GtC yr<sup>-1</sup> in 2023.

1371 In addition to the large decline of the tropical land uptake, the northern extra tropics experienced warmer than  
1372 average conditions, in particular in the summer over North America and North Eurasia. In Canada alone, 2023  
1373 led to enhanced CO<sub>2</sub> release due to fires of 0.5-0.8 GtC yr<sup>-1</sup> (see Section 3.8.3). The atmospheric inversions do  
1374 simulate a slight reduction of the atmosphere-to-land flux in the northern extra-tropics (north of 30°N), from  
1375 1.6 GtC yr<sup>-1</sup> in 2022 to 1.4 GtC yr<sup>-1</sup> in 2023, while the DGVM fail to capture this pattern, with a simulated  
1376 northern extra-tropics net atmosphere-to-land flux larger in 2023 than in 2022 (1.0 vs 0.7 GtC yr<sup>-1</sup>).

### 1377 3.8.1.2 Net atmosphere-to-ocean flux

1378 For the 2014-2023 period, the GOBMs ( $2.6 \pm 0.4$  GtC yr<sup>-1</sup>) produce a lower estimate for  $S_{\text{OCEAN}}$  than the  $f\text{CO}_2$ -  
1379 products with 3.1 [2.9, 3.7] GtC yr<sup>-1</sup>, which shows up in Figure 13 as separate peaks in the distribution from the  
1380 GOBMs (dark blue symbols) and from the  $f\text{CO}_2$ -products (light blue symbols). Atmospheric inversions (3.1  
1381 [2.4, 4.1] GtC yr<sup>-1</sup>) suggest an ocean uptake more in line with the  $f\text{CO}_2$ -products for the recent decade (Table 7),  
1382 although the inversions range includes both the GOBMs and  $f\text{CO}_2$ -products estimates (Figure 14 top row) and  
1383 the inversions are not fully independent as 6 out of 10 inversions covering the last decade use  $f\text{CO}_2$ -products as  
1384 ocean priors and one uses a GOBM (Table S4). The independent constraint based on atmospheric O<sub>2</sub> ( $3.4 \pm 0.5$   
1385 GtC yr<sup>-1</sup>) is at the high end of the distribution of the other methods. However, as mentioned in section 2.8, the  
1386 O<sub>2</sub> method requires a correction for global air-sea O<sub>2</sub> flux, which induces a non-negligible uncertainty on the  
1387 decadal estimates (about 0.5 GtC yr<sup>-1</sup>). The large growth in the ocean carbon sink from O<sub>2</sub> is compatible with  
1388 the GOBMs and  $f\text{CO}_2$ -products estimates when accounting for their uncertainty ranges. Lastly, the ESMs  
1389 estimate, 2.5 [2.2, 2.8] GtC yr<sup>-1</sup>, suggest a moderate ocean carbon sink, comparable to the GOBMs estimate with  
1390 regard to mean and spread. We caution that the riverine transport of carbon taken up on land and outgassing  
1391 from the ocean, accounted for here, is a substantial ( $0.65 \pm 0.3$  GtC yr<sup>-1</sup>) and uncertain term (Crisp et al., 2022;  
1392 Gruber et al., 2023; DeVries et al., 2023) that separates the GOBMs, ESMs and oxygen-based estimates on the  
1393 one hand from the  $f\text{CO}_2$ -products and atmospheric inversions on the other hand.





1394 **3.8.2 Regional partitioning**

1395 Figure 14 shows the latitudinal partitioning of the global atmosphere-to-ocean ( $S_{\text{OCEAN}}$ ), atmosphere-to-land  
1396 ( $S_{\text{LAND}} - E_{\text{LUC}}$ ), and their sum ( $S_{\text{OCEAN}} + S_{\text{LAND}} - E_{\text{LUC}}$ ) according to the estimates from GOBMs and ocean  
1397  $f\text{CO}_2$ -products ( $S_{\text{OCEAN}}$ ), DGVMs ( $S_{\text{LAND}} - E_{\text{LUC}}$ ), and from atmospheric inversions ( $S_{\text{OCEAN}}$  and  $S_{\text{LAND}} - E_{\text{LUC}}$ ).

1398 **3.8.2.1 North**

1399 Despite being one of the most densely observed and studied regions of our globe, annual mean carbon sink  
1400 estimates in the northern extra-tropics (north of  $30^\circ\text{N}$ ) continue to differ. The atmospheric inversions suggest an  
1401 atmosphere-to-surface sink ( $S_{\text{OCEAN}} + S_{\text{LAND}} - E_{\text{LUC}}$ ) for 2014-2023 of  $2.6 [2.0 \text{ to } 3.4] \text{ GtC yr}^{-1}$ , which is slightly  
1402 higher than the process models' estimate of  $2.2 \pm 0.4 \text{ GtC yr}^{-1}$  (Figure 14). The GOBMs ( $1.2 \pm 0.2 \text{ GtC yr}^{-1}$ ),  
1403  $f\text{CO}_2$ -products ( $1.4 [1.3-1.5] \text{ GtC yr}^{-1}$ ), and inversion systems ( $1.2 [0.9 \text{ to } 1.4] \text{ GtC yr}^{-1}$ ) produce largely  
1404 consistent estimates of the ocean sink. However, the larger flux in the  $f\text{CO}_2$ -products may be related to data  
1405 sparsity (Mayot et al., 2024). Thus, the difference mainly arises from the net land flux ( $S_{\text{LAND}} - E_{\text{LUC}}$ ) estimate,  
1406 which is  $1.0 \pm 0.4 \text{ GtC yr}^{-1}$  in the DGVMs compared to  $1.5 [0.6 \text{ to } 2.3] \text{ GtC yr}^{-1}$  in the atmospheric inversions  
1407 (Figure 14, second row).

1408 Discrepancies in the northern land fluxes conforms with persistent issues surrounding the quantification of the  
1409 drivers of the global net land  $\text{CO}_2$  flux (Arneeth et al., 2017; Huntzinger et al., 2017; O'Sullivan et al., 2022) and  
1410 the distribution of atmosphere-to-land fluxes between the tropics and high northern latitudes (Baccini et al.,  
1411 2017; Schimel et al., 2015; Stephens et al., 2007; Ciais et al., 2019; Gaubert et al., 2019).

1412 In the northern extra-tropics, the process models, inversions, and  $f\text{CO}_2$ -products consistently suggest that most  
1413 of the interannual variability stems from the land (Figure 14). Inversions generally agree on the magnitude of  
1414 interannual variations (IAV) over land, more so than DGVMs ( $0.29-0.32$  vs  $0.14-0.63 \text{ GtC yr}^{-1}$ , averaged over  
1415 1990-2023).

1416 **3.8.2.2 Tropics**

1417 In the tropics ( $30^\circ\text{S}-30^\circ\text{N}$ ), both the atmospheric inversions and process models estimate a net carbon balance  
1418 ( $S_{\text{OCEAN}} + S_{\text{LAND}} - E_{\text{LUC}}$ ) that is relatively close to neutral over the past decade (inversions:  $0.3 [-0.4, 0.9] \text{ GtC yr}$   
1419  $^{-1}$ , process models:  $0.6 \pm 0.6 \text{ GtC yr}^{-1}$ ). The GOBMs ( $-0.03 \pm 0.3 \text{ GtC yr}^{-1}$ ),  $f\text{CO}_2$ -products ( $0.3 [0.1, 0.6] \text{ GtC yr}^{-1}$ ),  
1420 and inversion systems ( $0.3 [-0.1, 0.8] \text{ GtC yr}^{-1}$ ) indicate a neutral to positive tropical ocean flux (see Figure S1  
1421 for spatial patterns). DGVMs indicate a net land sink ( $S_{\text{LAND}} - E_{\text{LUC}}$ ) of  $0.6 \pm 0.4 \text{ GtC yr}^{-1}$ , whereas the inversion  
1422 systems indicate a neutral net land flux although with large model spread ( $-0.0 [-0.9, 0.8] \text{ GtC yr}^{-1}$ , (Figure 14,  
1423 third row).

1424 The tropical lands are the origin of most of the atmospheric  $\text{CO}_2$  interannual variability (Ahlström et al., 2015),  
1425 consistently among the process models and inversions (Figure 14). The interannual variability in the tropics is  
1426 similar among the ocean  $f\text{CO}_2$ -products ( $0.06-0.16 \text{ GtC yr}^{-1}$ ) and the GOBMs ( $0.07-0.16 \text{ GtC yr}^{-1}$ , Figure S2).  
1427 The DGVMs and inversions indicate that atmosphere-to-land  $\text{CO}_2$  fluxes are more variable than atmosphere-to-



1428 ocean CO<sub>2</sub> fluxes in the tropics, with interannual variability of 0.37 to 1.33 and 0.86-0.96 GtC yr<sup>-1</sup> for DGVMs  
1429 and inversions, respectively.

### 1430 3.8.2.3 South

1431 In the southern extra-tropics (south of 30°S), the atmospheric inversions suggest a net atmosphere-to-surface  
1432 sink (SOCEAN+SLAND-ELUC) for 2014-2023 of 1.5 [1.2, 1.9] GtC yr<sup>-1</sup>, identical to the process models' estimate of  
1433 1.5 ± 0.4 GtC yr<sup>-1</sup> (Figure 14). An approximately neutral net land flux (SLAND-ELUC) for the southern extra-  
1434 tropics is estimated by both the DGVMs (0.05 ± 0.1 GtC yr<sup>-1</sup>) and the inversion systems (-0.03 [-0.11, 0.08] GtC  
1435 yr<sup>-1</sup>). This means nearly all carbon uptake is due to oceanic sinks south of 30°S. The Southern Ocean flux in the  
1436 fCO<sub>2</sub>-products (1.5[1.3, 1.7 GtC] yr<sup>-1</sup>) and inversion estimates (1.6 [1.2, 1.9] GtCyr-1) is marginally higher than  
1437 in the GOBMs (1.4 ± 0.4 GtC yr<sup>-1</sup>) (Figure 14, bottom row). This agreement is subject to the choice of the river  
1438 flux adjustment (Lacroix et al., 2020, Hauck et al., 2023b). Nevertheless, the time-series of atmospheric  
1439 inversions and fCO<sub>2</sub>-products diverge from the GOBMs. A substantial overestimation of the trends in the fCO<sub>2</sub>-  
1440 products could be explained by sparse and unevenly distributed observations, especially in wintertime (Figure  
1441 S1; Hauck et al., 2023a; Gloege et al., 2021). Model biases may contribute as well, with biases in mode water  
1442 formation, stratification, and the chemical buffer capacity known to play a role in Earth System Models (Terhaar  
1443 et al., 2021, Bourgeois et al., 2022, Terhaar et al., 2022).

1444 The interannual variability in the southern extra-tropics is low because of the dominance of ocean areas with  
1445 low variability compared to land areas. The split between land (SLAND-ELUC) and ocean (SOCEAN) shows a  
1446 substantial contribution to variability in the south coming from the land, with no consistency between the  
1447 DGVMs and the inversions or among inversions. This is expected due to the difficulty of separating exactly the  
1448 land and oceanic fluxes when viewed from atmospheric observations alone. The SOCEAN interannual variability  
1449 was found to be higher in the fCO<sub>2</sub>-products (0.04-0.20 GtC yr<sup>-1</sup>) compared to GOBMs (0.04 to 0.06 GtC yr<sup>-1</sup>)  
1450 in 1990-2023 (Figure S2). Inversions give an interannual variability of 0.10 to 0.13 GtC yr<sup>-1</sup>. Model  
1451 subsampling experiments recently illustrated that fCO<sub>2</sub>-products may overestimate decadal variability in the  
1452 Southern Ocean carbon sink by 30% and the trend since 2000 by 50-130% due to data sparsity, based on one  
1453 and two fCO<sub>2</sub>-products with strong variability (Gloege et al., 2021, Hauck et al., 2023a). The trend benchmark  
1454 test using the method of Hauck et al., (2023a) and a subset of 6 fCO<sub>2</sub>-products confirms the sensitivity of the  
1455 decadal trends in fCO<sub>2</sub>-products to reconstruction biases, particularly in the Southern Ocean, indicating an  
1456 overestimation of the ensemble mean trend. However, we also find compensating positive biases in the  
1457 ensemble so that the ensemble mean bias is smaller than the bias from some individual fCO<sub>2</sub>-products.

### 1458 3.8.2.4 RECCAP2 regions

1459 Aligning with the RECCAP-2 initiative (Ciais et al., 2022; Poulter et al., 2022; DeVries et al., 2023), we  
1460 provide a breakdown of this GCB paper estimate of the ELUC, SLAND, Net land (SLAND - ELUC), and SOCEAN fluxes  
1461 over the 10 land, and 5 ocean RECCAP-2 regions, averaged over the period 2014-2023 (Figure 15). The  
1462 DGVMs and inversions suggest a positive net land sink in all regions, except for South America and Africa,



1463 where the inversions indicate a small net source of respectively  $-0.1 [-0.8, 0.3]$   $\text{GtC yr}^{-1}$  and  $-0.3 [-0.7, -0.1]$   
1464  $\text{GtC yr}^{-1}$ , compared to a small sink of  $0.1 \pm 0.3$   $\text{GtC yr}^{-1}$  and  $0.3 \pm 0.1$   $\text{GtC yr}^{-1}$  for the DGVMs. However, for  
1465 South America, there is substantial uncertainty in both products (ensembles span zero). For the DGVMs, this is  
1466 driven by uncertainty in both  $S_{\text{LAND}}$  ( $0.5 \pm 0.4$   $\text{GtC yr}^{-1}$ ) and  $E_{\text{LUC}}$  ( $0.4 \pm 0.2$   $\text{GtC yr}^{-1}$ ). The bookkeeping models  
1467 also suggest an  $E_{\text{LUC}}$  source of around  $0.4$   $\text{GtC yr}^{-1}$  in South America and Africa, in line with the DGVMs  
1468 estimates. Bookkeeping models and DGVMs similarly estimate a source of  $0.3$ - $0.4$   $\text{GtC yr}^{-1}$  in Southeast Asia,  
1469 with DGVMs suggesting a small net land sink ( $0.1 \pm 0.1$   $\text{GtC yr}^{-1}$ ). This is similar to the inversion mean estimate  
1470 of a  $0.1 [-0.3, 0.8]$   $\text{GtC yr}^{-1}$  sink, although the inversion spread is substantial. The inversions suggest the largest  
1471 net land sinks are located in North America ( $0.5 [-0.1, 1.0]$   $\text{GtC yr}^{-1}$ ), Russia ( $0.6 [0.1, 0.9]$   $\text{GtC yr}^{-1}$ ), and East  
1472 Asia ( $0.4 [-0.2, 1.3]$   $\text{GtC yr}^{-1}$ ). This agrees well with the DGVMs in North America ( $0.4 \pm 0.1$   $\text{GtC yr}^{-1}$ ), which  
1473 indicate a large natural land sink ( $S_{\text{LAND}}$ ) of  $0.6 \pm 0.2$   $\text{GtC yr}^{-1}$ , being slightly reduced by land-use related carbon  
1474 losses ( $0.2 \pm 0.1$   $\text{GtC yr}^{-1}$ ). The DGVMs suggest a smaller net land sink in Russia compared to inversions  
1475 ( $0.3 \pm 0.2$   $\text{GtC yr}^{-1}$ ), and a similar net sink in East Asia ( $0.2 \pm 0.1$   $\text{GtC yr}^{-1}$ ).

1476 There is generally a higher level of agreement in the estimates of regional  $S_{\text{OCEAN}}$  between the different data  
1477 streams (GOBMs,  $f\text{CO}_2$ -products and atmospheric inversions) on decadal scale, compared to the agreement  
1478 between the different land flux estimates. All data streams agree that the largest contribution to  $S_{\text{OCEAN}}$  stems  
1479 from the Southern Ocean due to a combination of high flux density and large surface area, but with important  
1480 contributions also from the Atlantic (high flux density) and Pacific (large area) basins. In the Southern Ocean,  
1481 GOBMs suggest a sink of  $1.0 \pm 0.3$   $\text{GtC yr}^{-1}$ , in line with the  $f\text{CO}_2$ -products ( $1.0 [0.8, 1.3]$   $\text{GtC yr}^{-1}$ ) and  
1482 atmospheric inversions ( $1.0 [0.7, 1.4]$   $\text{GtC yr}^{-1}$ ). There is similar agreement in the Pacific ocean, with GOBMs,  
1483  $f\text{CO}_2$ -products, and atmospheric inversions indicating a sink of  $0.6 \pm 0.2$   $\text{GtC yr}^{-1}$ ,  $0.7 [0.6, 1.0]$   $\text{GtC yr}^{-1}$ , and  
1484  $0.6 [0.1, 1.0]$   $\text{GtC yr}^{-1}$ , respectively. However, in the Atlantic ocean, GOBMs simulate a sink of  $0.5 \pm 0.1$   $\text{GtC}$   
1485  $\text{yr}^{-1}$ , noticeably lower than both the  $f\text{CO}_2$ -products ( $0.8 [0.7, 1.0]$   $\text{GtC yr}^{-1}$ ) and atmospheric inversions ( $0.7$   
1486  $[0.4, 1.1]$   $\text{GtC yr}^{-1}$ ). It is important to note the  $f\text{CO}_2$ -products and atmospheric inversions have a substantial and  
1487 uncertain river flux adjustment in the Atlantic ocean ( $0.3$   $\text{GtC yr}^{-1}$ ) that also leads to a mean offset between  
1488 GOBMs and  $f\text{CO}_2$ -products/inversions in the latitude band of the tropics (Figure 14). The Indian Ocean due its  
1489 smaller size and the Arctic Ocean due to its size and sea-ice cover that prevents air-sea gas-exchange are  
1490 responsible for smaller but non negligible  $S_{\text{OCEAN}}$  fluxes (Indian Ocean:  $0.3 [0.2, 0.3]$   $\text{GtC yr}^{-1}$ ,  $0.3 [0.3, 0.4]$   
1491  $\text{GtC yr}^{-1}$ , and  $0.4 [0.3, 0.6]$   $\text{GtC yr}^{-1}$  for GOBMs,  $f\text{CO}_2$ -products, and atmospheric inversions, respectively, and  
1492 Arctic Ocean:  $0.1 [0.1, 0.1]$   $\text{GtC yr}^{-1}$ ,  $0.2 [0.1, 0.2]$   $\text{GtC yr}^{-1}$ , and  $0.1 [0.1, 0.2]$   $\text{GtC yr}^{-1}$  for GOBMs,  $f\text{CO}_2$ -  
1493 products, and atmospheric inversions, respectively). Note that the  $S_{\text{OCEAN}}$  numbers presented here deviate from  
1494 numbers reported in RECCAP-2 where the net air-sea  $\text{CO}_2$  flux is reported (i.e. without river flux adjustment for  
1495  $f\text{CO}_2$ -products and inversions, and with river flux adjustment subtracted from GOBMs in most chapters, or  
1496 comparing unadjusted datasets with discussion of uncertain regional riverine fluxes as major uncertainty, e.g.  
1497 Sarma et al., 2023, DeVries et al., 2023).



1498 **3.8.2.5 Tropical vs northern land uptake**

1499 A continuing conundrum is the partitioning of the global atmosphere-land flux between the northern hemisphere  
1500 land and the tropical land (Stephens et al., 2017; Pan et al., 2011; Gaubert et al., 2019). It is of importance  
1501 because each region has its own history of land-use change, climate drivers, and impact of increasing  
1502 atmospheric CO<sub>2</sub> and nitrogen deposition. Quantifying the magnitude of each sink is a prerequisite to  
1503 understanding how each individual driver impacts the tropical and mid/high-latitude carbon balance.

1504 We define the North-South (N-S) difference as net atmosphere-land flux north of 30°N minus the net  
1505 atmosphere-land flux south of 30°N. For the inversions, the N-S difference is 1.50 [0.05,3.0] GtC yr<sup>-1</sup> across  
1506 this year's inversion ensemble. An apparent clustering of six satellite-driven solutions towards a common NH  
1507 land sink noted in GCB2023 is no longer clear.

1508 In the ensemble of DGVMs the N-S difference is  $0.4 \pm 0.5$  GtC yr<sup>-1</sup>, a much narrower range than the one from  
1509 atmospheric inversions. Only three out of twenty DGVMs have a N-S difference larger than 1.0 GtC yr<sup>-1</sup>,  
1510 compared to half of the inversion systems simulating a difference at least this large. The smaller spread across  
1511 DGVMs than across inversions is to be expected as there is no correlation between Northern and Tropical land  
1512 sinks in the DGVMs as opposed to the inversions where the sum of the two regions being well-constrained by  
1513 atmospheric observations leads to an anti-correlation between these two regions. This atmospheric N-S gradient  
1514 could be used as an additional way to evaluate tropical and NH uptake in DGVMs, if their fluxes were  
1515 combined with multiple transport models. Vice versa, the much smaller spread in the N-S difference between  
1516 the DGVMs could help to scrutinise the inverse systems further. For example, a large northern land sink and a  
1517 tropical land source in an inversion would suggest a large sensitivity to CO<sub>2</sub> fertilisation (the dominant factor  
1518 driving the land sinks) for Northern ecosystems, which would be not mirrored by tropical ecosystems. Such a  
1519 combination could be hard to reconcile with the process understanding gained from the DGVM ensembles and  
1520 independent measurements (e.g. Free Air CO<sub>2</sub> Enrichment experiments).

1521 **3.8.3 Fire Emissions in 2024**

1522 Fire emissions so far in 2024 have been above the average of recent decades, chiefly due to synchronous large  
1523 emissions fluxes from North and South America. Figure S9 shows global and regional emissions estimates for  
1524 the period 1st Jan-30th September in each year 2003-2024. Estimates derive from two global fire emissions  
1525 products: the global fire emissions database (GFED, version 4.1s; van der Werf et al., 2017), and the global fire  
1526 assimilation system (GFAS, operated by the Copernicus Atmosphere Service; Kaiser et al., 2012). The two  
1527 products estimate that global emissions from fires were 1.6-2.2 GtC yr<sup>-1</sup> during January-September 2024. These  
1528 estimates are 11-32% above the 2014-2023 average for the same months (1.5-1.7 GtC yr<sup>-1</sup>). In the GFED4.1s  
1529 product, the year-to-date emissions in 2024 were highest since 2003, exceeding even the large emissions  
1530 estimate of 2023, whereas the GFAS product showed lower emissions in 2024 than in 2023 and six other years  
1531 since 2003.



1532 The pattern of high fire emissions from Canada in 2023, which were record-breaking (Jones et al., 2024b, Byrne  
1533 et al., 2024), continued into 2024. In January-September 2024, emissions from Canada ( $0.2\text{--}0.3\text{ GtC yr}^{-1}$ ) were  
1534 half as great as in the same months of 2023 ( $0.5\text{--}0.8\text{ GtC yr}^{-1}$ ) but still 2.1-2.3 times the average of January-  
1535 September periods in 2014-2023 (and 4-6 times greater than the average of those months in 2003-2022  
1536 [excluding the record-breaking year in 2023]; Figure S9). The continued anomaly in Canada propagated to the  
1537 northern hemisphere, where emissions of  $0.5\text{--}0.6\text{ GtC yr}^{-1}$  were 26-44% above the average of 2014-2023.

1538 In January-September 2024, fire emissions from South America ( $0.4\text{--}0.6\text{ GtC yr}^{-1}$ ) were 94-164% above the  
1539 average of January-September periods in 2014-2023, marking 2024 out as a year with synchronous high fire  
1540 emissions across the Americas. Emissions from Brazil in January-September 2024 ( $0.2\text{--}0.3\text{ GtC yr}^{-1}$ ) were 91-  
1541 118% above the average of January-September periods of 2014-2023 and were at a level not seen since the  
1542 major drought year of 2010 (Figure S9; Aragão et al., 2018, Silva Junior et al., 2019). In 2023, deforestation fire  
1543 activity in the Brazilian Amazon was below the average levels recorded in national recording systems and  
1544 attributed to renewed environmental policy implementation, however the fall in Amazon deforestation fire  
1545 activity was largely offset by above-average wildfires related to historic drought (Mataveli et al. 2024).  
1546 According to the National Center for Monitoring and Early Warning of Natural Disasters (CEMADEN), drought  
1547 conditions continued into 2024 and the current drought is the most intense and widespread Brazil has  
1548 experienced since records began in 1950 (CEMADEN, 2024), prompting large wildfires anomalies across the  
1549 Amazon, Cerrado and Pantanal regions (INPE, 2024).

1550 Emissions anomalies in Africa strongly influence global totals because the continent typically contributed 41-  
1551 47% of global fire emissions during 2014-2023 (average of January-September periods). GFAS suggests that  
1552 fire emissions in Africa through September 2024 ( $0.6\text{ GtC yr}^{-1}$ ) were slightly below the average of 2014-2023,  
1553 whereas GFED4.1s suggests that fire emissions through September 2024 were slightly above the average of  
1554 2014-2023 ( $0.8\text{ GtC yr}^{-1}$ ).

1555 Tropical fire emissions through September 2024 ( $1.1\text{--}1.6\text{ GtC yr}^{-1}$ ) accounted for 69-74% of the global total  
1556 emissions, which is close to the average of the 2014-2023 period ( $1.1\text{--}1.2\text{ GtC yr}^{-1}$ ; 72-75%). This marks a  
1557 return to a more typical distribution of fire emissions between the tropics and extratropics after the tropical  
1558 contribution fell to just 55-59% during January-September 2023 (Figure S9).

1559 We caution that the fire emissions fluxes presented here should not be compared directly with other fluxes of the  
1560 budget (e.g.  $S_{\text{LAND}}$  or  $E_{\text{LUC}}$ ) due to incompatibilities between the observable fire emission fluxes and what is  
1561 quantified in the  $S_{\text{LAND}}$  and  $E_{\text{LUC}}$  components of the budget. The fire emission estimates from global fire  
1562 products relate to all fire types that can be observed in Earth Observations (Giglio et al., 2018; Randerson et al.,  
1563 2012; Kaiser et al., 2012), including (i) fires occurring as part of natural disturbance-recovery cycles that would  
1564 also have occurred in the pre-industrial period (Yue et al., 2016; Keeley and Pausas, 2019; Zou et al., 2019), (ii)  
1565 fires occurring above and beyond natural disturbance-recovery cycle due to changes in climate,  $\text{CO}_2$  and N  
1566 fertilisation and to an increased frequency of extreme drought and heatwave events (Abatzoglou et al., 2019;  
1567 Jones et al., 2022; Zheng et al., 2021; Burton et al., 2024), and (iii) fires occurring in relation to land use and  
1568 land use change, such as deforestation fires and agricultural fires (van der Werf et al., 2010; Magi et al., 2012).



1569 In the context of the global carbon budget, only the portion of fire emissions associated with (ii) should be  
1570 included in the  $S_{\text{LAND}}$  component, and fire emissions associated with (iii) should already be accounted for in the  
1571  $E_{\text{LUC}}$  component. Emissions associated with (i) should not be included in the global carbon budget. It is not  
1572 currently possible to derive specific estimates for fluxes (i), (ii), and (iii) using global fire emission products  
1573 such as GFED or GFAS. In addition, the fire emissions estimates from global fire emissions products represent  
1574 a gross flux of carbon to the atmosphere, whereas the  $S_{\text{LAND}}$  component of the budget is a net flux that should  
1575 also include post-fire recovery fluxes. Even if emissions from fires of type (ii) could be separated from those of  
1576 type (i), these fluxes may be partially or wholly offset in subsequent years by post-fire fluxes as vegetation  
1577 recovers, sequestering carbon from the atmosphere to the terrestrial biosphere (Yue et al., 2016; Jones et al.,  
1578 2024c). Increases in forest fire emissions and severity (emissions per unit area) from globally during the past  
1579 two decades have highlighted the increasing potential for fire emissions fluxes to outweigh post-fire recovery  
1580 fluxes, though long-term monitoring of vegetation recovery is required to quantify the net effect on terrestrial C  
1581 storage (Jones et al., 2024c).

### 1582 **3.9 Closing the Global Carbon Cycle**

#### 1583 **3.9.1 Partitioning of Cumulative Emissions and Sink Fluxes**

1584 Emissions during the period 1850–2023 amounted to  $710 \pm 70$  GtC and were partitioned among the atmosphere  
1585 ( $285 \pm 5$  GtC; 40%), ocean ( $185 \pm 35$  GtC; 26%), and land ( $220 \pm 60$  GtC; 32%). The cumulative land sink is  
1586 almost equal to the cumulative land-use emissions ( $225 \pm 65$  GtC), making the global land nearly neutral over  
1587 the whole 1850–2023 period (Figure 3).

1588 The use of nearly independent estimates for the individual terms of the global carbon budget shows a cumulative  
1589 budget imbalance of 25 GtC (3% of total emissions) during 1850–2023 (Figure 3, Table 8), which, if correct,  
1590 suggests that emissions could be slightly too high by the same proportion or that the combined land and ocean  
1591 sinks are slightly underestimated (by about 6%), although these are well within the uncertainty range of each  
1592 component of the budget. Nevertheless, part of the imbalance could originate from the estimation of significant  
1593 increase in  $E_{\text{FOS}}$  and  $E_{\text{LUC}}$  between the mid 1920s and the mid 1960s which is unmatched by a similar growth in  
1594 atmospheric  $\text{CO}_2$  concentration as recorded in ice cores (Figure 3). However, the known loss of additional sink  
1595 capacity of 30–40 GtC (over the 1850–2020 period) due to reduced forest cover has not been accounted for in  
1596 our method and would exacerbate the budget imbalance (see Section 2.10 and Supplement S.6.4).

1597 For the more recent 1960–2023 period where direct atmospheric  $\text{CO}_2$  measurements are available, total  
1598 emissions ( $E_{\text{FOS}} + E_{\text{LUC}}$ ) amounted to  $500 \pm 50$  GtC, of which  $410 \pm 20$  GtC (82%) were caused by fossil  $\text{CO}_2$   
1599 emissions, and  $90 \pm 45$  GtC (18%) by land-use change (Table 8). The total emissions were partitioned among  
1600 the atmosphere ( $220 \pm 5$  GtC; 45%), ocean ( $130 \pm 26$  GtC; 25%), and the land ( $150 \pm 40$  GtC; 30%), with a near  
1601 zero ( $<1$  GtC) unattributed budget imbalance. All components except land-use change emissions have  
1602 significantly grown since 1960, with important interannual variability in the growth rate in atmospheric  $\text{CO}_2$   
1603 concentration and in the land  $\text{CO}_2$  sink (Figure 4), and some decadal variability in all terms (Table 7).  
1604 Differences with previous budget releases are documented in Figure S6.



1605 The global carbon budget averaged over the last decade (2014-2023) is shown in Figure 2, Figure 16 (right  
1606 panel) and Table 7. For this period, 90% of the total emissions ( $E_{\text{FOS}} + E_{\text{LUC}}$ ) were from fossil CO<sub>2</sub> emissions  
1607 ( $E_{\text{FOS}}$ ), and 10% from land-use change ( $E_{\text{LUC}}$ ). The total emissions were partitioned among the atmosphere  
1608 (48%), ocean (26%) and land (30%), with a small negative budget imbalance ( $\sim 4\%$ ,  $0.4 \text{ GtC yr}^{-1}$ ). For single  
1609 years, the budget imbalance can be larger (Figure 4). For 2023, the combination of our estimated sources ( $11.1 \pm$   
1610  $0.9 \text{ GtC yr}^{-1}$ ) and sinks ( $11.1 \pm 0.9 \text{ GtC yr}^{-1}$ ) leads to a  $B_{\text{IM}}$  of  $-0.02 \text{ GtC}$ , suggesting a near perfect closure of  
1611 the global carbon budget.

### 1612 3.9.2 Trend and Variability in the Carbon Budget Imbalance

1613 The carbon budget imbalance ( $B_{\text{IM}}$ ; Eq. 1, Figure 4) quantifies the mismatch between the estimated total  
1614 emissions and the estimated changes in the atmosphere, land, and ocean reservoirs. The budget imbalance from  
1615 1960 to 2023 is very small ( $0.5 \text{ GtC}$  over the period, i.e.  $<0.01 \text{ GtC yr}^{-1}$  on average) and shows no trend over the  
1616 full time series (Figure 4e). The process models (GOBMs and DGVMs) and  $f_{\text{CO}_2}$ -products have been selected  
1617 to match observational constraints in the 1990s, but no further constraints have been applied to their  
1618 representation of trend and variability. Therefore, the near-zero mean and trend in the budget imbalance is seen  
1619 as evidence of a coherent community understanding of the emissions and their partitioning on those time scales  
1620 (Figure 4). However, the budget imbalance shows substantial variability of the order of  $\pm 1 \text{ GtC yr}^{-1}$ , particularly  
1621 over semi-decadal time scales, although most of the variability is within the uncertainty of the estimates. The  
1622 positive carbon imbalance during the 1960s, and early 1990s, indicates that either the emissions were  
1623 overestimated, or the sinks were underestimated during these periods. The reverse is true for the 1970s, and to a  
1624 lesser extent for the 1980s and 2014-2023 period (Figure 4, Table 7).

1625 We cannot attribute the cause of the variability in the budget imbalance with our analysis, we only note that the  
1626 budget imbalance is unlikely to be explained by errors or biases in the emissions alone because of its large semi-  
1627 decadal variability component, a variability that is atypical of emissions and has not changed in the past 60 years  
1628 despite a near tripling in emissions (Figure 4). Errors in  $S_{\text{LAND}}$  and  $S_{\text{OCEAN}}$  are more likely to be the main cause  
1629 for the budget imbalance, especially on interannual to semi-decadal timescales. For example, underestimation of  
1630 the  $S_{\text{LAND}}$  by DGVMs has been reported following the eruption of Mount Pinatubo in 1991 possibly due to  
1631 missing responses to changes in diffuse radiation (Mercado et al., 2009). Although since GCB2021 we  
1632 accounted for aerosol effects on solar radiation quantity and quality (diffuse vs direct), most DGVMs only used  
1633 the former as input (i.e., total solar radiation) (Table S1). Thus, the ensemble mean may not capture the full  
1634 effects of volcanic eruptions, i.e. associated with high light scattering sulphate aerosols, on the land carbon sink  
1635 (O'Sullivan et al., 2021). DGVMs are suspected to overestimate the land sink in response to the wet decade of  
1636 the 1970s (Sitch et al., 2008). Quasi-decadal variability in the ocean sink has also been reported, with all  
1637 methods agreeing on a smaller than expected ocean CO<sub>2</sub> sink in the 1990s and a larger than expected sink in the  
1638 2000s (Figure 11; Landschützer et al., 2016, DeVries et al., 2019, Hauck et al., 2020, McKinley et al., 2020,  
1639 Gruber et al., 2023) and the climate-driven variability could be substantial but is not well constrained (DeVries  
1640 et al., 2023, Müller et al., 2023). Errors in sink estimates could also be driven by errors in the climatic forcing  
1641 data, particularly precipitation for  $S_{\text{LAND}}$  and wind for  $S_{\text{OCEAN}}$ . Also, the  $B_{\text{IM}}$  shows substantial departure from



1642 zero on yearly time scales (Figure 4e), highlighting unresolved variability of the carbon cycle, likely in the land  
1643 sink ( $S_{\text{LAND}}$ ), given its large year to year variability (Figure 4d and 9).

1644 Both the budget imbalance ( $B_{\text{IM}}$ , Table 7) and the residual land sink from the global budget ( $E_{\text{FOS}}+E_{\text{LUC}}-G_{\text{ATM}}-$   
1645  $S_{\text{OCEAN}}$ , Table 5) include an error term due to the inconsistencies that arises from combining  $E_{\text{LUC}}$  from  
1646 bookkeeping models with  $S_{\text{LAND}}$  from DGVMs, most notably the loss of additional sink capacity (see Section  
1647 2.10 and Supplement S.6.4). Other differences include a better accounting of land use changes practices and  
1648 processes in bookkeeping models than in DGVMs, or the bookkeeping models error of having present-day  
1649 observed carbon densities fixed in the past. That the budget imbalance shows no clear trend towards larger  
1650 values over time is an indication that these inconsistencies probably play a minor role compared to other errors  
1651 in  $S_{\text{LAND}}$  or  $S_{\text{OCEAN}}$ .

1652 Although the budget imbalance is near zero for the recent decades, it could be due to a compensation of errors.  
1653 We cannot exclude an overestimation of  $\text{CO}_2$  emissions, particularly from land-use change, given their large  
1654 uncertainty, as has been suggested elsewhere (Piao et al., 2018), and/or an underestimate of the sinks. A larger  
1655 DGVM estimate of the atmosphere-land  $\text{CO}_2$  flux ( $S_{\text{LAND}}-E_{\text{LUC}}$ ) over the extra-tropics would reconcile model  
1656 results with inversion estimates for fluxes in the total land during the past decade (Figure 14; Table 5).  
1657 Likewise, a larger  $S_{\text{OCEAN}}$  is also possible given the higher estimates from the  $f\text{CO}_2$ -products, inversions and  
1658 oxygen based estimates (see Section 3.6.2, Figure 11 and Figure 14), the underestimation of interior ocean  
1659 anthropogenic carbon accumulation in the GOBMs (Section 3.6.5, Müller et al., 2023), known biases of ocean  
1660 models (e.g., Terhaar et al., 2022; 2024), the role of potential temperature bias and skin effects in  $f\text{CO}_2$ -products  
1661 (Watson et al., 2020; Dong et al., 2022; Bellenger et al., 2023, Figure 11) and regionally larger estimates based  
1662 e.g. on eddy covariance measurements and aircraft data (Dong et al., 2024a; Long et al., 2021; Jin et al., 2024).  
1663 More integrated use of observations in the Global Carbon Budget, either on their own or for further constraining  
1664 model results, should help resolve some of the budget imbalance (Peters et al., 2017a).

#### 1665 **4 Tracking progress towards mitigation targets**

1666 The average growth in global fossil  $\text{CO}_2$  emissions peaked at nearly +3% per year during the 2000s, driven by  
1667 the rapid growth in emissions in China. In the last decade, however, the global growth rate has slowly declined,  
1668 reaching a low +0.6% per year over 2014-2023. While this slowdown in global fossil  $\text{CO}_2$  emissions growth is  
1669 welcome, global fossil  $\text{CO}_2$  emissions continue to grow, far from the rapid emission decreases needed to be  
1670 consistent with the temperature goals of the Paris Agreement.

1671 Since the 1990s, the average growth rate of fossil  $\text{CO}_2$  emissions has continuously declined across the group of  
1672 developed countries of the Organisation for Economic Co-operation and Development (OECD), with emissions  
1673 peaking in around 2005 and declining at  $1.4\% \text{ yr}^{-1}$  in the decade 2014-2023, compared to a decline of  $0.9\% \text{ yr}^{-1}$   
1674 during the 2004-2013 period (Table 9). In the decade 2014-2023, territorial fossil  $\text{CO}_2$  emissions decreased  
1675 significantly (at the 95% confidence level) in 22 countries/economies whose economies grew significantly (also  
1676 at the 95% confidence level): Belgium, Czechia, Denmark, Estonia, Finland, France, Germany, Jordan,  
1677 Luxembourg, Netherlands, New Zealand, Norway, Portugal, South Korea, Romania, Slovenia, Somalia, Spain,





1678 Sweden, Switzerland, United Kingdom, USA (updated from Le Quéré et al., 2019). Altogether, these 22  
1679 countries emitted 2.2 GtC yr<sup>-1</sup> (8.1 GtCO<sub>2</sub> yr<sup>-1</sup>) on average over the last decade, about 23% of world CO<sub>2</sub> fossil  
1680 emissions. For comparison, 18 countries showed a significant decrease in territorial fossil CO<sub>2</sub> emissions over  
1681 the previous decade (2004-2013).

1682 Decomposing emission changes into the components of growth, a Kaya decomposition, helps give an initial  
1683 understanding of the drivers of the changes (Peters et al., 2017b). The reduction in growth in global fossil CO<sub>2</sub>  
1684 emissions in the last decade is due to slightly weaker economic growth, accelerating declines in CO<sub>2</sub> emissions  
1685 per unit energy, and sustained declines in energy per unit GDP (Figure 17). These trends are a supposition of the  
1686 trends at the national level. Fossil CO<sub>2</sub> emission declines in the USA and the EU27 are primarily driven by  
1687 slightly weaker economic growth since the Global Financial Crisis (GFC) in 2008/2009, sustained declines in  
1688 energy per GDP, and sustained declines in CO<sub>2</sub> emissions per unit energy with a slight acceleration in the USA  
1689 in the last decade. In contrast, fossil CO<sub>2</sub> emissions continue to grow in non-OECD countries, although the  
1690 growth rate has slowed from 4.9% yr<sup>-1</sup> during the 2004-2013 decade to 1.8% yr<sup>-1</sup> in the last decade (Table 9).  
1691 Representing 47% of non-OECD emissions in 2023, a large part of this slowdown is due to China, which has  
1692 seen emissions growth decline from 7.5% yr<sup>-1</sup> in the 2004-2013 decade to 1.9% yr<sup>-1</sup> in the last decade.  
1693 Excluding China, non-OECD emissions grew at 3% yr<sup>-1</sup> in the 2004-2013 decade compared to 1.7% yr<sup>-1</sup> in the  
1694 last decade. China has had weaker economic growth in the 2000s compared to the 2010s, and the rate of  
1695 reduction in the energy intensity of economic production has weakened significantly since 2015 with  
1696 accelerating declines in CO<sub>2</sub> emissions per unit energy (Figure 17). India has had strong economic growth that is  
1697 not offset by declines in energy per GDP or declines in CO<sub>2</sub> emissions per unit energy, driving up fossil CO<sub>2</sub>  
1698 emissions. Despite the high deployment of renewables in some countries (e.g., China, India), fossil energy  
1699 sources continue to grow to meet growing energy demand (Le Quéré et al., 2019). In the rest of the world,  
1700 economic growth has slowed considerably in the last decade, but is only partly offset by declines in energy or  
1701 carbon intensity, leading to growing emissions.

1702 Globally, fossil CO<sub>2</sub> emissions growth is slowing, and this is due in part to the emergence of climate policy  
1703 (Eskander and Fankhauser 2020; Le Quere et al 2019) and technological change, which is leading to a shift from  
1704 coal to gas and growth in renewable energies, and reduced expansion of coal capacity. At the aggregated global  
1705 level, decarbonisation shows a strong and growing signal in the last decade, with smaller contributions from  
1706 lower economic growth and declines in energy per GDP (Figure 17). Altogether, global fossil CO<sub>2</sub> emissions are  
1707 still growing (average of 0.6% per year over the 2014-2023 decade), far from the reductions needed to meet the  
1708 ambitious climate goals of the UNFCCC Paris agreement.

1709 Last, we update the remaining carbon budget (RCB) based on two studies, the IPCC AR6 (Canadell et al., 2021)  
1710 and the revision of the IPCC AR6 estimates (Forster et al., 2024, Lamboll et al., 2023). We update the RCB  
1711 assessed by the IPCC AR6 (Canadell et al., 2021), accounting for the 2020 to 2024 estimated emissions from  
1712 fossil fuel combustion (E<sub>FOS</sub>) and land use changes (E<sub>LUC</sub>). From January 2025, the IPCC AR6 RCB (50%  
1713 likelihood) for limiting global warming to 1.5°C, 1.7°C and 2°C is estimated to amount to 85, 180, and 315 GtC  
1714 (305, 655, 1155 GtCO<sub>2</sub>). The Forster et al. (2024) study proposed a significantly lower RCB than IPCC AR6,



1715 with the largest reduction being due to an update of the climate emulator (MAGICC) used to estimate the  
1716 warming contribution of non-CO<sub>2</sub> agents, and to the warming (i.e. emissions) that occurred over the 2020-2023  
1717 period. We update the Forster et al., budget accounting for the 2024 estimated emissions from fossil fuel  
1718 combustion (E<sub>FOS</sub>) and land use changes (E<sub>LUC</sub>). From January 2025, the Forster et al., (2024) RCB (50%  
1719 likelihood) for limiting global warming to 1.5°C, 1.7°C and 2°C is estimated to amount to 45, 140, and 290 GtC  
1720 (160, 510, 1060 GtCO<sub>2</sub>), significantly smaller than the updated IPCC AR6 estimate. Both the original IPCC  
1721 AR6 and Forster et al. (2024) estimates include the Earth System uncertainty on the climate response to  
1722 cumulative CO<sub>2</sub> emissions, which is reflected through the percent likelihood of exceeding the given temperature  
1723 threshold, an additional uncertainty of 220GtCO<sub>2</sub> due to alternative non-CO<sub>2</sub> emission scenarios, and other  
1724 sources of uncertainties (see Canadell et al., 2021). The two sets of estimates overlap when considering all  
1725 uncertainties. The IPCC AR6 estimates have the advantage of a consensus building approach, while the Forster  
1726 et al. (2024) estimates include significant update estimates but without the backing of the IPCC yet.

1727 Here, we take the average of our 2024 update of both IPCC AR6 and Forster et al. (2024) estimates, giving a  
1728 remaining carbon (50% likelihood) for limiting global warming to 1.5°C, 1.7°C and 2°C of respectively 65, 160,  
1729 and 305 GtC (235, 585, 1110 GtCO<sub>2</sub>) starting from January 2025. We emphasise the large uncertainties,  
1730 particularly when close to the global warming limit of 1.5°C. These 1.5°C, 1.7°C and 2°C remaining carbon  
1731 budgets correspond respectively to about 6, 14 and 27 years from the beginning of 2025, at the 2024 level of  
1732 total anthropogenic CO<sub>2</sub> emissions. Reaching net-zero CO<sub>2</sub> emissions by 2050 entails cutting total  
1733 anthropogenic CO<sub>2</sub> emissions by about 0.4 GtC (1.6 GtCO<sub>2</sub>), 3.9% of 2024 emissions, each year on average,  
1734 comparable to the decrease in E<sub>FOS</sub> observed in 2020 during the COVID-19 pandemic. However, this would lead  
1735 to cumulative emissions over 2025-2050 of 145 GtC (530 GtCO<sub>2</sub>), well above the remaining carbon budget of  
1736 65 GtC to limit global warming to 1.5°C, but still within the remaining budget of 160 GtC to limit warming to  
1737 1.7°C (in phase with the “well below 2°C” ambition of the Paris Agreement). Even reaching net zero CO<sub>2</sub>  
1738 globally by 2040, which would require annual emissions cuts of 0.7 GtC (2.5 GtCO<sub>2</sub>) on average, would still  
1739 exceed the remaining carbon budget, with 90 GtC (325 GtCO<sub>2</sub>) cumulative emissions over 2025-2040, unless  
1740 the global emissions trajectory becomes net negative (i.e. more anthropogenic CO<sub>2</sub> sinks than emissions) after  
1741 2040.

## 1742 **5 Discussion**

1743 Each year when the global carbon budget is published, each flux component is updated for all previous years to  
1744 consider corrections that are the result of further scrutiny and verification of the underlying data in the primary  
1745 input datasets. Annual estimates may be updated with improvements in data quality and timeliness (e.g., to  
1746 eliminate the need for extrapolation of forcing data such as land-use). Of all terms in the global budget, only the  
1747 fossil CO<sub>2</sub> emissions and the growth rate in atmospheric CO<sub>2</sub> concentration are based primarily on empirical  
1748 inputs supporting annual estimates in this carbon budget. The carbon budget imbalance, yet an imperfect  
1749 measure, provides a strong indication of the limitations in observations, in understanding and representing  
1750 processes in models, and/or in the integration of the carbon budget components.



1751 The persistent unexplained variability in the carbon budget imbalance limits our ability to verify reported  
1752 emissions (Peters et al., 2017a) and suggests we do not yet have a complete understanding of the underlying  
1753 carbon cycle dynamics on annual to decadal timescales. Resolving most of this unexplained variability should  
1754 be possible through different and complementary approaches. First, as intended with our annual updates, the  
1755 imbalance as an error term should be reduced by improvements of individual components of the global carbon  
1756 budget that follow from improving the underlying data and statistics and by improving the models through the  
1757 resolution of some of the key uncertainties detailed in Table 10. Second, additional clues to the origin and  
1758 processes responsible for the variability in the budget imbalance could be obtained through a closer scrutiny of  
1759 carbon variability in light of other Earth system data (e.g., heat balance, water balance), and the use of a wider  
1760 range of biogeochemical observations to better understand the land-ocean partitioning of the carbon imbalance  
1761 such as the constraint from atmospheric oxygen included this year. Finally, additional information could also be  
1762 obtained through better inclusion of process knowledge at the regional level, and through the introduction of  
1763 inferred fluxes such as those based on satellite  $x\text{CO}_2$  retrievals. The limit of the resolution of the carbon budget  
1764 imbalance is yet unclear, but most certainly not yet reached given the possibilities for improvements that lie  
1765 ahead.

1766 Estimates of global fossil  $\text{CO}_2$  emissions from different datasets are in relatively good agreement when the  
1767 different system boundaries of these datasets are considered (Andrew, 2020a). But while estimates of  $E_{\text{FOS}}$  are  
1768 derived from reported activity data requiring much fewer complex transformations than some other components  
1769 of the budget, uncertainties remain, and one reason for the apparently low variation between datasets is precisely  
1770 the reliance on the same underlying reported energy data. The budget excludes some sources of fossil  $\text{CO}_2$   
1771 emissions, which available evidence suggests are relatively small (<1%). We have added emissions from lime  
1772 production in China and the US, but these are still absent in most other non-Annex I countries, and before 1990  
1773 in other Annex I countries.

1774 Estimates of  $E_{\text{LUC}}$  suffer from a range of intertwined issues, including the poor quality of historical land-cover  
1775 and land-use change maps, the rudimentary representation of management processes in most models, and the  
1776 confusion in methodologies and boundary conditions used across methods (e.g., Arneth et al., 2017; Pongratz et  
1777 al., 2014, see also Supplement S.6.4 on the loss of sink capacity; Bastos et al., 2021). Uncertainties in current  
1778 and historical carbon stocks in soils and vegetation also add uncertainty in the  $E_{\text{LUC}}$  estimates. Unless a major  
1779 effort to resolve these issues is made, little progress is expected in the resolution of  $E_{\text{LUC}}$ . This is particularly  
1780 concerning given the growing importance of  $E_{\text{LUC}}$  for climate mitigation strategies, and the large issues in the  
1781 quantification of the cumulative emissions over the historical period that arise from large uncertainties in  $E_{\text{LUC}}$ .

1782 By adding the DGVMs estimates of  $\text{CO}_2$  fluxes due to environmental change from countries' managed forest  
1783 areas (part of  $S_{\text{LAND}}$  in this budget) to the budget  $E_{\text{LUC}}$  estimate, we successfully reconciled the large gap  
1784 between our  $E_{\text{LUC}}$  estimate and the land use flux from NGHGs using the approach described in Grassi et al.  
1785 (2021) for future scenarios and in Grassi et al. (2023) using data from the Global Carbon Budget 2021. The  
1786 updated data presented here can be used as potential adjustment in the policy context, e.g., to help assess the  
1787 collective countries' progress towards the goal of the Paris Agreement and avoiding double-accounting for the



1788 sink in managed forests. In the absence of this adjustment, collective progress would hence appear better than it  
1789 is (Grassi et al., 2021). The application of this adjustment is also recommended in the UNFCCC Synthesis  
1790 report for the first Global Stocktake (UNFCCC, 2022) whenever a comparison between LULUCF fluxes  
1791 reported by countries and the global emission estimates of the IPCC is conducted. However, this adjustment  
1792 should be seen as a short-term and pragmatic fix based on existing data, rather than a definitive solution to  
1793 bridge the differences between global models and national inventories. Additional steps are needed to  
1794 understand and reconcile the remaining differences, some of which are relevant at the country level (Grassi, et  
1795 al., 2023, Schwingshackl, et al., 2022).

1796 The comparison of GOBMs,  $f\text{CO}_2$ -products, and inversions highlights substantial discrepancy in the temporal  
1797 evolution of  $\text{SO}_{\text{CEAN}}$  in the Southern Ocean and northern high-latitudes (Figure 14, Hauck et al., 2023a) and in  
1798 the mean  $\text{SO}_{\text{CEAN}}$  in the tropics. A large part of the uncertainty in the mean fluxes stems from the regional  
1799 distribution of the river flux adjustment term. The current distribution simulates the largest share of the  
1800 outgassing to occur in the tropics (Lacroix et al., 2020). The long-standing sparse data coverage of  $f\text{CO}_2$   
1801 observations in the Southern compared to the Northern Hemisphere (e.g., Takahashi et al., 2009) continues to  
1802 exist (Bakker et al., 2016, 2024, Figure S1) and to lead to substantially higher uncertainty in the  $\text{SO}_{\text{CEAN}}$  estimate  
1803 for the Southern Hemisphere (Watson et al., 2020, Gloege et al., 2021, Hauck et al., 2023a). This discrepancy,  
1804 which also hampers model improvement, points to the need for increased high-quality  $f\text{CO}_2$  observations  
1805 especially in the Southern Ocean. At the same time, model uncertainty is illustrated by the large spread of  
1806 individual GOBM estimates (indicated by shading in Figure 14) and highlights the need for model  
1807 improvement. The issue of diverging trends in  $\text{SO}_{\text{CEAN}}$  from different methods is smaller this year as the trend in  
1808 the  $f\text{CO}_2$ -products was revised downwards with the data available in this GCB release, but remains a matter of  
1809 concern. Recent and on-going work suggests that the  $f\text{CO}_2$ -products may overestimate the trend (Hauck et al.,  
1810 2023a, Supplement section S3.4), though the full  $f\text{CO}_2$ -product ensemble remains to be tested. A data-  
1811 constrained model approach suggests that the GOBMs underestimate the amplitude of decadal variability, but  
1812 that the  $f\text{CO}_2$ -products overestimate the trend (Mayot et al., 2024). At the same time, evidence is accumulating  
1813 that GOBMs likely underestimate the mean flux (Section 3.6.2, Terhaar et al., 2022, DeVries et al., 2023,  
1814 Müller et al., 2023, Dong et al., 2024). The independent constraint from atmospheric oxygen measurements  
1815 gives a larger sink for the past decade and a steeper trend. However, the estimate is consistent within  
1816 uncertainties with  $\text{SO}_{\text{CEAN}}$ , with the relatively larger ocean sink in the  $f\text{CO}_2$ -products and some of the GOBMs.  
1817 The assessment of the net land-atmosphere exchange from DGVMs and atmospheric inversions also shows  
1818 substantial discrepancy, particularly for the estimate of the net land flux over the northern extra-tropic. This  
1819 discrepancy highlights the difficulty to quantify complex processes ( $\text{CO}_2$  fertilisation, nitrogen deposition and  
1820 fertilisers, climate change and variability, land management, etc.) that collectively determine the net land  $\text{CO}_2$   
1821 flux. Resolving the differences in the Northern Hemisphere land sink will require the consideration and  
1822 inclusion of larger volumes of observations.

1823 We provide metrics for the evaluation of the ocean and land models and the atmospheric inversions (Figures S2  
1824 to S4, Table S11). These metrics expand the use of observations in the global carbon budget, helping 1) to  
1825 support improvements in the ocean and land carbon models that produce the sink estimates, and 2) to constrain



1826 the representation of key underlying processes in the models and to allocate the regional partitioning of the CO<sub>2</sub>  
1827 fluxes. The introduction of process-based metrics targeted to evaluate the simulation of SO<sub>CEAN</sub> in the ocean  
1828 biogeochemistry models is an important addition to the evaluation based on ocean carbon observations. This is  
1829 an initial step towards the introduction of a broader range of observations and more stringent model evaluation  
1830 that we hope will support continued improvements in the annual estimates of the global carbon budget.

1831 We assessed before that a sustained decrease of –1% in global emissions could be detected at the 66%  
1832 likelihood level after a decade only (Peters et al., 2017a). Similarly, a change in behaviour of the land and/or  
1833 ocean carbon sink would take as long to detect, and much longer if it emerges more slowly. To continue  
1834 reducing the carbon imbalance on annual to decadal time scales, regionalising the carbon budget, and integrating  
1835 multiple variables are powerful ways to shorten the detection limit and ensure the research community can  
1836 rapidly identify issues of concern in the evolution of the global carbon cycle under the current rapid and  
1837 unprecedented changing environmental conditions.

## 1838 **6 Conclusions**

1839 The estimation of global CO<sub>2</sub> emissions and sinks is a major effort by the carbon cycle research community that  
1840 requires a careful compilation and synthesis of measurements, statistical estimates, and model results. The  
1841 delivery of an annual carbon budget serves two purposes. First, there is a large demand for up-to-date  
1842 information on the state of the anthropogenic perturbation of the climate system and its underpinning causes. A  
1843 broad stakeholder community relies on the datasets associated with the annual carbon budget including  
1844 scientists, policy makers, businesses, journalists, and non-governmental organisations engaged in adapting to  
1845 and mitigating human-driven climate change. Second, over the last decades we have seen unprecedented  
1846 changes in the human and biophysical environments (e.g., changes in the growth of fossil fuel emissions, impact  
1847 of COVID-19 pandemic, Earth’s warming, and strength of the carbon sinks), which call for frequent  
1848 assessments of the state of the planet, a better quantification of the causes of changes in the contemporary global  
1849 carbon cycle, and an improved capacity to anticipate its evolution in the future. Building this scientific  
1850 understanding to meet the extraordinary climate mitigation challenge requires frequent, robust, transparent, and  
1851 traceable datasets and methods that can be scrutinised and replicated. This paper via ‘living data’ helps to keep  
1852 track of new budget updates.

## 1853 **7 Data availability**

1854 The data presented here are made available in the belief that their wide dissemination will lead to greater  
1855 understanding and new scientific insights of how the carbon cycle works, how humans are altering it, and how  
1856 we can mitigate the resulting human-driven climate change. Full contact details and information on how to cite  
1857 the data shown here are given at the top of each page in the accompanying database and summarised in Table 2.

1858 The accompanying database includes three Excel files organised in the following spreadsheets:

1859 File Global\_Carbon\_Budget\_2024v1.0.xlsx includes the following:



- 1860 1. Summary
- 1861 2. The global carbon budget (1959-2023);
- 1862 3. The historical global carbon budget (1750-2023);
- 1863 4. Global CO<sub>2</sub> emissions from fossil fuels and cement production by fuel type, and the per-capita emissions  
1864 (1850-2023);
- 1865 5. CO<sub>2</sub> emissions from land-use change from the individual bookkeeping models (1959-2023);
- 1866 6. Ocean CO<sub>2</sub> sink from the individual global ocean biogeochemistry models and  $f$ CO<sub>2</sub>-products (1959-  
1867 2023);
- 1868 7. Terrestrial CO<sub>2</sub> sink from the individual DGVMs (1959-2023);
- 1869 8. Cement carbonation CO<sub>2</sub> sink (1959-2023).
- 1870 File National\_Fossil\_Carbon\_Emissions\_2024v1.0.xlsx includes the following:
- 1871 1. Summary
- 1872 2. Territorial country CO<sub>2</sub> emissions from fossil fuels and cement production (1850-2023);
- 1873 3. Consumption country CO<sub>2</sub> emissions from fossil fuels and cement production and emissions transfer from  
1874 the international trade of goods and services (1990-2020) using CDIAC/UNFCCC data as reference;
- 1875 4. Emissions transfers (Consumption minus territorial emissions; 1990-2020);
- 1876 5. Country definitions.
- 1877 File National\_LandUseChange\_Carbon\_Emissions\_2024v1.0.xlsx includes the following:
- 1878 1. Summary
- 1879 2. Territorial country CO<sub>2</sub> emissions from Land Use Change (1850-2023) from three bookkeeping models;
- 1880 All three spreadsheets are published by the Integrated Carbon Observation System (ICOS) Carbon Portal and  
1881 are available at <https://doi.org/10.18160/GCP-2024> (Friedlingstein et al., 2024). National emissions data are also  
1882 available at <https://doi.org/10.5281/zenodo.13981696> (Andrew and Peters, 2024), from the Global Carbon Atlas  
1883 (<http://www.globalcarbonatlas.org/>, last access: 28 October 2024) and from Our World in Data  
1884 (<https://ourworldindata.org/co2-emissions>, last access: 28 October 2024).



1885 **Author contributions**

1886 PF, MO, MWJ, RMA, JH, PL, CLQ, HL, ITL, AO, GPP, WP, JP, CS, and SSi designed the study, conducted  
1887 the analysis, and wrote the paper with input from JGC, PCi and RBJ. RMA, GPP and JIK produced the fossil  
1888 CO<sub>2</sub> emissions and their uncertainties and analysed the emissions data. MH and GMa provided fossil fuel  
1889 emission data. JP, TGa, ZQ, and CS provided the bookkeeping land-use change emissions with synthesis by JP  
1890 and CS. SSm provided the estimates of non-vegetation CDR fluxes. LB, MC, ÖG, NG, TI, TJ, LR, JS, RS, and  
1891 HTs provided an update of the global ocean biogeochemical models; LMD, ARF, DJF, MG, LG, YI, AJ, CR,  
1892 AR, JZ, and PC provided an update of the ocean/CO<sub>2</sub>-data products, with synthesis on both streams by JH, PL  
1893 and NMa. SRA, NRB, MB, CFB, HCB, KC, KE, WE, RAF, TGk, SKL, NL, NMe, NMM, SN, LO, TO, DP,  
1894 AJS, ST, BT, CN, and RW provided ocean fCO<sub>2</sub> measurements for the year 2023, with synthesis by AO and TS.  
1895 AA, VA, PCa, THC, JD, CDR, AF, JHe, AKJ, EK, JK, PCM, LM, TN, MO, QS, HTi, XYa, WY, XYu, and SZ  
1896 provided an update of the Dynamic Global Vegetation Models, with synthesis by SSi and MO. HL, RSA, OT,  
1897 and ET provided estimates of land and ocean sinks from Earth System Models, as well as a projection of the  
1898 atmospheric growth rate for 2024. NC, FC, ARJ, FJ, ZJ, JL, SM, YN, PIP, CR, DY, and NZ provided an  
1899 updated atmospheric inversion, WP, FC, and ITL developed the protocol and produced the synthesis and  
1900 evaluation of the atmospheric inversions. RMA provided projections of the 2024 fossil emissions and  
1901 atmospheric CO<sub>2</sub> growth rate. PL provided the predictions of the 2024 ocean and land sinks. LPC, GCH, KKG,  
1902 TMR, GRvdW, WX, and ZY provided forcing data for land-use change. FT and GG provided data for the land-  
1903 use change NGHGI harmonisation. RFK provided key atmospheric CO<sub>2</sub> data. EJM and RFK provided the  
1904 atmospheric oxygen constraint on surface net carbon sinks. MWJ provided the historical atmospheric CO<sub>2</sub>  
1905 concentration and growth rate. MO and NB produced the aerosol diffuse radiative forcing for the DGVMs. IH  
1906 provided the climate forcing data for the DGVMs. PCM provided the evaluation of the DGVMs. MWJ provided  
1907 the emissions prior for use in the inversion systems. XD provided seasonal emissions data for most recent years  
1908 for the emission prior. PF, MO and MWJ coordinated the effort, revised all figures, tables, text and numbers to  
1909 ensure the update was clear from the 2023 edition and in line with the [globalcarbonatlas.org](https://globalcarbonatlas.org).

1910 **Competing interests.**

1911 At least one of the (co-)authors is a member of the editorial board of Earth System Science Data



1912

1913 **Acknowledgements**

1914 We thank all people and institutions who provided the data used in this global carbon budget 2024 and the Global  
1915 Carbon Project members for their input throughout the development of this publication. We thank Nigel Hawtin  
1916 for producing Figure 2 and Figure 15. We thank Alex Vermeulen and Hannah Ritchie for respectively hosting the  
1917 Global Carbon Budget datasets on the ICOS portal and the Our World in Data website. We thank Ian G. C. Ashton,  
1918 Dorothee Bakker, Sebastian Brune, Fatemeh Cheginig, Emeric Claudel, Lushanya Dayathilake, Christian Ethé,  
1919 Lonke Goddijn-Murphy, T. Holding, Fabrice Lacroix, Yi Liu, Damian Loher, Naiqing Pan, Paridhi Rustogi, J.  
1920 D. Shutler, Richard Sims, Phillip Townsend, Jing Wang, Andrew J. Watson, Kristina Frölich, Zoé Lloret, Adrien  
1921 Martinez, Lorna Nayagam, Rajesh Janardanan, Yakun Zhu, Ram Alkama, Simone Rossi, Stefanie Falk, Pengyue  
1922 Du, Peter Lawrence, Sean Swenson, Daniel Kennedy, Sam Levis, Erik Kluzek, Lachlan Whyborn, Drew  
1923 Holzworth, Ian Harman, Dr. Shufen Pan, Jason Cole, Victoria Spada, Vladimir Lapin, Raffaele Bernardello, K.  
1924 Toyama, H. Nakano, S. L. Urakawa, Anthony P. Walker, Tristan Quaife, and David K. Woolf for their  
1925 involvement in the development, use and analysis of the models and data-products used here. We thank Kim  
1926 Currie, Siyabulela Hamna, Mutshutshu Tsanwani, Pedro Monteiro, C. Lo Monaco, and Arne Körtzinger who  
1927 contributed to the provision of surface ocean CO<sub>2</sub> observations for the year 2023 (see Table S7). We also thank  
1928 Stephen D. Jones of the Ocean Thematic Centre of the EU Integrated Carbon Observation System (ICOS)  
1929 Research Infrastructure, Eugene Burger of NOAA's Pacific Marine Environmental Laboratory and Alex Kozyr of  
1930 NOAA's National Centers for Environmental Information, for their contribution to surface ocean CO<sub>2</sub> data and  
1931 metadata management. We thank the scientists, institutions, and funding agencies responsible for the collection  
1932 and quality control of the data in SOCAT as well as the International Ocean Carbon Coordination Project  
1933 (IOCCP), the Surface Ocean Lower Atmosphere Study (SOLAS) and the Integrated Marine Biosphere Research  
1934 (IMBeR) program for their support. We thank Nadine Goris and Lavinia Patara for support in calculating  
1935 observational ocean evaluation metrics. We thank Fortunat Joos, Samar Khatiwala and Timothy DeVries for  
1936 providing historical atmospheric and ocean data. We thank data providers ObsPack GLOBALVIEWplus v9.0 and  
1937 NRT v9.2 for atmospheric CO<sub>2</sub> observations. Ingrid T Lujikx and Wouter Peters thank the CarbonTracker Europe  
1938 team at Wageningen University, including Remco de Kok, Joram Hooghiem, Linda Kooijmans and Auke van der  
1939 Woude. Ian Harris thanks the Japan Meteorological Agency (JMA) for producing the Japanese 55-year Reanalysis  
1940 (JRA-55). Reinel Sospedra-Alfonso thanks William J. Merryfield, Woosung Lee, Jason Cole, and Victoria Spada





1941 for their help to set up and produce CanESM5 runs. Olivier Torres thanks Patricia Cadule, Juliette Mignot, Didier  
1942 Swingedouw, and Laurent Bopp for contributions to the IPSL-CM6-LR-ESMCO2 simulations. Yosuke Niwa  
1943 thanks CSIRO, EC, EMPA, FMI, IPEN, JMA, LSCE, NCAR, NIES, NILU, NIWA, NOAA, SIO, and TU/NIPR  
1944 for providing data for NISMON-CO2. Zhe Jin thanks Xiangjun Tian, Yilong Wang, Hongqin Zhang, Min Zhao,  
1945 Tao Wang, Jinzhi Ding and Shilong Piao for their contributions to the GONGGA inversion system. Paul I. Palmer  
1946 thanks Lian Fang and acknowledges ongoing support from the National Centre for Earth Observation. Ning Zeng  
1947 thanks Zhiqiang Liu, Yun Liu, Eugenia Kalnay, and Gassem Asrar for their contributions to the COLA system.  
1948 Fei Jiang acknowledges the High-Performance Computing Center (HPCC) of Nanjing University for doing the  
1949 inversions on its blade cluster system, and thanks Weimin Ju for updating the a priori fluxes of the terrestrial  
1950 ecosystems. Meike Becker and Are Olsen thank Sparebanken Vest / Agenda Vestlandet for their support for the  
1951 observations on the Statsraad Lehmkuhl. Wiley Evans and Katie Campbell thank the Tula Foundation for funding  
1952 support. Thanos Gkritzalis and the VLIZ ICOS team are thankful to the crew of the research vessel Simon Stevin  
1953 for all the support and help they provide. Bronte Tilbrook and Craig Neill thank Australia's Integrated Marine  
1954 Observing System (IMOS) for sourcing CO2 data. FAOSTAT is funded by FAO member states through their  
1955 contributions to the FAO Regular Programme, data contributions by national experts are greatly acknowledged.  
1956 The views expressed in this paper are the authors' only and do not necessarily reflect those of FAO. Finally, we  
1957 thank all funders who have supported the individual and joint contributions to this work (see details below), as  
1958 well as the two anonymous reviewers of this manuscript, and the many researchers who have provided feedback.

#### 1959 **Financial and computing support**

1960 This research was supported by the following sources of funding: The Argentinian-Uruguayan Joint Technical  
1961 Commission of the Maritime Front (Comisión Técnica Mixta del Frente Marítimo, CTMFM) (Argentina);  
1962 Instituto Nacional de Investigación y Desarrollo Pesquero (Argentina); Australia's Integrated Marine Observing  
1963 System (IMOS) which is enabled by the National Collaborative Research Infrastructure Strategy (NCRIS)  
1964 (Australia); Australian Earth-System Simulator National Research Infrastructure (ACCESS-NRI) (Australia);  
1965 Australian National Environmental Science Program, Climate Systems Hub (Australia); Research Foundation  
1966 Flanders (ICOS Flanders, grant no. I001821N) (Belgium); Tula Foundation (Canada); National Key Research and  
1967 Development Program (grant no. 2023YFF0805400) (China); National Key Research and Development Program  
1968 (grant no. 2023YFB3907404) (China); Jiangsu Provincial Science Fund for Distinguished Young Scholars (Grant  
1969 No: BK20231530) (China); National Natural Science Foundation (grant no. 42141020) (China); Carbon  
1970 Neutrality and Energy System Transformation (CNEST) Program led by Tsinghua University, granted by National  
1971 Key R&D Program of China (Grant No. 2023YFE0113000) (China); Second Tibetan Plateau Scientific  
1972 Expedition and Research Program (Grant: 2022QZKK0101) (China); CAS Project for Young Scientists in Basic



1973 Research, Grant No.YSBR-037 (China); grant no. 2021YFD2200405 (China); Copernicus Atmosphere  
1974 Monitoring Service, implemented by ECMWF (Grant: CAMS2 55) (European Commission); Copernicus Marine  
1975 Environment Monitoring Service, implemented by MOi (Grant: CMEMS-TAC-MOB) (European Commission);  
1976 H2020 4C (grant no. 821003) (European Commission); H2020 ESM2025 – Earth System Models for the Future  
1977 (grant no. 101003536) (European Commission); H2020 GEORGE (grant no. 101094716) (European  
1978 Commission); Horizon Europe (EYE-CLIMA: grant no. 101081395) (European Commission); ERC-2022-STG  
1979 OceanPeak (Grant 101077209) (European Commission); Horizon Europe Grant 101083922 (OceanICU  
1980 Improving Carbon Understanding) (European Commission); Horizon 2020 research and innovation programme  
1981 under Grant Agreements N° 101056939 (RESCUE project) (European Commission); COMFORT project (grant  
1982 no. 820989) (European Commission); Climate Space RECCAP-2 (European Space Agency); Ocean Carbon for  
1983 Climate (European Space Agency); EO-LINCS (European Space Agency); OceanSODA project, grant no.  
1984 4000112091/14/I-LG (European Space Agency); Institut National des Sciences de l’Univers (INSU) (France);  
1985 Institut Polaire français, Paul-Emile Victor (IPEV) (France); Observatoire des sciences de l’univers Ecce-Terra  
1986 (OSU at Sorbonne Université) (France); Institut de recherché français sur les ressources marines (IFREMER)  
1987 (France); French Oceanographic Fleet (FOF) (France); ICOS-France (France); Institut de Recherche pour le  
1988 Développement (IRD) (France); Agence Nationale de la Recherche - France 2030 (PEPR TRACCS programme  
1989 under grant number ANR-22-EXTR-0009) (France); Institut de l’Océan and the Institut des Sciences du Calcul et  
1990 des Données of Sorbonne University (IDEX SUPER 11-IDEX-0004, project-team FORMAL) (France); Federal  
1991 Ministry of Education and Research, collaborative project C-SCOPE (project no. 03F0877A) (Germany);  
1992 Helmholtz Association ATMO programme (Germany); Initiative and Networking Fund of the Helmholtz  
1993 Association (grant no. VH-NG-19-33) (Germany); ICOS Germany (Germany); German Federal Ministry of  
1994 Education and Research (BMBF), project STEPSEC (grant no. 01LS2102A) (Germany); Helmholtz Young  
1995 Investigator Group Marine Carbon and Ecosystem Feedbacks in the Earth System (MarESys), grant number VH-  
1996 NG-1301 (Germany); Deutsche Forschungsgemeinschaft (DFG) under Germany's Excellence Strategy – EXC  
1997 2037 ‘Climate, Climatic Change, and Society’ – Project Number: 390683824 (Germany); Arctic Challenge for  
1998 Sustainability phase II project (ArCS-II; grant no. JP-MXD1420318865) (Japan); Environment Research and  
1999 Technology Development Fund (grant no. JPMEERF24S12206) (Japan); CREST, Japan Science and Technology  
2000 Agency (grant no. JPMJCR23J4) (Japan); Global Environmental Research Coordination System, Ministry of the  
2001 Environment (grant no. E2252) (Japan); Meteorological Agency (Japan); Ministry of Education, Culture, Sports,  
2002 Science and Technology, MEXT program for the advanced studies of climate change projection (SENTAN) (grant  
2003 numbers JPMXD0722680395 and JPMXD0722681344) (Japan); Meteorological Research Institute and the  
2004 Environment Research and Technology Development Fund (JPMEERF24S12200) (Japan); NIES GOSAT project  
2005 (Japan); Research Council of Norway (N-ICOS-2, grant no. 296012) (Norway); Research Council of Norway  
2006 (grant no. 270061) (Norway); Swiss National Science Foundation (grant no. 200020-200511) (Switzerland);  
2007 Natural Environmental Research Council, National Centre for Earth Observation (NE/R016518/1) (UK); Natural  
2008 Environment Research Council, UK EO Climate Information Service (NE/X019071/1) (UK); Natural  
2009 Environment Research Council (NE/V01417X/1) (UK); Natural Environment Research Council, National Centre  
2010 for Atmospheric Science (UK); Natural Environment Research Council (NE/Y005260/1) (UK); UK Royal Society  
2011 (grant no. RP\R1\191063) (UK); Natural Environment Research Council (Grant Ref: NE/V013106/1) (UK);



2012 National Center for Atmospheric Research (NSF Cooperative Agreement No. 1852977) (USA); NOAA Ocean  
2013 Acidification Program (grant no. 100018228) (USA); NOAA Global Ocean Monitoring and Observing Program  
2014 (grant no. 100018302) (USA); NOAA cooperative agreement NA22OAR4320151 (USA); NOAA cooperative  
2015 agreement NA20OAR4310340 (USA); NOAA (grant no. 1305M322PNRMJ0338); NASA (grant no.  
2016 80NSSC22K0150); NASA (grant no. 80NM0018D0004); National Science Foundation (NSF-2019625) (USA);  
2017 National Science Foundation (NSF-831361857) (USA); NASA Terrestrial Ecology Program (USA); NASA  
2018 Carbon Monitoring System program (80NSSC21K1059) (USA); NASA Land Cover and Land Use Change  
2019 Program (80NSSC24K0920) (USA); National Science Foundation (NSF-1903722) (USA); National Science  
2020 Foundation (NSF-1852977) (USA); The U.S. Department of Energy, Office of Science, Office of Biological and  
2021 Environmental Research (USA); The Department for Education SciDac (grant number: DESC0012972) (USA);  
2022 IDS (grant number: 80NSSC17K0348) (USA); Schmidt Sciences, LLC (USA).

2023 We also acknowledge support from the following computing facilities: The Australian Earth-System Simulator  
2024 National Research Infrastructure (ACCESS-NRI) (Australia); Deutsches Klimarechenzentrum (DKRZ) granted  
2025 by its Scientific Steering Committee (WLA) under project ID bm0891 (Germany); HPC cluster Aether at the  
2026 University of Bremen, financed by DFG within the scope of the Excellence Initiative (Germany); HPC resources  
2027 of TGCC under the allocation A0150102201 awarded by GENCI and of CCRT under the Grant CCRT2024-  
2028 p24cheva awarded by CEA/DRF (France); HPC resources of Meteo-France (France); NIES supercomputer system  
2029 (Japan); UNINETT Sigma2, National Infrastructure for High Performance Computing and Data Storage in  
2030 Norway (NN2980K/NS2980K) (Norway); UK CEDA JASMIN supercomputer (UK); UEA (University of East  
2031 Anglia) high performance computing cluster (UK); Derecho supercomputer (doi:10.5065/D6RX99HX), provided  
2032 by the Computational and Information Systems Laboratory (CISL) at NCAR (USA); Oak Ridge Leadership  
2033 Computing Facility at the Oak Ridge National Laboratory (USA); ISAM simulations were performed using  
2034 Cheyenne, NCAR HPC resources managed by CISL (doi:10.5065/D6RX99HX) (USA).



2035

## References

- 2036 Andela, N., Morton, D. C., Giglio, L., Chen, Y., van der Werf, G. R., Kasibhatla, P. S., DeFries, R. S., Collatz, G. J.,  
2037 Hantson, S., Kloster, S., Bachelet, D., Forrest, M., Lasslop, G., Li, F., Mangeon, S., Melton, J. R., Yue, C., and Randerson, J.  
2038 T.: A human-driven decline in global burned area, *Science*, 356, 1356–1362, <https://doi.org/10.1126/science.aal4108>, 2017.
- 2039 Andrew, R. M.: A comparison of estimates of global carbon dioxide emissions from fossil carbon sources, *Earth Syst. Sci.*  
2040 *Data*, 12, 1437–1465, <https://doi.org/10.5194/essd-12-1437-2020>, 2020a.
- 2041 Andrew, R. M.: Timely estimates of India’s annual and monthly fossil CO<sub>2</sub> emissions, *Earth Syst. Sci. Data*, 12, 2411–2421,  
2042 <https://doi.org/10.5194/essd-12-2411-2020>, 2020b.
- 2043 Andrew, R. M. and Peters, G. P.: The Global Carbon Project’s fossil CO<sub>2</sub> emissions dataset (2024v17), Zenodo [dataset],  
2044 <https://doi.org/10.5281/zenodo.13981696>, 2024.
- 2045 Aragão, L. E. O. C., Anderson, L. O., Fonseca, M. G., Rosan, T. M., Vedovato, L. B., Wagner, F. H., Silva, C. V. J., Silva  
2046 Junior, C. H. L., Arai, E., Aguiar, A. P., Barlow, J., Berenguer, E., Deeter, M. N., Domingues, L. G., Gatti, L., Gloor, M.,  
2047 Malhi, Y., Marengo, J. A., Miller, J. B., Phillips, O. L., and Saatchi, S.: 21st Century drought-related fires counteract the  
2048 decline of Amazon deforestation carbon emissions, *Nat Commun*, 9, 536, <https://doi.org/10.1038/s41467-017-02771-y>,  
2049 2018.
- 2050 Archer, D., Eby, M., Brovkin, V., Ridgwell, A., Cao, L., Mikolajewicz, U., Caldeira, K., Matsumoto, K., Munhoven, G.,  
2051 Montenegro, A., and Tokos, K.: Atmospheric Lifetime of Fossil Fuel Carbon Dioxide, *Annu. Rev. Earth Planet. Sci.*, 37,  
2052 117–134, <https://doi.org/10.1146/annurev.earth.031208.100206>, 2009.
- 2053 Arneeth, A., Sitch, S., Pongratz, J., Stocker, B. D., Ciais, P., Poulter, B., Bayer, A. D., Bondeau, A., Calle, L., Chini, L. P.,  
2054 Gasser, T., Fader, M., Friedlingstein, P., Kato, E., Li, W., Lindeskog, M., Nabel, J. E. M. S., Pugh, T. A. M., Robertson, E.,  
2055 Viovy, N., Yue, C., and Zaehle, S.: Historical carbon dioxide emissions caused by land-use changes are possibly larger than  
2056 assumed, *Nature Geosci*, 10, 79–84, <https://doi.org/10.1038/ngeo2882>, 2017.
- 2057 Asaadi, A., Arora, V. K., Melton, J. R., and Bartlett, P.: An improved parameterization of leaf area index (LAI) seasonality  
2058 in the Canadian Land Surface Scheme (CLASS) and Canadian Terrestrial Ecosystem Model (CTEM) modelling framework,  
2059 15, 6885–6907, <https://doi.org/10.5194/bg-15-6885-2018>, 2018.
- 2060 Aumont, O., Orr, J. C., Monfray, P., Ludwig, W., Amiotte-Suchet, P., and Probst, J.-L.: Riverine-driven interhemispheric  
2061 transport of carbon, *Global Biogeochem. Cycles*, 15, 393–405, <https://doi.org/10.1029/1999GB001238>, 2001.
- 2062 Aumont, O., Ethé, C., Tagliabue, A., Bopp, L., and Gehlen, M.: PISCES-v2: an ocean biogeochemical model for carbon and  
2063 ecosystem studies, 8, 2465–2513, <https://doi.org/10.5194/gmd-8-2465-2015>, 2015.
- 2064 Baccini, A., Walker, W., Carvalho, L., Farina, M., Sulla-Menashe, D., and Houghton, R. A.: Tropical forests are a net carbon  
2065 source based on aboveground measurements of gain and loss, *Science*, 358, 230–234,  
2066 <https://doi.org/10.1126/science.aam5962>, 2017.
- 2067 Bakker, D. C. E., Pfeil, B., Landa, C. S., Metzler, N., O’Brien, K. M., Olsen, A., Smith, K., Cosca, C., Harasawa, S., Jones, S.  
2068 D., Nakaoka, S., Nojiri, Y., Schuster, U., Steinhoff, T., Sweeney, C., Takahashi, T., Tilbrook, B., Wada, C., Wanninkhof, R.,  
2069 Alin, S. R., Balestrini, C. F., Barbero, L., Bates, N. R., Bianchi, A. A., Bonou, F., Boutin, J., Bozec, Y., Burger, E. F., Cai,



- 2070 W.-J., Castle, R. D., Chen, L., Chierici, M., Currie, K., Evans, W., Featherstone, C., Feely, R. A., Fransson, A., Goyet, C.,  
2071 Greenwood, N., Gregor, L., Hankin, S., Hardman-Mountford, N. J., Harlay, J., Hauck, J., Hoppema, M., Humphreys, M. P.,  
2072 Hunt, C. W., Huss, B., Ibáñez, J. S. P., Johannessen, T., Keeling, R., Kitidis, V., Körtzinger, A., Kozyr, A., Krasakopoulou,  
2073 E., Kuwata, A., Landschützer, P., Lauvset, S. K., Lefèvre, N., Lo Monaco, C., Manke, A., Mathis, J. T., Merlivat, L.,  
2074 Millero, F. J., Monteiro, P. M. S., Munro, D. R., Murata, A., Newberger, T., Omar, A. M., Ono, T., Paterson, K., Pearce, D.,  
2075 Pierrot, D., Robbins, L. L., Saito, S., Salisbury, J., Schlitzer, R., Schneider, B., Schweitzer, R., Sieger, R., Skjelvan, I.,  
2076 Sullivan, K. F., Sutherland, S. C., Sutton, A. J., Tadokoro, K., Telszewski, M., Tuma, M., van Heuven, S. M. A. C.,  
2077 Vandemark, D., Ward, B., Watson, A. J., and Xu, S.: A multi-decade record of high-quality CO<sub>2</sub> data in version 3 of the  
2078 Surface Ocean CO<sub>2</sub> Atlas (SOCAT), *Earth Syst. Sci. Data*, 8, 383–413, <https://doi.org/10.5194/essd-8-383-2016>, 2016.
- 2079 Bakker, Dorothee C. E.; Alin, Simone R.; Bates, Nicholas; Becker, Meike; Gkritzalis, Thanos; Jones, Steve D.; Kozyr, Alex;  
2080 Lauvset, Siv K.; Metzl, Nicolas; Nakaoka, Shin-ichiro; O'Brien, Kevin M.; Olsen, Are; Pierrot, Denis; Steinhoff, Tobias;  
2081 Sutton, Adrienne J.; Takao, Shintaro; Tilbrook, Bronte; Wada, Chisato; Wanninkhof, Rik; Akl, John; Arbillá, Lisandro A.;  
2082 Arruda, Ricardo; Azetsu-Scott, Kumiko; Barbero, Leticia; Beatty, Cory M.; Berghoff, Carla F.; Bittig, Henry C.; Burger,  
2083 Eugene F.; Campbell, Katie; Cardin, Vanessa; Collins, Andrew; Coppola, Laurent; Cronin, Margot; Cross, Jessica N.;  
2084 Currie, Kim I.; Emerson, Steven R.; Enright, Matt P.; Enyo, Kazutaka; Evans, Wiley; Feely, Richard A.; Flohr, Anita;  
2085 Gehrung, Martina; Glockzin, Michael; González-Dávila, Melchor; Hamna, Siyabulela; Hartman, Sue; Howden, Stephan D.;  
2086 Kam, Kitty; Kamb, Linus; Körtzinger, Arne; Kosugi, Naohiro; Lefèvre, Nathalie; Lo Monaco, Claire; Macovei, Vlad A.;  
2087 Maenner Jones, Stacy; Manalang, Dana; Martz, Todd R.; Mdokwana, Baxolele; Monacci, Natalie M.; Monteiro, Pedro M.  
2088 S.; Mordy, Calvin; Morell, Julio M.; Murata, Akihiko; Neill, Craig; Noh, Jae-Hoon; Nojiri, Yukihiko; Ohman, Mark; Olivier,  
2089 Léa; Ono, Tsuneo; Petersen, Wilhelm; Plueddemann, Albert J.; Prytherch, John; Rehder, Gregor; Rutgersson, Anna;  
2090 Santana-Casiano, J. Magdalena; Schlitzer, Reiner; Send, Uwe; Skjelvan, Ingunn; Sullivan, Kevin F.; T'Jampens, Michiel;  
2091 Tadokoro, Kazuaki; Telszewski, Maciej; Theetaert, Hannelore; Tsanwani, Mutshutshu; Vandemark, Douglas; van Ooijen,  
2092 Erik; Vecchia, Martín H.; Voynova, Yoana G.; Wang, Hongjie; Weller, Robert A.; Woosley, Ryan J.: Surface Ocean CO<sub>2</sub>  
2093 Atlas Database Version 2024 (SOCATv2024) (NCEI Accession 0293257). NOAA National Centers for Environmental  
2094 Information, <https://doi.org/10.25921/9wpm-th28>, last access: 28 October 2024, 2024.
- 2095 Ballantyne, A. P., Alden, C. B., Miller, J. B., Tans, P. P., and White, J. W. C.: Increase in observed net carbon dioxide  
2096 uptake by land and oceans during the past 50 years, *Nature*, 488, 70–72, <https://doi.org/10.1038/nature11299>, 2012.
- 2097 Ballantyne, A. P., Andres, R., Houghton, R., Stocker, B. D., Wanninkhof, R., Anderegg, W., Cooper, L. A., DeGrandpre,  
2098 M., Tans, P. P., Miller, J. B., Alden, C., and White, J. W. C.: Audit of the global carbon budget: estimate errors and their  
2099 impact on uptake uncertainty, *Biogeosciences*, 12, 2565–2584, <https://doi.org/10.5194/bg-12-2565-2015>, 2015.
- 2100 Bastos, A., Hartung, K., Nützel, T. B., Nabel, J. E. M. S., Houghton, R. A., and Pongratz, J.: Comparison of uncertainties in  
2101 land-use change fluxes from bookkeeping model parameterisation, 12, 745–762, <https://doi.org/10.5194/esd-12-745-2021>,  
2102 2021.
- 2103 Battle, M. O., Raynor, R., Kesler, S., and Keeling, R.: Technical Note: The impact of industrial activity on the amount of  
2104 atmospheric O<sub>2</sub>, *Atmospheric Chem. Phys. Discuss.*, 1–17, <https://doi.org/10.5194/acp-2022-765>, 2023.  
2105
- 2106 Bellenger, H., Bopp, L., Ethé, C., Ho, D., Duvel, J. P., Flavoni, S., Guez, L., Kataoka, T., Perrot, X., Parc, L., and Watanabe,  
2107 M.: Sensitivity of the Global Ocean Carbon Sink to the Ocean Skin in a Climate Model, *J. Geophys. Res. Oceans*, 128,  
2108 e2022JC019479, <https://doi.org/10.1029/2022JC019479>, 2023.  
2109



- 2110 Bennington, V., Gloege, L., and McKinley, G. A.: Variability in the Global Ocean Carbon Sink From 1959 to 2020 by  
2111 Correcting Models with Observations, *Geophys. Res. Lett.*, 49, e2022GL098632, <https://doi.org/10.1029/2022GL098632>,  
2112 2022.
- 2113 Bernardello, R., Sicardi, V., Lapin, V., Ortega, P., Ruprich-Robert, Y., Tourigny, E. and Ferrer, E.: Ocean biogeochemical  
2114 reconstructions to estimate historical ocean CO<sub>2</sub> uptake. *Earth System Dynamics*, 15(5), pp.1255-1275,  
2115 <https://doi.org/10.5194/esd-15-1255-2024>, 2024.
- 2116 Berthet, S., Sférian, R., Bricaud, C., Chevallier, M., Voldoire, A., and Ethé, C.: Evaluation of an Online Grid-Coarsening  
2117 Algorithm in a Global Eddy-Admitting Ocean Biogeochemical Model, *J. Adv. Model Earth Sy.*, 11, 1759–1783,  
2118 <https://doi.org/10.1029/2019MS001644>, 2019.
- 2119 Betts, R. A., Jones, C. D., Knight, J. R., Keeling, R. F., and Kennedy, J. J.: El Niño and a record CO<sub>2</sub> rise, *Nat. Clim.*  
2120 *Change*, 6, 806–810, <https://doi.org/10.1038/nclimate3063>, 2016.
- 2121 Bilbao, R., Wild, S., Ortega, P., Acosta-Navarro, J., Arsouze, T., Bretonnière, P.A., Caron, L.P., Castrillo, M., Cruz-García,  
2122 R., Cvijanovic, I. and Doblas-Reyes, F.J.: Assessment of a full-field initialised decadal climate prediction system with the  
2123 CMIP6 version of EC-Earth. *Earth System Dynamics Discussions*, 2020, pp.1-30, <https://doi.org/10.5194/esd-12-173-2021>,  
2124 2020.
- 2125 Bloom, A. A. and Williams, M.: Constraining ecosystem carbon dynamics in a data-limited world: integrating ecological  
2126 “common sense” in a model–data fusion framework, *Biogeosciences*, 12, 1299–1315, [https://doi.org/10.5194/bg-12-1299-](https://doi.org/10.5194/bg-12-1299-2015)  
2127 2015, 2015.
- 2128
- 2129 Bloom, A. A., Exbrayat, J.-F., van der Velde, I. R., Feng, L., and Williams, M.: The decadal state of the terrestrial carbon  
2130 cycle: Global retrievals of terrestrial carbon allocation, pools, and residence times, *Proc. Natl. Acad. Sci.*, 113, 1285–1290,  
2131 <https://doi.org/10.1073/pnas.1515160113>, 2016.
- 2132
- 2133 Boer, G. J., Smith, D. M., Cassou, C., Doblas-Reyes, F., Danabasoglu, G., Kirtman, B., Kushnir, Y., Kimoto, M., Meehl, G.  
2134 A., Msadek, R., Mueller, W. A., Taylor, K. E., Zwiers, F., Rixen, M., Ruprich-Robert, Y., and Eade, R.: The Decadal  
2135 Climate Prediction Project (DCPP) contribution to CMIP6, *Geosci. Model Dev.*, 9, 3751–3777, [https://doi.org/10.5194/gmd-](https://doi.org/10.5194/gmd-9-3751-2016)  
2136 9-3751-2016, 2016.
- 2137
- 2138 Boucher, O., Servonnat, J., Albright, A. L., Aumont, O., Balkanski, Y., Bastrikov, V., Bekki, S., Bonnet, R., Bony, S., Bopp,  
2139 L., Braconnot, P., Brockmann, P., Cadule, P., Caubel, A., Cheruy, F., Codron, F., Cozic, A., Cugnet, D., D’Andrea, F.,  
2140 Davini, P., de Lavergne, C., Denvil, S., Deshayes, J., Devilliers, M., Ducharne, A., Dufresne, J.-L., Dupont, E., Éthé, C.,  
2141 Fairhead, L., Falletti, L., Flavoni, S., Foujols, M.-A., Gardoll, S., Gastineau, G., Ghattas, J., Grandpeix, J.-Y., Guenet, B.,  
2142 Guez, E., Lionel, Guilyardi, E., Guimberteau, M., Hauglustaine, D., Hourdin, F., Idelkadi, A., Joussaume, S., Kageyama, M.,  
2143 Khodri, M., Krinner, G., Lebas, N., Levvasseur, G., Lévy, C., Li, L., Lott, F., Lurton, T., Luysaert, S., Madec, G.,  
2144 Madeleine, J.-B., Maignan, F., Marchand, M., Marti, O., Mellul, L., Meurdesoif, Y., Mignot, J., Musat, I., Otlé, C., Peylin,  
2145 P., Planton, Y., Polcher, J., Rio, C., Rochetin, N., Rousset, C., Sepulchre, P., Sima, A., Swingedouw, D., Thiéblemont, R.,  
2146 Traore, A. K., Vancoppenolle, M., Vial, J., Vialard, J., Viovy, N., and Vuichard, N.: Presentation and Evaluation of the  
2147 IPSL-CM6A-LR Climate Model, *J. Adv. Model. Earth Syst.*, 12, e2019MS002010, <https://doi.org/10.1029/2019MS002010>,  
2148 2020.



- 2149 Bourgeois, T., Goris, N., Schwinger, J., and Tjiputra, J. F.: Stratification constrains future heat and carbon uptake in the  
2150 Southern Ocean between 30°S and 55°S, *Nat. Commun.*, 13, 340, <https://doi.org/10.1038/s41467-022-27979-5>, 2022.
- 2151 Bray, E.: 2017 Minerals Yearbook: Aluminum [Advance Release], Tech. rep., U.S. Geological Survey, [https://d9-wret.s3-us-](https://d9-wret.s3-us-west-2.amazonaws.com/assets/palladium/production/atoms/files/myb1-2017-alumi.pdf)  
2152 [west-2.amazonaws.com/assets/palladium/production/atoms/files/myb1-2017-alumi.pdf](https://d9-wret.s3-us-west-2.amazonaws.com/assets/palladium/production/atoms/files/myb1-2017-alumi.pdf), 2020.
- 2153 Brienen, R. J. W., Caldwell, L., Duchesne, L., Voelker, S., Barichivich, J., Baliva, M., Ceccantini, G., Di Filippo, A.,  
2154 Helama, S., Locosselli, G. M., Lopez, L., Piovesan, G., Schöngart, J., Villalba, R., and Gloor, E.: Forest carbon sink  
2155 neutralized by pervasive growth-lifespan trade-offs, *Nat. Commun.*, 11, 4241, <https://doi.org/10.1038/s41467-020-17966-z>,  
2156 2020.
- 2157 Brienen, R. J. W., Phillips, O. L., Feldpausch, T. R., Gloor, E., Baker, T. R., Lloyd, J., Lopez-Gonzalez, G., Monteagudo-  
2158 Mendoza, A., Malhi, Y., Lewis, S. L., Vásquez Martínez, R., Alexiades, M., Álvarez Dávila, E., Alvarez-Loayza, P.,  
2159 Andrade, A., Aragão, L. E. O. C., Araujo-Murakami, A., Arets, E. J. M. M., Arroyo, L., Aymard C., G. A., Bánki, O. S.,  
2160 Baraloto, C., Barroso, J., Bonal, D., Boot, R. G. A., Camargo, J. L. C., Castilho, C. V., Chama, V., Chao, K. J., Chave, J.,  
2161 Comiskey, J. A., Cornejo Valverde, F., da Costa, L., de Oliveira, E. A., Di Fiore, A., Erwin, T. L., Fauset, S., Forsthofer, M.,  
2162 Galbraith, D. R., Grahame, E. S., Groot, N., Hérault, B., Higuchi, N., Honorio Coronado, E. N., Keeling, H., Killeen, T. J.,  
2163 Laurance, W. F., Laurance, S., Licona, J., Magnussen, W. E., Marimon, B. S., Marimon-Junior, B. H., Mendoza, C., Neill,  
2164 D. A., Nogueira, E. M., Núñez, P., Pallqui Camacho, N. C., Parada, A., Pardo-Molina, G., Peacock, J., Peña-Claros, M.,  
2165 Pickavance, G. C., Pitman, N. C. A., Poorter, L., Prieto, A., Quesada, C. A., Ramírez, F., Ramírez-Angulo, H., Restrepo, Z.,  
2166 Roopsind, A., Rudas, A., Salomão, R. P., Schwarz, M., Silva, N., Silva-Espejo, J. E., Silveira, M., Stropp, J., Talbot, J., ter  
2167 Steege, H., Teran-Aguilar, J., Terborgh, J., Thomas-Caesar, R., Toledo, M., Torello-Raventos, M., Umetsu, R. K., van der  
2168 Heijden, G. M. F., van der Hout, P., Guimaraes Vieira, I. C., Vieira, S. A., Vilanova, E., Vos, V. A., and Zagt, R. J.: Long-  
2169 term decline of the Amazon carbon sink, 519, 344–348, <https://doi.org/10.1038/nature14283>, 2015.
- 2170 Bronselaer, B., Winton, M., Russell, J., Sabine, C. L., and Khatiwala, S.: Agreement of CMIP5 Simulated and Observed  
2171 Ocean Anthropogenic CO<sub>2</sub> Uptake, *Geophys. Res. Lett.*, 44, 12,298–12,305, <https://doi.org/10.1002/2017GL074435>, 2017.
- 2172 Bruno, M. and Joos, F.: Terrestrial carbon storage during the past 200 years: A Monte Carlo Analysis of CO<sub>2</sub> data from ice  
2173 core and atmospheric measurements, *Global Biogeochem. Cycles*, 11, 111–124, <https://doi.org/10.1029/96GB03611>, 1997.
- 2174 Burrows, S. M., Maltrud, M., Yang, X., Zhu, Q., Jeffery, N., Shi, X., Ricciuto, D., Wang, S., Bisht, G., Tang, J., Wolfe, J.,  
2175 Harrop, B. E., Singh, B., Brent, L., Baldwin, S., Zhou, T., Cameron-Smith, P., Keen, N., Collier, N., Xu, M., Hunke, E. C.,  
2176 Elliott, S. M., Turner, A. K., Li, H., Wang, H., Golaz, J.-C., Bond-Lamberty, B., Hoffman, F. M., Riley, W. J., Thornton, P.  
2177 E., Calvin, K., and Leung, L. R.: The DOE E3SM v1.1 Biogeochemistry Configuration: Description and Simulated  
2178 Ecosystem-Climate Responses to Historical Changes in Forcing, *J. Adv. Model. Earth Syst.*, 12, e2019MS001766,  
2179 <https://doi.org/10.1029/2019MS001766>, 2020.
- 2180 Bunsen, F., Nissen, C., and Hauck, J.: The Impact of Recent Climate Change on the Global Ocean Carbon Sink. *Geophysical*  
2181 *Research Letters*, 51(4), e2023GL107030, <https://doi.org/10.1029/2023GL107030>, 2024.
- 2182 Burton, C., Betts, R., Cardoso, M., Feldpausch, T. R., Harper, A., Jones, C. D., Kelley, D. I., Robertson, E., and Wiltshire,  
2183 A.: Representation of fire, land-use change and vegetation dynamics in the Joint UK Land Environment Simulator vn4.9  
2184 (JULES), *Geosci. Model Dev.*, 12, 179–193, <https://doi.org/10.5194/gmd-12-179-2019>, 2019.



- 2185 Burton, C., Lampe, S., Kelley, D. I., Thiery, W., Hantson, S., Christidis, N., Gudmundsson, L., Forrest, M., Burke, E.,  
2186 Chang, J., Huang, H., Ito, A., Kou-Giesbrecht, S., Lasslop, G., Li, W., Nieradzki, L., Li, F., Chen, Y., Randerson, J., Reyer,  
2187 C. P. O., and Mengel, M.: Global burned area increasingly explained by climate change, *Nature Climate Change*,  
2188 <https://doi.org/10.1038/s41558-024-02140-w>, 2024.
- 2189 Bushinsky, S. M., Landschützer, P., Rödenbeck, C., Gray, A. R., Baker, D., Mazloff, M. R., Resplandy, L., Johnson, K. S.,  
2190 and Sarmiento, J. L.: Reassessing Southern Ocean Air-Sea CO<sub>2</sub> Flux Estimates With the Addition of Biogeochemical Float  
2191 Observations, *Global Biogeochem. Cycles*, 33, 1370–1388, <https://doi.org/10.1029/2019GB006176>, 2019.
- 2192 Byrne, B., Liu, J., Bowman, K. W., Pascolini-Campbell, M., Chatterjee, A., Pandey, S., Miyazaki, K., van der Werf, G. R.,  
2193 Wunch, D., Wennberg, P. O., Roehl, C. M., and Sinha, S.: Carbon emissions from the 2023 Canadian wildfires. *Nature*, 633,  
2194 835–839, <https://doi.org/10.1038/s41586-024-07878-z>, 2024.
- 2195 Canadell, J. G., Le Quere, C., Raupach, M. R., Field, C. B., Buitenhuis, E. T., Ciais, P., Conway, T. J., Gillett, N. P.,  
2196 Houghton, R. A., and Marland, G.: Contributions to accelerating atmospheric CO<sub>2</sub> growth from economic activity, carbon  
2197 intensity, and efficiency of natural sinks, *Proceedings of the National Academy of Sciences*, 104, 18866–18870,  
2198 <https://doi.org/10.1073/pnas.0702737104>, 2007.
- 2199 Canadell, J. G., Monteiro, P. M. S., Costa, M. H., Cotrim da Cunha, L., Cox, P. M., Eliseev, A. V., Henson, S., Ishii, M.,  
2200 Jaccard, S., Koven, C., Lohila, A., Patra, P. K., Piao, S., Rogelj, J., Syampungani, S., Zaehle, S., and Zickfeld, K.: Global  
2201 Carbon and other Biogeochemical Cycles and Feedbacks. In: *Climate Change 2021: The Physical Science Basis*.  
2202 Contribution of Working Group I to the Sixth Assessment Report of the Intergovernmental Panel on Climate Change  
2203 [Masson-Delmotte, V., P. Zhai, A. Pirani, S. L. Connors, C. Péan, S. Berger, N. Caud, Y. Chen, L. Goldfarb, M. I. Gomis,  
2204 M. Huang, K. Leitzell, E. Lonnoy, J. B. R. Matthews, T. K. Maycock, T. Waterfield, O. Yelekçi, R. Yu and B. Zhou (eds.)].  
2205 Cambridge University Press, Cambridge, United Kingdom and New York, NY, USA, pp. 673–816,  
2206 <https://doi.org/10.1017/9781009157896.007>, 2021.
- 2207 Cao, Z., Myers, R. J., Lupton, R. C., Duan, H., Sacchi, R., Zhou, N., Reed Miller, T., Cullen, J. M., Ge, Q., and Liu, G.: The  
2208 sponge effect and carbon emission mitigation potentials of the global cement cycle, *Nat Commun*, 11, 3777,  
2209 <https://doi.org/10.1038/s41467-020-17583-w>, 2020.
- 2210 Centro Nacional de Monitoramento e Alertas de Desastres Naturais (CEMADEN): Monitoramento de secas e impactos no  
2211 Brasil - Agosto 2024, available at: [https://www.gov.br/cemaden/pt-br/assuntos/monitoramento/monitoramento-de-seca-para-](https://www.gov.br/cemaden/pt-br/assuntos/monitoramento/monitoramento-de-seca-para-o-brasil/monitoramento-de-secas-e-impactos-no-brasil-agosto-2024)  
2212 [o-brasil/monitoramento-de-secas-e-impactos-no-brasil-agosto-2024](https://www.gov.br/cemaden/pt-br/assuntos/monitoramento/monitoramento-de-seca-para-o-brasil/monitoramento-de-secas-e-impactos-no-brasil-agosto-2024), last access: 28 October 2024.
- 2213 Céspedes, J., Sylvester, J. M., Pérez-Marulanda, L., Paz-García, P., Reymondin, L., Khodadadi, M., Tello, J. J., and Castro-  
2214 Nunez, A.: Has global deforestation accelerated due to the COVID-19 pandemic?, *J. For. Res.*, 34, 1153–1165,  
2215 <https://doi.org/10.1007/s11676-022-01561-7>, 2023.
- 2216 Chandra, N., Patra, P. K., Niwa, Y., Ito, A., Iida, Y., Goto, D., Morimoto, S., Kondo, M., Takigawa, M., Hajima, T., and  
2217 Watanabe, M.: Estimated regional CO<sub>2</sub> flux and uncertainty based on an ensemble of atmospheric CO<sub>2</sub> inversions,  
2218 *Atmospheric Chem. Phys.*, 22, 9215–9243, <https://doi.org/10.5194/acp-22-9215-2022>, 2022.
- 2219 Chatfield, C.: The Holt-Winters Forecasting Procedure, *J. Roy. Stat. Soc. C.*, 27, 264–279, <https://doi.org/10.2307/2347162>,  
2220 1978.





- 2221 Chau, T. T. T., Gehlen, M., and Chevallier, F.: A seamless ensemble-based reconstruction of surface ocean  $p\text{CO}_2$  and air–sea  
2222  $\text{CO}_2$  fluxes over the global coastal and open oceans, *Biogeosciences*, 19, 1087–1109, [https://doi.org/10.5194/bg-19-1087-](https://doi.org/10.5194/bg-19-1087-2022)  
2223 2022, 2022.
- 2224 Chevallier, F., Fisher, M., Peylin, P., Serrar, S., Bousquet, P., Bréon, F.-M., Chédin, A., and Ciais, P.: Inferring  $\text{CO}_2$   
2225 sources and sinks from satellite observations: Method and application to TOVS data, *J. Geophys. Res.*, 110, D24309,  
2226 <https://doi.org/10.1029/2005JD006390>, 2005.
- 2227 Ciais, P., Sabine, C., Bala, G., Bopp, L., Brovkin, V., Canadell, J. G., Chhabra, A., DeFries, R., Galloway, J., Heimann, M.,  
2228 Jones, C., Le Quéré, C., Myneni, R., Piao, S., Thornton, P., Willem, J., Friedlingstein, P., and Munhoven, G.: Carbon and  
2229 Other Biogeochemical Cycles, in *Climate Change 2013: The Physical Science Basis, Contribution of Working Group I to the  
2230 Fifth Assessment Report of the Intergovernmental Panel on Climate Change*, edited by: Intergovernmental Panel on Climate  
2231 Change, Cambridge University Press, Cambridge, United Kingdom and New York, NY, USA,  
2232 <https://doi.org/10.1017/CBO9781107415324.015>, 2013.
- 2233 Ciais, P., Tan, J., Wang, X., Roedenbeck, C., Chevallier, F., Piao, S.-L., Moriarty, R., Broquet, G., Le Quéré, C., Canadell, J.  
2234 G., Peng, S., Poulter, B., Liu, Z., and Tans, P.: Five decades of northern land carbon uptake revealed by the interhemispheric  
2235  $\text{CO}_2$  gradient, *Nature*, 568, 221–225, <https://doi.org/10.1038/s41586-019-1078-6>, 2019.
- 2236 Ciais, P., Bastos, A., Chevallier, F., Lauerwald, R., Poulter, B., Canadell, P., Hugelius, G., Jackson, R. B., Jain, A., Jones,  
2237 M., Kondo, M., Luijkx, I. T., Patra, P. K., Peters, W., Pongratz, J., Petrescu, A. M. R., Piao, S., Qiu, C., Von Randow, C.,  
2238 Regnier, P., Saunois, M., Scholes, R., Shvidenko, A., Tian, H., Yang, H., Wang, X., and Zheng, B.: Definitions and methods  
2239 to estimate regional land carbon fluxes for the second phase of the REgional Carbon Cycle Assessment and Processes  
2240 Project (RECCAP-2), *Geosci. Model Dev.*, 15, 1289–1316, <https://doi.org/10.5194/gmd-15-1289-2022>, 2022.
- 2241 Collier, N., Hoffman, F. M., Lawrence, D. M., Keppel-Aleks, G., Koven, C. D., Riley, W. J., Mu, M., and Randerson, J. T.:  
2242 The International Land Model Benchmarking (ILAMB) System: Design, Theory, and Implementation, *J. Adv. Model. Earth  
2243 Syst.*, 10, 2731–2754, <https://doi.org/10.1029/2018MS001354>, 2018.
- 2244 Cox, P. M., Pearson, D., Booth, B. B., Friedlingstein, P., Huntingford, C., Jones, C. D., and Luke, C. M.: Sensitivity of  
2245 tropical carbon to climate change constrained by carbon dioxide variability, *Nature*, 494, 341–344,  
2246 <https://doi.org/10.1038/nature11882>, 2013.
- 2247 De Kauwe, M. G., Medlyn, B. E., Zaehle, S., Walker, A. P., Dietze, M. C., Wang, Y.-P., Luo, Y., Jain, A. K., El-Masri, B.,  
2248 Hickler, T., Wärlind, D., Weng, E., Parton, W. J., Thornton, P. E., Wang, S., Prentice, I. C., Asao, S., Smith, B., McCarthy,  
2249 H. R., Iversen, C. M., Hanson, P. J., Warren, J. M., Oren, R., and Norby, R. J.: Where does the carbon go? A model–data  
2250 intercomparison of vegetation carbon allocation and turnover processes at two temperate forest free-air  $\text{CO}_2$  enrichment  
2251 sites, *New Phytol.*, 203, 883–899, <https://doi.org/10.1111/nph.12847>, 2014.
- 2252 Delire, C., Séférian, R., Decharme, B., Alkama, R., Calvet, J.-C., Carrer, D., Gibelin, A.-L., Joetzjer, E., Morel, X., Rocher,  
2253 M., and Tzanos, D.: The Global Land Carbon Cycle Simulated With ISBA-CTRIP: Improvements Over the Last Decade, *J.  
2254 Adv. Model. Earth Syst.*, 12, e2019MS001886, <https://doi.org/10.1029/2019MS001886>, 2020.
- 2255 Denman, K. L., Brasseur, G., Chidthaisong, A., Ciais, P., Cox, P. M., Dickinson, R. E., Hauglustaine, D., Heinze, C.,  
2256 Holland, E., Jacob, D., Lohmann, U., Ramachandran, S., Leite da Silva Dias, P., Wofsy, S. C., and Zhang, X.: Couplings  
2257 Between Changes in the Climate System and Biogeochemistry, in: *Climate Change 2007: The Physical Science Basis*.



- 2258 Contribution of Working Group I to the Fourth Assessment Report of the Intergovernmental Panel on Climate Change,  
2259 edited by: Solomon, S., Qin, D., Manning, M., Marquis, M., Averyt, K., Tignor, M. M. B., Miller, H. L., and Chen, Z. L.,  
2260 Cambridge University Press, Cambridge, UK and New York, USA, 499–587, ISBN: 9780521705967, 2007.
- 2261 Denvil-Sommer, A., Gehlen, M., and Vrac, M.: Observation system simulation experiments in the Atlantic Ocean for  
2262 enhanced surface ocean pCO<sub>2</sub> reconstructions, *Ocean Sci.*, 17, 1011–1030, <https://doi.org/10.5194/os-17-1011-2021>, 2021.
- 2263 DeVries, T., Holzer, M., and Primeau, F.: Recent increase in oceanic carbon uptake driven by weaker upper-ocean  
2264 overturning, *Nature*, 542, 215–218, <https://doi.org/10.1038/nature21068>, 2017.
- 2265 DeVries, T., Quéré, C. L., Andrews, O., Berthet, S., Hauck, J., Ilyina, T., Landschützer, P., Lenton, A., Lima, I. D., Nowicki,  
2266 M., Schwinger, J., and Séférian, R.: Decadal trends in the ocean carbon sink, *PNAS*, 116, 11646–11651,  
2267 <https://doi.org/10.1073/pnas.1900371116>, 2019.
- 2268 DeVries, T., Yamamoto, K., Wanninkhof, R., Gruber, N., Hauck, J., Müller, J. D., Bopp, L., Carroll, D., Carter, B., Chau,  
2269 T.-T.-T., Doney, S. C., Gehlen, M., Gloege, L., Gregor, L., Henson, S., Kim, J. H., Iida, Y., Ilyina, T., Landschützer, P., Le  
2270 Quéré, C., Munro, D., Nissen, C., Patara, L., Pérez, F. F., Resplandy, L., Rodgers, K. B., Schwinger, J., Séférian, R., Sicardi,  
2271 V., Terhaar, J., Triñanes, J., Tsujino, H., Watson, A., Yasunaka, S., and Zeng, J.: Magnitude, trends, and variability of the  
2272 global ocean carbon sink from 1985–2018, *Glob. Biogeochem. Cycles*, n/a, e2023GB007780,  
2273 <https://doi.org/10.1029/2023GB007780>, 2023.  
2274
- 2275 Döscher, R., Acosta, M., Alessandri, A., Anthoni, P., Armeth, A., Arsouze, T., Bergmann, T., Bernadello, R., Bousetta, S.,  
2276 Caron, L.P. and Carver, G.: The EC-earth3 Earth system model for the climate model intercomparison project 6.  
2277 Geoscientific Model Development Discussions, 2021, pp.1-90, <https://doi.org/10.5194/gmd-15-2973-2022>, 2021.  
2278
- 2279 Forster, P. M., Smith, C., Walsh, T., Lamb, W. F., Lamboll, R., Hall, B., Hauser, M., Ribes, A., Rosen, D., Gillett, N. P.,  
2280 Palmer, M. D., Rogelj, J., von Schuckmann, K., Trewin, B., Allen, M., Andrew, R., Betts, R. A., Borger, A., Boyer, T.,  
2281 Broersma, J. A., Buontempo, C., Burgess, S., Cagnazzo, C., Cheng, L., Friedlingstein, P., Gettelman, A., Gütschow, J., Ishii,  
2282 M., Jenkins, S., Lan, X., Morice, C., Mühle, J., Kadow, C., Kennedy, J., Killick, R. E., Krummel, P. B., Minx, J. C., Myhre,  
2283 G., Naik, V., Peters, G. P., Pirani, A., Pongratz, J., Schleussner, C.-F., Seneviratne, S. I., Szopa, S., Thorne, P., Kovilakam,  
2284 M. V. M., Majamäki, E., Jalkanen, J.-P., van Marle, M., Hoesly, R. M., Rohde, R., Schumacher, D., van der Werf, G., Vose,  
2285 R., Zickfeld, K., Zhang, X., Masson-Delmotte, V., and Zhai, P.: Indicators of Global Climate Change 2023: annual update of  
2286 key indicators of the state of the climate system and human influence, *Earth Syst. Sci. Data*, 16, 2625–2658,  
2287 <https://doi.org/10.5194/essd-16-2625-2024>, 2024.
- 2288 Doney, S. C., Lima, I., Feely, R. A., Glover, D. M., Lindsay, K., Mahowald, N., Moore, J. K., and Wanninkhof, R.:  
2289 Mechanisms governing interannual variability in upper-ocean inorganic carbon system and air–sea CO<sub>2</sub> fluxes: Physical  
2290 climate and atmospheric dust, *Deep Sea Research Part II: Topical Studies in Oceanography*, 56, 640–655,  
2291 <https://doi.org/10.1016/j.dsr2.2008.12.006>, 2009.
- 2292 Dong, Y., Bakker, D. C. E., Bell, T. G., Huang, B., Landschützer, P., Liss, P. S., and Yang, M.: Update on the Temperature  
2293 Corrections of Global Air–Sea CO<sub>2</sub> Flux Estimates, *Glob. Biogeochem. Cycles*, 36, e2022GB007360,  
2294 <https://doi.org/10.1029/2022GB007360>, 2022.  
2295



- 2296 Dong, Y., Bakker, D. C. E., Bell, T. G., Yang, M., Landschützer, P., Hauck, J., Rödenbeck, C., Kitidis, V., Bushinsky, S. M.,  
2297 and Liss, P. S. (2024). Direct observational evidence of strong CO<sub>2</sub> uptake in the Southern Ocean. *Science Advances*,  
2298 10(30), eadn5781, <https://doi.org/10.1126/sciadv.adn5781>, 2024a.  
2299
- 2300 Dong, Y., Bakker, D. C. E., and Landschützer, P.: Accuracy of ocean CO<sub>2</sub> uptake estimates at a risk by a reduction in the  
2301 data collection. *Geophysical Research Letters*, 51, e2024GL108502, <https://doi.org/10.1029/2024GL108502>, 2024b.  
2302
- 2303 Dorgeist, L., Schwingshackl, C., Bultan, S., and Pongratz, J.: A consistent budgeting of terrestrial carbon fluxes. *Nature*  
2304 *Communications*, 15(1), 7426, <https://doi.org/10.1038/s41467-024-51126-x>, 2024.  
2305
- 2306 Dou, X., Wang, Y., Ciais, P., Chevallier, F., Davis, S. J., Crippa, M., Janssens-Maenhout, G., Guizzardi, D., Solazzo, E.,  
2307 Yan, F., Huo, D., Zheng, B., Zhu, B., Cui, D., Ke, P., Sun, T., Wang, H., Zhang, Q., Gentine, P., Deng, Z., and Liu, Z.: Near-  
2308 real-time global gridded daily CO<sub>2</sub> emissions, *The Innovation*, 3, 100182, <https://doi.org/10.1016/j.xinn.2021.100182>, 2022.
- 2309 Edson, J. B., Jampana, V., Weller, R. A., Bigorre, S. P., Plueddemann, A. J., Fairall, C. W., Miller, S. D., Mahrt, L., Vickers,  
2310 D., and Hersbach, H.: On the Exchange of Momentum over the Open Ocean, *J. Phys. Oceanogr.*, 43, 1589–1610,  
2311 <https://doi.org/10.1175/JPO-D-12-0173.1>, 2013.
- 2312 EIA. Short-Term Energy Outlook: September 2023. U.S. Energy Information Administration [dataset]. Available at:  
2313 <http://www.eia.gov/forecasts/steo/outlook.cfm>, last access: 28 October 2024, 2023.
- 2314 Embury, O., Merchant, C.J., Good, S.A., Rayner, N.A., Hoyer, J.L., Atkinson, C., Block, T., Alerskans, E., Pearson, K.J.,  
2315 Worsfold, M. and McCarroll, N. and Donlon, C.: Satellite-based time-series of sea-surface temperature since 1980 for  
2316 climate applications. *Scientific Data*, 11(1), 326, <https://doi.org/10.1038/s41597-024-03147-w>, 2024.
- 2317 Erb, K.-H., Kastner, T., Luyssaert, S., Houghton, R. A., Kuemmerle, T., Olofsson, P., and Haberl, H.: Bias in the attribution  
2318 of forest carbon sinks, *Nature Clim Change*, 3, 854–856, <https://doi.org/10.1038/nclimate2004>, 2013.
- 2319 Erb, K.-H., Kastner, T., Plutzer, C., Bais, A. L. S., Carvalhais, N., Fetzel, T., Gingrich, S., Haberl, H., Lauk, C.,  
2320 Niedertscheider, M., Pongratz, J., Thurner, M., and Luyssaert, S.: Unexpectedly large impact of forest management and  
2321 grazing on global vegetation biomass, *Nature*, 553, 73–76, <https://doi.org/10.1038/nature25138>, 2018.
- 2322 Eskander, S. M. S. U. and Fankhauser, S.: Reduction in greenhouse gas emissions from national climate legislation, *Nat.*  
2323 *Clim. Chang.*, 10, 750–756, <https://doi.org/10.1038/s41558-020-0831-z>, 2020.
- 2324 Etheridge, D. M., Steele, L. P., Langenfelds, R. L., Francey, R. J., Barnola, J.-M., and Morgan, V. I.: Natural and  
2325 anthropogenic changes in atmospheric CO<sub>2</sub> over the last 1000 years from air in Antarctic ice and firn, *J. Geophys. Res.*,  
2326 101, 4115–4128, <https://doi.org/10.1029/95JD03410>, 1996.
- 2327 Eyring, V., Bony, S., Meehl, G. A., Senior, C. A., Stevens, B., Stouffer, R. J., and Taylor, K. E.: Overview of the Coupled  
2328 Model Intercomparison Project Phase 6 (CMIP6) experimental design and organization, *Geosci. Model Dev.*, 9, 1937–1958,  
2329 <https://doi.org/10.5194/gmd-9-1937-2016>, 2016.
- 2330 FAO, Food and Agriculture Organization of the United Nations (FAO): Impact of the Ukraine-Russia conflict on global food  
2331 security and related matters under the mandate of the Food and Agriculture Organization of the United Nations (FAO),



- 2332 Hundred and Seventieth Session of the Council, <https://www.fao.org/3/nj164en/nj164en.pdf>, last access: 28 October 2024,  
2333 2023.
- 2334 Fay, A. R., Gregor, L., Landschützer, P., McKinley, G. A., Gruber, N., Gehlen, M., Iida, Y., Laruelle, G. G., Rödenbeck, C.,  
2335 Roobaert, A., and Zeng, J.: SeaFlux: harmonization of air–sea CO<sub>2</sub> fluxes from surface pCO<sub>2</sub> data products using a  
2336 standardized approach, *Earth System Science Data*, 13, 4693–4710, <https://doi.org/10.5194/essd-13-4693-2021>, 2021.
- 2337 Feng, L., Palmer, P. I., Bösch, H., and Dance, S.: Estimating surface CO<sub>2</sub> fluxes from space-borne CO<sub>2</sub> dry air mole fraction  
2338 observations using an ensemble Kalman Filter, *Atmospheric Chem. Phys.*, 9, 2619–2633, [https://doi.org/10.5194/acp-9-](https://doi.org/10.5194/acp-9-2619-2009)  
2339 2619-2009, 2009.
- 2340 Feng, L., Palmer, P. I., Parker, R. J., Deutscher, N. M., Feist, D. G., Kivi, R., Morino, I., and Sussmann, R.: Estimates of  
2341 European uptake of CO<sub>2</sub> inferred from GOSAT XCO<sub>2</sub> retrievals: sensitivity to measurement bias inside and outside Europe,  
2342 *Atmos. Chem. Phys.*, 16, 1289–1302, <https://doi.org/10.5194/acp-16-1289-2016>, 2016.
- 2343 Flanagan, D.: 2017 Minerals Yearbook: Copper [Advance Release], Tech. rep., U.S. Geological Survey,  
2344 <https://pubs.usgs.gov/myb/vol11/2017/myb1-2017-copper.pdf>, 2021.
- 2345 Ford, D., Blannin, J., Watts, J., Watson, A., Landschützer, P., Jersild, A. and Shutler, J.: A comprehensive analysis of air-sea  
2346 CO<sub>2</sub> flux uncertainties constructed from surface ocean data products, *Global Biogeochemical Cycles*, accepted, 2024.
- 2347 Friedlingstein, P., Houghton, R. A., Marland, G., Hackler, J., Boden, T. A., Conway, T. J., Canadell, J. G., Raupach, M. R.,  
2348 Ciais, P., and Le Quéré, C.: Update on CO<sub>2</sub> emissions, *Nature Geosci*, 3, 811–812, <https://doi.org/10.1038/ngeo1022>, 2010.
- 2349 Friedlingstein, P., Andrew, R. M., Rogelj, J., Peters, G. P., Canadell, J. G., Knutti, R., Luderer, G., Raupach, M. R.,  
2350 Schaeffer, M., van Vuuren, D. P., and Le Quéré, C.: Persistent growth of CO<sub>2</sub> emissions and implications for reaching  
2351 climate targets, *Nature Geosci*, 7, 709–715, <https://doi.org/10.1038/ngeo2248>, 2014.
- 2352 Friedlingstein, P., Jones, M. W., O’Sullivan, M., Andrew, R. M., Hauck, J., Peters, G. P., Peters, W., Pongratz, J., Sitch, S.,  
2353 Le Quéré, C., Bakker, D. C. E., Canadell, J. G., Ciais, P., Jackson, R. B., Anthoni, P., Barbero, L., Bastos, A., Bastrikov, V.,  
2354 Becker, M., Bopp, L., Buitenhuis, E., Chandra, N., Chevallier, F., Chini, L. P., Currie, K. I., Feely, R. A., Gehlen, M.,  
2355 Gilfillan, D., Gkritzalis, T., Goll, D. S., Gruber, N., Gutekunst, S., Harris, I., Haverd, V., Houghton, R. A., Hurtt, G., Ilyina,  
2356 T., Jain, A. K., Joetzer, E., Kaplan, J. O., Kato, E., Klein Goldewijk, K., Korsbakken, J. I., Landschützer, P., Lauvset, S. K.,  
2357 Lefèvre, N., Lenton, A., Lienert, S., Lombardozi, D., Marland, G., McGuire, P. C., Melton, J. R., Metzl, N., Munro, D. R.,  
2358 Nabel, J. E. M. S., Nakaoka, S.-I., Neill, C., Omar, A. M., Ono, T., Pregon, A., Pierrot, D., Poulter, B., Rehder, G.,  
2359 Resplandy, L., Robertson, E., Rödenbeck, C., Séférian, R., Schwinger, J., Smith, N., Tans, P. P., Tian, H., Tilbrook, B.,  
2360 Tubiello, F. N., van der Werf, G. R., Wiltshire, A. J., and Zaehle, S.: Global Carbon Budget 2019, *Earth Syst. Sci. Data*, 11,  
2361 1783–1838, <https://doi.org/10.5194/essd-11-1783-2019>, 2019.
- 2362 Friedlingstein, P., O’Sullivan, M., Jones, M. W., Andrew, R. M., Hauck, J., Olsen, A., Peters, G. P., Peters, W., Pongratz, J.,  
2363 Sitch, S., Le Quéré, C., Canadell, J. G., Ciais, P., Jackson, R. B., Alin, S., Aragão, L. E. O. C., Armeth, A., Arora, V., Bates,  
2364 N. R., Becker, M., Benoit-Cattin, A., Bittig, H. C., Bopp, L., Bultan, S., Chandra, N., Chevallier, F., Chini, L. P., Evans, W.,  
2365 Florentie, L., Forster, P. M., Gasser, T., Gehlen, M., Gilfillan, D., Gkritzalis, T., Gregor, L., Gruber, N., Harris, I., Hartung,  
2366 K., Haverd, V., Houghton, R. A., Ilyina, T., Jain, A. K., Joetzer, E., Kadono, K., Kato, E., Kitidis, V., Korsbakken, J. I.,  
2367 Landschützer, P., Lefèvre, N., Lenton, A., Lienert, S., Liu, Z., Lombardozi, D., Marland, G., Metzl, N., Munro, D. R.,  
2368 Nabel, J. E. M. S., Nakaoka, S.-I., Niwa, Y., O’Brien, K., Ono, T., Palmer, P. I., Pierrot, D., Poulter, B., Resplandy, L.,



- 2369 Robertson, E., Rödenbeck, C., Schwinger, J., Séférian, R., Skjelvan, I., Smith, A. J. P., Sutton, A. J., Tanhua, T., Tans, P. P.,  
2370 Tian, H., Tilbrook, B., van der Werf, G., Vuichard, N., Walker, A. P., Wanninkhof, R., Watson, A. J., Willis, D., Wiltshire,  
2371 A. J., Yuan, W., Yue, X., and Zaehle, S.: Global Carbon Budget 2020, *Earth Syst. Sci. Data*, 12, 3269–3340,  
2372 <https://doi.org/10.5194/essd-12-3269-2020>, 2020.
- 2373 Friedlingstein, P., Jones, M. W., O’Sullivan, M., Andrew, R. M., Bakker, D. C. E., Hauck, J., Le Quéré, C., Peters, G. P.,  
2374 Peters, W., Pongratz, J., Sitch, S., Canadell, J. G., Ciais, P., Jackson, R. B., Alin, S. R., Anthoni, P., Bates, N. R., Becker, M.,  
2375 Bellouin, N., Bopp, L., Chau, T. T. T., Chevallier, F., Chini, L. P., Cronin, M., Currie, K. I., Decharme, B., Djeutchouang, L.  
2376 M., Dou, X., Evans, W., Feely, R. A., Feng, L., Gasser, T., Gilfillan, D., Gkritzalis, T., Grassi, G., Gregor, L., Gruber, N.,  
2377 Gürses, Ö., Harris, I., Houghton, R. A., Hurtt, G. C., Iida, Y., Ilyina, T., Luijkx, I. T., Jain, A., Jones, S. D., Kato, E.,  
2378 Kennedy, D., Klein Goldewijk, K., Knauer, J., Korsbakken, J. I., Körtzinger, A., Landschützer, P., Lauvset, S. K., Lefèvre,  
2379 N., Lienert, S., Liu, J., Marland, G., McGuire, P. C., Melton, J. R., Munro, D. R., Nabel, J. E. M. S., Nakaoka, S.-I., Niwa,  
2380 Y., Ono, T., Pierrot, D., Poulter, B., Rehder, G., Resplandy, L., Robertson, E., Rödenbeck, C., Rosan, T. M., Schwinger, J.,  
2381 Schwingshackl, C., Séférian, R., Sutton, A. J., Sweeney, C., Tanhua, T., Tans, P. P., Tian, H., Tilbrook, B., Tubiello, F., van  
2382 der Werf, G. R., Vuichard, N., Wada, C., Wanninkhof, R., Watson, A. J., Willis, D., Wiltshire, A. J., Yuan, W., Yue, C.,  
2383 Yue, X., Zaehle, S., and Zeng, J.: Global Carbon Budget 2021, *Earth Syst. Sci. Data*, 14, 1917–2005,  
2384 <https://doi.org/10.5194/essd-14-1917-2022>, 2022a.
- 2385 Friedlingstein, P., O’Sullivan, M., Jones, M. W., Andrew, R. M., Gregor, L., Hauck, J., Le Quéré, C., Luijkx, I. T., Olsen, A.,  
2386 Peters, G. P., Peters, W., Pongratz, J., Schwingshackl, C., Sitch, S., Canadell, J. G., Ciais, P., Jackson, R. B., Alin, S. R.,  
2387 Alkama, R., Arneeth, A., Arora, V. K., Bates, N. R., Becker, M., Bellouin, N., Bittig, H. C., Bopp, L., Chevallier, F., Chini, L.  
2388 P., Cronin, M., Evans, W., Falk, S., Feely, R. A., Gasser, T., Gehlen, M., Gkritzalis, T., Gloege, L., Grassi, G., Gruber, N.,  
2389 Gürses, Ö., Harris, I., Hefner, M., Houghton, R. A., Hurtt, G. C., Iida, Y., Ilyina, T., Jain, A. K., Jersild, A., Kadono, K.,  
2390 Kato, E., Kennedy, D., Klein Goldewijk, K., Knauer, J., Korsbakken, J. I., Landschützer, P., Lefèvre, N., Lindsay, K., Liu,  
2391 J., Liu, Z., Marland, G., Mayot, N., McGrath, M. J., Metzl, N., Monacchi, N. M., Munro, D. R., Nakaoka, S., Niwa, Y.,  
2392 O’Brien, K., Ono, T., Palmer, P. I., Pan, N., Pierrot, D., Pockock, K., Poulter, B., Resplandy, L., Robertson, E., Rödenbeck,  
2393 C., Rodriguez, C., Rosan, T. M., Schwinger, J., Séférian, R., Shutler, J. D., Skjelvan, I., Steinhoff, T., Sun, Q., Sutton, A. J.,  
2394 Sweeney, C., Takao, S., Tanhua, T., Tans, P. P., Tian, X., Tian, H., Tilbrook, B., Tsujino, H., Tubiello, F., van der Werf, G.  
2395 R., Walker, A. P., Wanninkhof, R., Whitehead, C., Willstrand Wranne, A., Wright, R., Yuan, W., Yue, C., Yue, X., Zaehle,  
2396 S., Zeng, J., and Zheng, B.: Global Carbon Budget 2022, *Earth Syst. Sci. Data*, 14, 4811–4900, <https://doi.org/10.5194/essd-14-4811-2022>, 2022b.
- 2397  
2398
- 2399 Friedlingstein, P., O’Sullivan, M., Jones, M. W., Andrew, R. M., Bakker, D. C. E., Hauck, J., Landschützer, P., Le Quéré, C.,  
2400 Luijkx, I. T., Peters, G. P., Peters, W., Pongratz, J., Schwingshackl, C., Sitch, S., Canadell, J. G., Ciais, P., Jackson, R. B.,  
2401 Alin, S. R., Anthoni, P., Barbero, L., Bates, N. R., Becker, M., Bellouin, N., Decharme, B., Bopp, L., Brasika, I. B. M.,  
2402 Cadule, P., Chamberlain, M. A., Chandra, N., Chau, T.-T.-T., Chevallier, F., Chini, L. P., Cronin, M., Dou, X., Enyo, K.,  
2403 Evans, W., Falk, S., Feely, R. A., Feng, L., Ford, D. J., Gasser, T., Ghattas, J., Gkritzalis, T., Grassi, G., Gregor, L., Gruber,  
2404 N., Gürses, Ö., Harris, I., Hefner, M., Heinke, J., Houghton, R. A., Hurtt, G. C., Iida, Y., Ilyina, T., Jacobson, A. R., Jain, A.  
2405 K., Jarníková, T., Jersild, A., Jiang, F., Jin, Z., Joos, F., Kato, E., Keeling, R. F., Kennedy, D., Klein Goldewijk, K., Knauer,  
2406 J., Korsbakken, J. I., Körtzinger, A., Lan, X., Lefèvre, N., Li, H., Liu, J., Liu, Z., Ma, L., Marland, G., Mayot, N., McGuire,  
2407 P. C., McKinley, G. A., Meyer, G., Morgan, E. J., Munro, D. R., Nakaoka, S., Niwa, Y., O’Brien, K. M., Olsen, A., Omar, A.  
2408 M., Ono, T., Paulsen, M., Pierrot, D., Pockock, K., Poulter, B., Powis, C. M., Rehder, G., Resplandy, L., Robertson, E.,  
2409 Rödenbeck, C., Rosan, T. M., Schwinger, J., Séférian, R., Smallman, T. L., Smith, S. M., Sospedra-Alfonso, R., Sun, Q.,  
2410 Sutton, A. J., Sweeney, C., Takao, S., Tans, P. P., Tian, H., Tilbrook, B., Tsujino, H., Tubiello, F., van der Werf, G. R., van



- 2411 Ooijen, E., Wanninkhof, R., Watanabe, M., Wimart-Rousseau, C., Yang, D., Yang, X., Yuan, W., Yue, X., Zaehle, S., Zeng,  
2412 J., and Zheng, B.: Global Carbon Budget 2023, *Earth Syst. Sci. Data*, 15, 5301–5369, [https://doi.org/10.5194/essd-15-5301-](https://doi.org/10.5194/essd-15-5301-2023)  
2413 2023, 2023.
- 2414 Friedlingstein, P., O'Sullivan, M., Jones, M. W., Andrew, R. M., Hauck, J., Landschützer, P., Le Quéré, C., Li, H., Luijkx, I.  
2415 T., Olsen, A., Peters, G. P., Peters, W., Pongratz, J., Schwingshackl, C., Sitch, S., Canadell, J. G., Ciais, P., Jackson, R. B.,  
2416 Alin, S. R., Arneth, A., Arora, V., Bates, N. R., Becker, M., Bellouin, N., Berghoff, C. F., Bittig, H. C., Bopp, L., Cadule, P.,  
2417 Campbell, K., Chamberlain, M. A., Chandra, N., Chevallier, F., Chini, L. P., Colligan, T., Decayeux, J., Djeutchouang, L.  
2418 M., Dou, X., Duran Rojas, C., Enyo, K., Evans, W., Fay, A. R., Feely, R. A., Ford, D. J., Foster, A., Gasser, T., Gehlen, M.,  
2419 Gkritzalis, T., Grassi, G., Gregor, L., Gruber, N., Gürses, Ö., Harris, I., Hefner, M., Heinke, J., Hurtt, G. C., Iida, Y., Ilyina,  
2420 T., Jacobson, A. R., Jain, A. K., Jarníková, T., Jersild, A., Jiang, F., Jin, Z., Kato, E., Keeling, R. F., Klein Goldewijk, K.,  
2421 Knauer, J., Korsbakken, J. I., Lauvset, S. K., Lefèvre, N., Liu, Z., Liu, J., Ma, L., Maksyutov, S., Marland, G., Mayot, N.,  
2422 McGuire, P. C., Metz, N., Monacci, N. M., Morgan, E. J., Nakaoka, S., Neill, C., Niwa, Y., Nützel, T., Olivier, L., Ono, T.,  
2423 Palmer, P. I., Pierrot, D., Qin, Z., Resplandy, L., Roobaert, A., Rosan, T. M., Rödenbeck, C., Schwinger, J., Smallman, T. L.,  
2424 Smith, S. M., Sospedra-Alfonso, R., Steinhoff, T., Sun, Q., Sutton, A. J., Sférian, R., Takao, S., Tatebe, H., Tian, H.,  
2425 Tilbrook, B., Torres, O., Tourigny, E., Tsujino, H., Tubiello, F., van der Werf, G., Wanninkhof, R., Wang, X., Yang, D.,  
2426 Yang, X., Yu, Z., Yuan, W., Yue, X., Zaehle, S., Zeng, N., Zeng, J.: Supplemental data of the Global Carbon Budget 2024,  
2427 ICOS-ERIC Carbon Portal, <https://doi.org/10.18160/GCP-2024>, 2024.
- 2428 Ganzenmüller, R., Bultan, S., Winkler, K., Fuchs, R., Zabel, F., and Pongratz, J.: Land-use change emissions based on high-  
2429 resolution activity data substantially lower than previously estimated, *Environ. Res. Lett.*, 17, 064050,  
2430 <https://doi.org/10.1088/1748-9326/ac70d8>, 2022.
- 2431 Gasser, T., Crepin, L., Quilcaille, Y., Houghton, R. A., Ciais, P., and Obersteiner, M.: Historical CO<sub>2</sub> emissions from land  
2432 use and land cover change and their uncertainty, *Biogeosciences*, 17, 4075–4101, <https://doi.org/10.5194/bg-17-4075-2020>,  
2433 2020.
- 2434 Gaubert, B., Stephens, B. B., Basu, S., Chevallier, F., Deng, F., Kort, E. A., Patra, P. K., Peters, W., Rödenbeck, C., Saeki,  
2435 T., Schimel, D., Van der Laan-Luijkx, I., Wofsy, S., and Yin, Y.: Global atmospheric CO<sub>2</sub> inverse models converging on  
2436 neutral tropical land exchange, but disagreeing on fossil fuel and atmospheric growth rate, *Biogeosciences*, 16, 117–134,  
2437 <https://doi.org/10.5194/bg-16-117-2019>, 2019.
- 2438 GCP: The Global Carbon Budget 2007, available at: <http://www.globalcarbonproject.org/carbonbudget/archive.htm>, last  
2439 access: 28 October 2024, 2007.
- 2440 Giglio, L., Schroeder, W., and Justice, C. O.: The collection 6 MODIS active fire detection algorithm and fire products,  
2441 *Remote Sensing of Environment*, 178, 31–41, <https://doi.org/10.1016/j.rse.2016.02.054>, 2016.
- 2442 Gloege, L., McKinley, G. A., Landschützer, P., Fay, A. R., Frölicher, T. L., Fyfe, J. C., Ilyina, T., Jones, S., Lovenduski, N.  
2443 S., Rodgers, K. B., Schlunegger, S., and Takano, Y.: Quantifying Errors in Observationally Based Estimates of Ocean  
2444 Carbon Sink Variability, *Global Biogeochem. Cy.*, 35, e2020GB006788, <https://doi.org/10.1029/2020GB006788>, 2021.
- 2445 Gloege, L., Yan, M., Zheng, T., and McKinley, G. A.: Improved Quantification of Ocean Carbon Uptake by Using Machine  
2446 Learning to Merge Global Models and pCO<sub>2</sub> Data, *J. Adv. Model. Earth Syst.*, 14, e2021MS002620,  
2447 <https://doi.org/10.1029/2021MS002620>, 2022.



- 2448 Golar, G., Malik, A., Muis, H., Herman, A., Nurudin, N., and Lukman, L.: The social-economic impact of COVID-19  
2449 pandemic: implications for potential forest degradation, *Heliyon*, 6, e05354, <https://doi.org/10.1016/j.heliyon.2020.e05354>,  
2450 2020.
- 2451 Goris, N., Tjiputra, J. F., Olsen, A., Schwinger, J., Lauvset, S. K., and Jeansson, E.: Constraining Projection-Based Estimates  
2452 of the Future North Atlantic Carbon Uptake, *J. Clim.*, 31, 3959–3978, <https://doi.org/10.1175/JCLI-D-17-0564.1>, 2018.
- 2453 Grassi, G., House, J., Kurz, W. A., Cescatti, A., Houghton, R. A., Peters, G. P., Sanz, M. J., Viñas, R. A., Alkama, R.,  
2454 Arneeth, A., Bondeau, A., Dentener, F., Fader, M., Federici, S., Friedlingstein, P., Jain, A. K., Kato, E., Koven, C. D., Lee,  
2455 D., Nabel, J. E. M. S., Nassikas, A. A., Perugini, L., Rossi, S., Sitch, S., Viovy, N., Wiltshire, A., and Zachle, S.:  
2456 Reconciling global-model estimates and country reporting of anthropogenic forest CO<sub>2</sub> sinks, *Nature Clim Change*, 8, 914–  
2457 920, <https://doi.org/10.1038/s41558-018-0283-x>, 2018.
- 2458 Grassi, G., Stehfest, E., Rogelj, J., van Vuuren, D., Cescatti, A., House, J., Nabuurs, G.-J., Rossi, S., Alkama, R., Viñas, R.  
2459 A., Calvin, K., Ceccherini, G., Federici, S., Fujimori, S., Gusti, M., Hasegawa, T., Havlik, P., Humpenöder, F., Korosuo, A.,  
2460 Perugini, L., Tubiello, F. N., and Popp, A.: Critical adjustment of land mitigation pathways for assessing countries' climate  
2461 progress, *Nat. Clim. Chang.*, 11, 425–434, <https://doi.org/10.1038/s41558-021-01033-6>, 2021.
- 2462 Grassi, G., Schwingshackl, C., Gasser, T., Houghton, R. A., Sitch, S., Canadell, J. G., Cescatti, A., Ciais, P., Federici, S.,  
2463 Friedlingstein, P., Kurz, W. A., Sanz Sanchez, M. J., Abad Viñas, R., Alkama, R., Bultan, S., Ceccherini, G., Falk, S., Kato,  
2464 E., Kennedy, D., Knauer, J., Korosuo, A., Melo, J., McGrath, M. J., Nabel, J. E. M. S., Poulter, B., Romanovskaya, A. A.,  
2465 Rossi, S., Tian, H., Walker, A. P., Yuan, W., Yue, X., and Pongratz, J.: Harmonising the land-use flux estimates of global  
2466 models and national inventories for 2000–2020, *Earth Syst. Sci. Data*, 15, 1093–1114, [https://doi.org/10.5194/essd-15-1093-](https://doi.org/10.5194/essd-15-1093-2023)  
2467 2023, 2023.
- 2468 Gregor, L., Lebehot, A. D., Kok, S., and Scheel Monteiro, P. M.: A comparative assessment of the uncertainties of global  
2469 surface ocean CO<sub>2</sub> estimates using a machine-learning ensemble (CSIR-ML6 version 2019a)–have we hit the  
2470 wall?. *Geoscientific Model Development*, 12(12), 5113–5136, <https://doi.org/10.5194/gmd-12-5113-2019>, 2019.
- 2471 Gregor, L., Shutler, J., and Gruber, N.: High-resolution variability of the ocean carbon sink. *Global Biogeochemical Cycles*,  
2472 38(8), e2024GB008127, <https://doi.org/10.1029/2024GB008127>, 2024.
- 2473 Gruber, N., Bakker, D. C. E., DeVries, T., Gregor, L., Hauck, J., Landschützer, P., McKinley, G. A., and Müller, J. D.:  
2474 Trends and variability in the ocean carbon sink, *Nat. Rev. Earth Environ.*, 4, 119–134, [https://doi.org/10.1038/s43017-022-](https://doi.org/10.1038/s43017-022-00381-x)  
2475 00381-x, 2023.
- 2476 Gruber, N., Clement, D., Carter, B. R., Feely, R. A., van Heuven, S., Hoppema, M., Ishii, M., Key, R. M., Kozyr, A.,  
2477 Lauvset, S. K., Lo Monaco, C., Mathis, J. T., Murata, A., Olsen, A., Perez, F. F., Sabine, C. L., Tanhua, T., and Wanninkhof,  
2478 R.: The oceanic sink for anthropogenic CO<sub>2</sub> from 1994 to 2007, 363, 1193–1199, <https://doi.org/10.1126/science.aau5153>,  
2479 2019.
- 2480 Guan, D., Liu, Z., Geng, Y., Lindner, S., and Hubacek, K.: The gigatonne gap in China's carbon dioxide inventories, *Nature*  
2481 *Clim Change*, 2, 672–675, <https://doi.org/10.1038/nclimate1560>, 2012.
- 2482 Gulev, S. K., Thorne, P. W., Ahn, J., Dentener, F. J., Domingues, C. M., Gerland, S., Gong, D. S., Kaufman, S., Nnamchi,  
2483 H. C., Quaas, J., Rivera, J. A., Sathyendranath, S., Smith, S. L., Trewin, B., von Shuckmann, K., and Vose, R. S.: Changing



- 2484 State of the Climate System. In: Climate Change 2021: The Physical Science Basis. Contribution of Working Group I to the  
2485 Sixth Assessment Report of the Intergovernmental Panel on Climate Change [Masson-Delmotte, V., Zhai, P., Pirani, A.,  
2486 Connors, S. L., Péan, C., Berger, S., Caud, N., Chen, Y., Goldfarb, L., Gomis, M. I., Huang, M., Leitzell, K., Lonnoy, E.,  
2487 Matthews, J.B.R., Maycock, T.K., Waterfield, T., Yelekçi, O., Yu, R. and Zhou, B. (eds.)]. Cambridge University Press,  
2488 Cambridge, United Kingdom and New York, NY, USA, pp. 287–422, <https://doi.org/10.1017/9781009157896.004>, 2021.
- 2489 Guo, R., Wang, J., Bing, L., Tong, D., Ciais, P., Davis, S. J., Andrew, R. M., Xi, F., and Liu, Z.: Global CO<sub>2</sub> uptake by  
2490 cement from 1930 to 2019, 13, 1791–1805, <https://doi.org/10.5194/essd-13-1791-2021>, 2021.
- 2491 Gürses, Ö., Oziel, L., Karakuş, O., Sidorenko, D., Völker, C., Ye, Y., Zeising, M., Butzin, M., and Hauck, J.: Ocean  
2492 biogeochemistry in the coupled ocean–sea ice–biogeochemistry model FESOM2.1–REcoM3, *Geosci. Model Dev.*, 16,  
2493 4883–4936, <https://doi.org/10.5194/gmd-16-4883-2023>, 2023.
- 2494 Gütschow, J., Jeffery, M. L., Gieseke, R., Gebel, R., Stevens, D., Krapp, M., and Rocha, M.: The PRIMAP-hist national  
2495 historical emissions time series, 8, 571–603, <https://doi.org/10.5194/essd-8-571-2016>, 2016.
- 2496 Gütschow, J., Busch, D. and Pflüger, M.: The PRIMAP-hist national historical emissions time series (1750-2023) v2.6,  
2497 Zenodo [dataset], <https://doi.org/10.5281/zenodo.13752654>, 2023.
- 2498 Hall, B. D., Crotwell, A. M., Kitzis, D. R., Mefford, T., Miller, B. R., Schibig, M. F., and Tans, P. P.: Revision of the World  
2499 Meteorological Organization Global Atmosphere Watch (WMO/GAW) CO<sub>2</sub> calibration scale, 14, 3015–3032,  
2500 <https://doi.org/10.5194/amt-14-3015-2021>, 2021.
- 2501 Hansis, E., Davis, S. J., and Pongratz, J.: Relevance of methodological choices for accounting of land use change carbon  
2502 fluxes, *Global Biogeochem. Cycles*, 29, 1230–1246, <https://doi.org/10.1002/2014GB004997>, 2015.
- 2503 Hauck, J., Nissen, C., Landschützer, P., Rödenbeck, C., Bushinsky, S., and Olsen, A.: Sparse observations induce large  
2504 biases in estimates of the global ocean CO<sub>2</sub> sink: an ocean model subsampling experiment, *Philos. Trans. R. Soc. Math.*  
2505 *Phys. Eng. Sci.*, 381, 20220063, <https://doi.org/10.1098/rsta.2022.0063>, 2023a.
- 2506  
2507 Hauck, J., Gregor, L., Nissen, C., Patara, L., Hague, M., Mongwe, P., Bushinsky, S., Doney, S. C., Gruber, N., Le Quéré, C.,  
2508 Manizza, M., Mazloff, M., Monteiro, P. M. S., and Terhaar, J.: The Southern Ocean Carbon Cycle 1985–2018: Mean,  
2509 Seasonal Cycle, Trends, and Storage. *Global Biogeochemical Cycles*, 37(11), e2023GB007848,  
2510 <https://doi.org/10.1029/2023GB007848>, 2023b.
- 2511 Hauck, J., Zeising, M., Le Quéré, C., Gruber, N., Bakker, D. C. E., Bopp, L., Chau, T. T. T., Gürses, Ö., Ilyina, T.,  
2512 Landschützer, P., Lenton, A., Resplandy, L., Rödenbeck, C., Schwinger, J., and Séférian, R.: Consistency and Challenges in  
2513 the Ocean Carbon Sink Estimate for the Global Carbon Budget, *Front. Mar. Sci.*, 7, 571720,  
2514 <https://doi.org/10.3389/fmars.2020.571720>, 2020.
- 2515 Haverd, V., Smith, B., Nieradzik, L., Briggs, P. R., Woodgate, W., Trudinger, C. M., Canadell, J. G., and Cuntz, M.: A new  
2516 version of the CABLE land surface model (Subversion revision r4601) incorporating land use and land cover change, woody  
2517 vegetation demography, and a novel optimisation-based approach to plant coordination of photosynthesis, *Geosci. Model*  
2518 *Dev.*, 11, 2995–3026, <https://doi.org/10.5194/gmd-11-2995-2018>, 2018.





- 2519 Heinke, J., Rolinski, S., and Müller, C.: Modelling the role of livestock grazing in C and N cycling in grasslands with  
2520 LPJmL5.0-grazing, *Geosci. Model Dev.*, 16, 2455–2475, <https://doi.org/10.5194/gmd-16-2455-2023>, 2023.
- 2521 Hefner, M., Marland, G., Boden, T., Andres, R.: Global, Regional, and National Fossil-Fuel CO<sub>2</sub> Emissions: 1751-2020  
2522 CDIAC-FF [dataset], available at: <https://energy.appstate.edu/cdiac-appstate/data-products>, last access: 28 October 2024,  
2523 2023.
- 2524 Hefner, M; Marland G; (2023): Global, Regional, and National Fossil-Fuel CO<sub>2</sub> Emissions: 1751-2020 CDIAC-FF,  
2525 Research Institute for Environment, Energy, and Economics, Appalachian State University,  
2526 <https://ricee.appstate.edu/projects-programs/cdiac>
- 2527 Hickler, T., Smith, B., Prentice, I. C., Mjöfors, K., Miller, P., Arneth, A., and Sykes, M. T.: CO<sub>2</sub> fertilization in temperate  
2528 FACE experiments not representative of boreal and tropical forests, *Glob. Change Biol.*, 14, 1531–1542,  
2529 <https://doi.org/10.1111/j.1365-2486.2008.01598.x>, 2008.
- 2530 Hoesly, R. M., Smith, S. J., Feng, L., Klimont, Z., Janssens-Maenhout, G., Pitkanen, T., Seibert, J. J., Vu, L., Andres, R. J.,  
2531 Bolt, R. M., Bond, T. C., Dawidowski, L., Kholod, N., Kurokawa, J., Li, M., Liu, L., Lu, Z., Moura, M. C. P., O'Rourke, P.  
2532 R., and Zhang, Q.: Historical (1750–2014) anthropogenic emissions of reactive gases and aerosols from the Community  
2533 Emissions Data System (CEDs), *Geosci. Model Dev.*, 11, 369–408, <https://doi.org/10.5194/gmd-11-369-2018>, 2018.
- 2534 Hoesly, R., Smith, S. J., Prime, N., Ahsan, H., Suchyta, H., O'Rourke, P., Crippa, M., Klimont, Z., Guizzardi, D., Behrendt,  
2535 J., Feng, L., Harkins, C., McDonald, B., Mott, A., McDuffie, A., Nicholson, M. and Wang, S.: CEDs v\_2024\_07\_08  
2536 Release Emission Data, Zenodo [dataset], <https://doi.org/10.5281/zenodo.12803196>, 2024.
- 2537 Hong, C., Burney, J. A., Pongratz, J., Nabel, J. E. M. S., Mueller, N. D., Jackson, R. B., and Davis, S. J.: Global and regional  
2538 drivers of land-use emissions in 1961–2017, *Nature*, 589, 554–561, <https://doi.org/10.1038/s41586-020-03138-y>, 2021.
- 2539 Holding, T., Ashton, I. G., Shutler, J. D., Land, P. E., Nightingale, P. D., Rees, A. P., Brown, I., Piolle, J.-F., Kock, A.,  
2540 Bange, H. W., Woolf, D. K., Goddijn-Murphy, L., Pereira, R., Paul, F., Girard-Arduin, F., Chapron, B., Rehder, G.,  
2541 Arduin, F., and Donlon, C. J.: The FluxEngine air–sea gas flux toolbox: simplified interface and extensions for in situ  
2542 analyses and multiple sparingly soluble gases, *Ocean Sci.*, 15, 1707–1728, <https://doi.org/10.5194/os-15-1707-2019>, 2019.
- 2543 Houghton, R. A. and Castanho, A.: Annual emissions of carbon from land use, land-use change, and forestry from 1850 to  
2544 2020, *Earth Syst. Sci. Data*, 15, 2025–2054, <https://doi.org/10.5194/essd-15-2025-2023>, 2023.
- 2545 Houghton, R. A., House, J. I., Pongratz, J., van der Werf, G. R., DeFries, R. S., Hansen, M. C., Le Quéré, C., and  
2546 Ramankutty, N.: Carbon emissions from land use and land-cover change, *Biogeosciences*, 9, 5125–5142,  
2547 <https://doi.org/10.5194/bg-9-5125-2012>, 2012.
- 2548 Huang, B., Thorne, P. W., Banzon, V. F., Boyer, T., Chepurin, G., Lawrimore, J. H., Menne, M. J., Smith, T. M., Vose, R.  
2549 S., and Zhang, H.-M.: NOAA Extended Reconstructed Sea Surface Temperature (ERSST), Version 5,  
2550 <https://doi.org/10.7289/V5T72FNM>, 2017.
- 2551 Hubau, W., Lewis, S.L., Phillips, O.L., Affum-Baffoe, K., Beeckman, H., Cuni-Sanchez, A., Daniels, A.K., Ewango, C.E.N.,  
2552 Fauset, S., Mukinzi, J.M., Sheil, D., Sonké, B., Sullivan, M.J.P., Sunderland, T.C.H., Taedoumg, H., Thomas, S.C., White,  
2553 L.J.T., Abernethy, K.A., Adu-Bredu, S., Amani, C.A., Baker, T.R., Banin, L.F., Baya, F., Begne, S.K., Bennett, A.C.,



- 2554 Benedet, F., Bitariho, R., Bocko, Y.E., Boeckx, P., Boundja, P., Brienen, R.J.W., Brncic, T., Chezeaux, E., Chuyong, G.B.,  
2555 Clark, C.J., Collins, M., Comiskey, J.A., Coomes, D.A., Dargie, G.C., de Haulleville, T., Kamdem, M.N.D., Doucet, J.-L.,  
2556 Esquivel-Muelbert, A., Feldpausch, T.R., Fofanah, A., Foli, E.G., Gilpin, M., Gloor, E., Gonmadje, C., Gourlet-Fleury, S.,  
2557 Hall, J.S., Hamilton, A.C., Harris, D.J., Hart, T.B., Hockemba, M.B.N., Hladik, A., Ifo, S.A., Jeffery, K.J., Jucker, T.,  
2558 Yakusu, E.K., Kearsley, E., Kenfack, D., Koch, A., Leal, M.E., Levesley, A., Lindsell, J.A., Lisingo, J., Lopez-Gonzalez, G.,  
2559 Lovett, J.C., Makana, J.-R., Malhi, Y., Marshall, A.R., Martin, J., Martin, E.H., Mbayu, F.M., Medjibe, V.P., Mihindou, V.,  
2560 Mitchard, E.T.A., Moore, S., Munishi, P.K.T., Bengone, N.N., Ojo, L., Ondo, F.E., Peh, K.S.-H., Pickavance, G.C., Poulsen,  
2561 A.D., Poulsen, J.R., Qie, L., Reitsma, J., Rovero, F., Swaine, M.D., Talbot, J., Taplin, J., Taylor, D.M., Thomas, D.W.,  
2562 Toirambe, B., Mukendi, J.T., Tuagben, D., Umunay, P.M., van der Heijden, G.M.F., Verbeeck, H., Vleminckx, J., Willcock,  
2563 S., Wöll, H., Woods, J.T., Zomagho, L.: Asynchronous carbon sink saturation in African and Amazonian tropical forests,  
2564 *Nature*, 579, 80–87, <https://doi.org/10.1038/s41586-020-2035-0>, 2020.
- 2565 Humphrey, V., Zscheischler, J., Ciais, P., Gudmundsson, L., Sitch, S., and Seneviratne, S. I.: Sensitivity of atmospheric CO<sub>2</sub>  
2566 growth rate to observed changes in terrestrial water storage, *Nature*, 560, 628–631, [https://doi.org/10.1038/s41586-018-](https://doi.org/10.1038/s41586-018-0424-4)  
2567 0424-4, 2018.
- 2568 Humphrey, V., Berg, A., Ciais, P., Gentine, P., Jung, M., Reichstein, M., Seneviratne, S. I., and Frankenberg, C.: Soil  
2569 moisture–atmosphere feedback dominates land carbon uptake variability, *Nature*, 592, 65–69,  
2570 <https://doi.org/10.1038/s41586-021-03325-5>, 2021.
- 2571 Huntzinger, D. N., Michalak, A. M., Schwalm, C., Ciais, P., King, A. W., Fang, Y., Schaefer, K., Wei, Y., Cook, R. B.,  
2572 Fisher, J. B., Hayes, D., Huang, M., Ito, A., Jain, A. K., Lei, H., Lu, C., Maignan, F., Mao, J., Parazoo, N., Peng, S., Poulter,  
2573 B., Ricciuto, D., Shi, X., Tian, H., Wang, W., Zeng, N., and Zhao, F.: Uncertainty in the response of terrestrial carbon sink to  
2574 environmental drivers undermines carbon-climate feedback predictions, *Sci Rep*, 7, 4765, [https://doi.org/10.1038/s41598-](https://doi.org/10.1038/s41598-017-03818-2)  
2575 017-03818-2, 2017.
- 2576 Iida, Y., Takatani, Y., Kojima, A., and Ishii, M.: Global trends of ocean CO<sub>2</sub> sink and ocean acidification: an observation-  
2577 based reconstruction of surface ocean inorganic carbon variables, *J Oceanogr*, 77, 323–358, [https://doi.org/10.1007/s10872-](https://doi.org/10.1007/s10872-020-00571-5)  
2578 020-00571-5, 2021.
- 2579 Ilyina, T., Li, H., Spring, A., Müller, W. A., Bopp, L., Chikamoto, M. O., Danabasoglu, G., Dobrynin, M., Dunne, J.,  
2580 Fransner, F., Friedlingstein, P., Lee, W., Lovenduski, N. S., Merryfield, W. J., Mignot, J., Park, J. Y., Séférian, R., Sospedra-  
2581 Alfonso, R., Watanabe, M., and Yeager, S.: Predictable Variations of the Carbon Sinks and Atmospheric CO<sub>2</sub> Growth in a  
2582 Multi-Model Framework, *Geophys. Res. Lett.*, 48, e2020GL090695, <https://doi.org/10.1029/2020GL090695>, 2021.
- 2583 IMF: International Monetary Fund: World Economic Outlook, available at: <http://www.imf.org>, last access: 28 October  
2584 2024, 2023.
- 2585 Instituto Nacional de Pesquisas Espaciais (INPE): Portal TerraBrasilis, available at: [http://terrabrasilis.dpi.inpe.br/en/home-](http://terrabrasilis.dpi.inpe.br/en/home-page/)  
2586 [page/](http://terrabrasilis.dpi.inpe.br/en/home-page/), last access: 28 October 2024.
- 2587 IPCC: Annex II: Glossary [Möller, V, J.B.R. Matthews, R. van Diemen, C. Méndez, S. Semenov, J.S. Fuglestedt, A.  
2588 Reisinger (eds.)]. In: *Climate Change 2022: Impacts, Adaptation, and Vulnerability. Contribution of Working Group II to the*  
2589 *Sixth Assessment Report of the Intergovernmental Panel on Climate Change* [H.-O. Pörtner, D.C. Roberts, M. Tignor, E.S.  
2590 Poloczanska, K. Mintenbeck, A. Alegría, M. Craig, S. Langsdorf, S. Lösschke, V. Möller, A. Okem, B. Rama (eds.)], in:



- 2591 Climate Change 2022 – Impacts, Adaptation and Vulnerability: Working Group II Contribution to the Sixth Assessment  
2592 Report of the Intergovernmental Panel on Climate Change [Möller, V, J.B.R. Matthews, R. van Diemen, C. Méndez, S.  
2593 Semenov, J.S. Fuglestvedt, A. Reisinger (eds.)], Cambridge University Press, Cambridge, UK and New York, NY, 2897–  
2594 2930, <https://doi.org/10.1017/9781009325844.029>, 2023.
- 2595 Ito, A. and Inatomi, M.: Use of a process-based model for assessing the methane budgets of global terrestrial ecosystems and  
2596 evaluation of uncertainty, 9, 759–773, <https://doi.org/10.5194/bg-9-759-2012>, 2012.
- 2597 Jackson, R. B., Canadell, J. G., Le Quéré, C., Andrew, R. M., Korsbakken, J. I., Peters, G. P., and Nakicenovic, N.:  
2598 Reaching peak emissions, *Nature Clim Change*, 6, 7–10, <https://doi.org/10.1038/nclimate2892>, 2016.
- 2599 Jackson, R. B., Le Quéré, C., Andrew, R. M., Canadell, J. G., Korsbakken, J. I., Liu, Z., Peters, G. P., and Zheng, B.: Global  
2600 energy growth is outpacing decarbonization, *Environ. Res. Lett.*, 13, 120401, <https://doi.org/10.1088/1748-9326/aaf303>,  
2601 2018.
- 2602 Jackson, R. B., Friedlingstein, P., Andrew, R. M., Canadell, J. G., Le Quéré, C., and Peters, G. P.: Persistent fossil fuel  
2603 growth threatens the Paris Agreement and planetary health, *Environ. Res. Lett.*, 14, 121001, <https://doi.org/10.1088/1748-9326/ab57b3>, 2019.
- 2605 Jackson, R. B., Friedlingstein, P., Quéré, C. L., Abernethy, S., Andrew, R. M., Canadell, J. G., Ciais, P., Davis, S. J., Deng,  
2606 Z., Liu, Z., Korsbakken, J. I., and Peters, G. P.: Global fossil carbon emissions rebound near pre-COVID-19 levels, *Environ.*  
2607 *Res. Lett.*, 17, 031001, <https://doi.org/10.1088/1748-9326/ac55b6>, 2022.
- 2608 Jacobson, A. R., Schuldt, K. N., Tans, P., Andrews, A., Miller, J. B., Oda, T., Basu, S., Mund, J., Weir, B., Ott, L., Aalto, T.,  
2609 Abshire, J. B., Aikin, K., Aoki, S., Apadula, F., Arnold, S., Baier, B., Bartyzel, J., Beyersdorf, A., Biermann, T., Biraud, S.  
2610 C., Boenisch, H., Brailsford, G., Brand, W. A., Chen, G., Chen, H., Chmura, L., Clark, S., Colomb, A., Commane, R., Conil,  
2611 S., Couret, C., Cox, A., Cristofanelli, P., Cuevas, E., Curcoll, R., Daube, B., Davis, K. J., De Wekker, S., Della Coletta, J.,  
2612 Delmotte, M., DiGangi, E., DiGangi, J. P., di Sarra, A. G., Dlugokencky, E., Elkins, J. W., Emmenegger, L., Fang, S.,  
2613 Fischer, M. L., Forster, G., Frumau, A., Galkowski, M., Gatti, L. V., Gehrlein, T., Gerbig, C., Gheusi, F., Gloor, E., Gomez-  
2614 Trueba, V., Goto, D., Griffis, T., Hammer, S., Hanson, C., Haszpra, L., Hatakka, J., Heimann, M., Heliasz, M., Hensen, A.,  
2615 Hermansen, O., Hints, E., Holst, J., Ivakhov, V., Jaffé, D. A., Jordan, A., Joubert, W., Karion, A., Kawa, S. R., Kazan, V.,  
2616 Keeling, R. F., Keronen, P., Kneuer, T., Kolari, P., Komínková, K., Kort, E., Kozlova, E., Krummel, P., Kubistin, D.,  
2617 Labuschagne, C., Lam, D. H. Y., Lan, X., Langenfelds, R. L., Laurent, O., Laurila, T., Lauvaux, T., Lavric, J., Law, B. E.,  
2618 Lee, J., Lee, O. S. M., Lehner, I., Lehtinen, K., Leppert, R., Leskinen, A., Leuenberger, M., Levin, I., Levula, J., Lin, J.,  
2619 Lindauer, M., Loh, Z., Lopez, M., Luijkx, I. T., Lunder, C. R., Machida, T., Mammarella, I., Manca, G., Manning, A.,  
2620 Manning, A., Marek, M. V., Martin, M. Y., Matsueda, H., McKain, K., Meijer, H., Meinhardt, F., Merchant, L.,  
2621 Mihalopoulos, N., Miles, N. L., Miller, C. E., Mitchell, L., Mölder, M., Montzka, S., Moore, F., Moossen, H., Morgan, E.,  
2622 Morgui, J.-A., Morimoto, S., Müller-Williams, J., Munger, J. W., Munro, D., Myhre, C. L., Nakaoka, S.-I., Necki, J.,  
2623 Newman, S., Nichol, S., Niwa, Y., Obersteiner, F., O'Doherty, S., Paplawsky, B., Peischl, J., Peltola, O., Piacentino, S.,  
2624 Pichon, J.-M., Pickers, P., Piper, S., Pitt, J., Plass-Dülmer, C., Platt, S. M., Prinzivalli, S., Ramonet, M., Ramos, R., Reyes-  
2625 Sanchez, E., Richardson, S. J., Riris, H., Rivas, P. P., Ryerson, T., Saito, K., Sargent, M., Sasakawa, M., Scheeren, B.,  
2626 Schuck, T., Schumacher, M., Seifert, T., Sha, M. K., Shepson, P., Shook, M., Sloop, C. D., Smith, P., Stanley, K.,  
2627 Steinbacher, M., Stephens, B., Sweeney, C., Thoning, K., Timas, H., Torn, M., Tørseth, K., Trisolino, P., Turnbull, J., van  
2628 den Bulk, P., van Dinter, D., Vermeulen, A., Viner, B., Vitkova, G., Walker, S., Watson, A., Wofsy, S. C., Worsley, J.,



- 2629 Worthy, D., Young, D., Zaehle, S., Zahn, A., and Zimnoch, M.: CarbonTracker CT2022, NOAA GML [dataset],  
2630 <https://doi.org/10.25925/Z1GJ-3254>, 2023a.
- 2631 Jacobson, A. R., Schuldt, K. N., Tans, P., Andrews, A., Miller, J. B., Oda, T., Basu, S., Mund, J., Weir, B., Ott, L., Aalto, T.,  
2632 Abshire, J. B., Aikin, K., Aoki, S., Apadula, F., Arnold, S., Baier, B., Bartyzel, J., Beyersdorf, A., Biermann, T., Biraud, S.  
2633 C., Boenisch, H., Brailsford, G., Brand, W. A., Chen, G., Chen, H., Chmura, L., Clark, S., Colomb, A., Commane, R., Conil,  
2634 S., Couret, C., Cox, A., Cristofanelli, P., Cuevas, E., Curcoll, R., Daube, B., Davis, K. J., De Wekker, S., Della Coletta, J.,  
2635 Delmotte, M., DiGangi, E., DiGangi, J. P., di Sarra, A. G., Dlugokencky, E., Elkins, J. W., Emmenegger, L., Fang, S.,  
2636 Fischer, M. L., Forster, G., Frumau, A., Galkowski, M., Gatti, L. V., Gehrlein, T., Gerbig, C., Gheusi, F., Gloor, E., Gomez-  
2637 Trueba, V., Goto, D., Griffis, T., Hammer, S., Hanson, C., Haszpra, L., Hatakka, J., Heimann, M., Heliasz, M., Hensen, A.,  
2638 Hermansen, O., Hintsa, E., Holst, J., Ivakhov, V., Jaffe, D. A., Jordan, A., Joubert, W., Karion, A., Kawa, S. R., Kazan, V.,  
2639 Keeling, R. F., Keronen, P., Kneuer, T., Kolari, P., Komínková, K., Kort, E., Kozlova, E., Krummel, P., Kubistin, D.,  
2640 Labuschagne, C., Lam, D. H. Y., Lan, X., Langenfelds, R. L., Laurent, O., Laurila, T., Lauvaux, T., Lavric, J., Law, B. E.,  
2641 Lee, J., Lee, O. S. M., Lehner, I., Lehtinen, K., Leppert, R., Leskinen, A., Leuenberger, M., Levin, I., Levula, J., Lin, J.,  
2642 Lindauer, M., Loh, Z., Lopez, M., Luijkx, I. T., Lunder, C. R., Machida, T., Mammarella, I., Manca, G., Manning, A.,  
2643 Manning, A., Marek, M. V., Martin, M. Y., Matsueda, H., McKain, K., Meijer, H., Meinhardt, F., Merchant, L.,  
2644 Mihalopoulos, N., Miles, N. L., Miller, C. E., Mitchell, L., Mölder, M., Montzka, S., Moore, F., Moossen, H., Morgan, E.,  
2645 Morgui, J.-A., Morimoto, S., Müller-Williams, J., Munger, J. W., Munro, D., Myhre, C. L., Nakaoka, S.-I., Necki, J.,  
2646 Newman, S., Nichol, S., Niwa, Y., Obersteiner, F., O'Doherty, S., Paplawsky, B., Peischl, J., Peltola, O., Piacentino, S.,  
2647 Pichon, J.-M., Pickers, P., Piper, S., Pitt, J., Plass-Dülmer, C., Platt, S. M., Prinzivalli, S., Ramonet, M., Ramos, R., Reyes-  
2648 Sanchez, E., Richardson, S. J., Riris, H., Rivas, P. P., Ryerson, T., Saito, K., Sargent, M., Sasakawa, M., Scheeren, B.,  
2649 Schuck, T., Schumacher, M., Seifert, T., Sha, M. K., Shepson, P., Shook, M., Sloop, C. D., Smith, P., Stanley, K.,  
2650 Steinbacher, M., Stephens, B., Sweeney, C., Thoning, K., Timas, H., Torn, M., Tørseth, K., Trisolino, P., Turnbull, J., van  
2651 den Bulk, P., van Dinter, D., Vermeulen, A., Viner, B., Vitkova, G., Walker, S., Watson, A., Wofsy, S. C., Worsley, J.,  
2652 Worthy, D., Young, D., Zaehle, S., Zahn, A., and Zimnoch, M.: CarbonTracker CT-NRT.v2023-3, NOAA GML [dataset],  
2653 <https://doi.org/10.25925/TTAF-J322>, 2023b.
- 2654 Jain, P., Barber, Q. E., Taylor, S. W., Whitman, E., Castellanos Acuna, D., Boulanger, Y., Chavardès, R. D., Chen, J.,  
2655 Englefield, P., Flannigan, M., Girardin, M. P., Hanes, C. C., Little, J., Morrison, K., Skakun, R. S., Thompson, D. K., Wang,  
2656 X., Parisien, M.-A.: Drivers and Impacts of the Record-Breaking 2023 Wildfire Season in Canada. *Nature Communications*,  
2657 15(1), p.6764, <https://doi.org/10.1038/s41467-024-51154-7>, 2024.
- 2658 Janssens-Maenhout, G., Crippa, M., Guizzardi, D., Muntean, M., Schaaf, E., Dentener, F., Bergamaschi, P., Pagliari, V.,  
2659 Olivier, J. G. J., Peters, J. A. H. W., van Aardenne, J. A., Monni, S., Doering, U., Petrescu, A. M. R., Solazzo, E., and  
2660 Oreggioni, G. D.: EDGAR v4.3.2 Global Atlas of the three major greenhouse gas emissions for the period 1970–2012, *Earth*  
2661 *Syst. Sci. Data*, 11, 959–1002, <https://doi.org/10.5194/essd-11-959-2019>, 2019.
- 2662 Jean-Michel, L., Eric, G., Romain, B.-B., Gilles, G., Angélique, M., Marie, D., Clément, B., Mathieu, H., Olivier, L. G.,  
2663 Charly, R., Tony, C., Charles-Emmanuel, T., Florent, G., Giovanni, R., Mounir, B., Yann, D., and Pierre-Yves, L. T.: The  
2664 Copernicus Global 1/12° Oceanic and Sea Ice GLORYS12 Reanalysis, *Front. Earth Sci.*, 9, 2021.
- 2665 Jiang, F., Ju, W., He, W., Wu, M., Wang, H., Wang, J., Jia, M., Feng, S., Zhang, L., and Chen, J. M.: A 10-year global  
2666 monthly averaged terrestrial net ecosystem exchange dataset inferred from the ACOS GOSAT v9 XCO2 retrievals  
2667 (GCAS2021), *Earth Syst. Sci. Data*, 14, 3013–3037, <https://doi.org/10.5194/essd-14-3013-2022>, 2022.



- 2668 Jiang, F., Wang, H., Chen, J. M., Ju, W., Tian, X., Feng, S., Li, G., Chen, Z., Zhang, S., Lu, X., Liu, J., Wang, H., Wang, J.,  
2669 He, W., and Wu, M.: Regional CO<sub>2</sub> fluxes from 2010 to 2015 inferred from GOSAT XCO<sub>2</sub> retrievals using a new version  
2670 of the Global Carbon Assimilation System, *Atmospheric Chem. Phys.*, 21, 1963–1985, [https://doi.org/10.5194/acp-21-1963-](https://doi.org/10.5194/acp-21-1963-2021)  
2671 2021, 2021.
- 2672
- 2673 Jin, Y., Keeling, R. F., Stephens, B. B., Long, M. C., Patra, P. K., Rödenbeck, C., Morgan, E. J., Kort, E. A., and Sweeney,  
2674 C.: Improved atmospheric constraints on Southern Ocean CO<sub>2</sub> exchange. *Proceedings of the National Academy of*  
2675 *Sciences*, 121(6), e2309333121, <https://doi.org/10.1073/pnas.2309333121>, 2024.
- 2676
- 2677 Jin, Z., Wang, T., Zhang, H., Wang, Y., Ding, J., and Tian, X.: Constraint of satellite CO<sub>2</sub> retrieval on the global carbon  
2678 cycle from a Chinese atmospheric inversion system, *Sci. China Earth Sci.*, 66, 609–618, [https://doi.org/10.1007/s11430-022-](https://doi.org/10.1007/s11430-022-1036-7)  
2679 1036-7, 2023.
- 2680
- 2681 Joos, F. and Spahni, R.: Rates of change in natural and anthropogenic radiative forcing over the past 20,000 years,  
*Proceedings of the National Academy of Sciences*, 105, 1425–1430, <https://doi.org/10.1073/pnas.0707386105>, 2008.
- 2682
- 2683 Jones, C. D., Hickman, J. E., Rumbold, S. T., Walton, J., Lamboll, R. D., Skeie, R. B., Fiedler, S., Forster, P. M., Rogelj, J.,  
2684 Abe, M., Botzet, M., Calvin, K., Cassou, C., Cole, J. N. S., Davini, P., Deushi, M., Dix, M., Fyfe, J. C., Gillett, N. P., Ilyina,  
2685 T., Kawamiya, M., Kelley, M., Kharin, S., Koshiro, T., Li, H., Mackallah, C., Müller, W. A., Nabat, P., van Noije, T., Nolan,  
2686 P., Ohgaito, R., Olivieri, D., Oshima, N., Parodi, J., Reerink, T. J., Ren, L., Romanou, A., Séférian, R., Tang, Y., Timmreck,  
2687 C., Tjiputra, J., Tourigny, E., Tsigaridis, K., Wang, H., Wu, M., Wyser, K., Yang, S., Yang, Y., and Ziehn, T.: The Climate  
2688 Response to Emissions Reductions Due to COVID-19: Initial Results From CovidMIP, *Geophys. Res. Lett.*, 48,  
2689 e2020GL091883, <https://doi.org/10.1029/2020GL091883>, 2021a.
- 2690
- 2691 Jones, M. W., Abatzoglou, J. T., Veraverbeke, S., Andela, N., Lasslop, G., Forkel, M., Smith, A. J. P., Burton, C., Betts, R.  
2692 A., van der Werf, G. R., Sitch, S., Canadell, J. G., Santín, C., Kolden, C., Doerr, S. H., and Le Quéré, C.: Global and  
2693 Regional Trends and Drivers of Fire Under Climate Change, *Rev. Geophys.*, 60, e2020RG000726,  
<https://doi.org/10.1029/2020RG000726>, 2022.
- 2694
- 2695 Jones, M. W., Andrew, R. M., Peters, G. P., Janssens-Maenhout, G., De-Gol, A. J., Ciais, P., Patra, P. K., Chevallier, F., and  
2696 Le Quéré, C.: Gridded fossil CO<sub>2</sub> emissions and related O<sub>2</sub> combustion consistent with national inventories 1959–2018, *Sci*  
*Data*, 8, 2, <https://doi.org/10.1038/s41597-020-00779-6>, 2021b.
- 2697
- 2698 Jones, M. W., Andrew, R. M., Peters, G. P., Janssens-Maenhout, G., De-Gol, A. J., Dou, X., Liu, Z., Pickers, P., Ciais, P.,  
2699 Patra, P. K., Chevallier, F., and Le Quéré, C.: Gridded fossil CO<sub>2</sub> emissions and related O<sub>2</sub> combustion consistent with  
2700 national inventories, Zenodo [dataset], <https://doi.org/10.5281/zenodo.13909046>, 2024a.
- 2701
- 2702 Jones, M. W., Kelley, D. I., Burton, C. A., Di Giuseppe, F., Barbosa, M. L. F., Brambleby, E., Hartley, A. J., Lombardi, A.,  
2703 Mataveli, G., McNorton, J. R., Spuler, F. R., Wessel, J. B., Abatzoglou, J. T., Anderson, L. O., Andela, N., Archibald, S.,  
2704 Armenteras, D., Burke, E., Carmenta, R., Chuvieco, E., Clarke, H., Doerr, S. H., Fernandes, P. M., Giglio, L., Hamilton, D.  
2705 S., Hantson, S., Harris, S., Jain, P., Kolden, C. A., Kurvits, T., Lampe, S., Meier, S., New, S., Parrington, M., Perron, M. M.  
2706 G., Qu, Y., Ribeiro, N. S., Saharjo, B. H., San-Miguel-Ayanz, J., Shuman, J. K., Tanpipat, V., van der Werf, G. R.,  
2707 Veraverbeke, S., and Xanthopoulos, G.: State of Wildfires 2023–2024, *Earth System Science Data*, 16, 3601–3685,  
<https://doi.org/10.5194/essd-16-3601-2024>, 2024b.



- 2707 Jones, M.W., Veraverbeke, S., Andela, N., Doerr, S.H., Kolden, C., Mataveli, G., Pettinari, M.L., Le Quéré, C., Rosan, T.M.,  
2708 van der Werf, G.R. and van Wees, D.: Global rise in forest fire emissions linked to climate change in the extratropics.  
2709 *Science*, 386(6719), p.ead15889, 2024c.
- 2710 Jung, M., Reichstein, M., Schwalm, C. R., Huntingford, C., Sitch, S., Ahlström, A., Arneth, A., Camps-Valls, G., Ciais, P.,  
2711 Friedlingstein, P., Gans, F., Ichii, K., Jain, A. K., Kato, E., Papale, D., Poulter, B., Raduly, B., Rödenbeck, C., Tramontana,  
2712 G., Viovy, N., Wang, Y.-P., Weber, U., Zaehle, S., and Zeng, N.: Compensatory water effects link yearly global land CO<sub>2</sub>  
2713 sink changes to temperature, *Nature*, 541, 516–520, <https://doi.org/10.1038/nature20780>, 2017.
- 2714 Kaiser, J. W., Heil, A., Andreae, M. O., Benedetti, A., Chubarova, N., Jones, L., Morcrette, J.-J., Razinger, M., Schultz, M.  
2715 G., Suttie, M., and van der Werf, G. R.: Biomass burning emissions estimated with a global fire assimilation system based  
2716 on observed fire radiative power, *Biogeosciences*, 9, 527–554, <https://doi.org/10.5194/bg-9-527-2012>, 2012.
- 2717 Kato, E., Kinoshita, T., Ito, A., Kawamiya, M., and Yamagata, Y.: Evaluation of spatially explicit emission scenario of land-  
2718 use change and biomass burning using a process-based biogeochemical model, *J. Land Use Sci.*, 8, 104–122,  
2719 <https://doi.org/10.1080/1747423X.2011.628705>, 2013.
- 2720 Kawasaki, T., Hasumi, H., and Tanaka, Y.: Role of tide-induced vertical mixing in the deep Pacific Ocean circulation, *J.*  
2721 *Oceanogr.*, 77, 173–184, <https://doi.org/10.1007/s10872-020-00584-0>, 2021.
- 2722 Ke, P., Ciais, P., Sitch, S., Li, W., Bastos, A., Liu, Z., Xu, Y., Gui, X., Bian, J., Goll, D. S., Xi, Y., Li, W., O'Sullivan, M.,  
2723 Goncalves de Souza, J., Friedlingstein, P., Chevallier, F.: Low latency carbon budget analysis reveals a large decline of the  
2724 land carbon sink in 2023. *National Science Review*, p.nwae367, <https://doi.org/10.1093/nsr/nwae367>, 2024.  
2725
- 2726 Keeley, J. E. and Pausas, J. G.: Distinguishing disturbance from perturbations in fire-prone ecosystems, *Int. J. Wildland Fire*,  
2727 28, 282–287, <https://doi.org/10.1071/WF18203>, 2019.
- 2728 Keeling, C. D., Bacastow, R. B., Bainbridge, A. E., Ekdahl, C. A., Guenther, P. R., Waterman, L. S., and Chin, J. F. S.:  
2729 Atmospheric carbon dioxide variations at Mauna Loa Observatory, Hawaii, *Tellus A.*, 28, 538–551,  
2730 <https://doi.org/10.1111/j.2153-3490.1976.tb00701.x>, 1976.
- 2731 Keeling R.F.: Development of an Interferometric Oxygen Analyzer for Precise Measurement of the Atmospheric O<sub>2</sub> Mole  
2732 Fraction, PhD thesis, Harvard University, Cambridge, Massachusetts, available at:  
2733 [https://bluemoon.ucsd.edu/publications/ralph/34\\_PhDthesis.pdf](https://bluemoon.ucsd.edu/publications/ralph/34_PhDthesis.pdf), last access: 28 October 2024, 1988.
- 2734 Keeling, R. F., Manning, A. C., Paplawsky, W. J., and Cox, A. C.: On the long-term stability of reference gases for  
2735 atmospheric O<sub>2</sub>/N<sub>2</sub> and CO<sub>2</sub> measurements, *Tellus B Chem. Phys. Meteorol.*, 59, 3–14, [https://doi.org/10.1111/j.1600-  
2736 0889.2006.00196.x](https://doi.org/10.1111/j.1600-), 2007.  
2737
- 2738 Keeling, R. F. and Manning, A. C.: 5.15 - Studies of Recent Changes in Atmospheric O<sub>2</sub> Content, in: *Treatise on*  
2739 *Geochemistry (Second Edition)*, edited by: Holland, H. D. and Turekian, K. K., Elsevier, Oxford, 385–404,  
2740 <https://doi.org/10.1016/B978-0-08-095975-7.00420-4>, 2014.
- 2741 Keppler, L. and Landschützer, P.: Regional Wind Variability Modulates the Southern Ocean Carbon Sink, *Sci Rep*, 9, 7384,  
2742 <https://doi.org/10.1038/s41598-019-43826-y>, 2019.



- 2743 Khatiwala, S., Primeau, F., and Hall, T.: Reconstruction of the history of anthropogenic CO<sub>2</sub> concentrations in the ocean,  
2744 *Nature*, 462, 346–349, <https://doi.org/10.1038/nature08526>, 2009.
- 2745 Khatiwala, S., Tanhua, T., Mikaloff Fletcher, S., Gerber, M., Doney, S. C., Graven, H. D., Gruber, N., McKinley, G. A.,  
2746 Murata, A., Ríos, A. F., and Sabine, C. L.: Global ocean storage of anthropogenic carbon, *Biogeosciences*, 10, 2169–2191,  
2747 <https://doi.org/10.5194/bg-10-2169-2013>, 2013.
- 2748 Kong, Y., Zheng, B., Zhang, Q., and He, K.: Global and regional carbon budget for 2015–2020 inferred from OCO-2 based  
2749 on an ensemble Kalman filter coupled with GEOS-Chem, *Atmospheric Chem. Phys.*, 22, 10769–10788,  
2750 <https://doi.org/10.5194/acp-22-10769-2022>, 2022.
- 2751 Korsbakken, J. I., Peters, G. P., and Andrew, R. M.: Uncertainties around reductions in China’s coal use and CO<sub>2</sub> emissions,  
2752 *Nature Clim Change*, 6, 687–690, <https://doi.org/10.1038/nclimate2963>, 2016.
- 2753 Krinner, G., Viovy, N., de Noblet-Ducoudré, N., Ogée, J., Polcher, J., Friedlingstein, P., Ciais, P., Sitch, S., and Prentice, I.  
2754 C.: A dynamic global vegetation model for studies of the coupled atmosphere-biosphere system: DVGCM for coupled climate  
2755 studies, *Global Biogeochem. Cycles*, 19, GB1015, <https://doi.org/10.1029/2003GB002199>, 2005.
- 2756 Lacroix, F., Ilyina, T., and Hartmann, J.: Oceanic CO<sub>2</sub> outgassing and biological production hotspots induced by pre-  
2757 industrial river loads of nutrients and carbon in a global modeling approach, *Biogeosciences*, 17, 55–88,  
2758 <https://doi.org/10.5194/bg-17-55-2020>, 2020.
- 2759 Lacroix, F., Ilyina, T., Mathis, M., Laruelle, G. G., and Regnier, P.: Historical increases in land-derived nutrient inputs may  
2760 alleviate effects of a changing physical climate on the oceanic carbon cycle, *Glob Change Biol*, 27, 5491–5513,  
2761 <https://doi.org/10.1111/gcb.15822>, 2021.
- 2762 Lamboll, R. D., Nicholls, Z. R. J., Smith, C. J., Kikstra, J. S., Byers, E., and Rogelj, J.: Assessing the size and uncertainty of  
2763 remaining carbon budgets, *Nat. Clim. Change*, <https://doi.org/10.1038/s41558-023-01848-5>, 2023.  
2764
- 2765 Lamboll, R. D., Jones, C. D., Skeie, R. B., Fiedler, S., Samset, B. H., Gillett, N. P., Rogelj, J., Forster, P. M., 2021:  
2766 Modifying emissions scenario projections to account for the effects of COVID-19: protocol for CovidMIP, *Geosci. Model*  
2767 *Dev.*, 14, 3683–3695, <https://doi.org/10.5194/gmd-14-3683-2021>, 2021.
- 2768 Lan, X., Tans, P. and K.W. Thoning: Trends in globally-averaged CO<sub>2</sub> determined from NOAA Global Monitoring  
2769 Laboratory measurements, Version 2024-09. National Oceanic and Atmospheric Administration, Global Monitoring  
2770 Laboratory (NOAA/GML) [dataset], available at: <https://gml.noaa.gov/ccgg/trends/global.html>, last access: 28 October  
2771 2024, 2024.
- 2772 Landschützer, P., Gruber, N., Haumann, F. A., Rödenbeck, C., Bakker, D. C. E., van Heuven, S., Hoppema, M., Metzl, N.,  
2773 Sweeney, C., Takahashi, T., Tilbrook, B., and Wanninkhof, R.: The reinvigoration of the Southern Ocean carbon sink,  
2774 *Science*, 349, 1221–1224, <https://doi.org/10.1126/science.aab2620>, 2015.
- 2775 Landschützer, P., Gruber, N., and Bakker, D. C. E.: Decadal variations and trends of the global ocean carbon sink: decadal  
2776 air-sea CO<sub>2</sub> flux variability, *Global Biogeochem. Cycles*, 30, 1396–1417, <https://doi.org/10.1002/2015GB005359>, 2016.



- 2777 Lapola, D. M., Pinho, P., Barlow, J., Aragão, L. E. O. C., Berenguer, E., Carmenta, R., Liddy, H. M., Seixas, H., Silva, C. V.  
2778 J., Silva-Junior, C. H. L., Alencar, A. A. C., Anderson, L. O., Armenteras, D., Brovkin, V., Calders, K., Chambers, J., Chini,  
2779 L., Costa, M. H., Faria, B. L., Fearnside, P. M., Ferreira, J., Gatti, L., Gutierrez-Velez, V. H., Han, Z., Hibbard, K., Koven,  
2780 C., Lawrence, P., Pongratz, J., Portela, B. T. T., Rounsevell, M., Ruane, A. C., Schaldach, R., da Silva, S. S., von Randow,  
2781 C., Walker, W. S.: The drivers and impacts of Amazon forest degradation. *Science*, 379(6630), p.eabp8622,  
2782 <https://doi.org/10.1126/science.abp8622>, 2023.
- 2783 Law, R. M., Ziehn, T., Matear, R. J., Lenton, A., Chamberlain, M. A., Stevens, L. E., Wang, Y.-P., Srbnovsky, J., Bi, D.,  
2784 Yan, H., and Vohralik, P. F.: The carbon cycle in the Australian Community Climate and Earth System Simulator  
2785 (ACCESS-ESM1) – Part 1: Model description and pre-industrial simulation, *Geosci. Model Dev.*, 10, 2567–2590,  
2786 <https://doi.org/10.5194/gmd-10-2567-2017>, 2017.
- 2787 Lawrence, D. M., Fisher, R. A., Koven, C. D., Oleson, K. W., Swenson, S. C., Bonan, G., Collier, N., Ghimire, B., van  
2788 Kampenhout, L., Kennedy, D., Kluzek, E., Lawrence, P. J., Li, F., Li, H., Lombardozzi, D., Riley, W. J., Sacks, W. J., Shi,  
2789 M., Vertenstein, M., Wieder, W. R., Xu, C., Ali, A. A., Badger, A. M., Bisht, G., van den Broeke, M., Brunke, M. A., Burns,  
2790 S. P., Buzan, J., Clark, M., Craig, A., Dahlin, K., Drewniak, B., Fisher, J. B., Flanner, M., Fox, A. M., Gentine, P., Hoffman,  
2791 F., Keppel-Aleks, G., Knox, R., Kumar, S., Lenaerts, J., Leung, L. R., Lipscomb, W. H., Lu, Y., Pandey, A., Pelletier, J. D.,  
2792 Perket, J., Randerson, J. T., Ricciuto, D. M., Sanderson, B. M., Slater, A., Subin, Z. M., Tang, J., Thomas, R. Q., Val Martin,  
2793 M., and Zeng, X.: The Community Land Model Version 5: Description of New Features, Benchmarking, and Impact of  
2794 Forcing Uncertainty, *J. Adv. Model Earth, Sy.*, 11, 4245–4287, <https://doi.org/10.1029/2018MS001583>, 2019.
- 2795 Le Quéré, C., Rödenbeck, C., Buitenhuis, E. T., Conway, T. J., Langenfelds, R., Gomez, A., Labuschagne, C., Ramonet, M.,  
2796 Nakazawa, T., Metzl, N., Gillett, N., and Heimann, M.: Saturation of the Southern Ocean CO<sub>2</sub> Sink Due to Recent Climate  
2797 Change, *Science*, 316, 1735–1738, <https://doi.org/10.1126/science.1136188>, 2007.
- 2798 Le Quéré, C., Raupach, M. R., Canadell, J. G., Marland, G., Bopp, L., Ciais, P., Conway, T. J., Doney, S. C., Feely, R. A.,  
2799 Foster, P., Friedlingstein, P., Gurney, K., Houghton, R. A., House, J. I., Huntingford, C., Levy, P. E., Lomas, M. R., Majkut,  
2800 J., Metzl, N., Ometto, J. P., Peters, G. P., Prentice, I. C., Randerson, J. T., Running, S. W., Sarmiento, J. L., Schuster, U.,  
2801 Sitch, S., Takahashi, T., Viovy, N., van der Werf, G. R., and Woodward, F. I.: Trends in the sources and sinks of carbon  
2802 dioxide, *Nature Geosci.*, 2, 831–836, <https://doi.org/10.1038/ngeo689>, 2009.
- 2803 Le Quéré, C., Andres, R. J., Boden, T., Conway, T., Houghton, R. A., House, J. I., Marland, G., Peters, G. P., van der Werf,  
2804 G. R., Ahlström, A., Andrew, R. M., Bopp, L., Canadell, J. G., Ciais, P., Doney, S. C., Enright, C., Friedlingstein, P.,  
2805 Huntingford, C., Jain, A. K., Jourdain, C., Kato, E., Keeling, R. F., Klein Goldewijk, K., Levis, S., Levy, P., Lomas, M.,  
2806 Poulter, B., Raupach, M. R., Schwinger, J., Sitch, S., Stocker, B. D., Viovy, N., Zaehle, S., and Zeng, N.: The global carbon  
2807 budget 1959–2011, *Earth Syst. Sci. Data*, 5, 165–185, <https://doi.org/10.5194/essd-5-165-2013>, 2013.
- 2808 Le Quéré, C., Peters, G. P., Andres, R. J., Andrew, R. M., Boden, T. A., Ciais, P., Friedlingstein, P., Houghton, R. A.,  
2809 Marland, G., Moriarty, R., Sitch, S., Tans, P., Armeth, A., Arvanitis, A., Bakker, D. C. E., Bopp, L., Canadell, J. G., Chini, L.  
2810 P., Doney, S. C., Harper, A., Harris, I., House, J. I., Jain, A. K., Jones, S. D., Kato, E., Keeling, R. F., Klein Goldewijk, K.,  
2811 Körtzinger, A., Koven, C., Lefèvre, N., Maignan, F., Omar, A., Ono, T., Park, G.-H., Pfeil, B., Poulter, B., Raupach, M. R.,  
2812 Regnier, P., Rödenbeck, C., Saito, S., Schwinger, J., Segsneider, J., Stocker, B. D., Takahashi, T., Tilbrook, B., van  
2813 Heuven, S., Viovy, N., Wanninkhof, R., Wiltshire, A., and Zaehle, S.: Global carbon budget 2013, *Earth Syst. Sci. Data*, 6,  
2814 235–263, <https://doi.org/10.5194/essd-6-235-2014>, 2014.





- 2815 Le Quéré, C., Moriarty, R., Andrew, R. M., Peters, G. P., Ciais, P., Friedlingstein, P., Jones, S. D., Sitch, S., Tans, P.,  
2816 Armeth, A., Boden, T. A., Bopp, L., Bozec, Y., Canadell, J. G., Chini, L. P., Chevallier, F., Cosca, C. E., Harris, I.,  
2817 Hoppema, M., Houghton, R. A., House, J. I., Jain, A. K., Johannessen, T., Kato, E., Keeling, R. F., Kitidis, V., Klein  
2818 Goldewijk, K., Koven, C., Landa, C. S., Landschützer, P., Lenton, A., Lima, I. D., Marland, G., Mathis, J. T., Metzl, N.,  
2819 Nojiri, Y., Olsen, A., Ono, T., Peng, S., Peters, W., Pfeil, B., Poulter, B., Raupach, M. R., Regnier, P., Rödenbeck, C., Saito,  
2820 S., Salisbury, J. E., Schuster, U., Schwinger, J., Séférian, R., Segschneider, J., Steinhoff, T., Stocker, B. D., Sutton, A. J.,  
2821 Takahashi, T., Tilbrook, B., van der Werf, G. R., Viovy, N., Wang, Y.-P., Wanninkhof, R., Wiltshire, A., and Zeng, N.:  
2822 Global carbon budget 2014, *Earth Syst. Sci. Data*, 7, 47–85, <https://doi.org/10.5194/essd-7-47-2015>, 2015a.
- 2823 Le Quéré, C., Moriarty, R., Andrew, R. M., Canadell, J. G., Sitch, S., Korsbakken, J. I., Friedlingstein, P., Peters, G. P.,  
2824 Andres, R. J., Boden, T. A., Houghton, R. A., House, J. I., Keeling, R. F., Tans, P., Armeth, A., Bakker, D. C. E., Barbero,  
2825 L., Bopp, L., Chang, J., Chevallier, F., Chini, L. P., Ciais, P., Fader, M., Feely, R. A., Gkritzalis, T., Harris, I., Hauck, J.,  
2826 Ilyina, T., Jain, A. K., Kato, E., Kitidis, V., Klein Goldewijk, K., Koven, C., Landschützer, P., Lauvset, S. K., Lefèvre, N.,  
2827 Lenton, A., Lima, I. D., Metzl, N., Millero, F., Munro, D. R., Murata, A., Nabel, J. E. M. S., Nakaoka, S., Nojiri, Y.,  
2828 O'Brien, K., Olsen, A., Ono, T., Pérez, F. F., Pfeil, B., Pierrot, D., Poulter, B., Rehder, G., Rödenbeck, C., Saito, S.,  
2829 Schuster, U., Schwinger, J., Séférian, R., Steinhoff, T., Stocker, B. D., Sutton, A. J., Takahashi, T., Tilbrook, B., van der  
2830 Laan-Luijkx, I. T., van der Werf, G. R., van Heuven, S., Vandemark, D., Viovy, N., Wiltshire, A., Zaehle, S., and Zeng, N.:  
2831 Global Carbon Budget 2015, *Earth Syst. Sci. Data*, 7, 349–396, <https://doi.org/10.5194/essd-7-349-2015>, 2015b.
- 2832 Le Quéré, C., Andrew, R. M., Canadell, J. G., Sitch, S., Korsbakken, J. I., Peters, G. P., Manning, A. C., Boden, T. A., Tans,  
2833 P. P., Houghton, R. A., Keeling, R. F., Alin, S., Andrews, O. D., Anthoni, P., Barbero, L., Bopp, L., Chevallier, F., Chini, L.  
2834 P., Ciais, P., Currie, K., Delire, C., Doney, S. C., Friedlingstein, P., Gkritzalis, T., Harris, I., Hauck, J., Haverd, V.,  
2835 Hoppema, M., Klein Goldewijk, K., Jain, A. K., Kato, E., Körtzinger, A., Landschützer, P., Lefèvre, N., Lenton, A., Lienert,  
2836 S., Lombardozi, D., Melton, J. R., Metzl, N., Millero, F., Monteiro, P. M. S., Munro, D. R., Nabel, J. E. M. S., Nakaoka, S.,  
2837 O'Brien, K., Olsen, A., Omar, A. M., Ono, T., Pierrot, D., Poulter, B., Rödenbeck, C., Salisbury, J., Schuster, U., Schwinger,  
2838 J., Séférian, R., Skjelvan, I., Stocker, B. D., Sutton, A. J., Takahashi, T., Tian, H., Tilbrook, B., van der Laan-Luijkx, I. T.,  
2839 van der Werf, G. R., Viovy, N., Walker, A. P., Wiltshire, A. J., and Zaehle, S.: Global Carbon Budget 2016, *Earth Syst. Sci.*  
2840 *Data*, 8, 605–649, <https://doi.org/10.5194/essd-8-605-2016>, 2016.
- 2841 Le Quéré, C., Andrew, R. M., Friedlingstein, P., Sitch, S., Pongratz, J., Manning, A. C., Korsbakken, J. I., Peters, G. P.,  
2842 Canadell, J. G., Jackson, R. B., Boden, T. A., Tans, P. P., Andrews, O. D., Arora, V. K., Bakker, D. C. E., Barbero, L.,  
2843 Becker, M., Betts, R. A., Bopp, L., Chevallier, F., Chini, L. P., Ciais, P., Cosca, C. E., Cross, J., Currie, K., Gasser, T.,  
2844 Harris, I., Hauck, J., Haverd, V., Houghton, R. A., Hunt, C. W., Hurtt, G., Ilyina, T., Jain, A. K., Kato, E., Kautz, M.,  
2845 Keeling, R. F., Klein Goldewijk, K., Körtzinger, A., Landschützer, P., Lefèvre, N., Lenton, A., Lienert, S., Lima, I.,  
2846 Lombardozi, D., Metzl, N., Millero, F., Monteiro, P. M. S., Munro, D. R., Nabel, J. E. M. S., Nakaoka, S., Nojiri, Y., Padin,  
2847 X. A., Peregón, A., Pfeil, B., Pierrot, D., Poulter, B., Rehder, G., Reimer, J., Rödenbeck, C., Schwinger, J., Séférian, R.,  
2848 Skjelvan, I., Stocker, B. D., Tian, H., Tilbrook, B., Tubiello, F. N., van der Laan-Luijkx, I. T., van der Werf, G. R., van  
2849 Heuven, S., Viovy, N., Vuichard, N., Walker, A. P., Watson, A. J., Wiltshire, A. J., Zaehle, S., and Zhu, D.: Global Carbon  
2850 Budget 2017, *Earth Syst. Sci. Data*, 10, 405–448, <https://doi.org/10.5194/essd-10-405-2018>, 2018a.
- 2851 Le Quéré, C., Andrew, R. M., Friedlingstein, P., Sitch, S., Hauck, J., Pongratz, J., Pickers, P. A., Korsbakken, J. I., Peters, G.  
2852 P., Canadell, J. G., Armeth, A., Arora, V. K., Barbero, L., Bastos, A., Bopp, L., Chevallier, F., Chini, L. P., Ciais, P., Doney,  
2853 S. C., Gkritzalis, T., Goll, D. S., Harris, I., Haverd, V., Hoffman, F. M., Hoppema, M., Houghton, R. A., Hurtt, G., Ilyina, T.,  
2854 Jain, A. K., Johannessen, T., Jones, C. D., Kato, E., Keeling, R. F., Klein Goldewijk, K., Landschützer, P., Lefèvre, N.,



- 2855 Lienert, S., Liu, Z., Lombardozi, D., Metzl, N., Munro, D. R., Nabel, J. E. M. S., Nakaoka, S., Neill, C., Olsen, A., Ono, T.,  
2856 Patra, P., Peregon, A., Peters, W., Peylin, P., Pfeil, B., Pierrot, D., Poulter, B., Rehder, G., Resplandy, L., Robertson, E.,  
2857 Rocher, M., Rödenbeck, C., Schuster, U., Schwinger, J., Séférian, R., Skjelvan, I., Steinhoff, T., Sutton, A., Tans, P. P.,  
2858 Tian, H., Tilbrook, B., Tubiello, F. N., van der Laan-Luijkx, I. T., van der Werf, G. R., Viovy, N., Walker, A. P., Wiltshire,  
2859 A. J., Wright, R., Zaehle, S., and Zheng, B.: Global Carbon Budget 2018, *Earth Syst. Sci. Data*, 10, 2141–2194,  
2860 <https://doi.org/10.5194/essd-10-2141-2018>, 2018b.
- 2861 Le Quéré, C., Korsbakken, J. I., Wilson, C., Tosun, J., Andrew, R., Andres, R. J., Canadell, J. G., Jordan, A., Peters, G. P.,  
2862 and van Vuuren, D. P.: Drivers of declining CO<sub>2</sub> emissions in 18 developed economies, *Nat. Clim. Chang.*, 9, 213–217,  
2863 <https://doi.org/10.1038/s41558-019-0419-7>, 2019.
- 2864 Le Quéré, C., Peters, G. P., Friedlingstein, P., Andrew, R. M., Canadell, J. G., Davis, S. J., Jackson, R. B., and Jones, M. W.:  
2865 Fossil CO<sub>2</sub> emissions in the post-COVID-19 era, *Nat. Clim. Chang.*, 11, 197–199, [https://doi.org/10.1038/s41558-021-](https://doi.org/10.1038/s41558-021-01001-0)  
2866 01001-0, 2021.
- 2867 Levitus, S., Antonov, J. I., Boyer, T. P., Baranova, O. K., Garcia, H. E., Locarnini, R. A., Mishonov, A. V., Reagan, J. R.,  
2868 Seidov, D., Yarosh, E. S., and Zweng, M. M.: World ocean heat content and thermocline sea level change (0–2000 m),  
2869 1955–2010, *Geophys. Res. Lett.*, 39, <https://doi.org/10.1029/2012GL051106>, 2012.  
2870
- 2871 Li, H., Ilyina, T., Müller, W. A., and Sienz, F.: Decadal predictions of the North Atlantic CO<sub>2</sub> uptake, *Nat. Commun.*, 7,  
2872 11076, <https://doi.org/10.1038/ncomms11076>, 2016.  
2873
- 2874 Li, H., Ilyina, T., Müller, W. A., and Landschützer, P.: Predicting the variable ocean carbon sink, *Sci. Adv.*, 5, eaav6471,  
2875 <https://doi.org/10.1126/sciadv.aav6471>, 2019.  
2876
- 2877 Li, H., Ilyina, T., Loughran, T., Spring, A., and Pongratz, J.: Reconstructions and predictions of the global carbon budget  
2878 with an emission-driven Earth system model, *Earth Syst. Dyn.*, 14, 101–119, <https://doi.org/10.5194/esd-14-101-2023>, 2023.
- 2879 Li, W., Ciais, P., Peng, S., Yue, C., Wang, Y., Thurner, M., Saatchi, S. S., Armeth, A., Avitabile, V., Carvalhais, N., Harper,  
2880 A. B., Kato, E., Koven, C., Liu, Y. Y., Nabel, J. E. M. S., Pan, Y., Pongratz, J., Poulter, B., Pugh, T. A. M., Santoro, M.,  
2881 Sitch, S., Stocker, B. D., Viovy, N., Wiltshire, A., Yousefpour, R., and Zaehle, S.: Land-use and land-cover change carbon  
2882 emissions between 1901 and 2012 constrained by biomass observations, *Biogeosciences*, 14, 5053–5067,  
2883 <https://doi.org/10.5194/bg-14-5053-2017>, 2017.
- 2884 Liao, E., Resplandy, L., Liu, J., and Bowman, K. W.: Amplification of the Ocean Carbon Sink During El Niños: Role of  
2885 Poleward Ekman Transport and Influence on Atmospheric CO<sub>2</sub>, *Global Biogeochem. Cy.*, 34, e2020GB006574,  
2886 <https://doi.org/10.1029/2020GB006574>, 2020.
- 2887 Lienert, S. and Joos, F.: A Bayesian ensemble data assimilation to constrain model parameters and land-use carbon  
2888 emissions, *Biogeosciences*, 15, 2909–2930, <https://doi.org/10.5194/bg-15-2909-2018>, 2018.
- 2889 Liu, J., Baskaran, L., Bowman, K., Schimel, D., Bloom, A. A., Parazoo, N. C., Oda, T., Carroll, D., Menemenlis, D., Joiner,  
2890 J., Commane, R., Daube, B., Gatti, L. V., McKain, K., Miller, J., Stephens, B. B., Sweeney, C., and Wofsy, S.: Carbon  
2891 Monitoring System Flux Net Biosphere Exchange 2020 (CMS-Flux NBE 2020), 13, 299–330, [https://doi.org/10.5194/essd-](https://doi.org/10.5194/essd-13-299-2021)  
2892 13-299-2021, 2021.



- 2893 Liu, Z., Guan, D., Wei, W., Davis, S. J., Ciais, P., Bai, J., Peng, S., Zhang, Q., Hubacek, K., Marland, G., Andres, R. J.,  
2894 Crawford-Brown, D., Lin, J., Zhao, H., Hong, C., Boden, T. A., Feng, K., Peters, G. P., Xi, F., Liu, J., Li, Y., Zhao, Y.,  
2895 Zeng, N., and He, K.: Reduced carbon emission estimates from fossil fuel combustion and cement production in China,  
2896 *Nature*, 524, 335–338, <https://doi.org/10.1038/nature14677>, 2015.
- 2897 Liu, Z., Zeng, N., Liu, Y., Kalnay, E., Asrar, G., Wu, B., Cai, Q., Liu, D., and Han, P.: Improving the joint estimation of  
2898 CO<sub>2</sub> and surface carbon fluxes using a constrained ensemble Kalman filter in COLA (v1.0), *Geosci. Model Dev.*, 15, 5511–  
2899 5528, <https://doi.org/10.5194/gmd-15-5511-2022>, 2022.
- 2900
- 2901 Long, M. C., Stephens, B. B., McKain, K., Sweeney, C., Keeling, R. F., Kort, E. A., Morgan, E. J., Bent, J. D., Chandra, N.,  
2902 Chevallier, F., Commane, R., Daube, B. C., Krummel, P. B., Loh, Z., Lujikx, I. T., Munro, D., Patra, P., Peters, W.,  
2903 Ramonet, M., Rödenbeck, C., Stavert, A., Tans, P., Wofsy, S. C.: Strong Southern Ocean carbon uptake evident in airborne  
2904 observations. *Science*, 374(6572), 1275–1280, <https://doi.org/10.1126/science.abi4355>, 2021.
- 2905
- 2906 Lovenduski, N. S., Bonan, G. B., Yeager, S. G., Lindsay, K., and Lombardozzi, D. L.: High predictability of terrestrial  
2907 carbon fluxes from an initialized decadal prediction system, *Environ. Res. Lett.*, 14, 124074, <https://doi.org/10.1088/1748-9326/ab5c55>, 2019a.
- 2908
- 2909
- 2910 Lovenduski, N. S., Yeager, S. G., Lindsay, K., and Long, M. C.: Predicting near-term variability in ocean carbon uptake,  
2911 *Earth Syst. Dyn.*, 10, 45–57, <https://doi.org/10.5194/esd-10-45-2019>, 2019b.
- 2912 Lutz, F., Herzfeld, T., Heinke, J., Rolinski, S., Schaphoff, S., von Bloh, W., Stoorvogel, J. J., and Müller, C.: Simulating the  
2913 effect of tillage practices with the global ecosystem model LPJmL (version 5.0-tillage), *Geosci. Model Dev.*, 12, 2419–2440,  
2914 <https://doi.org/10.5194/gmd-12-2419-2019>, 2019.
- 2915 Ma, L., Hurtt, G., Ott, L., Sahajpal, R., Fisk, J., Lamb, R., Tang, H., Flanagan, S., Chini, L., Chatterjee, A., and Sullivan, J.:  
2916 Global evaluation of the Ecosystem Demography model (ED v3.0), *Geosci. Model Dev.*, 15, 1971–1994,  
2917 <https://doi.org/10.5194/gmd-15-1971-2022>, 2022.
- 2918
- 2919 Magi, B. I., Rabin, S., Shevliakova, E., and Pacala, S.: Separating agricultural and non-agricultural fire seasonality at  
2920 regional scales, *Biogeosciences*, 9, 3003–3012, <https://doi.org/10.5194/bg-9-3003-2012>, 2012.
- 2921
- 2922 Maksyutov, S., Oda, T., Saito, M., Janardanan, R., Belikov, D., Kaiser, J. W., Zhuravlev, R., Ganshin, A., Valsala, V. K.,  
2923 Andrews, A., Chmura, L., Dlugokencky, E., Haszpra, L., Langenfels, R. L., Machida, T., Nakazawa, T., Ramonet, M.,  
2924 Sweeney, C., and Worthy, D.: Technical note: A high-resolution inverse modelling technique for estimating surface CO<sub>2</sub>  
2925 fluxes based on the NIES-TM–FLEXPART coupled transport model and its adjoint, *Atmos. Chem. Phys.*, 21, 1245–1266,  
2926 <https://doi.org/10.5194/acp-21-1245-2021>, 2021.
- 2927 Masarie, K. A. and Tans, P. P.: Extension and integration of atmospheric carbon dioxide data into a globally consistent  
2928 measurement record, *J. Geophys. Res.*, 100, 11593, <https://doi.org/10.1029/95JD00859>, 1995.
- 2929 Mataveli, G., Jones, M.W., Carmenta, R., Sanchez, A., Dutra, D.J., Chaves, M., de Oliveira, G., Anderson, L.O. and Aragão,  
2930 L.E.: Deforestation falls but rise of wildfires continues degrading Brazilian Amazon forests. *Global Change Biology*, 30(2),  
2931 p.e17202, <https://doi.org/10.1111/gcb.17202>, 2024.



- 2932 Mather, A. S.: The transition from deforestation to reforestation in Europe, in: *Agricultural technologies and tropical*  
2933 *deforestation* (eds. Angelsen, A.; Kaimowitz, D.), CABI in association with centre for international Forestry Research, 35–  
2934 52, 2001.
- 2935 Mauritsen, T., Bader, J., Becker, T., Behrens, J., Bittner, M., Brokopf, R., Brovkin, V., Claussen, M., Crueger, T., Esch, M.,  
2936 Fast, I., Fiedler, S., Fläschner, D., Gayler, V., Giorgetta, M., Goll, D. S., Haak, H., Hagemann, S., Hedemann, C.,  
2937 Hohenegger, C., Ilyina, T., Jahns, T., Jiménez-de-la-Cuesta, D., Jungclaus, J., Kleinen, T., Kloster, S., Kracher, D., Kinne,  
2938 S., Kleberg, D., Lasslop, G., Kornbluh, L., Marotzke, J., Matei, D., Meraner, K., Mikolajewicz, U., Modali, K., Möbis, B.,  
2939 Müller, W. A., Nabel, J. E. M. S., Nam, C. C. W., Notz, D., Nyawira, S.-S., Paulsen, H., Peters, K., Pincus, R., Pohlmann,  
2940 H., Pongratz, J., Popp, M., Raddatz, T. J., Rast, S., Redler, R., Reick, C. H., Rohrschneider, T., Schemann, V., Schmidt, H.,  
2941 Schnur, R., Schulzweida, U., Six, K. D., Stein, L., Stemmler, I., Stevens, B., von Storch, J.-S., Tian, F., Voigt, A., Vrese, P.,  
2942 Wieners, K.-H., Wilkenskjeld, S., Winkler, A., and Roeckner, E.: Developments in the MPI-M Earth System Model version  
2943 1.2 (MPI-ESM1.2) and Its Response to Increasing CO<sub>2</sub>, *J. Adv. Model Earth Sy.*, 11, 998–1038,  
2944 <https://doi.org/10.1029/2018MS001400>, 2019.
- 2945 Mayot, N., Buitenhuis, E. T., Wright, R. M., Hauck, J., Bakker, D. C. E., and Le Quéré, C.: Constraining the trend in the  
2946 ocean CO<sub>2</sub> sink during 2000–2022. *Nat Commun* 15, 8429, <https://doi.org/10.1038/s41467-024-52641-7>, 2024.
- 2947 McGrath, M. J., Luysaert, S., Meyfroidt, P., Kaplan, J. O., Bürgi, M., Chen, Y., Erb, K., Gimmi, U., McInerney, D., Naudts,  
2948 K., Otto, J., Pasztor, F., Ryder, J., Schelhaas, M.-J., and Valade, A.: Reconstructing European forest management from 1600  
2949 to 2010, 12, 4291–4316, <https://doi.org/10.5194/bg-12-4291-2015>, 2015.
- 2950 McKinley, G. A., Fay, A. R., Eddebbar, Y. A., Gloege, L., and Lovenduski, N. S.: External Forcing Explains Recent  
2951 Decadal Variability of the Ocean Carbon Sink, *AGU Advances*, 1, e2019AV000149,  
2952 <https://doi.org/10.1029/2019AV000149>, 2020.
- 2953 McKinley, G. A., Fay, A. R., Lovenduski, N. S., and Pilcher, D. J.: Natural Variability and Anthropogenic Trends in the  
2954 Ocean Carbon Sink, *Annu. Rev. Mar. Sci.*, 9, 125–150, <https://doi.org/10.1146/annurev-marine-010816-060529>, 2017.
- 2955 Meiyappan, P., Jain, A. K., and House, J. I.: Increased influence of nitrogen limitation on CO<sub>2</sub> emissions from future land  
2956 use and land use change, *Global Biogeochem. Cycles*, 29, 1524–1548, <https://doi.org/10.1002/2015GB005086>, 2015.
- 2957 Melton, J. R., Arora, V. K., Wisernig-Cojoc, E., Seiler, C., Fortier, M., Chan, E., and Teckentrup, L.: CLASSIC v1.0: the  
2958 open-source community successor to the Canadian Land Surface Scheme (CLASS) and the Canadian Terrestrial Ecosystem  
2959 Model (CTEM) – Part 1: Model framework and site-level performance, *Geosci. Model Dev.*, 13, 2825–2850,  
2960 <https://doi.org/10.5194/gmd-13-2825-2020>, 2020.
- 2961 Mercado, L. M., Bellouin, N., Sitch, S., Boucher, O., Huntingford, C., Wild, M., and Cox, P. M.: Impact of changes in  
2962 diffuse radiation on the global land carbon sink, *Nature*, 458, 1014–1017, <https://doi.org/10.1038/nature07949>, 2009.
- 2963 Merchant, C. J., Embury, O., Bulgin, C. E., Block, T., Corlett, G. K., Fiedler, E., Good, S. A., Mittaz, J., Rayner, N. A.,  
2964 Berry, D., Eastwood, S., Taylor, M., Tsushima, Y., Waterfall, A., Wilson, R., and Donlon, C.: Satellite-based time-series of  
2965 sea-surface temperature since 1981 for climate applications, *Sci. Data*, 6, 223, <https://doi.org/10.1038/s41597-019-0236-x>,  
2966 2019.



- 2967 Moorcroft, P. R., Hurtt, G. C., and Pacala, S. W.: A Method for Scaling Vegetation Dynamics: The Ecosystem Demography  
2968 Model (ed), *Ecol. Monogr.*, 71, 557–586, [https://doi.org/10.1890/0012-9615\(2001\)071\[0557:AMFSVD\]2.0.CO;2](https://doi.org/10.1890/0012-9615(2001)071[0557:AMFSVD]2.0.CO;2), 2001.
- 2969 Müller, J. D., Gruber, N., Carter, B., Feely, R., Ishii, M., Lange, N., Lauvset, S. K., Murata, A., Olsen, A., Pérez, F. F.,  
2970 Sabine, C., Tanhua, T., Wanninkhof, R., and Zhu, D.: Decadal Trends in the Oceanic Storage of Anthropogenic Carbon  
2971 From 1994 to 2014, *AGU Adv.*, 4, e2023AV000875, <https://doi.org/10.1029/2023AV000875>, 2023.
- 2972 Nayagam, L., Maksyutov, S., Oda, T., Janardanan, R., Trisolino, P., Zeng J., Kaiser, J.W. and Matsunaga, T.: A top-down  
2973 estimation of subnational CO<sub>2</sub> budget using a global high-resolution inverse model with data from regional surface  
2974 networks, *Environ. Res. Lett.*, 19, 0140312024, <https://doi.org/10.1088/1748-9326/ad0f74>, 2024.
- 2975 NCEP: National Centers for Environmental Prediction. ONI Index. Cold & Warm Episodes by Season [dataset], available at:  
2976 [https://origin.cpc.ncep.noaa.gov/products/analysis\\_monitoring/ensostuff/ONI\\_v5.php](https://origin.cpc.ncep.noaa.gov/products/analysis_monitoring/ensostuff/ONI_v5.php), last access: 28 October 2024, 2023.
- 2977 Nevison, C.D., Mahowald, N.M., Doney, S.C., Lima, I.D. and Cassar, N.: Impact of variable air-sea O<sub>2</sub> and CO<sub>2</sub> fluxes on  
2978 atmospheric potential oxygen (APO) and land-ocean carbon sink partitioning. *Biogeosciences*, 5(3), pp.875-889,  
2979 <https://doi.org/10.5194/bg-5-875-2008>, 2008.
- 2980 Niu, G.-Y., Yang, Z.-L., Mitchell, K. E., Chen, F., Ek, M. B., Barlage, M., Kumar, A., Manning, K., Niyogi, D., Rosero, E.,  
2981 Tewari, M., and Xia, Y.: The community Noah land surface model with multiparameterization options (Noah-MP): 1. Model  
2982 description and evaluation with local-scale measurements, *J. Geophys. Res. Atmospheres*, 116,  
2983 <https://doi.org/10.1029/2010JD015139>, 2011.
- 2984 Niwa, Y., Ishijima, K., Ito, A., and Iida, Y.: Toward a long-term atmospheric CO<sub>2</sub> inversion for elucidating natural carbon  
2985 fluxes: technical notes of NISMON-CO<sub>2</sub> v2021.1, *Prog. Earth Planet Sci.*, 9, 42, [https://doi.org/10.1186/s40645-022-00502-](https://doi.org/10.1186/s40645-022-00502-6)  
2986 6, 2022.
- 2987 Niwa, Y., Langenfelds, R., Krummel, P., Loh, Zoe, Worthy, Doug, Hatakka, Juha, Aalto, Tuula, Ramonet, Michel,  
2988 Delmotte, Marc, Schmidt, Martina, Gheusi, Francois, Mihalopoulos, N., Morgui, J.A., Andrews, Arlyn, Dlugokencky, Ed,  
2989 Lee, John, Sweeney, Colm, Thoning, Kirk, Tans, Pieter, De Wekker, Stephan, Fischer, Marc L., Jaffe, Dan, McKain,  
2990 Kathryn, Viner, Brian, Miller, John B., Karion, Anna, Miller, Charles, Sloop, Christopher D., Saito, Kazuyuki, Aoki, Shuji,  
2991 Morimoto, Shinji, Goto, Daisuke, Steinbacher, Martin, Myhre, Cathrine Lund, Hermanssen, Ove, Stephens, Britton, Keeling,  
2992 Ralph, Afshar, Sara, Paplawsky, Bill, Cox, Adam, Walker, Stephen, Schuldt, Kenneth, Mukai, Hitoshi, Machida, Toshinobu,  
2993 Sasakawa, Motoki, Nomura, Shohei, Ito, Akihiko, Iida, Yosuke, and Jones, Matthew W.: Long-term global CO<sub>2</sub> fluxes  
2994 estimated by NICAM-based Inverse Simulation for Monitoring CO<sub>2</sub> (NISMON-CO<sub>2</sub>) (ver.2022.1), National Institute for  
2995 Environmental Studies Japan [dataset], <https://doi.org/10.17595/20201127.001>, 2020.
- 2996 Obermeier, W. A., Nabel, J. E. M. S., Loughran, T., Hartung, K., Bastos, A., Havermann, F., Anthoni, P., Arneht, A., Goll,  
2997 D. S., Lienert, S., Lombardozzi, D., Luyssaert, S., McGuire, P. C., Melton, J. R., Poulter, B., Sitch, S., Sullivan, M. O., Tian,  
2998 H., Walker, A. P., Wiltshire, A. J., Zaehle, S., and Pongratz, J.: Modelled land use and land cover change emissions – a  
2999 spatio-temporal comparison of different approaches, 12, 635–670, <https://doi.org/10.5194/esd-12-635-2021>, 2021.
- 3000 O'Rourke, P. R., Smith, S. J., Mott, A., Ahsan, H., McDuffie, E. E., Crippa, M., Klimont, Z., McDonald, B., Wang, S.,  
3001 Nicholson, M. B., Feng, L., and Hoesly, R. M.: CEDS v\_2021\_04\_21 Release Emission Data, Zenodo [dataset],  
3002 <https://doi.org/10.5281/zenodo.4741285>, 2021.



- 3003 O'Sullivan, M., Zhang, Y., Bellouin, N., Harris, I., Mercado, L. M., Sitch, S., Ciais, P., and Friedlingstein, P.: Aerosol–light  
3004 interactions reduce the carbon budget imbalance, *Environ. Res. Lett.*, 16, 124072, <https://doi.org/10.1088/1748-9326/ac3b77>,  
3005 2021.
- 3006 O'Sullivan, M., Friedlingstein, P., Sitch, S., Anthoni, P., Arneeth, A., Arora, V. K., Bastrikov, V., Delire, C., Goll, D. S., Jain,  
3007 A., Kato, E., Kennedy, D., Knauer, J., Lienert, S., Lombardozi, D., McGuire, P. C., Melton, J. R., Nabel, J. E. M. S.,  
3008 Pongratz, J., Poulter, B., Séférian, R., Tian, H., Vuichard, N., Walker, A. P., Yuan, W., Yue, X., and Zaehle, S.: Process-  
3009 oriented analysis of dominant sources of uncertainty in the land carbon sink, *Nat. Commun.*, 13, 4781,  
3010 <https://doi.org/10.1038/s41467-022-32416-8>, 2022.
- 3011 O'Sullivan, M., Spracklen, D. V., Batterman, S. A., Arnold, S. R., Gloor, M., and Buermann, W.: Have Synergies Between  
3012 Nitrogen Deposition and Atmospheric CO<sub>2</sub> Driven the Recent Enhancement of the Terrestrial Carbon Sink?, *Glob.*  
3013 *Biogeochem. Cycles*, 33, 163–180, <https://doi.org/10.1029/2018GB005922>, 2019.
- 3014 Palmer, P. I., Feng, L., Baker, D., Chevallier, F., Bösch, H., and Somkuti, P.: Net carbon emissions from African biosphere  
3015 dominate pan-tropical atmospheric CO<sub>2</sub> signal, *Nat Commun*, 10, 3344, <https://doi.org/10.1038/s41467-019-11097-w>, 2019.
- 3016 Pan, Y., Birdsey, R. A., Fang, J., Houghton, R., Kauppi, P. E., Kurz, W. A., Phillips, O. L., Shvidenko, A., Lewis, S. L.,  
3017 Canadell, J. G., Ciais, P., Jackson, R. B., Pacala, S. W., McGuire, A. D., Piao, S., Rautiainen, A., Sitch, S., and Hayes, D.: A  
3018 Large and Persistent Carbon Sink in the World's Forests, *Science*, 333, 988–993, <https://doi.org/10.1126/science.1201609>,  
3019 2011.
- 3020 Pendrill, F., Persson, U. M., Godar, J., Kastner, T., Moran, D., Schmidt, S., and Wood, R.: Agricultural and forestry trade  
3021 drives large share of tropical deforestation emissions, *Global Environmental Change*, 56, 1–10,  
3022 <https://doi.org/10.1016/j.gloenvcha.2019.03.002>, 2019.
- 3023 Pérez, F. F., Becker, M., Goris, N., Gehlen, M., López-Mozos, M., Tjiputra, J., Olsen, A., Müller, J. D., Huertas, I. E., Chau,  
3024 T. T. T., Cainzos, V., Velo, A., Benard, G., Hauck, J., Gruber, N., and Wanninkhof, R.: An Assessment of CO<sub>2</sub> Storage and  
3025 Sea–Air Fluxes for the Atlantic Ocean and Mediterranean Sea Between 1985 and 2018. *Global Biogeochemical Cycles*,  
3026 38(4), e2023GB007862, <https://doi.org/10.1029/2023GB007862>, 2024.
- 3027 Peters, G. P., Minx, J. C., Weber, C. L., and Edenhofer, O.: Growth in emission transfers via international trade from 1990 to  
3028 2008, *Proceedings of the National Academy of Sciences*, 108, 8903–8908, <https://doi.org/10.1073/pnas.1006388108>, 2011a.
- 3029 Peters, G. P., Marland, G., Le Quéré, C., Boden, T., Canadell, J. G., and Raupach, M. R.: Rapid growth in CO<sub>2</sub> emissions  
3030 after the 2008–2009 global financial crisis, *Nature Clim Change*, 2, 2–4, <https://doi.org/10.1038/nclimate1332>, 2012a.
- 3031 Peters, G. P., Andrew, R. M., Boden, T., Canadell, J. G., Ciais, P., Le Quéré, C., Marland, G., Raupach, M. R., and Wilson,  
3032 C.: The challenge to keep global warming below 2 °C, *Nature Clim Change*, 3, 4–6, <https://doi.org/10.1038/nclimate1783>,  
3033 2013.
- 3034 Peters, G. P., Le Quéré, C., Andrew, R. M., Canadell, J. G., Friedlingstein, P., Ilyina, T., Jackson, R. B., Joos, F.,  
3035 Korsbakken, J. I., McKinley, G. A., Sitch, S., and Tans, P.: Towards real-time verification of CO<sub>2</sub> emissions, *Nature Clim*  
3036 *Change*, 7, 848–850, <https://doi.org/10.1038/s41558-017-0013-9>, 2017a.



- 3037 Peters, G. P., Andrew, R. M., Canadell, J. G., Fuss, S., Jackson, R. B., Korsbakken, J. I., Le Quéré, C. and Nakicenovic, N.:  
3038 Key indicators to track current progress and future ambition of the Paris Agreement, 7, 118–122,  
3039 <https://doi.org/10.1038/nclimate3202>, 2017b.
- 3040 Peters, G. P., Andrew, R. M., Canadell, J. G., Friedlingstein, P., Jackson, R. B., Korsbakken, J. I., Le Quéré, C., and  
3041 Peregón, A.: Carbon dioxide emissions continue to grow amidst slowly emerging climate policies, *Nat. Clim. Chang.*, 10, 3–  
3042 6, <https://doi.org/10.1038/s41558-019-0659-6>, 2020.
- 3043 Peters, W., Miller, J. B., Whitaker, J., Denning, A. S., Hirsch, A., Krol, M. C., Zupanski, D., Bruhwiler, L., and Tans, P. P.:  
3044 An ensemble data assimilation system to estimate CO<sub>2</sub> surface fluxes from atmospheric trace gas observations, *J. Geophys.*  
3045 *Res. Atmospheres*, 110, <https://doi.org/10.1029/2005JD006157>, 2005.
- 3046 Petrescu, A. M. R., Peters, G. P., Janssens-Maenhout, G., Ciais, P., Tubiello, F. N., Grassi, G., Nabuurs, G.-J., Leip, A.,  
3047 Carmona-García, G., Winiwarter, W., Höglund-Isaksson, L., Günther, D., Solazzo, E., Kiesow, A., Bastos, A., Pongratz, J.,  
3048 Nabel, J. E. M. S., Conchedda, G., Pilli, R., Andrew, R. M., Schelhaas, M.-J., and Dolman, A. J.: European anthropogenic  
3049 AFOLU greenhouse gas emissions: a review and benchmark data, *Earth Syst. Sci. Data*, 12, 961–1001,  
3050 <https://doi.org/10.5194/essd-12-961-2020>, 2020.
- 3051 Pfeil, B., Olsen, A., Bakker, D. C. E., Hankin, S., Koyuk, H., Kozyr, A., Malczyk, J., Manke, A., Metz, N., Sabine, C. L.,  
3052 Akl, J., Alin, S. R., Bates, N., Bellerby, R. G. J., Borges, A., Boutin, J., Brown, P. J., Cai, W.-J., Chavez, F. P., Chen, A.,  
3053 Cosca, C., Fassbender, A. J., Feely, R. A., González-Dávila, M., Goyet, C., Hales, B., Hardman-Mountford, N., Heinze, C.,  
3054 Hood, M., Hoppema, M., Hunt, C. W., Hydes, D., Ishii, M., Johannessen, T., Jones, S. D., Key, R. M., Körtzinger, A.,  
3055 Landschützer, P., Lauvset, S. K., Lefèvre, N., Lenton, A., Lourantou, A., Merlivat, L., Midorikawa, T., Mintrop, L.,  
3056 Miyazaki, C., Murata, A., Nakadate, A., Nakano, Y., Nakaoka, S., Nojiri, Y., Omar, A. M., Padin, X. A., Park, G.-H.,  
3057 Paterson, K., Perez, F. F., Pierrot, D., Poisson, A., Ríos, A. F., Santana-Casiano, J. M., Salisbury, J., Sarma, V. V. S. S.,  
3058 Schlitzer, R., Schneider, B., Schuster, U., Sieger, R., Skjelvan, I., Steinhoff, T., Suzuki, T., Takahashi, T., Tedesco, K.,  
3059 Telszewski, M., Thomas, H., Tilbrook, B., Tjiputra, J., Vandemark, D., Veness, T., Wanninkhof, R., Watson, A. J., Weiss,  
3060 R., Wong, C. S., and Yoshikawa-Inoue, H.: A uniform, quality controlled Surface Ocean CO<sub>2</sub> Atlas (SOCAT), *Earth Syst.*  
3061 *Sci. Data*, 5, 125–143, <https://doi.org/10.5194/essd-5-125-2013>, 2013.
- 3062 Piao, S., Ciais, P., Friedlingstein, P., de Noblet-Ducoudré, N., Cadule, P., Viovy, N., and Wang, T.: Spatiotemporal patterns  
3063 of terrestrial carbon cycle during the 20th century, *Global Biogeochem. Cy.*, 23, GB4026,  
3064 <https://doi.org/10.1029/2008GB003339>, 2009.
- 3065 Piao, S., Huang, M., Liu, Z., Wang, X., Ciais, P., Canadell, J. G., Wang, K., Bastos, A., Friedlingstein, P., Houghton, R. A.,  
3066 Le Quéré, C., Liu, Y., Myneni, R. B., Peng, S., Pongratz, J., Sitch, S., Yan, T., Wang, Y., Zhu, Z., Wu, D., and Wang, T.:  
3067 Lower land-use emissions responsible for increased net land carbon sink during the slow warming period, *Nature Geosci.*, 11,  
3068 739–743, <https://doi.org/10.1038/s41561-018-0204-7>, 2018.
- 3069 Pongratz, J., Reick, C. H., Houghton, R. A., and House, J. I.: Terminology as a key uncertainty in net land use and land  
3070 cover change carbon flux estimates, *Earth Syst. Dynam.*, 5, 177–195, <https://doi.org/10.5194/esd-5-177-2014>, 2014.
- 3071 Pongratz, J., Smith, S. M., Schwingshackl, C., Dayathilake, L., Gasser, T., Grassi, G. and Pilli, R.: Chapter 7: Current levels  
3072 of CDR. in *The State of Carbon Dioxide Removal 2024 – 2nd Edition*, <https://doi.org/10.17605/OSF.IOZXSKB>, 2024.



- 3073 Poulter, B., Bastos, A., Canadell, J., Ciais, P., Gruber, N., Hauck, J., Jackson, R., Ishii, M., Müller, J., Patra, P., and Tian, H.:  
3074 Inventorying Earth's Land and Ocean Greenhouse Gases, *Eos*, 103, <https://doi.org/10.1029/2022EO179084>, 2022.
- 3075 Poulter, B., Frank, D. C., Hodson, E. L., and Zimmermann, N. E.: Impacts of land cover and climate data selection on  
3076 understanding terrestrial carbon dynamics and the CO<sub>2</sub> airborne fraction, *Biogeosciences*, 8, 2027–2036,  
3077 <https://doi.org/10.5194/bg-8-2027-2011>, 2011.
- 3078 Poulter, B., Freeborn, P. H., Jolly, W. M., and Varner, J. M.: COVID-19 lockdowns drive decline in active fires in  
3079 southeastern United States, *PNAS*, 118, e2105666118, <https://doi.org/10.1073/pnas.2105666118>, 2021.
- 3080 Powis, C. M., Smith, S. M., Minx, J. C., and Gasser, T.: Quantifying global carbon dioxide removal deployment, *Environ.*  
3081 *Res. Lett.*, 18, 024022, <https://doi.org/10.1088/1748-9326/acb450>, 2023.
- 3082 Prentice, I. C., Farquhar, G. D., Fasham, M. J. R., Goulden, M. L., Heimann, M., Jaramillo, V. J., Khashgi, H. S., Le Quéré,  
3083 C., Scholes, R. J., and Wallace, D. W. R.: The Carbon Cycle and Atmospheric Carbon Dioxide, in *Climate Change 2001:*  
3084 *The Scientific Basis. Contribution of Working Group I to the Third Assessment Report of the Intergovernmental Panel on*  
3085 *Climate Change*, edited by: Houghton, J. T., Ding, Y., Griggs, D. J., Noguer, M., van der Linden, P. J., Dai, X., Maskell, K.,  
3086 and Johnson, C. A., Cambridge University Press, Cambridge, United Kingdom and New York, NY, USA, 183–237, ISBN:  
3087 978-0521014953, 2001.
- 3088 Price, J. T. and Warren, R.: Literature Review of the Potential of “Blue Carbon” Activities to Reduce Emissions, available  
3089 at: [https://avoid-net-uk.cc.ic.ac.uk/wp-content/uploads/delightful-downloads/2016/03/Literature-review-of-the-potential-of-](https://avoid-net-uk.cc.ic.ac.uk/wp-content/uploads/delightful-downloads/2016/03/Literature-review-of-the-potential-of-blue-carbon-activities-to-reduce-emissions-AVOID2-WPE2.pdf)  
3090 [blue-carbon-activities-to-reduce-emissions-AVOID2-WPE2.pdf](https://avoid-net-uk.cc.ic.ac.uk/wp-content/uploads/delightful-downloads/2016/03/Literature-review-of-the-potential-of-blue-carbon-activities-to-reduce-emissions-AVOID2-WPE2.pdf), last access: 28 October 2024, 2016.
- 3091 Qin, Y., Xiao, X., Wigneron, J.-P., Ciais, P., Brandt, M., Fan, L., Li, X., Crowell, S., Wu, X., Doughty, R., Zhang, Y., Liu,  
3092 F., Sitch, S., and Moore, B.: Carbon loss from forest degradation exceeds that from deforestation in the Brazilian Amazon,  
3093 *Nat. Clim. Chang.*, 11, 442–448, <https://doi.org/10.1038/s41558-021-01026-5>, 2021.
- 3094 Qin, Z., Zhu, Y., Canadell, J. G., Chen, M., Li, T., Mishra, U. and Yuan, W.: Global spatially explicit carbon emissions from  
3095 land-use change over the past six decades (1961–2020). *One Earth*, 7(5), pp.835-847,  
3096 <https://doi.org/10.1016/j.oneear.2024.04.002>, 2024.
- 3097 Randerson, J. T., Chen, Y., van der Werf, G. R., Rogers, B. M., and Morton, D. C.: Global burned area and biomass burning  
3098 emissions from small fires: BURNED AREA FROM SMALL FIRES, *J. Geophys. Res. Biogeosciences*, 117, n/a-n/a,  
3099 <https://doi.org/10.1029/2012JG002128>, 2012.
- 3100 Raupach, M. R., Marland, G., Ciais, P., Le Quere, C., Canadell, J. G., Klepper, G., and Field, C. B.: Global and regional  
3101 drivers of accelerating CO<sub>2</sub> emissions, *Proceedings of the National Academy of Sciences*, 104, 10288–10293,  
3102 <https://doi.org/10.1073/pnas.0700609104>, 2007.
- 3103 Regnier, P., Resplandy, L., Najjar, R. G., and Ciais, P.: The land-to-ocean loops of the global carbon cycle, *Nature*, 603,  
3104 401–410, <https://doi.org/10.1038/s41586-021-04339-9>, 2022.
- 3105 Reick, C. H., Gayler, V., Goll, D., Hagemann, S., Heidkamp, M., Nabel, J. E. M. S., Raddatz, T., Roeckner, E., Schnur, R.,  
3106 110 and Wilkenskeld, S.: JSBACH 3 – The land component of the MPI Earth System Model: documentation of version 3.2,  
3107 available at: <https://doi.org/10.17617/2.3279802>, 2021.





- 3108 Remaud, M., Chevallier, F., Cozic, A., Lin, X., and Bousquet, P.: On the impact of recent developments of the LMDz  
3109 atmospheric general circulation model on the simulation of CO<sub>2</sub> transport, 11, 4489, [https://doi.org/10.5194/gmd-11-4489-](https://doi.org/10.5194/gmd-11-4489-2018)  
3110 2018, 2018.
- 3111 Resplandy, L., Keeling, R. F., Rödenbeck, C., Stephens, B. B., Khatiwala, S., Rodgers, K. B., Long, M. C., Bopp, L., and  
3112 Tans, P. P.: Revision of global carbon fluxes based on a reassessment of oceanic and riverine carbon transport, *Nature*  
3113 *Geosci*, 11, 504–509, <https://doi.org/10.1038/s41561-018-0151-3>, 2018.
- 3114 Resplandy, L., Keeling, R. F., Edehbar, Y., Brooks, M., Wang, R., Bopp, L., Long, M. C., Dunne, J. P., Koeve, W., and  
3115 Oeschles, A.: Quantification of ocean heat uptake from changes in atmospheric O<sub>2</sub> and CO<sub>2</sub> composition, *Scientific Reports*,  
3116 9, 20244, <https://doi.org/10.1038/s41598-019-56490-z>, 2019.
- 3117 Rodenbeck, C., Houweling, S., Gloor, M., and Heimann, M.: CO<sub>2</sub> flux history 1982–2001 inferred from atmospheric data  
3118 using a global inversion of atmospheric transport, *Atmos Chem Phys*, 3, 1919–1964, 2003.
- 3119 Rödenbeck, C., Bakker, D. C. E., Metzl, N., Olsen, A., Sabine, C., Cassar, N., Reum, F., Keeling, R. F., and Heimann, M.:  
3120 Interannual sea–air CO<sub>2</sub> flux variability from an observation-driven ocean mixed-layer scheme, 11, 4599–4613,  
3121 <https://doi.org/10.5194/bg-11-4599-2014>, 2014.
- 3122 Rödenbeck, C., Zaehe, S., Keeling, R., and Heimann, M.: History of El Niño impacts on the global carbon cycle 1957–  
3123 2017: a quantification from atmospheric CO<sub>2</sub> data, 373, 20170303, <https://doi.org/10.1098/rstb.2017.0303>, 2018.
- 3124 Rödenbeck, C., DeVries, T., Hauck, J., Le Quéré, C., and Keeling, R. F.: Data-based estimates of interannual sea–air CO<sub>2</sub>  
3125 flux variations 1957–2020 and their relation to environmental drivers, *Biogeosciences*, 19, 2627–2652,  
3126 <https://doi.org/10.5194/bg-19-2627-2022>, 2022.
- 3127 Rosan, T. M., Klein Goldewijk, K., Ganzenmüller, R., O’Sullivan, M., Pongratz, J., Mercado, L. M., Aragao, L. E. O. C.,  
3128 Heinrich, V., Randow, C. V., Wiltshire, A., Tubiello, F. N., Bastos, A., Friedlingstein, P., and Sitch, S.: A multi-data  
3129 assessment of land use and land cover emissions from Brazil during 2000–2019, *Environ. Res. Lett.*, 16, 074004,  
3130 <https://doi.org/10.1088/1748-9326/ac08c3>, 2021.
- 3131 Sakamoto, K., H. Nakano, S. Urakawa, T. Toyoda, Y. Kawakami, H. Tsujino, G. Yamanaka, 2023: Reference manual for the  
3132 Meteorological Research Institute Community Ocean Model version 5 (MRI.COMv5), Technical Reports of the  
3133 Meteorological Research Institute, No.87, <https://doi.org/10.11483/mritechrepo.87>.
- 3134 Sarma, V. V. S. S., Sridevi, B., Metzl, N., Patra, P. K., Lachkar, Z., Chakraborty, K., Goyet, C., Levy, M., Mehari, M., and  
3135 Chandra, N.: Air-Sea Fluxes of CO<sub>2</sub> in the Indian Ocean Between 1985 and 2018: A Synthesis Based on Observation-Based  
3136 Surface CO<sub>2</sub>, Hindcast and Atmospheric Inversion Models, *Glob. Biogeochem. Cycles*, 37, e2023GB007694,  
3137 <https://doi.org/10.1029/2023GB007694>, 2023.
- 3138 Schaphoff, S., von Bloh, W., Rammig, A., Thonicke, K., Biemans, H., Forkel, M., Gerten, D., Heinke, J., Jägermeyr, J.,  
3139 Knauer, J., Langerwisch, F., Lucht, W., Müller, C., Rolinski, S., and Waha, K.: LPJmL4 – a dynamic global vegetation  
3140 model with managed land – Part 1: Model description, *Geosci. Model Dev.*, 11, 1343–1375, [https://doi.org/10.5194/gmd-11-](https://doi.org/10.5194/gmd-11-1343-2018)  
3141 1343-2018, 2018.



- 3142 Schimel, D., Alves, D., Enting, I. G., Heimann, M., Joos, F., Raynaud, D., Wigley, T., Prater, M., Derwent, R., Ehhalt, D.,  
3143 Fraser, P., Sanhueza, E., Zhou, X., Jonas, P., Charlson, R., Rodhe, H., Sadasivan, S., Shine, K. P., Fouquart, Y.,  
3144 Ramaswamy, V., Solomon, S., Srinivasan, J., Albritton, D., Derwent, R., Isaksen, I., Lal, M., and Wuebbles, D.: Radiative  
3145 Forcing of Climate Change, in: *Climate Change 1995: The Science of Climate Change, Contribution of Working Group I to*  
3146 *the Second Assessment Report of the Intergovernmental Panel on Climate Change* [Houghton, J. T., Meira Rilho, L. G.,  
3147 Callander, B. A., Harris, N., Kattenberg, A., and Maskell, K. (eds.)], Cambridge University Press, Cambridge, United  
3148 Kingdom and New York, NY, USA, ISBN: 978-0521559621, 1995.
- 3149 Schimel, D., Stephens, B. B., and Fisher, J. B.: Effect of increasing CO<sub>2</sub> on the terrestrial carbon cycle, *Proc Natl Acad Sci*  
3150 *USA*, 112, 436–441, <https://doi.org/10.1073/pnas.1407302112>, 2015.
- 3151 Schuh, A. E., Jacobson, A. R., Basu, S., Weir, B., Baker, D., Bowman, K., Chevallier, F., Crowell, S., Davis, K. J., Deng, F.,  
3152 Denning, S., Feng, L., Jones, D., Liu, J., and Palmer, P. I.: Quantifying the Impact of Atmospheric Transport Uncertainty on  
3153 CO<sub>2</sub> Surface Flux Estimates, *Global Biogeochem. Cycles*, 33, 484–500, <https://doi.org/10.1029/2018GB006086>, 2019.
- 3154 Schuldt, K. N., Mund, J., Aalto, T., Abshire, J. B., Aikin, K., Allen, G., Andrews, A., Apadula, F., Arnold, S., Baier, B.,  
3155 Bakwin, P., Bartyzel, J., Bentz, G., Bergamaschi, P., Beyersdorf, A., Biermann, T., Biraud, S. C., Blanc, P.-E., Boenisch, H.,  
3156 Bowling, D., Brailsford, G., Brand, W. A., Brunner, D., Bui, T. P., Băni, L., Calzolari, F., Chang, C. S., Chen, H., Chen, G.,  
3157 Chmura, L., Clark, S., Climadat, S., Colomb, A., Commane, R., Conen, F., Conil, S., Couret, C., Cristofanelli, P., Cuevas,  
3158 E., Curcoll, R., Daube, B., Davis, K. J., De Mazière, M., De Wekker, S., Dean-Day, J. M., Della Coletta, J., Delmotte, M.,  
3159 Di Iorio, T., DiGangi, E., DiGangi, J. P., Elkins, J. W., Elsasser, M., Emmenegger, L., Fang, S., Fischer, M. L., Forster, G.,  
3160 France, J., Frumau, A., Fuente-Lastra, M., Galkowski, M., Gatti, L. V., Gehrlein, T., Gerbig, C., Gheusi, F., Gloor, E., Goto,  
3161 D., Griffis, T., Hammer, S., Hanisco, T. F., Hanson, C., Haszpra, L., Hatakka, J., Heimann, M., Heliasz, M., Heltai, D.,  
3162 Henne, S., Hensen, A., Hermans, C., Hermansen, O., Hintsa, E., Hoheisel, A., Holst, J., Iraci, L. T., Ivakhov, V., Jaffé, D.  
3163 A., Jordan, A., Joubert, W., Karion, A., Kawa, S. R., Kazan, V., Keeling, R. F., Keronen, P., Kim, J., Klausen, J., Kneuer, T.,  
3164 Kolari, P., Kominkova, K., Kort, E., Kozlova, E., Krummel, P. B., Kubistin, D., Kulawik, S. S., Kumps, N., Labuschagne,  
3165 C., Lam, D. H., Lan, X., Langenfelds, R. L., Lanza, A., Laurent, O., Laurila, T., Lauvaux, T., Lavric, J., Law, B. E., Lee, J.,  
3166 Lehner, I., Lehtinen, K., Leppert, R., Leskinen, A., Leuenberger, M., Leung, W. H., Levin, I., Levula, J., Lin, J., Lindauer,  
3167 M., Lindroth, A., Loh, Z. M., Lopez, M., Lunder, C. R., Löfvenius, M. O., Machida, T., Mammarella, I., Manca, G.,  
3168 Manning, A., Manning, A., Marek, M. V., Marklund, P., Marrero, J. E., Martin, D., Martin, M. Y., Martins, G. A., Matsueda,  
3169 H., McKain, K., Meijer, H., Meinhardt, F., Merchant, L., Metzger, J.-M., Mihalopoulos, N., Miles, N. L., Miller, J. B.,  
3170 Miller, C. E., Mitchell, L., Monteiro, V., Montzka, S., Moore, F., Moossen, H., Morgan, E., Morgui, J.-A., Morimoto, S.,  
3171 Munger, J. W., Munro, D., Mutuku, M., Myhre, C. L., Mölder, M., Müller-Williams, J., Necki, J., Newman, S., Nichol, S.,  
3172 Nisbet, E., Niwa, Y., Njiru, D. M., Noe, S. M., Nojiri, Y., O'Doherty, S., Obersteiner, F., Paplawsky, B., Parworth, C. L.,  
3173 Peischl, J., Peltola, O., Peters, W., Philippon, C., Piacentino, S., Pichon, J. M., Pickers, P., Piper, S., Pitt, J., Plass-Dülmer,  
3174 C., Platt, S. M., Prinziavalli, S., Ramonet, M., Ramos, R., Reyes-Sanchez, E., Richardson, S. J., Rigouleau, L.-J., Riris, H.,  
3175 Rivas, P. P., Rothe, M., Roulet, Y.-A., Ryerson, T., Ryoo, J.-M., Sargent, M., Sasakawa, M., Scheeren, B., Schmidt, M.,  
3176 Schuck, T., Schumacher, M., Seibel, J., Seifert, T., Sha, M. K., Shepson, P., Shook, M., Sloop, C. D., Smith, P. D., Spain,  
3177 G., St. Clair, J. M., Steger, D., Steinbacher, M., Stephens, B., Sweeney, C., Sørensen, L. L., Taipale, R., Takatsuji, S., Tans,  
3178 P., Thoning, K., Timas, H., Torn, M., Trisolino, P., Turnbull, J., Vermeulen, A., Viner, B., Vitkova, G., Walker, S., Watson,  
3179 A., Weiss, R., Weyrauch, D., Wofsy, S. C., Worsley, J., Worthy, D., Xueref-Remy, I., Yates, E. L., Young, D., Yver-Kwok,  
3180 C., Zaehle, S., Zahn, A., Zellweger, C., Zimnoch, M., de Souza, R. A., di Sarra, A. G., van Dinter, D., and van den Bulk, P.  
3181 (2023) Multi-laboratory compilation of atmospheric carbon dioxide data for the period 1957-2022;



- 3182 obspack\_co2\_1\_GLOBALVIEWplus\_v9.0\_2023-09-09; NOAA Earth System Research Laboratory, Global Monitoring  
3183 Laboratory, <http://doi.org/10.25925/20230801>.
- 3184 Schuldt, K. N., Jacobson, A. R., Aalto, T., Andrews, A., Apadula, F., Arnold, S., Bakwin, P., Bartyzel, J., Bergamaschi, P.,  
3185 Biermann, T., Biraud, S. C., Blanc, P.-E., Böni, L., Calzolari, F., Chen, H., Chmura, L., Colomb, A., Condori, L., Conen, F.,  
3186 Conil, S., Couret, C., Cristofanelli, P., Cuevas, E., De Mazière, M., De Wekker, S., Della Coletta, J., Delmotte, M., Di Iorio,  
3187 T., Elsasser, M., Emmenegger, L., Fischer, M. L., Forster, G., Frumau, A., Fuente-Lastra, M., Galkowski, M., Gheusi, F.,  
3188 Hammer, S., Hatakka, J., Heliasz, M., Heltai, D., Hensen, A., Hermans, C., Hermansen, O., Hoheisel, A., Holst, J., Jaffe, D.,  
3189 A., Karion, A., Kazan, V., Keronen, P., Kneuer, T., Kolari, P., Kominkova, K., Krummel, P. B., Kubistin, D., Kumps, N.,  
3190 Lan, X., Langenfelds, R. L., Lanza, A., Laurent, O., Laurila, T., Lee, J., Lehner, I., Lehtinen, K., Leskinen, A., Leuenberger,  
3191 M., Levin, I., Levula, J., Lindauer, M., Lindroth, A., Loh, Z. M., Lopez, M., Lunder, C. R., Löfvenius, M. O., Mammarella,  
3192 I., Manca, G., Manning, A., Manning, A., Marek, M. V., Marklund, P., McKain, K., Meijer, H., Meinhardt, F., Metzger, J.-  
3193 M., Miller, C. E., Miller, J. B., Myhre, C. L., Mölder, M., Müller-Williams, J., Necki, J., O'Doherty, S., Peltola, O.,  
3194 Philippon, C., Piacentino, S., Pichon, J. M., Pickers, P., Pitt, J., Plass-Dülmer, C., Platt, S. M., Ramonet, M., Ramos, R.,  
3195 Reyes-Sanchez, E., Rigouleau, L.-J., Rivas, P. P., Roulet, Y.-A., Scheeren, B., Schmidt, M., Schumacher, M., Sha, M. K.,  
3196 Sloop, C. D., Smith, P. D., Steger, D., Steinbacher, M., Sweeney, C., Sørensen, L. L., Taipale, R., Tans, P., Thoning, K.,  
3197 Trisolino, P., Turnbull, J., Vermeulen, A., Viner, B., Vitkova, G., Weyrauch, D., Worthly, D., Xueref-Remy, I., Young, D.,  
3198 Yver-Kwok, C., Zimnoch, M., di Sarra, A. G., van Dinter, D., and van den Bulk, P. (2024) Multi-laboratory compilation of  
3199 atmospheric carbon dioxide data for the period 2023-2024; obspack\_co2\_1\_NRT\_v9.2\_2024-03-25; NOAA Earth System  
3200 Research Laboratory, Global Monitoring Laboratory, <http://doi.org/10.25925/20240215>.
- 3201 Schwinger, J., Goris, N., Tjiputra, J. F., Kriest, I., Bentsen, M., Bethke, I., Ilicak, M., Assmann, K. M., and Heinze, C.:  
3202 Evaluation of NorESM-OC (versions 1 and 1.2), the ocean carbon-cycle stand-alone configuration of the Norwegian Earth  
3203 System Model (NorESM1), *Geosci. Model Dev.*, 9, 2589–2622, <https://doi.org/10.5194/gmd-9-2589-2016>, 2016.
- 3204 Schwingshackl, C., Obermeier, W. A., Bultan, S., Grassi, G., Canadell, J. G., Friedlingstein, P., Gasser, T., Houghton, R. A.,  
3205 Kurz, W. A., Sitch, S., and Pongratz, J.: Differences in land-based mitigation estimates reconciled by separating natural and  
3206 land-use CO<sub>2</sub> fluxes at the country level, *One Earth*, 5, 1367–1376, <https://doi.org/10.1016/j.oneear.2022.11.009>, 2022.
- 3207 Séférian, R., Nabat, P., Michou, M., Saint-Martin, D., Voltaire, A., Colin, J., Decharme, B., Delire, C., Berthet, S.,  
3208 Chevallier, M., Sénési, S., Franchisteguy, L., Vial, J., Mallet, M., Joetzjer, E., Geoffroy, O., Guérémy, J.-F., Moine, M.-P.,  
3209 Msadek, R., Ribes, A., Rocher, M., Roehrig, R., Salas-y-Méla, D., Sanchez, E., Terray, L., Valcke, S., Waldman, R.,  
3210 Aumont, O., Bopp, L., Deshayes, J., Éthé, C., and Madec, G.: Evaluation of CNRM Earth System Model, CNRM-ESM2-1:  
3211 Role of Earth System Processes in Present-Day and Future Climate, *Journal of Advances in Modeling Earth Systems*, 11,  
3212 4182–4227, <https://doi.org/10.1029/2019MS001791>, 2019.
- 3213 Seiler, C., Melton, J. R., Arora, V. K., Sitch, S., Friedlingstein, P., Anthoni, P., Goll, D., Jain, A. K., Joetzjer, E., Lienert, S.,  
3214 Lombardozi, D., Luyssaert, S., Nabel, J. E. M. S., Tian, H., Vuichard, N., Walker, A. P., Yuan, W., and Zaehle, S.: Are  
3215 Terrestrial Biosphere Models Fit for Simulating the Global Land Carbon Sink?, *J. Adv. Model. Earth Syst.*, 14,  
3216 e2021MS002946, <https://doi.org/10.1029/2021MS002946>, 2022.
- 3217 Sellar, A. A., Jones, C. G., Mulcahy, J. P., Tang, Y., Yool, A., Wiltshire, A., O'Connor, F. M., Stringer, M., Hill, R.,  
3218 Palmieri, J., Woodward, S., Mora, L., Kuhlbrodt, T., Rumbold, S. T., Kelley, D. I., Ellis, R., Johnson, C. E., Walton, J.,  
3219 Abraham, N. L., Andrews, M. B., Andrews, T., Archibald, A. T., Berthou, S., Burke, E., Blockley, E., Carslaw, K., Dalvi,  
3220 M., Edwards, J., Folberth, G. A., Gedney, N., Griffiths, P. T., Harper, A. B., Hendry, M. A., Hewitt, A. J., Johnson, B.,



- 3221 Jones, A., Jones, C. D., Keeble, J., Liddicoat, S., Morgenstern, O., Parker, R. J., Predoi, V., Robertson, E., Siahhan, A.,  
3222 Smith, R. S., Swaminathan, R., Woodhouse, M. T., Zeng, G., and Zerroukat, M.: UKESM1: Description and Evaluation of  
3223 the U.K. Earth System Model, *J. Adv. Model. Earth Syst.*, 11, 4513–4558, <https://doi.org/10.1029/2019MS001739>, 2019.
- 3224 Shu, S., Jain, A. K., Koven, C. D., and Mishra, U.: Estimation of Permafrost SOC Stock and Turnover Time Using a Land  
3225 Surface Model With Vertical Heterogeneity of Permafrost Soils, *Global Biogeochem. Cy.*, 34, e2020GB006585,  
3226 <https://doi.org/10.1029/2020GB006585>, 2020.
- 3227 Shutler, J. D., Land, P. E., Piolle, J.-F., Woolf, D. K., Goddijn-Murphy, L., Paul, F., Girard-Arduin, F., Chapron, B., and  
3228 Donlon, C. J.: FluxEngine: A Flexible Processing System for Calculating Atmosphere–Ocean Carbon Dioxide Gas Fluxes  
3229 and Climatologies, *J. Atmospheric Ocean. Technol.*, 33, 741–756, <https://doi.org/10.1175/JTECH-D-14-00204.1>, 2016.
- 3230 Silva Junior, C.H., Anderson, L.O., Silva, A.L., Almeida, C.T., Dalagnol, R., Pletsch, M.A., Penha, T.V., Paloschi, R.A. and  
3231 Aragão, L.E.: Fire responses to the 2010 and 2015/2016 Amazonian droughts. *Frontiers in Earth Science*, 7, p.97,  
3232 <https://doi.org/10.3389/feart.2019.00097>, 2019.
- 3233 Sitch, S., Huntingford, C., Gedney, N., Levy, P. E., Lomas, M., Piao, S. L., Betts, R., Ciais, P., Cox, P., Friedlingstein, P.,  
3234 Jones, C. D., Prentice, I. C., and Woodward, F. I.: Evaluation of the terrestrial carbon cycle, future plant geography and  
3235 climate–carbon cycle feedbacks using five Dynamic Global Vegetation Models (DGVMs): Uncertainty In Land Carbon  
3236 Cycle Feedbacks, *Glob. Change Biol.*, 14, 2015–2039, <https://doi.org/10.1111/j.1365-2486.2008.01626.x>, 2008.
- 3237 Sitch, S., O’Sullivan, M., Robertson, E., Friedlingstein, P., Albergel, C., Anthoni, P., Arneeth, A., Arora, V. K., Bastos, A.,  
3238 Bastrov, V., Bellouin, N., Canadell, J. G., Chini, L., Ciais, P., Falk, S., Harris, I., Hurtt, G., Ito, A., Jain, A. K., Jones, M.  
3239 W., Joos, F., Kato, E., Kennedy, D., Klein Goldewijk, K., Kluzek, E., Knauer, J., Lawrence, P. J., Lombardozzi, D., Melton,  
3240 J. R., Nabel, J. E. M. S., Pan, N., Peylin, P., Pongratz, J., Poulter, B., Rosan, T. M., Sun, Q., Tian, H., Walker, A. P., Weber,  
3241 U., Yuan, W., Yue, X., Zaehle, S.: Trends and Drivers of Terrestrial Sources and Sinks of Carbon Dioxide: An Overview of  
3242 the TRENDY Project, *Global Biogeochemical Cycles*, 38(7), e2024GB008102, <https://doi.org/10.1029/2024GB008102>,  
3243 2024.
- 3244 Smallman, T. L., Milodowski, D. T., Neto, E. S., Koren, G., Ometto, J., and Williams, M.: Parameter uncertainty dominates  
3245 C-cycle forecast errors over most of Brazil for the 21st century, *Earth Syst. Dyn.*, 12, 1191–1237,  
3246 <https://doi.org/10.5194/esd-12-1191-2021>, 2021.
- 3247 Smith, B., Wårlind, D., Arneeth, A., Hickler, T., Leadley, P., Siltberg, J., and Zaehle, S.: Implications of incorporating N  
3248 cycling and N limitations on primary production in an individual-based dynamic vegetation model, *Biogeosciences*, 11,  
3249 2027–2054, <https://doi.org/10.5194/bg-11-2027-2014>, 2014.
- 3250 Smith, S. M., Geden, O., Gidden, M. J., Lamb, W. F., Nemet, G. F., Minx, J. C., Buck, H., Burke, J., Cox, E., Edwards, M.  
3251 R., Fuss, S., Johnstone, I., Müller-Hansen, F., Pongratz, J., Probst, B. S., Roe, S., Schenuit, F., Schulte, I., and Vaughan, N.  
3252 E. The State of Carbon Dioxide Removal 2024 - 2nd Edition, <http://dx.doi.org/10.17605/OSF.IO/F85QJ>, 2024.
- 3253 Sospedra-Alfonso, R., Merryfield, W. J., Boer, G. J., Kharin, V. V., Lee, W.-S., Seiler, C., and Christian, J. R.: Decadal  
3254 climate predictions with the Canadian Earth System Model version 5 (CanESM5), *Geosci. Model Dev.*, 14, 6863–6891,  
3255 <https://doi.org/10.5194/gmd-14-6863-2021>, 2021.



- 3256 Stephens, B. B., Gurney, K. R., Tans, P. P., Sweeney, C., Peters, W., Bruhwiler, L., Ciais, P., Ramonet, M., Bousquet, P.,  
3257 Nakazawa, T., Aoki, S., Machida, T., Inoue, G., Vinnichenko, N., Lloyd, J., Jordan, A., Heimann, M., Shibistova, O.,  
3258 Langenfelds, R. L., Steele, L. P., Francey, R. J., and Denning, A. S.: Weak Northern and Strong Tropical Land Carbon  
3259 Uptake from Vertical Profiles of Atmospheric CO<sub>2</sub>, *Science*, 316, 1732–1735, <https://doi.org/10.1126/science.1137004>,  
3260 2007.
- 3261 Stephens, B. B., Keeling, R. F., Heimann, M., Six, K. D., Murnane, R., and Caldeira, K.: Testing global ocean carbon cycle  
3262 models using measurements of atmospheric O<sub>2</sub> and CO<sub>2</sub> concentration, *Glob. Biogeochem. Cycles*, 12, 213–230,  
3263 <https://doi.org/10.1029/97GB03500>, 1998.
- 3264 Stocker, T., Qin, D., and Plattner, G.-K.: *Climate Change 2013: The Physical Science Basis. Contribution of Working Group*  
3265 *I to the Fifth Assessment Report of the Intergovernmental Panel on Climate Change [Intergovernmental Panel on Climate*  
3266 *Change (eds.)]*, Cambridge University Press, Cambridge, ISBN: 9789291691388, 2013.
- 3267 Swart, N. C., Cole, J. N. S., Kharin, V. V., Lazare, M., Scinocca, J. F., Gillett, N. P., Anstey, J., Arora, V., Christian, J. R.,  
3268 Hanna, S., Jiao, Y., Lee, W. G., Majaess, F., Saenko, O. A., Seiler, C., Seinen, C., Shao, A., Sigmond, M., Solheim, L., von  
3269 Salzen, K., Yang, D., and Winter, B.: The Canadian Earth System Model version 5 (CanESM5.0.3), *Geosci. Model Dev.*, 12,  
3270 4823–4873, <https://doi.org/10.5194/gmd-12-4823-2019>, 2019.
- 3271 SX Coal: Monthly coal consumption estimates, <http://www.sxcoal.com/>, last access: 28 October 2024, 2022.
- 3272 Takahashi, T., Sutherland, S. C., Wanninkhof, R., Sweeney, C., Feely, R. A., Chipman, D. W., Hales, B., Friederich, G.,  
3273 Chavez, F., Sabine, C., Watson, A., Bakker, D. C. E., Schuster, U., Metzl, N., Yoshikawa-Inoue, H., Ishii, M., Midorikawa,  
3274 T., Nojiri, Y., Körtzinger, A., Steinhoff, T., Hoppema, M., Olafsson, J., Arnarson, T. S., Tilbrook, B., Johannessen, T.,  
3275 Olsen, A., Bellerby, R., Wong, C. S., Delille, B., Bates, N. R., and de Baar, H. J. W.: Climatological mean and decadal  
3276 change in surface ocean pCO<sub>2</sub>, and net sea–air CO<sub>2</sub> flux over the global oceans, *Deep Sea Research Part II: Topical Studies*  
3277 *in Oceanography*, 56, 554–577, <https://doi.org/10.1016/j.dsr2.2008.12.009>, 2009.
- 3278 Terhaar, J., Frölicher, T. L., and Joos, F.: Southern Ocean anthropogenic carbon sink constrained by sea surface salinity, *Sci.*  
3279 *Adv.*, 7, eabd5964, <https://doi.org/10.1126/sciadv.abd5964>, 2021.
- 3280 Terhaar, J., Frölicher, T. L., and Joos, F.: Observation-constrained estimates of the global ocean carbon sink from Earth  
3281 system models, *Biogeosciences*, 19, 4431–4457, <https://doi.org/10.5194/bg-19-4431-2022>, 2022.
- 3282 Terhaar, J., Goris, N., Müller, J. D., DeVries, T., Gruber, N., Hauck, J., Perez, F. F., and Séférian, R.: Assessment of Global  
3283 Ocean Biogeochemistry Models for Ocean Carbon Sink Estimates in RECCAP2 and Recommendations for Future Studies.  
3284 *Journal of Advances in Modeling Earth Systems*, 16(3), e2023MS003840, <https://doi.org/10.1029/2023MS003840>, 2024.
- 3285 Tian, H., Xu, X., Lu, C., Liu, M., Ren, W., Chen, G., Melillo, J., and Liu, J.: Net exchanges of CO<sub>2</sub>, CH<sub>4</sub>, and N<sub>2</sub>O between  
3286 China’s terrestrial ecosystems and the atmosphere and their contributions to global climate warming, *J. Geophys. Res.*  
3287 *Biogeosciences*, 116, G02011, <https://doi.org/10.1029/2010JG001393>, 2011.
- 3288 Tian, H., Chen, G., Lu, C., Xu, X., Hayes, D. J., Ren, W., Pan, S., Huntzinger, D. N., and Wofsy, S. C.: North American  
3289 terrestrial CO<sub>2</sub> uptake largely offset by CH<sub>4</sub> and N<sub>2</sub>O emissions: toward a full accounting of the greenhouse gas budget,  
3290 *Climatic Change*, 129, 413–426, <https://doi.org/10.1007/s10584-014-1072-9>, 2015.



- 3291 Tsujino, H., Nakano, H., Sakamoto, K., Urakawa, L. S., Toyama, K., Kosugi, N., Kitamura, Y., Ishii, M., Nishikawa, S.,  
3292 Nishikawa, H., Sugiyama, T., and Ishikawa, Y.: Impact of increased horizontal resolution of an ocean model on carbon  
3293 circulation in the North Pacific Ocean. *Journal of Advances in Modeling Earth Systems*, 16, e2023MS003720,  
3294 <https://doi.org/10.1029/2023MS003720>, 2024.
- 3295 Tubiello, F. N., Conchedda, G., Wanner, N., Federici, S., Rossi, S., and Grassi, G.: Carbon emissions and removals from  
3296 forests: new estimates, 1990–2020, *Earth Syst. Sci. Data*, 13, 1681–1691, <https://doi.org/10.5194/essd-13-1681-2021>, 2021.
- 3297 Tuck, C.: 2022 Mineral Commodity Summary: Iron Ore, Tech. rep., U.S. Geological Survey,  
3298 <https://pubs.usgs.gov/periodicals/mcs2022/mcs2022-iron-ore.pdf>, 2022.
- 3299 UNFCCC: Synthesis report for the technical assessment component of the first global stocktake, available at:  
3300 <https://unfccc.int/documents/461466>, last access: 28 October 2024, 2022.
- 3301 Vale, M. M., Berenguer, E., Argollo de Menezes, M., Viveiros de Castro, E. B., Pugliese de Siqueira, L., and Portela, R. de  
3302 C. Q.: The COVID-19 pandemic as an opportunity to weaken environmental protection in Brazil, *Biological Conservation*,  
3303 255, 108994, <https://doi.org/10.1016/j.biocon.2021.108994>, 2021.
- 3304 van der Laan-Luijkx, I. T., van der Velde, I. R., van der Veen, E., Tsuruta, A., Stanislawski, K., Babenhausserheide, A.,  
3305 Zhang, H. F., Liu, Y., He, W., Chen, H., Masarie, K. A., Krol, M. C., and Peters, W.: The CarbonTracker Data Assimilation  
3306 Shell (CTDAS) v1.0: implementation and global carbon balance 2001–2015, *Geosci. Model Dev.*, 10, 2785–2800,  
3307 <https://doi.org/10.5194/gmd-10-2785-2017>, 2017.
- 3308 van der Velde, I. R., van der Werf, G. R., Houweling, S., Maasackers, J. D., Borsdorff, T., Landgraf, J., Tol, P., van  
3309 Kempen, T. A., van Hees, R., Hoogeveen, R., Veeffkind, J. P., and Aben, I.: Vast CO<sub>2</sub> release from Australian fires in 2019–  
3310 2020 constrained by satellite, *Nature*, 597, 366–369, <https://doi.org/10.1038/s41586-021-03712-y>, 2021.
- 3311 van der Werf, G. R., Randerson, J. T., Giglio, L., Collatz, G. J., Mu, M., Kasibhatla, P. S., Morton, D. C., DeFries, R. S., Jin,  
3312 Y., and van Leeuwen, T. T.: Global fire emissions and the contribution of deforestation, savanna, forest, agricultural, and  
3313 peat fires (1997–2009), *Atmospheric Chem. Phys.*, 10, 11707–11735, <https://doi.org/10.5194/acp-10-11707-2010>, 2010.
- 3314 van der Werf, G. R., Randerson, J. T., Giglio, L., van Leeuwen, T. T., Chen, Y., Rogers, B. M., Mu, M., van Marle, M. J. E.,  
3315 Morton, D. C., Collatz, G. J., Yokelson, R. J., and Kasibhatla, P. S.: Global fire emissions estimates during 1997–2016,  
3316 *Earth Syst. Sci. Data*, 9, 697–720, <https://doi.org/10.5194/essd-9-697-2017>, 2017.
- 3317 van Wees, D., van der Werf, G. R., Randerson, J. T., Andela, N., Chen, Y., and Morton, D. C.: The role of fire in global  
3318 forest loss dynamics, *Glob. Change Biol.*, 27, 2377–2391, <https://doi.org/10.1111/gcb.15591>, 2021.
- 3319 von Bloh, W., Schaphoff, S., Müller, C., Rolinski, S., Waha, K., and Zaehle, S.: Implementing the nitrogen cycle into the  
3320 dynamic global vegetation, hydrology, and crop growth model LPJmL (version 5.0), *Geosci. Model Dev.*, 11, 2789–2812,  
3321 <https://doi.org/10.5194/gmd-11-2789-2018>, 2018.
- 3322 Vaithinada Ayar, P., Bopp, L., Christian, J. R., Ilyina, T., Krasting, J. P., Séférian, R., Tsujino, H., Watanabe, M., Yool, A.,  
3323 and Tjiputra, J.: Contrasting projections of the ENSO-driven CO<sub>2</sub> flux variability in the equatorial Pacific under high-  
3324 warming scenario, *Earth Syst. Dynam.*, 13, 1097–1118, <https://doi.org/10.5194/esd-13-1097-2022>, 2022.



- 3325 Vuichard, N., Messina, P., Luysaert, S., Guenet, B., Zaehle, S., Ghattas, J., Bastrikov, V., and Peylin, P.: Accounting for  
3326 carbon and nitrogen interactions in the global terrestrial ecosystem model ORCHIDEE (trunk version, rev 4999): multi-scale  
3327 evaluation of gross primary production, *Geosci. Model Dev.*, 12, 4751–4779, <https://doi.org/10.5194/gmd-12-4751-2019>,  
3328 2019.
- 3329 Walker, A. P., Quaife, T., Bodegom, P. M., De Kauwe, M. G., Keenan, T. F., Joiner, J., Lomas, M. R., MacBean, N., Xu, C.,  
3330 Yang, X., and Woodward, F. I.: The impact of alternative trait-scaling hypotheses for the maximum photosynthetic  
3331 carboxylation rate ( $V_{cmax}$ ) on global gross primary production, *New Phytol.*, 215, 1370–1386,  
3332 <https://doi.org/10.1111/nph.14623>, 2017.
- 3333 Walker, A. P., De Kauwe, M. G., Bastos, A., Belmecheri, S., Georgiou, K., Keeling, R. F., McMahon, S. M., Medlyn, B. E.,  
3334 Moore, D. J. P., Norby, R. J., Zaehle, S., Anderson-Teixeira, K. J., Battipaglia, G., Brienen, R. J. W., Cabugao, K. G.,  
3335 Cailleret, M., Campbell, E., Canadell, J. G., Ciais, P., Craig, M. E., Ellsworth, D. S., Farquhar, G. D., Fatichi, S., Fisher, J.  
3336 B., Frank, D. C., Graven, H., Gu, L., Haverd, V., Heilman, K., Heimann, M., Hungate, B. A., Iversen, C. M., Joos, F., Jiang,  
3337 M., Keenan, T. F., Knauer, J., Körner, C., Leshyk, V. O., Leuzinger, S., Liu, Y., MacBean, N., Malhi, Y., McVicar, T. R.,  
3338 Penuelas, J., Pongratz, J., Powell, A. S., Riutta, T., Sabot, M. E. B., Schleucher, J., Sitch, S., Smith, W. K., Sulman, B.,  
3339 Taylor, B., Terrer, C., Torn, M. S., Treseder, K. K., Trugman, A. T., Trumbore, S. E., van Mantgem, P. J., Voelker, S. L.,  
3340 Whelan, M. E., and Zuidema, P. A.: Integrating the evidence for a terrestrial carbon sink caused by increasing atmospheric  
3341 CO<sub>2</sub>, *New Phytol.*, 229, 2413–2445, <https://doi.org/10.1111/nph.16866>, 2021.
- 3342 Watanabe, M., Tatebe, H., Koyama, H., Hajima, T., Watanabe, M., and Kawamiya, M.: Importance of El Niño  
3343 reproducibility for reconstructing historical CO<sub>2</sub> flux variations in the equatorial Pacific, *Ocean Sci.*, 16, 1431–1442,  
3344 <https://doi.org/10.5194/os-16-1431-2020>, 2020.
- 3345 Watson, A. J., Schuster, U., Shutler, J. D., Holding, T., Ashton, I. G. C., Landschützer, P., Woolf, D. K., and Goddijn-  
3346 Murphy, L.: Revised estimates of ocean-atmosphere CO<sub>2</sub> flux are consistent with ocean carbon inventory, *Nat Commun*, 11,  
3347 4422, <https://doi.org/10.1038/s41467-020-18203-3>, 2020.
- 3348 Watson, R. T., Rohde, H., Oeschger, H., and Siegenthaler, U.: Greenhouse Gases and Aerosols, in: *Climate Change: The*  
3349 *IPCC Scientific Assessment. Intergovernmental Panel on Climate Change (IPCC)*, edited by: Houghton, J. T., Jenkins, G. J.,  
3350 and Ephraums, J. J., Cambridge University Press, Cambridge, ISBN: 978-0521403603, 1990.
- 3351 Wenzel, S., Cox, P. M., Eyring, V., and Friedlingstein, P.: Projected land photosynthesis constrained by changes in the  
3352 seasonal cycle of atmospheric CO<sub>2</sub>, *Nature*, 538, 499–501, <https://doi.org/10.1038/nature19772>, 2016.
- 3353 Wilkenskjeld, S., Kloster, S., Pongratz, J., Raddatz, T., and Reick, C. H.: Comparing the influence of net and gross  
3354 anthropogenic land-use and land-cover changes on the carbon cycle in the MPI-ESM, *Biogeosciences*, 11, 4817–4828,  
3355 <https://doi.org/10.5194/bg-11-4817-2014>, 2014.
- 3356 Wiltshire, A. J., Burke, E. J., Chadburn, S. E., Jones, C. D., Cox, P. M., Davies-Barnard, T., Friedlingstein, P., Harper, A. B.,  
3357 Liddicoat, S., Sitch, S., and Zaehle, S.: JULES-CN: a coupled terrestrial carbon–nitrogen scheme (JULES vn5.1), 14, 2161–  
3358 2186, <https://doi.org/10.5194/gmd-14-2161-2021>, 2021.
- 3359 Winkler, K., Yang, H., Ganzenmüller, R., Fuchs, R., Ceccherini, G., Duveiller, G., Grassi, G., Pongratz, J., Bastos, A.,  
3360 Shvidenko, A., Araza, A., Herold, M., Wigneron, J.-P., and Ciais, P.: Changes in land use and management led to a decline



- 3361 in Eastern Europe's terrestrial carbon sink, *Commun. Earth Environ.*, 4, 1–14, <https://doi.org/10.1038/s43247-023-00893-4>,  
3362 2023.
- 3363 Woodward, F. I. and Lomas, M. R.: Vegetation dynamics – simulating responses to climatic change, *Biol. Rev.*, 79, 643–  
3364 670, <https://doi.org/10.1017/S1464793103006419>, 2004.
- 3365 Wright, R. M., Le Quéré, C., Buitenhuis, E., Pitois, S., and Gibbons, M. J.: Role of jellyfish in the plankton ecosystem  
3366 revealed using a global ocean biogeochemical model, 18, 1291–1320, <https://doi.org/10.5194/bg-18-1291-2021>, 2021.
- 3367 Wunder, S., Kaimowitz, D., Jensen, S., and Feder, S.: Coronavirus, macroeconomy, and forests: What likely impacts?, *For.*  
3368 *Policy Econ.*, 131, 102536, <https://doi.org/10.1016/j.forpol.2021.102536>, 2021.
- 3369 Xi, F., Davis, S. J., Ciais, P., Crawford-Brown, D., Guan, D., Pade, C., Shi, T., Syddall, M., Lv, J., Ji, L., Bing, L., Wang, J.,  
3370 Wei, W., Yang, K.-H., Lagerblad, B., Galan, I., Andrade, C., Zhang, Y., and Liu, Z.: Substantial global carbon uptake by  
3371 cement carbonation, *Nature Geosci.*, 9, 880–883, <https://doi.org/10.1038/ngeo2840>, 2016.
- 3372 Xia, J., Chen, Y., Liang, S., Liu, D., and Yuan, W.: Global simulations of carbon allocation coefficients for deciduous  
3373 vegetation types, *Tellus B*, 67, 28016, <https://doi.org/10.3402/tellusb.v67.28016>, 2015.
- 3374 Yang, D., Liu, Y., Feng, L., Wang, J., Yao, L., Cai, Z., Zhu, S., Lu, N., and Lyu, D.: The First Global Carbon Dioxide Flux  
3375 Map Derived from TanSat Measurements, *Adv. Atmospheric Sci.*, 38, 1433–1443, <https://doi.org/10.1007/s00376-021->  
3376 1179-7, 2021.
- 3377 Yang, X., Thornton, P., Ricciuto, D., Wang, Y., and Hoffman, F.: Global evaluation of terrestrial biogeochemistry in the  
3378 Energy Exascale Earth System Model (E3SM) and the role of the phosphorus cycle in the historical terrestrial carbon  
3379 balance, *Biogeosciences*, 20, 2813–2836, <https://doi.org/10.5194/bg-20-2813-2023>, 2023.
- 3380 Yu, Z., Ciais, P., Piao, S., Houghton, R. A., Lu, C., Tian, H., Agathokleous, E., Kattel, G. R., Sitch, S., Goll, D., Yue, X.,  
3381 Walker, A., Friedlingstein, P., Jain, A. K., Liu, S., and Zhou, G.: Forest expansion dominates China's land carbon sink since  
3382 1980, *Nat. Commun.*, 13, 5374, <https://doi.org/10.1038/s41467-022-32961-2>, 2022.
- 3383 Yue, X. and Unger, N.: The Yale Interactive terrestrial Biosphere model version 1.0: description, evaluation and  
3384 implementation into NASA GISS ModelE2, *Geosci. Model Dev.*, 8, 2399–2417, <https://doi.org/10.5194/gmd-8-2399-2015>,  
3385 2015.
- 3386 Yuan, W., Liu, D., Dong, W., Liu, S., Zhou, G., Yu, G., Zhao, T., Feng, J., Ma, Z., Chen, J., Chen, Y., Chen, S., Han, S.,  
3387 Huang, J., Li, L., Liu, H., Liu, S., Ma, M., Wang, Y., Xia, J., Xu, W., Zhang, Q., Zhao, X., and Zhao, L.: Multiyear  
3388 precipitation reduction strongly decreases carbon uptake over northern China, *J. Geophys. Res.-Biogeo.*, 119, 881–896,  
3389 <https://doi.org/10.1002/2014JG002608>, 2014.
- 3390 Yue, C., Ciais, P., Zhu, D., Wang, T., Peng, S. S., and Piao, S. L.: How have past fire disturbances contributed to the current  
3391 carbon balance of boreal ecosystems?, *Biogeosciences*, 13, 675–690, <https://doi.org/10.5194/bg-13-675-2016>, 2016.
- 3392 Zaehle, S. and Friend, A. D.: Carbon and nitrogen cycle dynamics in the O-CN land surface model: 1. Model description,  
3393 site-scale evaluation, and sensitivity to parameter estimates: Site-scale evaluation of a C-N model, *Global Biogeochem.*  
3394 *Cycles*, 24, GB1005, <https://doi.org/10.1029/2009GB003521>, 2010.





- 3395 Zaehle, S., Ciais, P., Friend, A. D., and Prieur, V.: Carbon benefits of anthropogenic reactive nitrogen offset by nitrous oxide  
3396 emissions, *Nature Geosci.*, 4, 601–605, <https://doi.org/10.1038/ngeo1207>, 2011.
- 3397 Zaehle, S., Medlyn, B. E., De Kauwe, M. G., Walker, A. P., Dietze, M. C., Hickler, T., Luo, Y., Wang, Y.-P., El-Masri, B.,  
3398 Thornton, P., Jain, A., Wang, S., Warlind, D., Weng, E., Parton, W., Iversen, C. M., Gallet-Budynek, A., McCarthy, H.,  
3399 Finzi, A., Hanson, P. J., Prentice, I. C., Oren, R., and Norby, R. J.: Evaluation of 11 terrestrial carbon–nitrogen cycle models  
3400 against observations from two temperate Free-Air CO<sub>2</sub> Enrichment studies, *New Phytol.*, 202, 803–822,  
3401 <https://doi.org/10.1111/nph.12697>, 2014.
- 3402 Zeng, J., Iida, Y., Matsunaga, T., and Shirai, T.: Surface ocean CO<sub>2</sub> concentration and air-sea flux estimate by machine  
3403 learning with modelled variable trends, *Front. Mar. Sci.*, 9, <https://doi.org/10.3389/fmars.2022.989233>, 2022.
- 3404 Zheng, B., Ciais, P., Chevallier, F., Chuvieco, E., Chen, Y., and Yang, H.: Increasing forest fire emissions despite the  
3405 decline in global burned area, *Sci. Adv.*, 7, eabh2646, <https://doi.org/10.1126/sciadv.abh2646>, 2021.
- 3406 Zou, Y., Wang, Y., Ke, Z., Tian, H., Yang, J., and Liu, Y.: Development of a REgion-Specific Ecosystem Feedback Fire  
3407 (RESFire) Model in the Community Earth System Model, *J. Adv. Model. Earth Syst.*, 11, 417–445,  
3408 <https://doi.org/10.1029/2018MS001368>, 2019.
- 3409 Zscheischler, J., Mahecha, M. D., Avitabile, V., Calle, L., Carvalhais, N., Ciais, P., Gans, F., Gruber, N., Hartmann, J.,  
3410 Herold, M., Ichii, K., Jung, M., Landschützer, P., Laruelle, G. G., Lauerwald, R., Papale, D., Peylin, P., Poulter, B., Ray, D.,  
3411 Regnier, P., Rödenbeck, C., Roman-Cuesta, R. M., Schwalm, C., Tramontana, G., Tyukavina, A., Valentini, R., van der  
3412 Werf, G., West, T. O., Wolf, J. E., and Reichstein, M.: Reviews and syntheses: An empirical spatiotemporal description of  
3413 the global surface–atmosphere carbon fluxes: opportunities and data limitations, *Biogeosciences*, 14, 3685–3703,  
3414 <https://doi.org/10.5194/bg-14-3685-2017>, 2017.



3415 **Tables**

3416 **Table 1.** Factors used to convert carbon in various units (by convention, Unit 1 = Unit 2 × conversion).

Unit 1	Unit 2	Conversion	Source
GtC (gigatonnes of carbon)	ppm (parts per million) (a)	2.124 (b)	Ballantyne et al. (2012)
GtC (gigatonnes of carbon)	PgC (petagrams of carbon)		1 SI unit conversion
GtCO <sub>2</sub> (gigatonnes of carbon dioxide)	GtC (gigatonnes of carbon)	3.664	44.01/12.011 in mass equivalent
(a) Measurements of atmospheric CO <sub>2</sub> concentration have units of dry-air mole fraction. ‘ppm’ is an abbreviation for micromole/mol, dry air.			
(b) The use of a factor of 2.124 assumes that all the atmosphere is well mixed within one year. In reality, only the troposphere is well mixed and the growth rate of CO <sub>2</sub> concentration in the less well-mixed stratosphere is not measured by sites from the NOAA network. Using a factor of 2.124 makes the approximation that the growth rate of CO <sub>2</sub> concentration in the stratosphere equals that of the troposphere on a yearly basis.			

3417

3418

3419



3420 **Table 2.** How to cite the individual components of the global carbon budget presented here.

Component	Primary reference
Global fossil CO <sub>2</sub> emissions (EFOS), total and by fuel type	Andrew and Peters (2024)
National territorial fossil CO <sub>2</sub> emissions (EFOS)	Hefner and Marland (2023), UNFCCC (2024)
National consumption-based fossil CO <sub>2</sub> emissions (EFOS) by country (consumption)	Peters et al. (2011a) updated as described in this paper
Net land-use change flux (ELUC)	This paper (see Table 4 for individual model references).
Growth rate in atmospheric CO <sub>2</sub> concentration (GATM)	Lan et al. (2024)
Ocean and land CO <sub>2</sub> sinks (SOCEAN and SLAND)	This paper (see Table 4 for individual model and data products references).

3421

3422



**Table 3.** Main methodological changes in the global carbon budget since 2020. Methodological changes introduced in one year are kept for the following years unless noted. Empty cells mean there were no methodological changes introduced that year. Table S9 lists methodological changes from the first global carbon budget publication up to 2019.

Publication year	Fossil fuel emissions		LUC emissions	Reservoirs			Other changes
	Global	Country (territorial)		Atmosphere	Ocean	Land	
2020	Cement carbonation now included in the EFOS estimate, reducing EFOS by about 0.2GtC yr <sup>-1</sup> for the last decade	India's emissions from Andrew (2020: India); Corrections to Netherland Antilles and Aruba and Soviet emissions before 1950 as per Andrew (2020: CO <sub>2</sub> ); China's coal emissions in 2019 derived from official statistics, emissions now shown for EU27 instead of EU28. Projection for 2020 based on assessment of four approaches.	Average of three bookkeeping models; use of 17 DGVMs. Estimate of gross land use sources and sinks provided	Use of six atmospheric inversions	Based on nine models. River flux revised and partitioned NH, Tropics, SH	Based on 17 models	
Friedlingstein et al. (2020) GCB2020							
2021	Projections are no longer an assessment of four approaches.	Official data included for a number of additional countries, new estimates for South Korea, added emissions from lime production in China.	ELUC estimate compared to the estimates adopted in national GHG inventories		Average of means of eight models and means of seven data-products. Current year prediction of SOCEAN using a feed-forward neural network method	Current year prediction of SLAND using a feed-forward neural network method	
Friedlingstein et al. (2022a) GCB2021							
2022			ELUC provided at country level. Revised components decomposition of ELUC fluxes. Revision of LUC	Use of nine atmospheric inversions	Average of means of ten models and means of seven data-products	Based on 16 models. Revision of LUC maps for Brazil.	
Friedlingstein et al. (2022) GCB2022							



			maps for Brazil. New datasets for peat drainage.				
2023			Refined components decomposition of ELUC. Revision of LUC maps for Indonesia. Use of updated peat drainage estimates.	Use of 14 atmospheric inversions. Additional use of 4 Earth System Models to estimate current year CO2	Additional use of 4 Earth System Models and atmospheric oxygen method to assess SOCEAN. Regional distribution of river flux adjustment revised.	Based on 20 models. Additional use of 4 Earth System Models and atmospheric oxygen method to assess the net atmosphere-land flux.	Inclusion of an estimate of Carbon Dioxide Removal
Friedlingstein et al. (2023) GCB2023							
2024			Fourth bookkeeping estimate (LUCE). Update in land-use data (HYDE3.4) including revision of LUC maps for China. Updated definition of forest (re-)growth fluxes (consistent with 2nd State of CDR Report).	Use of 14 atmospheric inversions models	Use of 10 GOBMs, 8 fCO2-products. Added evaluation for fCO2-products.	Use of 20 DGVMs	
This study	Inclusion of 2024 projections from Carbon Monitor	Inclusion of 2024 projections from Carbon Monitor for China, USA, EU27, India, and Rest of the World					



**Table 4.** References for the process models, bookkeeping models, ocean data products, and atmospheric inversions. All models and products are updated with new data to the end of year 2023.

Model/data name	Reference	Change from Global Carbon Budget 2023 (Friedlingstein et al., 2023)
<b><i>Bookkeeping models for land-use change emissions</i></b>		
BLUE	Hansis et al. (2015)	No change to model, but simulations performed with LUH2-GCB2024 forcing. Update in added peat drainage emissions.
H&C2023	Houghton and Castanho (2023)	No change to model. Data for years after last modelled year (2020) extrapolated based on anomalies in deforestation fires from GFED. Update in added peat drainage emissions.
OSCAR	Gasser et al. (2020)	No change to model, but land-use forcing changed to LUH2-GCB2024 and FRA2020 extrapolated to 2023. Constraining based on GCB2023 data for SLAND over 1960-2022. Update in added peat drainage emissions.
LUCE	Qin et al. (2024)	New model in GCB2024.
<b><i>Dynamic global vegetation models</i></b>		
CABLE-POP	Haverd et al. (2018)	Bug fix applied to land use change calculations enabling variable crop and pasture fractions; corrections to the pre-industrial primary forest fraction in Europe; minor parameter changes
CLASSIC	Melton et al. (2020), Asaadi et al. (2018)	Permeable soil depth reduced to 4 m ; 15 soil layers in the top 4 m permeable soil and 5 bed rock layers from 4 m to 62 m; saturated hydraulic conductivity decreases with depth in the permeable soil layers; transpiration occurs from a partially-wet canopy leaves. These changes yield better runoff seasonality and a more realistic partitioning of precipitation into runoff and evapotranspiration.
CLM6.0	Lawrence et al. (2019)	Updates to surface datasets; improvement of roughness length calculation; updates to snow optical properties and snow thermal conductivity; improved excess ice; improved simulation of burial of vegetation by snow; urban updates, including transient urban, urban properties, and air conditioning; improvements to biomass heat storage; tillage and residue removal; crop phenology and planting dates; improvement to irrigation methods; PFT parameter update.



DLEM	Tian et al. (2015), You et al. (2022)	Incorporate mechanistic representations of dynamic crop growth and development processes, such as crop-specific phenological development, carbon allocation, yield formation, and biological N fixation. Agricultural management practices such as N fertiliser use, irrigation, tillage, manure application, dynamic crop rotation, cover cropping, and genetic improvements are also included (You et al. 2022).
EDv3	Moorcroft et al. (2001), Ma et al. (2022)	Minor bug fixes, updated fire submodule
ELM	Yang et al.(2023), Burrows et al.(2020)	No change
IBIS	Xia et al., (2024)	Improved algorithm of leaf area index
iMAPLE	Yue et al. (2024)	The updated version of YIBs model with dynamic coupling between carbon and water cycles.
ISAM	Jain et al. (2013), Meiyappan et al. (2015), Shu et al. (2020)	Vertically resolved soil biogeochemistry (carbon and nitrogen) module, following Shu et al. (2020),
ISBA-CTrip	Delire et al. (2020)	No change.
JSBACH	Mauritsen et al. (2019), Reick et al. (2021)	Minor bug fixes in post-processing
JULES-ES	Wiltshire et al. (2021), Sellar et al. (2019), Burton et al. (2019)	Minor bug fixes. (Using JULES v7.4)
LPJ-GUESS	Smith et al. (2014)	No change.
LPJml	Schaphoff et al., 2018, von Bloh et al., 2018, Lutz et al., 2019 (tillage), Heinke et al., 2023 (livestock grazing)	No change
LPJwsl	Poulter et al. (2011) (d)	Minor bug fixes, weighting of fire carbon by GFED to simulate annual cycle
LPX-Bern	Lienert and Joos (2018)	No change.
OCN	Zaehle and Friend (2010), Zaehle et al. (2011)	No change.
ORCHIDEEv3	Krinner et al. (2005), Zaehle and Friend (2010), Vuichard et al. (2019)	No change.
SDGVM	Woodward and Lomas (2004), Walker et al. (2017)	Parameter adjustment for reducing evaporation from vegetation that intercepted precipitation, as well as other adjustments to the calculation of evapotranspiration; bug fix in output of monthly NEP, NBP, soilr, and rh; bug fix on cLeaf monthly output; further development on gross land-use transitions, tracking of carbon from wood & crop harvest, and tracking of primary & secondary vegetation.
VISIT	Ito and Inatomi (2012), Kato et al. (2013)	No change.



<b>Intermediate complexity land carbon cycle model</b>		
CARDAMOM	Bloom et al. (2016), Smallman et al. (2021)	No change.
<b>Global ocean biogeochemistry models</b>		
NEMO-PlankTOM12	Wright et al. (2021)	Minor bug fixes, change to salinity restoring and restart file. New atmospheric CO2 input for simulations A and C.
NEMO4.2-PISCES (IPSL)	Aumont et al. (2015)	Switch to the new model version NEMO4.2-PISCES. Update following the new protocol (with 1750 preindustrial CO2 for spin-up). New atmospheric CO2 input for simulations A and C.
MICOM-HAMOCC (NorESM1-OCv1.2)	Schwinger et al. (2016)	No change in model set-up. New atmospheric CO2 file for simulations A and C. Corrected diagnostic output for pco2atm; diagnostic output for sfco2 and spco2 provided at the air-sea interface (not with respect to dry air at 1 atm).
MPIOM-HAMOCC6	Lacroix et al. Global Change Biology 2021	No change; only updated atmosphere CO2 input for A and C experiments and run 1948-2023.
NEMO3.6-PISCESv2-gas (CNRM)	Berthet et al. (2019) Séfériat et al. (2019)	Updated simulations using 1750 preindustrial conditions instead of 1850. No change in model configuration. New atmospheric CO2 input for simulations A and C
FESOM2.1-REcoM3	Gürses et al. (2023)	Updated atmospheric CO2 for simulations A and C.
MOM6-COBALT (Princeton)	Liao et al. (2020)	No change.
CESM-ETHZ	Doney et al. (2009)	Compared to the 2023 submission, the spinup was extended to 1422 years before 1750. Also, starting at 1751 the new atmospheric CO2 concentrations provided by GCB have been used for simulations A and C.
MRI-ESM2-3	Tsujino et al. (2024), Sakamoto et al. (2023)	Iron circulation and its limitation on primary production are introduced. Updated atmospheric CO2 for simulations A and C
ACCESS (CSIRO)	Law et al. (2017)	No change in model set-up (since GCB2023). Updated atmospheric CO2 for simulations A and C.
<b>fCO2-products</b>		
VLIZ-SOMFFN (former MPI-SOM-FFN)	Landschützer et al. (2016)	Time period 1982-2023; The estimate now covers the full open ocean and coastal domain as well as the Arctic Ocean extension by merging 2 MLD proxies for year round full coverage. Additionally, in the SOM step, the Seaflux climatology is now used
Jena-MLS	Rödenbeck et al. (2014) updated to	Time period extended to 2023





	Rödenbeck et al (2022)	
CMEMS-LSCE-FFNNv2	Chau et al. (2022)	Time period now 1985-2023
UEXP-FNN-U (previously Watson et al.)	Watson et al. (2020) and Ford et al. (accepted)	Updated CCI-SST to v3 (Embury et al. 2024), with cool bias with respect to global drifter observations corrected following recommendations in Dong et al. (2022). Updated SOM-FFN implementation to Python.
NIES-ML3	Zeng et al. (2022)	Updated time period 1982-2023.
JMA-MLR	Iida et al. (2021)	Time period extended to 2023
OceanSODA-ETHZv2	Gregor et al. (2024)	Updated method following Gregor et al 2024 and time period extended to 2023
LDEO-HPD	Gloege et al. 2022 and Bennington et al. 2022	Time period extended to 2023
CSIR-ML6	Gregor et al. (2019)	Time period 1982-2023.
<b>Atmospheric inversions</b>		
Jena CarboScope	Rödenbeck et al. (2018), Stephens et al. (2007)	Extension to end of year 2023. Slight change in station set. In the NBE-T inversion, removal of the relaxation term, instead, filtering out decadal variations from air temperature. Adding an additive correction to the result of the NBE-T inversion, to account for CO <sub>2</sub> flux IAV not related to air temperature, based on 8 long atmospheric records available near-continuously since at least 1976. TM3 driven by ERA5 rather than NCEP.
CAMS	Chevallier et al. (2005), Remaud et al. (2018)	Extension to year 2023. Increase of the 3D resolution with hexagonal prisms rather than rectangular parallelepipeds (3 times more 3D cells than the previous submission). Update of the prior fluxes.
CarbonTracker Europe (CTE)	van der Laan-Luijkx et al. (2017)	Extension to 2023, update of prior fluxes.
NISMON-CO <sub>2</sub>	Niwa et al. (2022), Niwa et al. (2017).	Extension to 2023, update of prior fluxes.
CT-NOAA	Jacobson et al. (2023a), Jacobson et al. (2024), Byrne et al. (2023), Krol et al. (2005), Peiro et al. (2022)	Extended to 2023 using the CarbonTracker Near-Real Time release CT-NRT.v2024-1 (Jacobson et al. 2024).
CMS-Flux	Liu et al. (2021)	Extension to 2023, update of prior fluxes.
CAMS-Satellite	Chevallier et al. (2005), Remaud et al. (2018)	Extension to year 2023. Increase of the 3D resolution with hexagonal prisms rather than rectangular parallelepipeds (3 times more 3D cells than the previous submission). Update of the prior fluxes.



GONGGA	Jin et al. (2023), Nassar et al. (2010)	Extension to 2023, update of prior fluxes.
COLA	Liu et al. (2022)	Extension to 2023, update of prior fluxes.
GCASv2	Jiang et al. (2021) & Emmons et al. (2010)	Extension to 2023, update of prior fluxes.
UoE in-situ	Feng et al. (2016) & Palmer et al. (2019)	Extension to 2023, update of prior fluxes.
IAPCAS	Yang et al. (2021) & Feng et al. (2016)	Extension to 2023, update of prior fluxes.
MIROC4-ACTM	Chandra et al. (2022) & Patra et al. (2018)	Extension to 2023, update of prior fluxes using only CASA and not VISIT. Less observation sites used in the assimilation (46 instead of 50).
NTFVAR	Nayagam et al. (2024) & Maksyutov et al. (2021)	New this year
<b>Earth System Models</b>		
CanESM5	Swart et al. (2019), Sospedra-Alfonso et al. (2021)	Reconstructions are extended to 1960-2023, and predictions are extended to 2024.
EC-Earth3-CC	Döscher et al. (2021), Bilbao et al. (2021), Bernardello et al. (2024)	New this year.
IPSL-CM6A-CO2-LR	Boucher et al. (2020)	Reconstructions are extended to 1960-2023, and predictions are extended to 2024. No change to model, the CMIP6 CovidMIP CO2 emissions after 2015 are used.
MIROC-ES2L	Watanabe et al. (2020)	Reconstructions are extended to 1960-2023, and predictions are extended to 2024. No change to model, the simulations were rerun including a long spinup.
MPI-ESM1-2-LR	Mauritsen et al. (2019), Li et al. (2023)	Reconstructions are extended to 1960-2023, and predictions are extended to 2024.



**Table 5.** Comparison of results from the bookkeeping method and budget residuals with results from the DGVMs, as well as additional estimates from atmospheric oxygen, atmospheric inversions and Earth System Models (ESMs) for different periods, the last decade, and the last year available. All values are in GtCyr<sup>-1</sup>. See Figure 7 for explanation of the bookkeeping component fluxes. The DGVM uncertainties represent ±1σ of the decadal or annual (for 2023) estimates from the individual DGVMs: for the inverse systems the mean and range of available results is given. All values are rounded to the nearest 0.1 GtC and therefore columns do not necessarily add to zero.

		<i>Mean (GtC/yr)</i>						
		1960s	1970s	1980s	1990s	2000s	2014-2023	2023
Land-use change emissions (ELUC)	Bookkeeping (BK) Net flux (1a)	1.6±0.7	1.4±0.7	1.4±0.7	1.6±0.7	1.4±0.7	1.1±0.7	1±0.7
	BK - deforestation (total)	1.7 [1.3,2.2]	1.6 [1.2,2]	1.6 [1.3,1.9]	1.8 [1.6,2]	1.9 [1.6,2.2]	1.7 [1.4,2.3]	1.7 [1.3,2.3]
	BK - forest regrowth (total)	-0.8 [- 1.1,- 0.6]	-0.9 [- 1.1,-0.7]	-0.9 [- 1,-0.7]	-0.9 [- 1.1,-0.8]	-1.1 [- 1.2,-0.9]	-1.2 [- 1.5,-0.9]	-1.2 [- 1.5,-0.9]
	BK - other transitions	0.3 [0.3,0.4]	0.2 [0.2,0.3]	0.2 [0.1,0.3]	0.1 [0,0.2]	0.1 [0,0.1]	0.1 [0,0.1]	0 [0,0.1]
	BK - peat drainage & peat fires	0.2 [0.1,0.2]	0.2 [0.1,0.2]	0.2 [0.2,0.2]	0.3 [0.2,0.3]	0.2 [0.2,0.3]	0.2 [0.2,0.3]	0.2 [0.2,0.3]
	BK - wood harvest & forest management	0.2 [- 0.2,0.6]	0.3 [- 0.2,0.6]	0.3 [- 0.2,0.7]	0.3 [- 0.1,0.6]	0.3 [- 0.1,0.6]	0.3 [0,0.6]	0.3 [0,0.7]
	DGVMs-net flux (1b)	1.5±0.5	1.5±0.5	1.5±0.5	1.7±0.5	1.7±0.6	1.5±0.6	1.2±0.7
Terrestrial sink (SLAND)	Residual sink from global budget (E <sub>FOS</sub> +E <sub>ELUC</sub> (1a)-G <sub>ATM-SOCEAN</sub> ) (2a)	1.7±0.8	1.9±0.8	1.6±0.9	2.6±0.9	2.8±0.9	2.7±0.9	2.3±1
	DGVMs (2b)	1.2±0.5	2±0.8	1.8±0.8	2.5±0.6	2.8±0.7	3.2±0.9	2.3±1
Net land fluxes (SLAND-ELUC)	GCB2024 Budget (2b-1a)	- 0.4±0.9	0.5±1.1	0.4±1.1	0.9±0.9	1.4±1	2.1±1.1	1.3±1.2
	Atmospheric O <sub>2</sub>	---	---	---	1.3±0.7	1±0.7	1±0.8	-
	DGVMs-net (2b-1b)	- 0.3±0.5	0.5±0.7	0.3±0.6	0.8±0.4	1.1±0.4	1.7±0.6	1.1±0.8
	Inversions*	- [-,-]	- [-,-]	0.3 [0.3,0.4] (2)	0.9 [0.6,1.1] (3)	1.2 [0.6,1.5] (4)	1.4 [0.3,2.2] (10)	0.9 [- 0.1-2.7] (14)
	ESMs	0 [- 0.7,0.5]	1.5 [1.2,2]	1 [0.5,1.4]	1.7 [1.2,2.4]	1.8 [0.4,2.7]	2.2 [0.3,3.6]	1.8 [- 2.9-3.7]

\*Estimates are adjusted for the pre-industrial influence of river fluxes, for the cement carbonation sink, and adjusted to common EFOS (Sect. 2.7). The ranges given include varying numbers (in parentheses) of inversions in each decade (Table A4)



**Table 6:** Comparison of results for the ocean sink from the  $f\text{CO}_2$ -products, from global ocean biogeochemistry models (GOBMs), the best estimate for GCB2024 as calculated from  $f\text{CO}_2$ -products and GOBMs that is used in the budget Table 7, as well as additional estimates from atmospheric oxygen, atmospheric inversions and Earth System Models (ESMs) for different periods, the last decade, and the last year available. All values are in  $\text{GtCyr}^{-1}$ . Uncertainties represent  $\pm 1\sigma$  of the estimates from the GOBMs ( $N > 10$ ) and range of ensemble members is given for ensembles with  $N < 10$  ( $f\text{CO}_2$ -products, inversions, ESMs). The uncertainty of the GCB2024 budget estimate is based on expert judgement (Section 2 and Supplementary S1 to S4) and for oxygen it is the standard deviation of a Monte Carlo ensemble (Section 2.8).

<i>Mean (GtC/yr)</i>							
Product	1960s	1970s	1980s	1990s	2000s	2014-2023	2023
$f\text{CO}_2$ -products	---	---	---	2.3 [1.9,2.9]	2.5 [2.3,2.7]	3.1 [2.9,3.7]	3 [2.3,4]
GOBMs	1±0.2	1.3±0.3	1.8±0.3	2±0.3	2.2±0.3	2.6±0.4	2.7±0.4
GCB2024 Budget	1.2±0.4	1.5±0.4	1.9±0.4	2.1±0.4	2.3±0.4	2.9±0.4	2.9±0.4
Atmospheric O <sub>2</sub>	---	---	---	2±0.5	2.8±0.4	3.4±0.5	-
Inversions	- [-,-]	- [-,-]	1.8 [1.8,1.9] (2)	2.3 [2.1,2.5] (3)	2.5 [2.3,3.1] (4)	3.1 [2.4,4.1] (10)	3 [1.8-4.1] (14)
ESMs	0.7 [0.1,1.1]	1 [0.4,1.4]	1.4 [0.7,1.7]	1.7 [1.1,2]	1.9 [1.5,2.2]	2.5 [2.2,2.8]	2.5 [2.2-3]



**Table 7:** Decadal mean in the five components of the anthropogenic CO<sub>2</sub> budget for different periods, and last year available. All values are in GtC yr<sup>-1</sup>, and uncertainties are reported as ±1σ. Fossil CO<sub>2</sub> emissions include cement carbonation. The table also shows the budget imbalance (BIM), which provides a measure of the discrepancies among the nearly independent estimates. A positive imbalance means the emissions are overestimated and/or the sinks are too small. All values are rounded to the nearest 0.1 GtC and therefore columns do not necessarily add to zero.

		<i>Mean (GtC/yr)</i>							
		1960s	1970s	1980s	1990s	2000s	2014-2023	2023	2024 (Projection)
Total emissions (EFOS + ELUC)	Fossil CO <sub>2</sub> emissions (EFOS)*	3±0.2	4.7±0.2	5.5±0.3	6.4±0.3	7.8±0.4	9.7±0.5	10.1±0.5	10.2±0.5
	Land-use change emissions (ELUC)	1.6±0.7	1.4±0.7	1.4±0.7	1.6±0.7	1.4±0.7	1.1±0.7	1±0.7	1.1±0.7
	Total emissions	4.6±0.7	6.1±0.7	6.9±0.8	7.9±0.8	9.2±0.8	10.8±0.9	11.1±0.9	11.3±0.9
	Growth rate in atmospheric CO <sub>2</sub> (GATM)	1.7±0.07	2.8±0.07	3.4±0.02	3.1±0.02	4±0.02	5.2±0.02	5.9±0.2	5.9±0.5
Partitioning	Ocean sink (SOCEAN)	1.2±0.4	1.5±0.4	1.9±0.4	2.1±0.4	2.3±0.4	2.9±0.4	2.9±0.4	3±0.6
	Terrestrial sink (SLAND)	1.2±0.5	2±0.8	1.8±0.8	2.5±0.6	2.8±0.7	3.2±0.9	2.3±1	3.2±1.5
Budget Imbalance	BIM=E FOS+E LUC-(GATM +SOCEAN)	0.5	-0.1	-0.2	0.1	0	-0.4	0	-0.7



	1960s	1970s	1980s	1990s	2000s	2014- 2023	2023	2024 (Projec tion)
AN+SL AND)								

\*Fossil emissions excluding the cement carbonation sink amount to  $3\pm 0.2$  GtC/yr,  $4.7\pm 0.2$  GtC/yr,  $5.5\pm 0.3$  GtC/yr,  $6.4\pm 0.3$  GtC/yr,  $7.9\pm 0.4$  GtC/yr, and  $9.9\pm 0.5$  GtC/yr for the decades 1960s to 2010s respectively and to  $10.3\pm 0.5$  GtC/yr for 2023, and  $10.4\pm 0.5$  GtC/yr for 2024.



**Table 8.** Cumulative CO<sub>2</sub> for different time periods in gigatonnes of carbon (GtC). Fossil CO<sub>2</sub> emissions include cement carbonation. The budget imbalance (B<sub>IM</sub>) provides a measure of the discrepancies among the nearly independent estimates. All values are rounded to the nearest 5 GtC and therefore columns do not necessarily add to zero. Uncertainties are reported as follows: E<sub>FOS</sub> is 5% of cumulative emissions; E<sub>LUC</sub> prior to 1959 is 1σ spread from the DGVMs, E<sub>LUC</sub> post-1959 is 0.7\*number of years (where 0.7 GtC/yr is the uncertainty on the annual E<sub>LUC</sub> flux estimate); G<sub>ATM</sub> uncertainty is held constant at 5 GtC for all time periods; S<sub>OCEAN</sub> uncertainty is 20% of the cumulative sink (20% relates to the annual uncertainty of 0.4 GtC/yr, which is ~20% of the current ocean sink); and S<sub>LAND</sub> is the 1σ spread from the DGVMs estimates.

		1750-2023	1850-2014	1850-2023	1960-2023	1850-2024
Emissions	Fossil CO <sub>2</sub> emissions (EFOS)	490±25	400±20	490±25	410±20	500±25
	Land-use change emissions (ELUC)	255±75	215±60	225±65	90±45	225±65
	Total emissions	745±80	615±65	710±70	500±50	725±70
Partitioning	Growth rate in atmos CO <sub>2</sub> (G <sub>ATM</sub> )	305±5	235±5	285±5	220±5	290±5
	Ocean sink (S <sub>OCEAN</sub> )	195±40	160±30	185±35	130±25	185±35
	Terrestrial sink (S <sub>LAND</sub> )	245±65	190±55	220±60	150±40	225±60
Budget imbalance	BIM=EFOS+ELUC-(G <sub>ATM</sub> +S <sub>OCEAN</sub> +S <sub>LAND</sub> )	0	30	25	0	20



**Table 9.** Average annual growth rate in fossil CO<sub>2</sub> emissions over the most recent decade (2014-2023) and the previous decade (2004-2013). The data for the World include the cement carbonation sink. IAS are emissions from international aviation and shipping. Rest of the World is World minus China, USA, EU27, India and IAS.

	World	China	USA	EU27	India	OECD	Non-OECD	IAS	Rest of the World
2004-2013	2.4%	7.5%	-1.4%	-1.8%	6.4%	-0.9%	4.9%	2.6%	1.9%
2014-2023	0.6%	1.9%	-1.2%	-2.1%	3.6%	-1.4%	1.8%	-1.6%	0.4%





**Table 10.** Major known sources of uncertainties in each component of the Global Carbon Budget, defined as input data or processes that have a demonstrated effect of at least  $\pm 0.3$  GtC yr<sup>-1</sup>.

Source of uncertainty	Time scale (years)	Location	Evidence
<b>Fossil CO<sub>2</sub> emissions (EFOS; Section 2.1)</b>			
energy statistics	annual to decadal	global, but mainly China & major developing countries	(Korsbakken et al., 2016, Guan et al., 2012)
carbon content of coal	annual to decadal	global, but mainly China & major developing countries	(Liu et al., 2015)
system boundary	annual to decadal	all countries	(Andrew, 2020a)
<b>Net land-use change flux (ELUC; section 2.2)</b>			
land-cover and land-use change statistics	continuous	global; in particular tropics	(Houghton et al., 2012, Gasser et al., 2020, Ganzenmüller et al., 2022, Yu et al. 2022)
sub-grid-scale transitions	annual to decadal	global	(Wilkenskjeld et al., 2014, Bastos et al., 2021)
vegetation biomass	annual to decadal	global; in particular tropics	(Houghton et al., 2012, Bastos et al., 2021)
forest degradation (fire, selective logging)	annual to decadal	tropics; Amazon	(Aragão et al., 2018, Qin et al., 2021, Lapola et al., 2023)
wood and crop harvest	annual to decadal	global; SE Asia	(Arneth et al., 2017, Erb et al., 2018)
peat burning	multi-decadal trend	global	(van der Werf et al., 2010, 2017)
loss of additional sink capacity	multi-decadal trend	global	(Pongratz et al., 2014, Gasser et al., 2020; Obermeier et al., 2021; Dorgeist et al., 2024)
environmental effects	multi-decadal trend	global	(Gasser et al. 2020, Dorgeist et al., 2024)
Atmospheric growth rate (GATM; section 2.4) no demonstrated uncertainties larger than $\pm 0.3$ GtC yr <sup>-1</sup> . The uncertainties in GATM have been estimated as $\pm 0.2$ GtC yr <sup>-1</sup> , although the conversion of the growth rate into a global annual flux assuming instantaneous mixing throughout the atmosphere introduces additional errors that have not yet been quantified.			
Ocean sink (SOCEAN; section 2.5)			



sparsity in surface fCO <sub>2</sub> observations	mean, decadal variability and trend	global, in particular southern hemisphere	(Gloege et al., 2021, Denvil-Sommer et al., 2021, Hauck et al., 2023a; Dong et al., 2024b)
riverine carbon outgassing and its anthropogenic perturbation	annual to decadal	global, in particular partitioning between Tropics and South	(Aumont et al., 2001, Lacroix et al., 2020, Crisp et al., 2022)
Models underestimate interior ocean anthropogenic carbon storage	annual to decadal	global	(Friedlingstein et al., 2022a, this study, DeVries et al., 2023, Müller et al., 2023)
near-surface temperature and salinity gradients	mean on all time-scales	global	(Watson et al., 2020, Dong et al., 2022, Bellenger et al., 2023, Dong et al., 2024a)
Land sink (SLAND; section 2.6)			
strength of CO <sub>2</sub> fertilisation	multi-decadal trend	global	(Wenzel et al., 2016; Walker et al., 2021)
response to variability in temperature and rainfall	annual to decadal	global; in particular tropics	(Cox et al., 2013; Jung et al., 2017; Humphrey et al., 2018; 2021)
nutrient limitation and supply	annual to decadal	global	(Zaehle et al., 2014)
carbon allocation and tissue turnover rates	annual to decadal	global	(De Kauwe et al., 2014; O'Sullivan et al., 2022)
tree mortality	annual	global in particular tropics	(Hubau et al., 2021; Brienen et al., 2020)
response to diffuse radiation	annual	global	(Mercado et al., 2009; O'Sullivan et al., 2021)
estimation under constant pre-industrial land cover	multi-decadal trend	global	(Gasser et al. 2020, Dorgeist et al., 2024)



## Figures and Captions

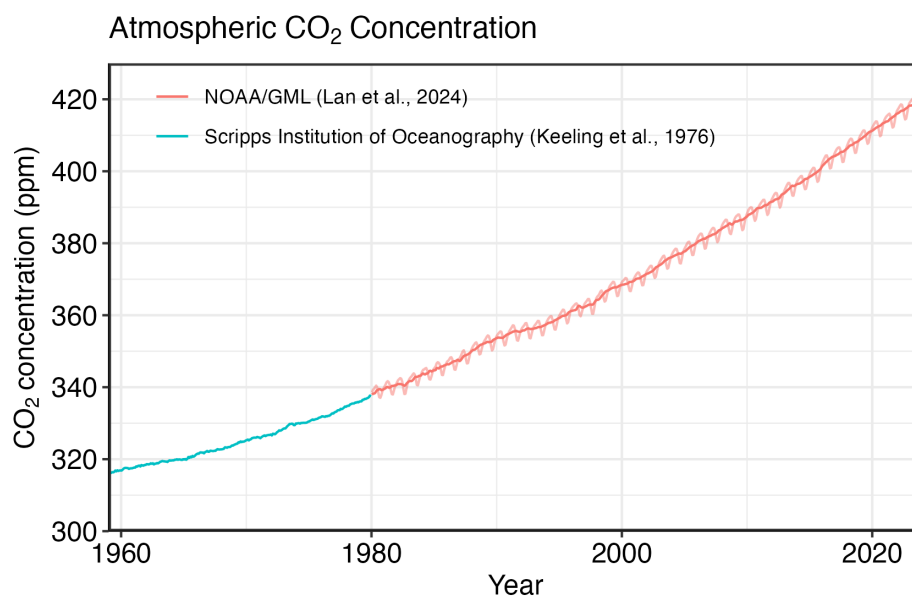
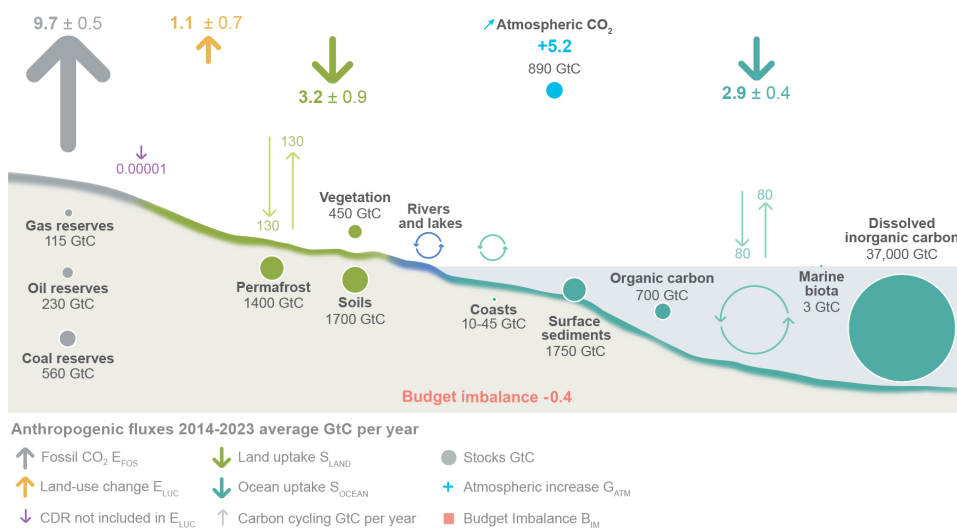


Figure 1. Surface average atmospheric CO<sub>2</sub> concentration (ppm). Since 1980, monthly data are from NOAA/GML (Lan et al., 2024) and are based on an average of direct atmospheric CO<sub>2</sub> measurements from multiple stations in the marine boundary layer (Masarie and Tans, 1995). The 1958-1979 monthly data are from the Scripps Institution of Oceanography, based on an average of direct atmospheric CO<sub>2</sub> measurements from the Mauna Loa and South Pole stations (Keeling et al., 1976). To account for the difference of mean CO<sub>2</sub> and seasonality between the NOAA/GML and the Scripps station networks used here, the Scripps surface average (from two stations) was de-seasonalised and adjusted to match the NOAA/GML surface average (from multiple stations) by adding the mean difference of 0.667 ppm, calculated here from overlapping data during 1980-2012.



## The global carbon cycle



**Figure 2.** Schematic representation of the overall perturbation of the global carbon cycle caused by anthropogenic activities, averaged globally for the decade 2014-2023. See legends for the corresponding arrows. Fluxes estimates and their 1 standard deviation uncertainty are as reported in Table 7. The CDR estimate is for the year 2023 only. The uncertainty in the atmospheric CO<sub>2</sub> growth rate is very small ( $\pm 0.02$  GtC yr<sup>-1</sup>) and is neglected for the figure. The anthropogenic perturbation occurs on top of an active carbon cycle, with fluxes and stocks represented in the background and taken from Canadell et al. (2021) for all numbers, except for the carbon stocks in coasts which is from a literature review of coastal marine sediments (Price and Warren, 2016). Fluxes are in GtC yr<sup>-1</sup> and reservoirs in GtC.

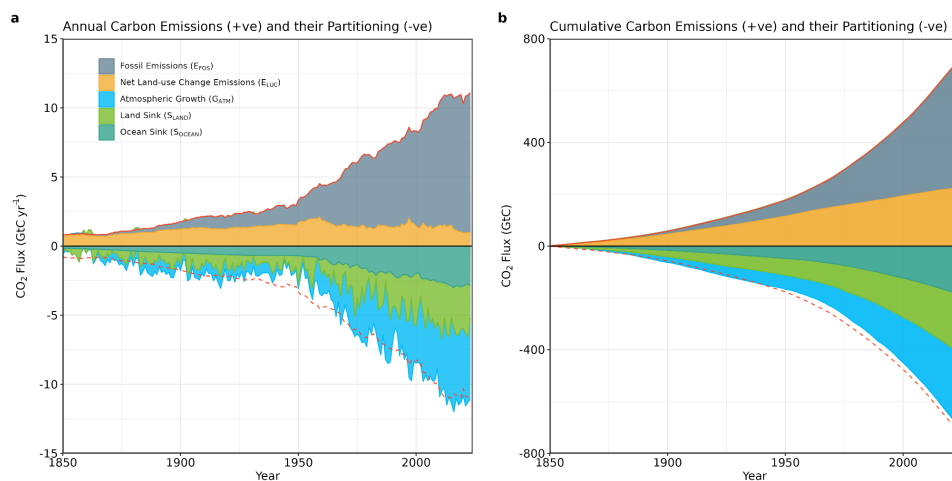


**Figure 3.** Combined components of the global carbon budget as a function of time, for fossil CO<sub>2</sub> emissions (E<sub>FOS</sub>, including a small sink from cement carbonation; grey) and emissions from land-use change (E<sub>LUC</sub>; brown), as well as their partitioning among the atmosphere (G<sub>ATM</sub>; cyan), ocean (S<sub>OCEAN</sub>; blue), and land (S<sub>LAND</sub>; green). Panel (a) shows annual estimates of each flux (in GtC yr<sup>-1</sup>) and panel (b) the cumulative flux (the sum of all prior annual fluxes, in GtC) since the year 1850. The partitioning is based on nearly independent estimates from observations (for G<sub>ATM</sub>) and from process model ensembles constrained by data (for S<sub>OCEAN</sub> and S<sub>LAND</sub>) and does not exactly add up to the sum of the emissions, resulting in a budget imbalance (B<sub>IM</sub>) which is represented by the difference between the bottom red line (mirroring total emissions) and the sum of carbon fluxes in the ocean, land, and atmosphere reservoirs. All data are in GtC yr<sup>-1</sup> (panel a) and GtC (panel b). The E<sub>FOS</sub> estimate is based on a mosaic of different datasets, and has an uncertainty of ±5% (±1σ). The E<sub>LUC</sub> estimate is from four bookkeeping models (Table 4) with uncertainty of ±0.7 GtC yr<sup>-1</sup>. The G<sub>ATM</sub> estimates prior to 1959 are from Joos and Spahni (2008) with uncertainties equivalent to about ±0.1-0.15 GtC yr<sup>-1</sup> and from Lan et al. (2024) since 1959 with uncertainties of about ±0.07 GtC yr<sup>-1</sup> during 1959-1979 and ±0.02 GtC yr<sup>-1</sup> since 1980. The S<sub>OCEAN</sub> estimate is the average from Khatiwala et al. (2013) and DeVries (2014) with uncertainty of about ±30% prior to 1959, and the average of an ensemble of models and an ensemble of fCO<sub>2</sub>-products (Table 4) with uncertainties of about ±0.4 GtC yr<sup>-1</sup> since 1959. The S<sub>LAND</sub> estimate is the average of an ensemble of models (Table 4) with uncertainties of about ±1 GtC yr<sup>-1</sup>. See the text for more details of each component and their uncertainties.

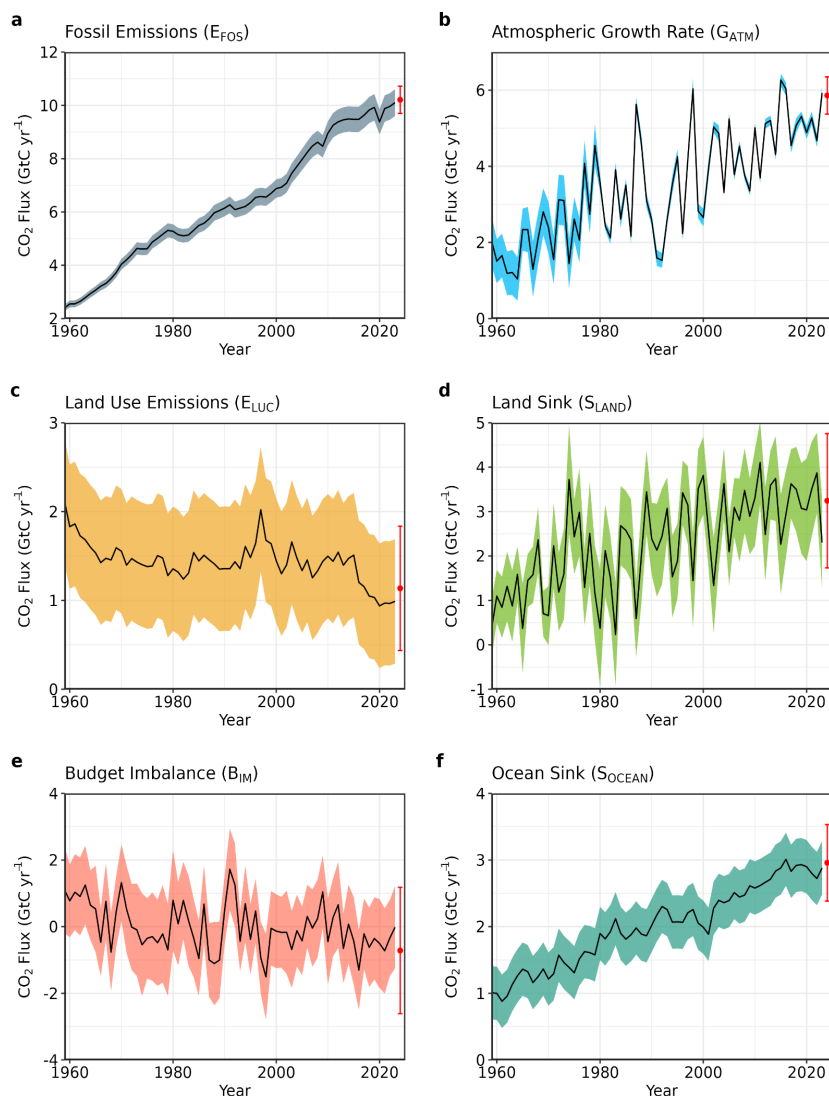


**Figure 4.** Components of the global carbon budget and their uncertainties as a function of time, presented individually for (a) fossil CO<sub>2</sub>, including cement carbonation emissions ( $E_{FOS}$ ), (b) growth rate in atmospheric CO<sub>2</sub> concentration ( $G_{ATM}$ ), (c) emissions from land-use change ( $E_{LUC}$ ), (d) the land CO<sub>2</sub> sink ( $S_{LAND}$ ), (e) the ocean CO<sub>2</sub> sink ( $S_{OCEAN}$ ), (f) the budget imbalance ( $B_{IM}$ ) that is not accounted for by the other terms. Positive values of  $S_{LAND}$  and  $S_{OCEAN}$  represent a flux from the atmosphere to land or the ocean. All data are in GtC yr<sup>-1</sup> with the uncertainty bounds representing  $\pm 1$  standard deviation in shaded colour. Data sources are as in Figure 3. The red dots indicate our projections for the year 2024 and the red error bars the uncertainty in the 2024 projections (see methods).

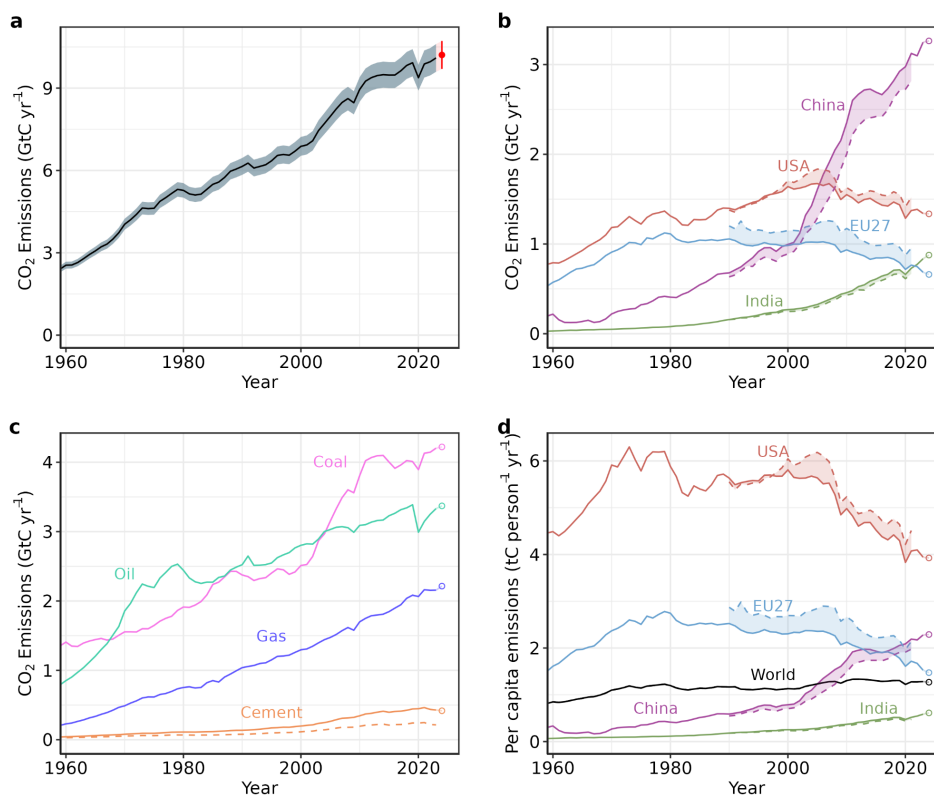


**Figure 5.** Fossil CO<sub>2</sub> emissions for (a) the globe, including an uncertainty of  $\pm 5\%$  (grey shading) and a projection through the year 2024 (red dot and uncertainty range), (b) territorial (solid lines) and consumption (dashed lines) emissions for the top three country emitters (USA, China, India) and for the European Union (EU27), (c) global emissions by fuel type, including coal, oil, gas, and cement, and cement minus cement carbonation (dashed), and (d) per-capita emissions the world and for the large emitters as in panel (b). Territorial emissions are primarily from a draft update of Hefner and Marland (2023) except for national data for most Annex I countries for 1990-2022, which are reported to the UNFCCC as detailed in the text, as well as some improvements in individual countries, and extrapolated forward to 2023 using data from Energy Institute. Consumption-based emissions are updated from Peters et al. (2011a). See Section 2.1 and Supplement S.1 for details of the calculations and data sources.

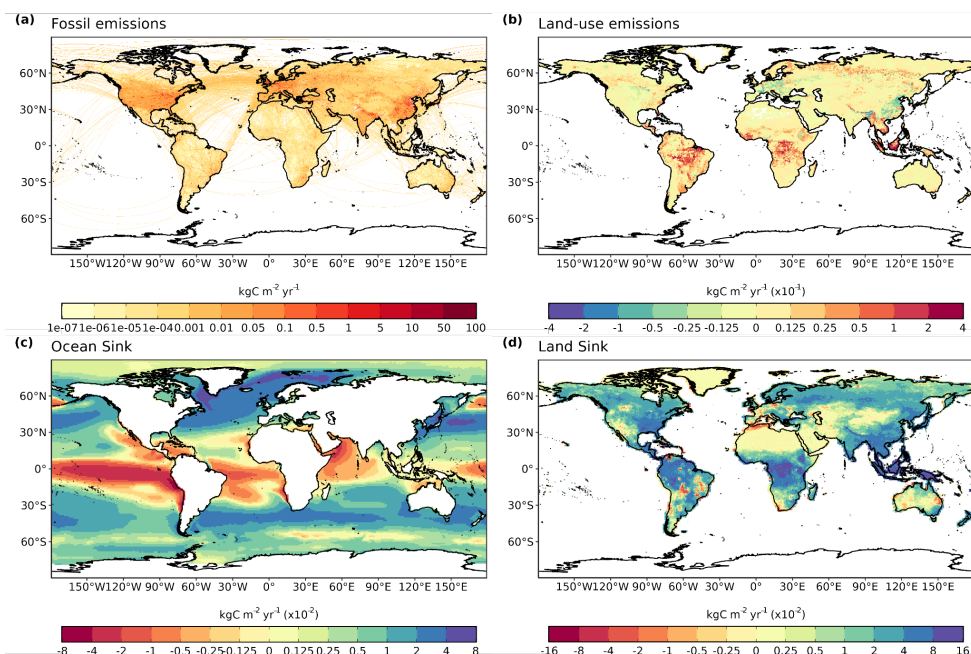


**Figure 6.** The 2014–2023 decadal mean components of the global carbon budget, presented for (a) fossil CO<sub>2</sub> emissions ( $E_{FOS}$ ), (b) land-use change emissions ( $E_{LUC}$ ), (c) the ocean CO<sub>2</sub> sink ( $S_{OCEAN}$ ), and (d) the land CO<sub>2</sub> sink ( $S_{LAND}$ ). Positive values for  $E_{FOS}$  and  $E_{LUC}$  represent a flux to the atmosphere, whereas positive values of  $S_{OCEAN}$  and  $S_{LAND}$  represent a flux from the atmosphere to the ocean or the land (carbon sink). In all panels, yellow/red colours represent a source (flux from the land/ocean to the atmosphere), green/blue colours represent a sink (flux from the atmosphere into the land/ocean). All units are in  $\text{kgC m}^{-2} \text{yr}^{-1}$ . Note the different scales in each panel.  $E_{FOS}$  data shown is from GCP-GridFEDv2024.0 and does not include cement carbonation. The  $E_{LUC}$  map shows the average  $E_{LUC}$  from the four bookkeeping models plus emissions from peat drainage and peat fires. BLUE and LUCE provide spatially explicit estimates at  $0.25^\circ$  resolution. Gridded  $E_{LUC}$  estimates for H&C2023 and OSCAR are derived by spatially distributing their national data based on the spatial patterns of BLUE gross fluxes in each country (see Schwingshackl et al., 2022, for more details about the methodology).  $S_{OCEAN}$  data shown is the average of GOBMs and  $f_{CO_2}$ -products means, using GOBMs simulation A, no adjustment for bias and drift applied to the gridded fields (see Section 2.5).  $S_{LAND}$  data shown is the average of the DGVMs for simulation S2 (see Section 2.6).



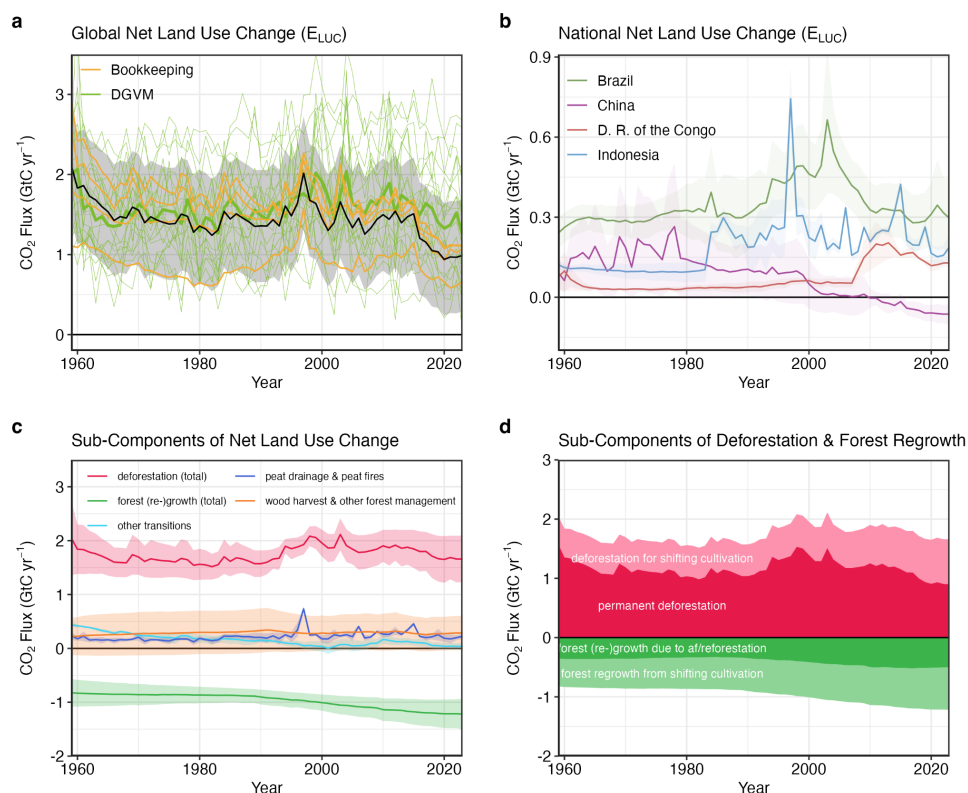


**Figure 7.** Net CO<sub>2</sub> exchanges between the atmosphere and the terrestrial biosphere related to land use change. (a) Net CO<sub>2</sub> emissions from land-use change ( $E_{LUC}$ ) with estimates from the four bookkeeping models (yellow lines) and the budget estimate (black with  $\pm 1\sigma$  uncertainty), which is the average of the four bookkeeping models. Estimates from individual DGVMs (narrow green lines) and the DGVM ensemble mean (thick green line) are also shown. (b) Net CO<sub>2</sub> emissions from land-use change from the four countries with largest cumulative emissions since 1959. Values shown are the average of the four bookkeeping models, with shaded regions as  $\pm 1\sigma$  uncertainty. (c) Sub-components of  $E_{LUC}$ : (i) emissions from deforestation (including permanent deforestation and deforestation in shifting cultivation cycles), (ii) emissions from peat drainage & peat fires, (iii) removals from forest (re-)growth (including forest (re-)growth due to afforestation and reforestation and forest regrowth in shifting cultivation cycles), (iv) fluxes from wood harvest and other forest management (comprising slash and product decay following wood harvest, regrowth after wood harvest, and fire suppression), and (v) emissions and removals related to other land-use transitions. The sum of the five components is  $E_{LUC}$  shown in panel (a). (d) Sub-components of ‘deforestation (total)’ and of ‘forest (re-)growth (total)’: (i) deforestation in shifting cultivation cycles, (ii) permanent deforestation, (iii) forest (re-)growth due to afforestation and/or reforestation, and (iv) forest regrowth in shifting cultivation cycles.

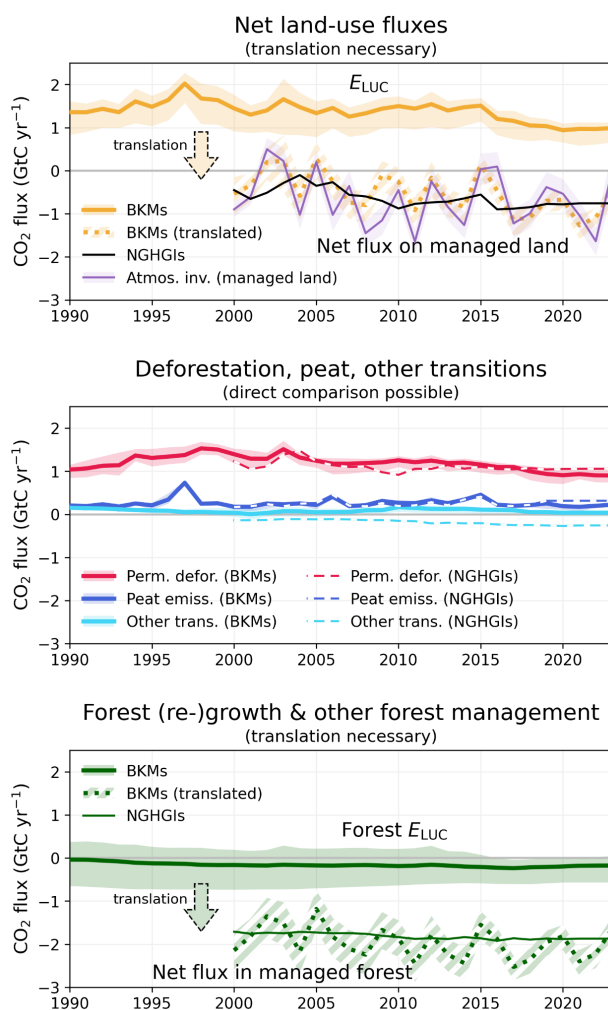


**Figure 8.** Comparison of land-use flux estimates from bookkeeping models (BKMs; following the GCB definition of  $E_{LUC}$ ), national GHG inventories (NGHGs; following IPCC guidelines and thus including all carbon fluxes on managed land), and atmospheric inversion systems (considering fluxes on managed land only). To compare BKM results with NGHGs, a translation is necessary for some subcomponents. (a) Net land-use fluxes, for which a translation of BKMs is necessary, (b) subcomponents permanent deforestation, peat drainage & peat fires, and other transitions, which can be directly compared and (c) subcomponent forest (re-)growth & other forest management, for which a translation is necessary. The lines represent the mean of 4 BKMs and 14 atmospheric inversion estimates, respectively; Shaded areas denote the full range across BKM estimates and the standard deviation for atmospheric inversions, respectively. The subcomponent forest (re-)growth & other forest management includes removals from forest (re-)growth (permanent), emissions and removals from wood harvest & other forest management, and emissions and removals in shifting cultivation cycles. The translation of



BKM estimates to NGHGI estimates in (a) and (c) is done by adding the natural land sink in managed forests to the BKM estimates (see also Table S10). The GCB definition of ELUC and the NGHGI definition of land-use fluxes are equally valid, each in its own context. For illustrative purposes we only show the translation of BKM estimates to the NGHGI definition.

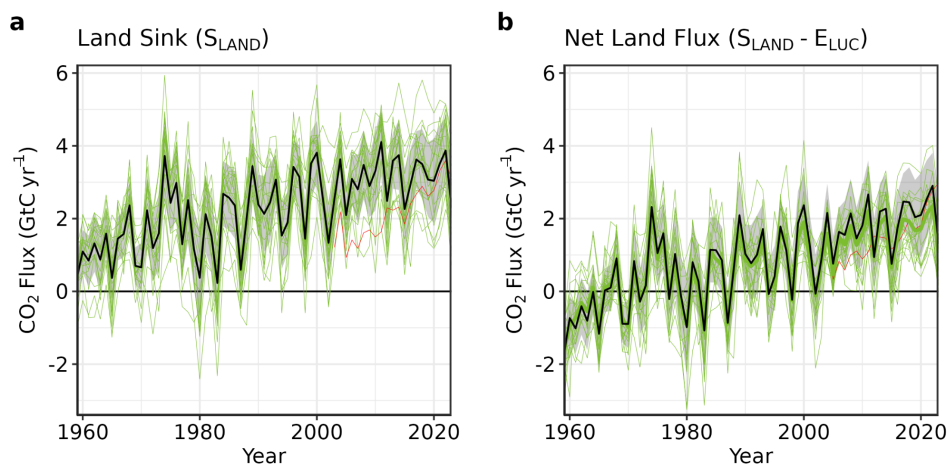


**Figure 9.** (a) The land  $\text{CO}_2$  sink ( $S_{\text{LAND}}$ ) estimated by individual DGVMs (green), and CARDAMOM (red), as well as the budget estimate (black with  $\pm 1\sigma$  uncertainty), which is the average of all DGVMs. (b) Net atmosphere-land  $\text{CO}_2$  fluxes ( $S_{\text{LAND}} - E_{\text{LUC}}$ ). The budget estimate of the net land flux (black with  $\pm 1\sigma$  uncertainty) combines the DGVM estimate of  $S_{\text{LAND}}$  from panel (a) with the bookkeeping estimate of  $E_{\text{LUC}}$  from Figure 7a. Uncertainties are similarly propagated in quadrature. DGVMs also provide estimates of  $E_{\text{LUC}}$  (see Figure 7a), which can be combined with their own estimates of the land sink. Hence panel (b) also includes an estimate for the net land flux for individual DGVMs (thin green lines) and their multi-model mean (thick green line).

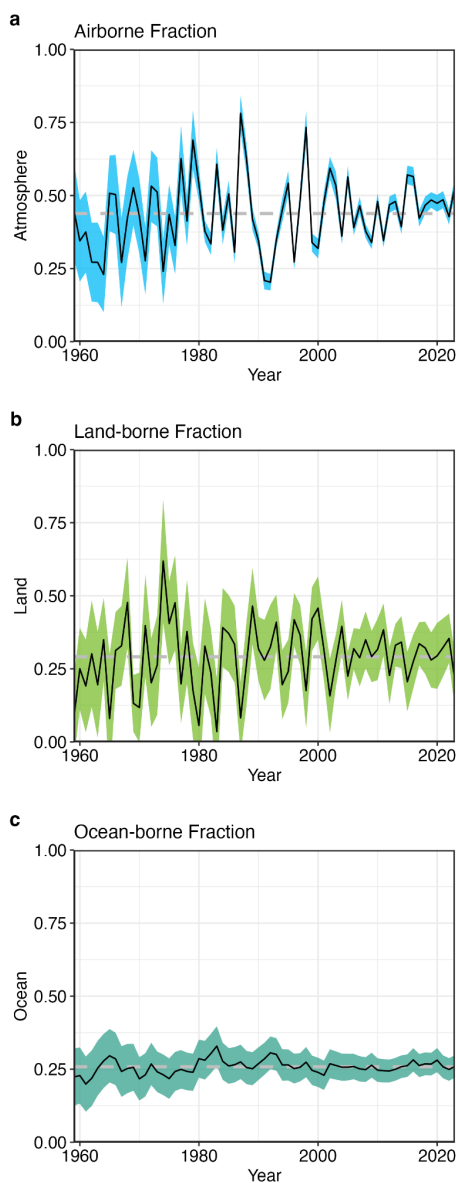


**Figure 10.** The partitioning of total anthropogenic CO<sub>2</sub> emissions ( $E_{FOS} + E_{LUC}$ ) across (a) the atmosphere (airborne fraction), (b) land (land-borne fraction), and (c) ocean (ocean-borne fraction). Black lines represent the central estimate, and the coloured shading represents the uncertainty. The grey dashed lines represent the long-term average of the airborne (44%), land-borne (30%) and ocean-borne (25%) fractions during 1960-2023 (with a  $B_{IM}$  of 1%).

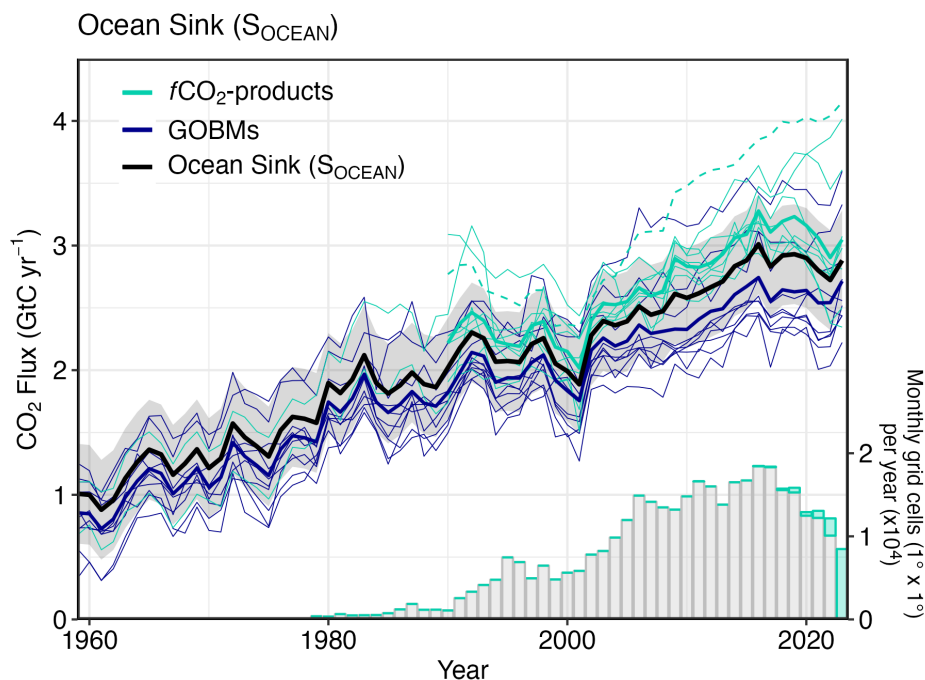


**Figure 11.** Comparison of the anthropogenic atmosphere-ocean CO<sub>2</sub> flux showing the budget values of  $S_{OCEAN}$  (black; with the uncertainty in grey shading), individual ocean models (royal blue), and the ocean  $fCO_2$ -products (cyan; with UExp-FFN-U, previously Watson et al. (2020), in dashed line as not used for ensemble mean). Two  $fCO_2$ -products (Jena-MLS, LDEO-HPD) extend back to 1959. The  $fCO_2$ -products were adjusted for the pre-industrial ocean source of CO<sub>2</sub> from river input to the ocean, by subtracting a source of 0.65 GtC yr<sup>-1</sup> to make them comparable to  $S_{OCEAN}$  (see Section 2.5). Bar-plot in the lower right illustrates the number of monthly gridded values in the SOCAT v2024 database (Bakker et al., 2024). Grey bars indicate the number of grid cells in SOCAT v2023, and coloured bars indicate the newly added grid cells in v2024.

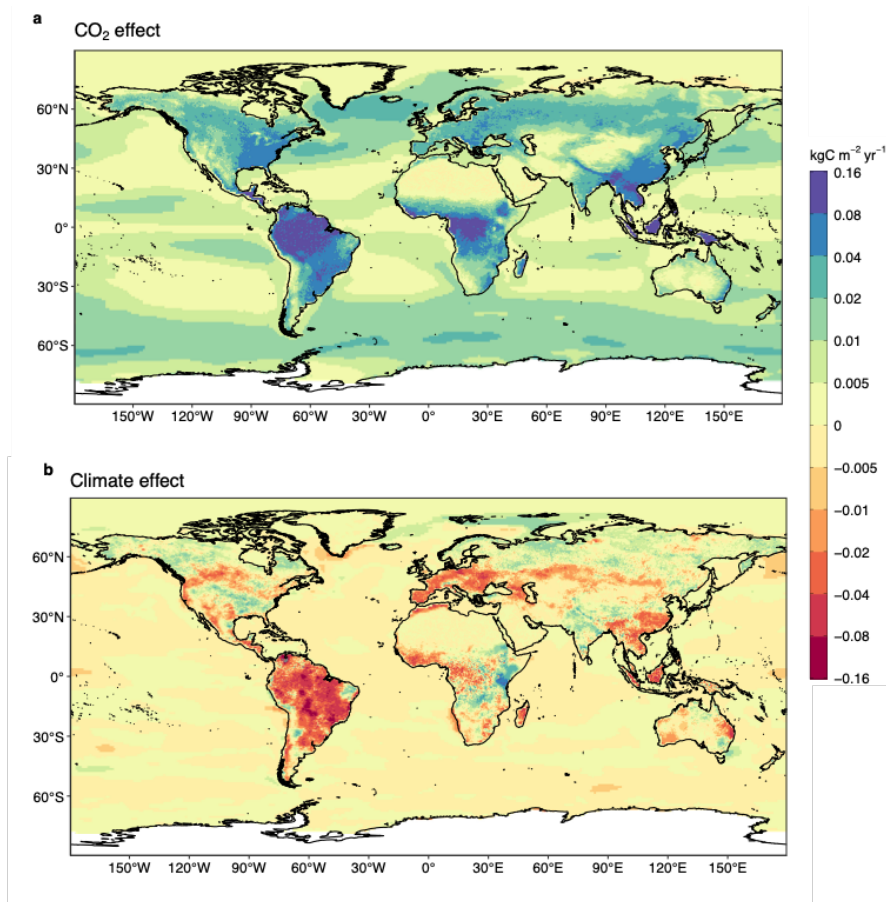


**Figure 12.** Attribution of the atmosphere-ocean ( $S_{\text{OCEAN}}$ ) and atmosphere-land ( $S_{\text{LAND}}$ ) CO<sub>2</sub> fluxes to (a) increasing atmospheric CO<sub>2</sub> concentrations and (b) changes in climate, averaged over the previous decade 2014–2023. All data shown is from the processed-based GOBMs and DGVMs. Note that the sum of ocean CO<sub>2</sub> and climate effects shown here will not equal the ocean sink shown in Figure 6, which includes the  $f\text{CO}_2$ -products. See Supplement S.3.2 and S.4.1 for attribution methodology. Units are in kgC m<sup>-2</sup> yr<sup>-1</sup> (note the non-linear colour scale). Positive values (blue) are CO<sub>2</sub> sinks, negative values (red) are CO<sub>2</sub> sources.

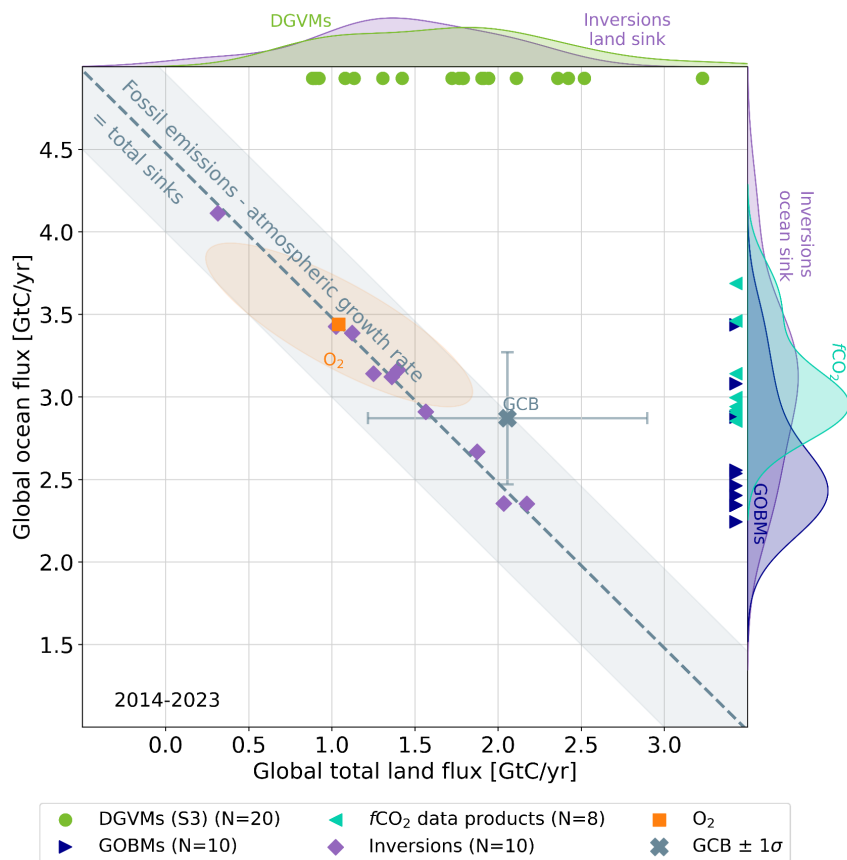


**Figure 13.** The 2014-2023 decadal mean global net atmosphere-ocean and atmosphere-land fluxes derived from the ocean models and  $f\text{CO}_2$  products (y-axis, right and left pointing blue triangles respectively), and from the DGVMs (x-axis, green symbols), and the same fluxes estimated from the atmospheric inversions (purple symbols). The shaded distributions show the densities of the ensembles of individual estimates. The grey central cross is the mean ( $\pm 1\sigma$ ) of  $S_{\text{OCEAN}}$  and  $(S_{\text{LAND}} - E_{\text{LUC}})$  as assessed in this budget. The grey diagonal line represents the constraint on the global land + ocean net flux, i.e. global fossil fuel emissions minus the atmospheric growth rate from this budget ( $E_{\text{FOS}} - G_{\text{ATM}}$ ). The orange square represents the same global net atmosphere-ocean and atmosphere-land fluxes as estimated from the atmospheric  $\text{O}_2$  constraint (the ellipse drawn around the central atmospheric  $\text{O}_2$  estimate is a contour representing the  $1\sigma$  uncertainty of the land and ocean fluxes as a joint probability distribution). Positive values are  $\text{CO}_2$  sinks. Note that the inverse estimates have been scaled for a minor difference between  $E_{\text{FOS}}$  and GridFEDv2024.0 (Jones et al., 2024a).



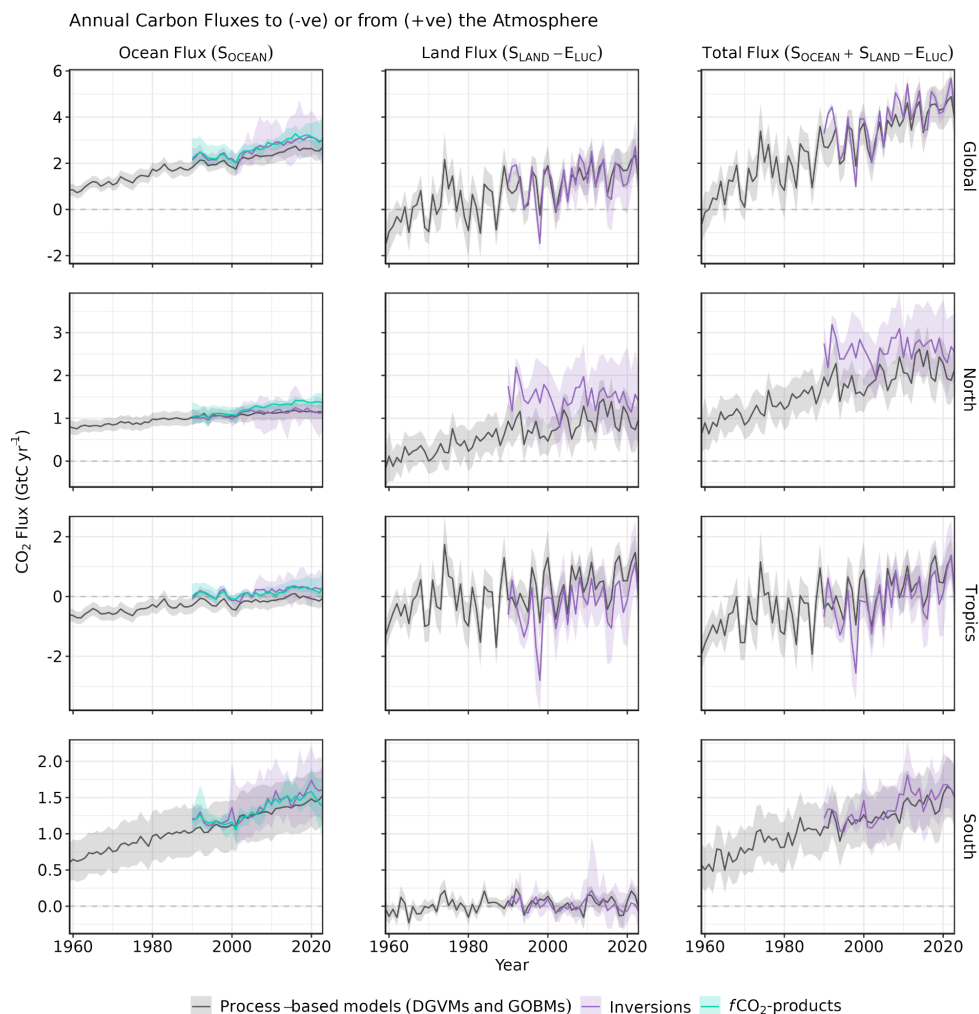


**Figure 14.** CO<sub>2</sub> fluxes between the atmosphere and the Earth's surface separated between land and oceans, globally and in three latitude bands. The ocean flux is  $S_{\text{OCEAN}}$  and the land flux is the net atmosphere-land fluxes from the DGVMs. The latitude bands are (top row) global, (2<sup>nd</sup> row) north ( $>30^{\circ}\text{N}$ ), (3<sup>rd</sup> row) tropics ( $30^{\circ}\text{S}$ - $30^{\circ}\text{N}$ ), and (bottom row) south ( $<30^{\circ}\text{S}$ ), and over ocean (left column), land (middle column), and total (right column). Estimates are shown for: process-based models (DGVMs for land, GOBMs for oceans); inversion systems (land and ocean); and  $f\text{CO}_2$ -products (ocean only). Positive values are CO<sub>2</sub> sinks. Mean estimates from the combination of the process models for the land and oceans are shown (black line) with  $\pm 1 \sigma$  of the model ensemble (grey shading). For the total uncertainty in the process-based estimate of the total sink, uncertainties are summed in quadrature. Mean estimates from the atmospheric inversions are shown (purple lines) with their full spread (purple shading). Mean estimates from the  $f\text{CO}_2$ -products are shown for the ocean domain (light blue



lines) with full model spread (light blue shading). The global  $S_{OCEAN}$  (upper left) and the sum of  $S_{OCEAN}$  in all three regions represents the anthropogenic atmosphere-to-ocean flux based on the assumption that the preindustrial ocean sink was  $0 \text{ GtC yr}^{-1}$  when riverine fluxes are not considered. This assumption does not hold at the regional level, where preindustrial fluxes can be significantly different from zero. Hence, the regional panels for  $S_{OCEAN}$  represent a combination of natural and anthropogenic fluxes. Bias-correction and area-weighting were only applied to global  $S_{OCEAN}$ ; hence the sum of the regions is slightly different from the global estimate ( $<0.07 \text{ GtC yr}^{-1}$ ).

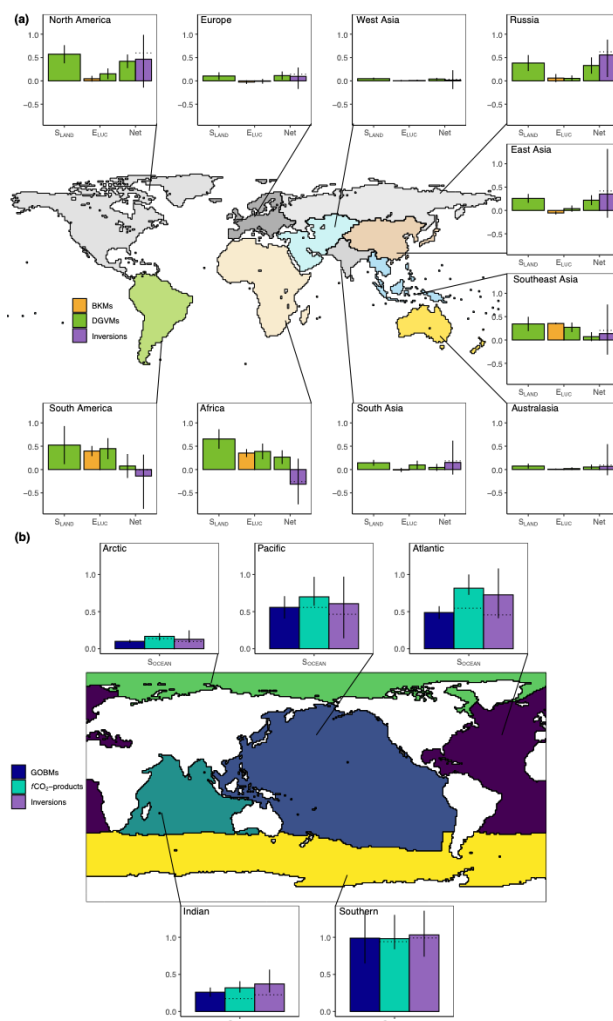


**Figure 15.** Decadal mean (a) land and (b) ocean fluxes for RECCAP-2 regions over 2014-2023. For land fluxes,  $S_{LAND}$  is estimated by the DGVMs (green bars), with the error bar as  $\pm 1\sigma$  spread among models. A positive  $S_{LAND}$  is a net transfer of carbon from the atmosphere to the land.  $E_{LUC}$  fluxes are shown for both DGVMs (green) and bookkeeping models (orange), again with the uncertainty calculated as the  $\pm 1\sigma$  spread. Note, a positive  $E_{LUC}$  flux indicates a loss of carbon from the land. The net land flux is shown for both DGVMs (green) and atmospheric inversions (purple), including the full model spread for inversions. The net ocean sink ( $Socean$ ) is estimated by GOBMs (royal blue),  $fCO_2$ -products (cyan), and atmospheric inversions (purple). Uncertainty is estimated as the  $\pm 1\sigma$  spread for GOBMs, and the full model spread for the other two datasets. The dotted lines show the  $fCO_2$ -products and inversion results without river flux adjustment. Positive values are  $CO_2$  sinks.



# Anthropogenic carbon flows

(a) Cumulative changes 1850-2023 GtC

(b) Mean fluxes 2014-2023 GtC per year

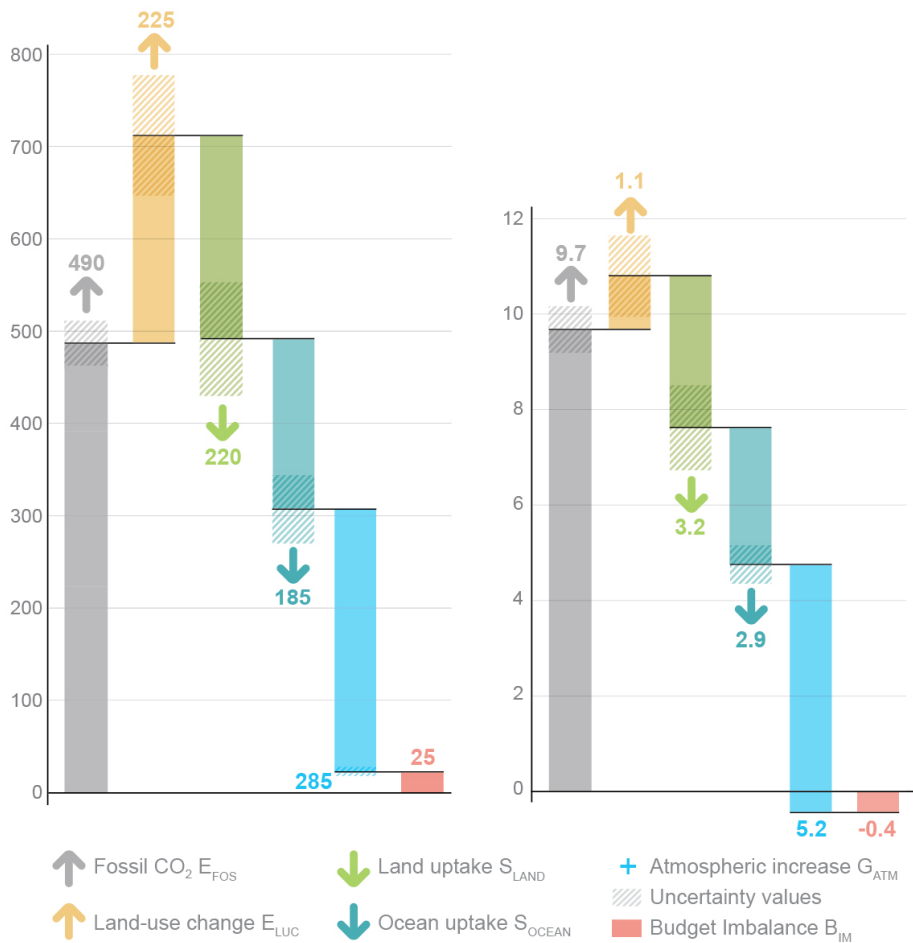


**Figure 16.** Cumulative changes over the 1850-2023 period (left) and average fluxes over the 2014-2023 period (right) for the anthropogenic perturbation of the global carbon cycle. See the caption of Figure 3 for key information and the methods in text for full details.



**Figure 17.** Kaya decomposition of the main drivers of fossil CO<sub>2</sub> emissions, considering population, GDP per person, Energy per GDP, and CO<sub>2</sub> emissions per energy, for China (top left), USA (top right), EU27 (middle left), India (middle right), Rest of the World (bottom left), and World (bottom right). Black dots are the annual fossil CO<sub>2</sub> emissions growth rate, coloured bars are the contributions from the different drivers to this growth rate. A general trend is that population and GDP growth put upward pressure on emissions (positive values), while energy per GDP and, more recently, CO<sub>2</sub> emissions per energy put downward pressure on emissions (negative values). Both the COVID-19 induced drop during 2020 and the recovery in 2021 led to a stark contrast to previous years, with different drivers in each region.